THE SYNTHESIS OF COMPOSITE SPECTRA: A STUDY OF FOUR GLOBULAR CLUSTERS OF THE GALAXY, FIVE GLOBULAR CLUSTERS OF M31, AND THE NUCLEUS OF NGC 205

Thesis by

Clark G. Christensen

In Partial Fulfillment of the Requirements

For the Degree of

Doctor of Philosophy

California Institute of Technology

Pasadena, California

1972

(Submitted January 24, 1972)

ACKNOWLEDGEMENTS

I am most appreciative of the direction and encouragement provided by my research co-advisors Dr. W. L. W. Sargent and Dr. J. B. Oke. I am indebted to Dr. Oke for sharing three nights of 200-inch observing time. Dr. Oke also permitted me to use his scans of red-giants in M92. Both Dr. Sargent and Dr. Oke provided unpublished references for program stars.

Bob O'Connell was most helpful in extending advance data from his thesis and especially in advising me concerning spectral synthesis techniques. I am also indebted to Bob, as well as Dr. Oke, for supplying needed computer programs.

I thank Hyron Spinrad for advice and for pre-publication results of his work.

Darrell J. MacConnell and Howard E. Bond were very generous in sending lists of population II stars from their work.

My thanks also go to N. Visvanathan for encouragement and advice.

Dean Petersen provided me with a liquid copper sulfate filter and assisted me in maintaining it.

I am grateful to the staff of the Caltech Astroelectronics Lab. Larry Blakee and Martin Olsiewski were especially helpful in extending much-needed advice and in maintaining electronic equipment.

I appreciate the generous amount of observing time allotted by the Hale Observatories Observing Committee.

For their assistance and moral support I thank night assistants Henry Schaefer, Gene Hancock, Tom Gregor, Pete Mastrosimone, and Jim Dittmar of Mt. Wilson and Gary Tuton of Mt. Palomar. I also thank Larry Bornhurst and Warren Weaver of Mt. Wilson and Bill Van Hook and Chuck Kearns of Mt. Palomar for unscheduled mechanical aid with the telescopes and auxiliary equipment.

Finally, I express my deepest appreciation to my wife Vicki whose support, encouragement, and confidence have been of inestimable value.

National Science Foundation Graduate Fellowships, an ARCS Foundation Fellowship, and research assistantships from the California Institute of Technology have sustained me financially.

ABSTRACT

A spectral synthesis technique similar to that of Spinrad and Taylor (1971) has been applied to the integrated light of globular clusters M5, M13, M15, and M92 of the Galaxy; H12, H55, H140, B282, and MIV of M31; and to the nucleus of the elliptical galaxy NGC 205. The derived stellar contents of the four local clusters have been compared with color-magnitude diagrams and luminosity functions based on studies of individual stars within these systems. Results agree.

The technique yields information on both the metal content of clusters and their horizontal-branch colors and thus is useful for extracting the two parameters which apparently describe galactic globular clusters.

Principal results of the study of the six extragalactic systems are:

(1) The clusters H12 and H140 have similar metal contents and similar luminosity functions except along their horizontal branches where H12 is concentrated to the red, resembling 47 Tuc, and H140 is rather blue, resembling M5. This result suggests that M31 clusters belong to at least a two-parameter family as do clusters in the Galaxy.

(2) H55 and B282 have absorption features too strong to be artificially reproduced with a mixture of population I stellar spectra

of normal feature strengths. This confirms a similar result by Spinrad and Schweizer (1972) for B282.

(3) The strong-lined cluster H55 is a halo object. This corroborates van den Bergh's (1969) discovery of strong-lined halo clusters in M31.

(4) The metal-richness of the stellar contents of the clusters correlates well with van den Bergh's line index L. This correlation strengthens his result that M31 globular clusters are generally more metal-rich than their galactic counterparts.

(5) No firm evidence is found for the hot blue stars inferred to be present in B282 by Spinrad and Schweizer.

(6) The nucleus of NGC 205 is composed of mild population II stars like clusters H12 and H140. However its color-magnitude distribution is unlike that of any known globular cluster. V-light contributions are about sixty per cent from its main sequence and only three per cent from its giant branch. The domination by dwarfs is greater by a factor of two than in the M81, M32, and M31 nuclear models of Spinrad and Taylor (1971). The apparent explanation is a different luminosity function.

There is some evidence for dispersion in the initial luminosity functions of clusters. The best models for the metal-rich clusters H55 and B282 have about one-half more V-light arising from their main sequences than the other clusters. The giant branch of M5 appears to

contribute about one-third more V-light than giant branches of other clusters studied. There is some independent evidence for an abnormally heavily populated giant branch in M5.

TABLE OF CONTENTS

TABLE OF CONTENTS (continued)

I. INTRODUCTION

A) Stellar Populations, Globular Clusters, and Galactic Evolution

When Baade (1944) introduced his concept of stellar populations, he characterized population II by a lack of O- and B-type stars and red-supergiants, an abundance of short period (RR Lyrae) variables, condensation of stars into tight globular clusters rather than open galactic clusters, and a characteristic distribution in the H-R diagram. He also recognized that his population II was identifiable with the high-velocity substratum of the Galaxy which had been discovered by Oort (1926). Globular clusters, which exhibited all of the above properties, were designated a prototype of population II.

Although a weakness of cyanogen bands in high-velocity giants had long been known (Lindblad 1922), the metal deficiency of population II stars was not definitely established until Chamberlain and Aller (1951) analyzed metal abundances in the subdwarfs HD 19445 and HD 140283. Metal deficiencies in globular clusters were implied by the theoretical work of Hoyle and Schwarzchild (1955) and were later confirmed spectroscopically by Helfer, Wallerstein and Greenstein (1959). Thus differences in stellar populations which Baade had correctly attributed to age were better understood as manifestations of differences in

chemical composition.

When Burbidge, Burbidge, Fowler, and Hoyle (1957) firmly established the theory of nucleosynthesis in stellar interiors, an immediate result was an implied age-chemical composition correlation in stellar populations. It remained for Eggen, Lynden-Bell, and Sandage (1962) to relate all of the above stated properties of population II in their model of galactic collapse. Wide dispersions in population II properties which had been discovered since Baade's original work were explained by confining the collapse of the Galaxy and a period of rapid metal enrichment of the interstellar medium to a relatively short period at the beginning of the Galaxy's history.

Despite the progress made in understanding stellar populations and galactic evolution between the time of Baade's early work and the publication of Eggen et al., recent years have produced unexplained discoveries. As van den Bergh (1965) first concluded, variations in the color-magnitude diagrams of globular clusters cannot be explained by a wide dispersion in but one parameter, metal abundance. (Iben [1971] disputes this view.) More recent studies indicate, although not conclusively, that globular cluster color-magnitude diagrams can be classified in a two-dimensional scheme. (See for example Hartwick [1968] or Castellani, Giannone and Renzini [1970].) Thus at least one basic parameter besides metal-content varies from cluster to cluster.

The identification of this second parameter is of primary importance. If it is helium content, a view advocated by Sandage and Wildey (1967), then cluster comparisons will assume cosmological importance since the initial helium content of the universe is a fundamental parameter in discriminating among cosmologies, a fact realized after Penzias and Wilson (1965) strengthened the position of big-bang cosmologies by their discovery of the 3°K microwave background. If the helium content of clusters should turn out to have a large dispersion it would give impetus to the admittedly speculative idea of Burbidge (1969) that much of the helium may have been synthesized in extremely massive objects in an early, highly luminous phase of the Galaxy.

Rood and Iben (1968) have suggested that the second parameter is age. If correct, their view would necessitate a revision in the theory of Eggen, Lynden-Bell and Sandage.

Another possible second parameter is initial cluster luminosity function. The possibility also exists that metal content has been oversimplified as a single parameter. Iben (1971) asserts that if mass-loss rate on the giant branch is correlated with metal content it may be possible to explain the variations in color-magnitude diagrams as a result of dispersion in metal content only. Iben describes a correlation between metal content and mass-loss rate which could account for the lack of a monotonic correlation between metal content and the mean color of horizontal-branch stars, the primary evidence that a second

parameter is necessary.

A second major indication of the need for a more comprehensive view of galactic evolution and stellar populations was van den Bergh's (1969) discovery that the globular clusters in M31 are generally more metal-rich than those in the Galaxy. They also lack a discernible correlation between metal content and spatial distribution. Van den Bergh has also inferred that the M31 globulars may be systematically brighter than those of the Galaxy.

Spinrad and Schweizer (1972) have intensified the problem raised by van den Bergh with their claim that the strongest-line globular clusters in M31 are "super-metal-rich." Furthermore Spinrad and Schweizer have inferred that the metal-rich M31 clusters contain hot blue stars, in contrast to metal-rich globular clusters in the Galaxy where such stars are absent.

Concurrently with the rise of the aforementioned problems has been the development of a technique which may contribute to their solution. This technique is spectral synthesis, the reproduction of composite spectra from known mixtures of stellar spectra. Its usefulness rests on the assumption that the stellar compositions of such models are similar to those of the objects synthesized. Pioneering work in the field includes that by Wood (1963, 1966), Tull (1963), Spinrad (1966), McClure and van den Bergh (1968), Spinrad and Taylor (1971), O'Connell (1970), and Spinrad and Schweizer (1972). Fairly primitive

early techniques have progressively become more sophisticated.

Application of spectral synthesis, if valid, should prove especially valuable in facilitating studies of stellar content in other galaxies and in aggregate components of other galaxies such as globular and galactic clusters. In particular galaxy-to-galaxy comparisons of both integrated and cluster stellar content should extend the aforementioned discoveries of van den Bergh and of Spinrad and Schweizer and hopefully lead to their explanation through better theoretical models of galactic evolution.

B) Purposes of this Program

The purposes of the program of research described in this thesis in the context of section I A were as follows:

(1) To test the validity of Spinrad and Taylor's (1971) synthesis technique by applying it to globular clusters of known color-magnitude array. Contingent upon its validity the subsequent purposes were also adopted.

(2) Since the approach is basically one of trial and error, to systematize it, again by use of the clusters of known color-magnitude array.

(3) To apply the technique to at least one of van den Bergh's (1969) strong-lined clusters in the outer regions of M31, thereby to

test his claim that some strong-lined clusters occur in the extreme halo.

(4) To synthesize M31 clusters having a wide range in van den Bergh's line strength index L in order to test its validity as an indicator of metallic line strength. Confirmation of the validity of the L index would strengthen van den Bergh's claim that the M31 clusters are generally more metal-rich than those of the Galaxy.

(5) To test Spinrad and Schweizer's (1972) claim that some M31 clusters have abnormally strong spectral features. (The adjective "super-metal-rich" was used by Spinrad and Schweizer in describing these clusters. Use of their term in this thesis is meant only to imply stronger than normal spectral features).

(6) To test Spinrad and Schweizer's (1972) inference that hot blue stars are required to explain the spectra of strong-lined M31 clusters.

II. OBSERVATIONAL PROGRAM

A) Selection of Globular Clusters

The first step in executing the program outlined above was the selection of objects for spectral synthesis. Since clusters in the Galaxy were to be observed with the Palomar 200-inch prime-focus scanner attached to a 4-inch telescope (to be described in part D) with an 8.1 minute field, and since the M31 clusters were to be observed with the multi-channel spectrophotometric scanner mounted on the Palomar 200-inch telescope, it was necessary to choose objects compatible with those instruments. Because the technique of spectral synthesis requires observations at a large number of wavelengths (at least 35 wavelengths were observed in all clusters of the Galaxy and at least 32 usable features in the M31 clusters) and because the weakness of absorption features in population II necessitates the use of narrow bandpasses (20Å and 30Å in the blue and red respectively were used for the clusters of the Galaxy, and 20Å and 40Å for the clusters of M31), the limiting magnitudes for objects chosen were relatively bright. To obtain accuracies of about two per cent (three per cent in the ultraviolet) in 25 hours of observing time it was necessary to restrict observations of nearby clusters to those brighter than V = 6.5. To obtain

accuracies better than four per cent (about eight per cent in the ultraviolet) in one and one-half hours, M31 clusters were restricted to those brighter than V = 15.6.

To eliminate atmospheric extinction as a significant error source only objects with declinations northward of -15° were chosen for observation.

The elimination of sky background and dark count noise was accomplished by means of a chopper on both telescopes. Alternation of object plus sky and sky between two apertures was necessary to prevent errors caused by small instrumental asymmetries. Thus it was necessary to restrict observations to objects flanked on two sides by "typical" looking regions of sky. This was particularly a problem with the M31 clusters. Several of these were eliminated from consideration because of crowded fields. This was also a reason that the relatively metal-rich cluster M71 was not observed.

Another requirement governing the choice of objects was that they exhibit relatively little interstellar reddening. This criterion also discriminated against M71 and the centrally located clusters in M31.

Besides the criteria just noted, used to discriminate against objects which could not be accurately observed, several additional criteria were employed to insure the selection of interesting objects.

The necessity of finding nearby globular clusters with already-known color-magnitude arrays led to the choice of the bright and easily

observable clusters M3, M5, M13, M15, and M92, all of which have known arrays extending below the main sequence turnoff. Because of the close similarity between M3 and M5 it was decided that only one of the two would be included. Convenience initially favored M3, but after one scan was obtained bad weather reversed the choice to M5. For this reason a partial energy distribution is given later in this thesis for M3 but no synthesis was attempted since the spectrum does not extend to all program wavelengths and its accuracy is probably only 5 to 10 per cent.

It also seemed desirable to include nearby clusters spanning as wide a range in Morgan (1959) metallic-line classification and Kron and Mayall (1960) spectral type as possible. These criteria, because of the lack of sufficiently bright candidates, were not completely satisfied. Morgan types range from type I for M15 and M92 to type III for M13. Kron and Mayall spectral types vary from F1 for M92 to F6 for M5 and M13 (M3 is type F7).

In selecting candidates from M31 the adopted criteria were more successfully applied. The five objects chosen for observation represent the full range of van den Bergh's (1969) line-strength index L spanned by M31 clusters. Their apparent positions include points close to and distant from the disk. (However with such a small sample it is possible that all could be remote clusters, with projection being responsible for apparent proximity to the disk.)

TABLE 1

PROGRAM OBJECTS FOR SPECTRAL SYNTHESIS

Globular Clusters of the Galaxy

Name	Morgan Type (1)	Sp. Type (2)	Line Index (3)	b^{II} (4)	$D_{0,9}$ ['] (2)	V (4,5)	B-V (5)	U-B (5)	Q (5)	Rad. Vel. [km/sec] (4)	m - M	E_{B-V}
M3	II	F7	4	78°	9.3	6.17	.69	.09	-.41	-153	15.40 (6)	0.00 (8, 9, 10, 11)
M5	II	F6	6	47°	10.7	5.97	.72	.13	-.39	49	14.39 (7)	0.02 (7, 10)
M13	III	F6	3	41°	12.9	5.76	.67	.04	-.44	-241	14.30 (4,15)	0.02 (8, 9, 11)
M15	I	F2	-1	-27°	9.4	6.27	.69	.06	-.44	-107	15.50 (4)	0.12 (11)
M92	I	F1	0	33°	12.3	6.32	.62	.02	-.43	-118	14.62 (6)	0.02 (10, 11)

M31 Globular Clusters

Name	Line Index (3)	Projected Location	V (3)	B - V (3)	U - B (3)	Q (3)	Rad. Vel. [km/sec] (3)	m - M (13)	E_{B-V} (3, 9, 14)
H12	8	Disk Edge	14.24	.82	.16	-.43	-286	24.65	0.11
H55	11	Halo	15.56	.91	.49	-.17	-247	24.65	0.11
H140	8	Halo	15.16	.72	.12	-.40	-181	24.65	0.11
B282	15	Disk Edge	14.18	.92	.47	-.19	-170	24.65	0.11
MIV	0	Halo	15.06	.66	-.01	-.49	-348	24.65	0.11
NGC 205 (nucleus)	3p	-	8.25 (12)	.81 (12)	.10 (12)	-.48	-239 (12)	24.65	0.11

TABLE 1 (continued)

References

1. Morgan (1959)
2. Kron and Mayall (1960)
3. van den Bergh (1969)
4. Arp (1965)
5. van den Bergh (1967)
6. Sandage and Walker (1966)
7. Arp (1962)
8. Crawford and Barnes (1969)
9. McClure and Racine (1969)
10. McNamara and Langford (1969)
11. Sandage (1969)
12. de Vaucouleurs and de Vaucouleurs (1964)
13. van den Bergh (1968)
14. Sturch (1966)
15. Baum et al. (1959)

Plate 1: Positions of NGC 205 and the five program globular clusters associated with M31.

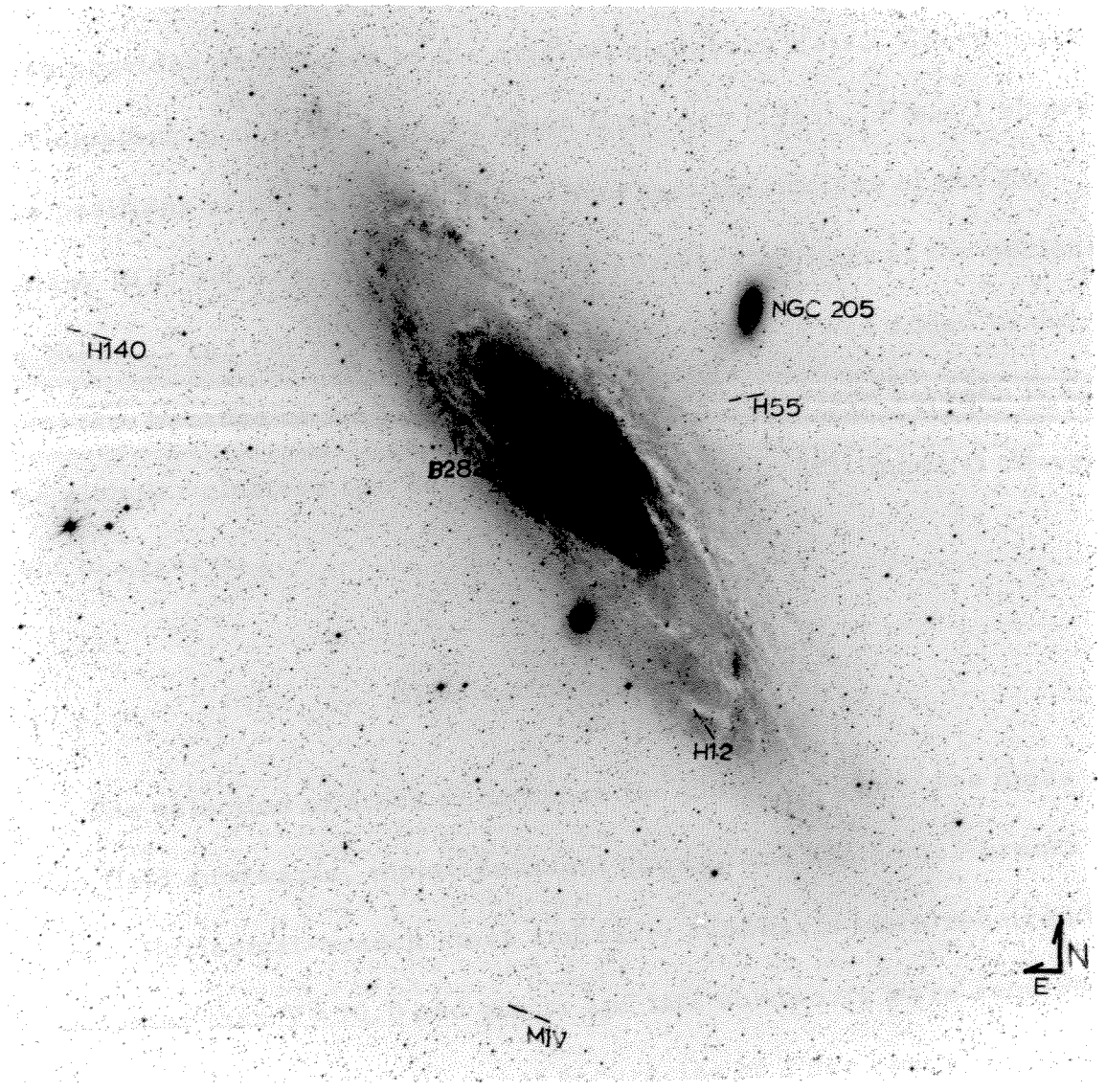

PLATE 1

Table 1 summarizes several properties of the clusters selected for observation. Sources of information are given in parentheses. Coordinates for the M31 clusters were taken from Vetešnik (1962) who also provides references to the original discovery lists. Coordinates for clusters of the Galaxy were taken from Arp (1965). Plate 1 shows the positions of the M31 clusters. (Note that the nucleus of the E6p galaxy NGC 205 has been included. The integrated light of the nucleus of NGC 205 has not been previously synthesized. It was added to the program because of the possibly interesting comparison between it and the globular clusters and because its proximity to M31 made it convenient to observe.)

B) Selection of Stars

The selection of stars to compose the cluster models was made from field subdwarfs, metal-deficient giants, and horizontal-branch stars. Horizontal-branch stars and early subdwarfs were required to be brighter than V = 10.0 and giants and late subdwarfs were required to be brighter than V = 9.0 so that accuracies of 2 per cent (3 per cent in the ultraviolet) could be achieved in three hours or less observing time with the Cassegrain scanner of the 60-inch and 100-inch Mount Wilson telescopes.

Stars were required to have declinations above -20°. Visual

binaries were rejected unless one component could be excluded from the aperture while the other was observed. HD 165195 and HDE 232078 were the only program stars with known color excesses greater than $E_{B-V} = 0.10$.

An attempt was made to include a two-dimensional sequence of stars representing the range of known population II spectral types (except for variables and planetary nebula nuclei) and a wide range of metal content. (Stars with measured or implied metal-deficiencies less than [-.5] were excluded.) Stars with abundance analyses were favored over those without.

Table 2 summarizes properties of stars included in the observing program. UBV photometry data are average values from the catalogue of Blanco et al. (1968). In most cases tabulated radial velocities are from the catalogues of Eggen (1962, 1964) and Wilson (1953). Other sources of these data and of abundance analyses and sources identifying objects as population II are given with the table. Ultraviolet excesses, where given, are either from one of the listed references or have been computed from the color-color relation of Johnson (1966). Not all of these stars turned out to be useful for inclusion in the stellar population models for the clusters. However energy distributions are given for all objects in Appendix B.

TABLE 2

PROGRAM STARS

Name	V	B-V	U-B	δ(U-B)	[Fe/H]	Rad. Vel. [km/sec]	References
HD 2665	7.65	1.00#			-1.68	-383	1
HD 3546	4.37	.87	.47	.10	-0.75	-84	2,3
HD 6755	7.68	.72	.08		-1.05	-320	1
HD 6833	6.74	1.18	.90		-0.82	-245	4
HD 9774	5.28	.96				-4	5
HD 10700	3.50	.73	.21	.09		-16	6,7,8
HD 19445	8.00	.47	-.24	.25	-1.75	-139	9,10,11
HD 25329	8.51	.87	.36	.28	-2.30	-30	8,12,13,14
HD 37160	4.08	.95	.64	.06	-0.73	99	2,3
HD 43039	4.33	1.02	.80	.10	-0.5	20	3
HD 44007	8.06	.85	.22			167	15
HD 46703	8.92	.50	.25	-.22		-75	16,17
HD 60552	6.70	.50*					18
HD 60778	9.10	.10	.14			39	19
HD 64090	8.34	.60	-.12	.25		-230	8,13,15
HD 73394	7.70	1.01*				-96	17
HD 74462	8.74	.97	.53			-168	15
HD 74721	8.72	.03	.13			9	18,19
HD 79452	5.97	.86	.37	.18	-0.85	56	2,3
HD 81192	6.44*	.94*				7	5
HD 84937	8.29	.41	-.23	.22		-18	8,15,20,21
HD 85504	6.01	-.04	-.07			97	22
HD 86986	7.99	.14	.16		-1.54	13	15,24,25
HD 88609	8.61	.90*				-31	17
HD 90362	5.58	1.52	1.86			32	26
HD 94028	8.21	.48	-.18	.20		62	8,13,20
HD 103095	6.45	.75	.17	.19	-1.50	-98	7,8,12,15
HD 106223	7.44	.30	-.08			-17	25,27,28
HD 107328	4.95	1.16	1.15	.05	-0.72	35	2,3
HD 109995	7.61	.04	.06		-1.44	-132	12,19,24,25,29
HD 117880	9.08	.04	.06			-45	15,19
HD 122563	6.20	.91	.38	.28	-2.65	-22	3,12,15,20,23
HD 123598	7.0	1.62	1.80			58	19
HD 126778	8.18	.92	.67			-131	19
HD 128167	4.46	.35	-.08			0	6,7,8
HD 130952	4.94	.99	.74	.07	-0.5	83	3

TABLE 2 (Continued)

Name	V	B-V	U-B	δ(U-B)	[Fe/H]	Rad. Vel. [km/sec]	References
HD 134439	9.12	.78	.19	.20		292	13
HD 134440	9.44	.86	.39	.16		306	13
HD 135722	3.50	.95	.68	.04	-0.57	-12	2,3
HD 140283	7.26	.48	-.20	.22	-2.06	-171	8,9,10,11,12, 15,20
HD 142574	5.44	1.59	1.94			-61	26
HD 144579	6.67	.73	.21	.15		-60	8
HD 148349	5.24	1.72	2.03			100	26
HD 151937	6.58	1.25	1.17			-43	30
-15° 4515	9.2	.61*					18
HD 157089	6.95	.66	-.02	.14	-0.57	-162	8,10,12
HD 161817	6.96	.18	.14	.00	-1.21	-363	9,12,15,19,20 24,25,27,31
HD 165195	7.35	1.18	.68	.18	-2.70	0	3,12,23
HD 165908	5.10	.52	-.10	.14	-0.51	1	10,12
HD 175305	7.17	.78	.16			-188	19,30
HD 182762	5.15	.99	.81			1	5
HDE 232078	8.48	1.95	2.15		-1.30	-387	12,32,33
HD 185657	6.5	1.00*				-85	12,34
HD 186776	6.4	1.58*				-97	26
HD 188510	8.83	.59	-.12	.24		-201	17,30
HD 193901	8.64	.55	-.13	.21		-175	8,30
HD 196610	6.3	1.30*				-66	26
HD 201626	8.14	1.11	.49		-1.45	-152	12,35
HD 205539	6.30	.37*				-42	17
+17° 4708	9.46	.44	-.20			-296	25
HD 215373	5.08	.97				13	5
HD 219615	3.69	.92	.57	.11		-14	36
HD 219617	8.17	.47	-.20	.21	-1.40	15	8,9,10,12,15
HD 221170	7.69	1.07	.62	.30	-2.70	-120	3,12,15,23
HD 222107	3.88	1.02	.68	.21	-0.78	7	2,3
M92 II-12@	14.58	.77	.21				37,38
M92 III-13@	12.05	1.46					37,38
M92 IV-2@	13.52	.90	.43				37,38
M92 VI-18@	13.76	.79	.29				37,38
M92 X-49@	12.16	1.19	1.10				37,38
M92 XII-8@	12.76	1.06	.57				37,38

*, #, @ See page 19.

TABLE 2 (continued)

References and Footnotes

1. Koelbloed (1967)
2. Helfer and Wallerstein (1968)
3. Wallerstein and Helfer (1966)
4. Cayrel de Strobel (1966)
5. Oke (1969b)
6. Strom, Cohen, and Strom (1967)
7. Sandage and Eggen (1959)
8. Strom and Strom (1967)
9. Aller and Greenstein (1960)
10. Wallerstein (1962)
11. Melbourne (1960)
12. Cayrel and Cayrel de Strobel (1966)
13. Cayrel (1968)
14. Pagel and Powell (1966)
15. Eggen and Sandage (1959)
16. Bidelman (1965)
17. Bond (1970b)
18. MacConnell (1970)
19. Eggen (1969)
20. Sandage (1964)
21. Greenstein (1965)
22. Eggen (1966)
23. Wallerstein et al. (1963)
24. Kodaira, Greenstein, and Oke (1969)
25. Oke, Greenstein, and Gunn (1966)
26. Deutsch, Wilson, and Keenan (1969)
27. Burbidge and Burbidge (1956)
28. Slettebak, Bahner, and Stock (1961)
29. Wallerstein and Hunziker (1964)
30. Eggen (1964)
31. Kodiara (1964)
32. Preston and Bidelman (1956)
33. Helfer, Wallerstein, and Greenstein (1959)
34. Pagel (1964)
35. Wallerstein and Greenstein (1964)
36. Greenstein and Keenan (1958)
37. Oke (1971)
38. Sandage and Walker (1966)

TABLE 2 (continued)

References and Footnotes (continued)

* No published datum was found. Value is inferred from present observations.

B-V for HD 2665 is about 0.77 according to present observations.

@ These faint globular cluster giants were observed by Oke. See section III A.

C) Selection of Wavelengths and Bandpasses

The criteria for selecting a suitable set of observational wavelengths for spectral synthesis have been discussed by O'Connell (1970). However they are reiterated and extended here:

(1) Only strong features are admissable. As with O'Connell's study, maximum equivalent widths in excess of 2Å in population I have been required for the present program. This criterion is even more important for syntheses of weak-lined population II composite spectra than for population I.

(2) Features need to be sensitive to temperature and/or luminosity and/or (for population II syntheses) chemical composition. The total list of features should include a mixture of these three sensitivities.

(3) It is helpful in carrying out the syntheses if the features contain lines or bands from only one element or molecule. The G-band feature measured at λ4305 does not satisfy this criterion, nor does the feature measured at λ3880 which contains part of the λ3883 CN band and also the blue wing of H zeta which is centered at λ3890. It is impossible shortward of λ4000 to find features which are not heavily blanketed by metallic lines and/or molecular bands in stars later than F0. Iron lines and CN bands are especially dominant in this spectral region.

(4) Continuum sidebands should be chosen for each line or band feature to serve as references from which quantitative measures of feature strengths can be made. Such sidebands should be as close to feature wavelengths and as free from line-blanketing as possible. Minnaert (1940), Wildey et al. (1962), Oke and Conti (1966), and Griffin (1968) are useful references for the selection of continuum wavelengths.

(5) Wavelengths where there is strong atmospheric absorption or contamination from terrestrial light sources should be avoided (the latter is not crucial when a chopper is used unless the contamination is very strong with respect to the signal).

Subject to the above criteria, the wavelengths employed in the present syntheses were mostly adopted from the program of O'Connell (1970). Choices of a few additional wavelengths were usually from Spinrad and Taylor's lists (1969, 1971). O'Connell's wavelengths were selected because (1) he had already chosen many of the optimum features for spectral synthesis and (2) it was anticipated that his population I data might be needed to synthesize strong-lined M31 clusters. For the same reasons the bandpasses used, 20Å in the blue and 30Å in the red, were the same as those of O'Connell. Program wavelengths, features, and bandpasses are given in Table 3.

Although some observations made early in the program were extended to wavelengths beyond λ8050, it was realized that prohibitive

TABLE 3

PROGRAM WAVELENGTHS

$\Delta\lambda$ = 20Å		$\Delta\lambda$ = 30Å	
λ[Å]	Feature	λ[Å]	Feature
3448	continuum	4780	MgH λ4845, TiO λ4762
3570	continuum	4970	TiO 4954
3620	continuum		
3784	continuum	5050	continuum
3798	H_{10}	5175	MgI, (MgH λ5211, TiO λ5167)
3815	continuum, (HeI)	5300	continuum
3835	H_9	5820	continuum, (TiO λ5814)
3860	CN λ3883	5892	NaI, (HeI λ5876, TiO λ5861)
3880	CN λ3883, H_8		
3910	continuum	6100	continuum
3933	CaII λ3933	6180	TiO $\lambda\lambda$6148, 6158
		6370	continuum
4015	continuum	6564	H alpha
4101	H delta		
4200	CN λ4216	7050	continuum, (TiO λ7054)
4226	CaI λ4227	7100	TiO $\lambda\lambda$7054, 7088
4270	continuum	7400	continuum
4305	CH λ4314, atomic lines		
4400	continuum	8050	continuum
4430	interstellar	8190	NaI
4500	continuum	8400	continuum
4780	MgH λ4845, TiO λ4762	8543	CaII
		8800	continuum
		8880	TiO $\lambda\lambda$8860, 8868
		9190	CN $\lambda\lambda$9194, 9198
		9950	continuum
		10400	continuum
		10800	continuum

amounts of observing time would be required to obtain accurate scans of the clusters beyond this wavelength because of the slowness of the S-1 photocathodes available for such observations. Thus later scans were restricted to the range λ3448 through λ8050, which includes all the wavelengths employed in the syntheses.

Observations are most easily interpreted if feature and continuum indices are formed from the measured fluxes. For convenience, indices were formed in the manner of O'Connell. Feature indices have been defined as the ratio of the flux per unit wavelength observed in a feature to the flux per unit wavelength at the feature wavelength as interpolated from its two sidebands. Continuum indices are the ratio of fluxes per unit wavelength in two different spectral regions. Two bandpasses per spectral region were used in forming the continuum indices. Feature wavelengths, sidebands, and wavelengths used in forming continuum indices are given in Table 4. In Table B5 of Appendix B indices are given for each mean stellar type. All indices used in the syntheses, i. e., those shortward of λ8050 are also plotted in Figures B1 - B19. The continuum index V/R, a relatively blanketing-free, temperature parameter serves as the abscissa. These figures illustrate the behavior of each index with respect to temperature, luminosity, and chemical composition. Brief descriptions of feature behaviors based largely on Figures B1 - B19 follow.

TABLE 4

LINE INDICES

Name	Sideband 1	Center	Sideband 2
H 3798	3784	3798	3815
H 3835	3815	3835	3860
CN 3860	3815	3860	3910
CN 3880	3815	3880	3910
CaII 3933	3910	3933	4015
H 4101	4015	4101	4270
CN 4200	4015	4200	4270
CaI 4226	4015	4226	4270
CH 4305	4270	4305	4400
Is 4430	4400	4430	4500
MgH 4780	4500	4780	5050
TiO 4970	4500	4970	5050
MgI 5175	5050	5175	5300
NaI 5892	5820	5892	6100
TiO 6180	6100	6180	6370
H 6564	6370	6564	7050
TiO 7100	7050	7100	7400
NaI 8190	8050	8190	8400
CaII 8543	8400	8543	8800
TiO 8880	8800	8880	9190
CN 9190	8800	9190	9950

CONTINUUM INDICES

Name	Lambda 1	Lambda 2	Lambda 3	Lambda 4
U/B	3570	3620	4270	4400
B/V	4270	4400	5300	5820
V/R	5300	5820	7050	7400
V/I	5300	5820	8400	8800
V/J	5300	5820	10400	10800

V/R

O'Connell (1970) found V/R to be tightly correlated with Spinrad and Taylor's (1969) T index. (T is proportional to the ratio of intensities at $\lambda\lambda$7000 and 7400 to that at λ5360.) O'Connell's comparison of population I V/R's with a black body V/R curve showed that V/R is increased by Paschen absorption in the R-band in stellar types B5 to F0 (about 1.3 to 0.9 in V/R). Later than K7 (V/R $\simeq$ .45) V/R is somewhat decreased by blanketing in the V-band. Of course the second effect is of less importance in population II stars.

U/B (Figure B1)

This index depends primarily upon the Balmer jump. Red horizontal-branch stars and early subdwarfs of the same V/R separate widely in U/B. To a lesser extent U/B is abundance sensitive because of differential blanketing in the U and B bands. Separation of mild and extreme population II sequences is quite perceptible in Figure B1, both among the subdwarfs and among the giants. Iron, nickel, and chromium absorption features in the U bands, especially λ3570, are responsible.

B/V (Figure B2)

This index is tightly correlated with Johnson's (1963) B - V color. Figure 1 shows the relation. All stars observed which had B - V colors

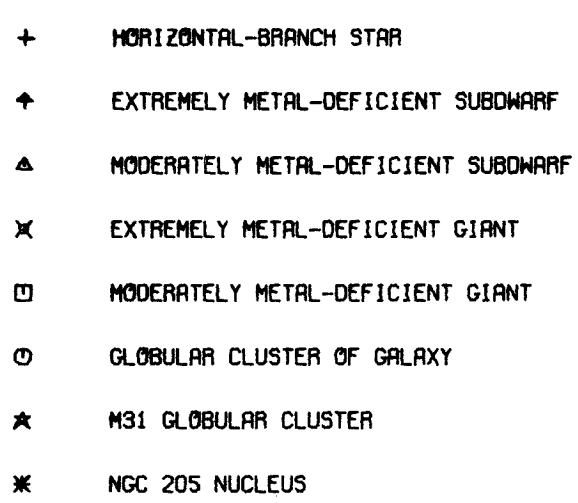

Figure 1: B - V versus B/V for the stars of Table 2. All program objects with published values of B - V are plotted, except HD 2665. B/V values are computed from the energy distributions in Table B2. Both indices have been corrected for interstellar reddening for the stars listed in Table A1. Symbols represent object types as follows:

FIGURE 1

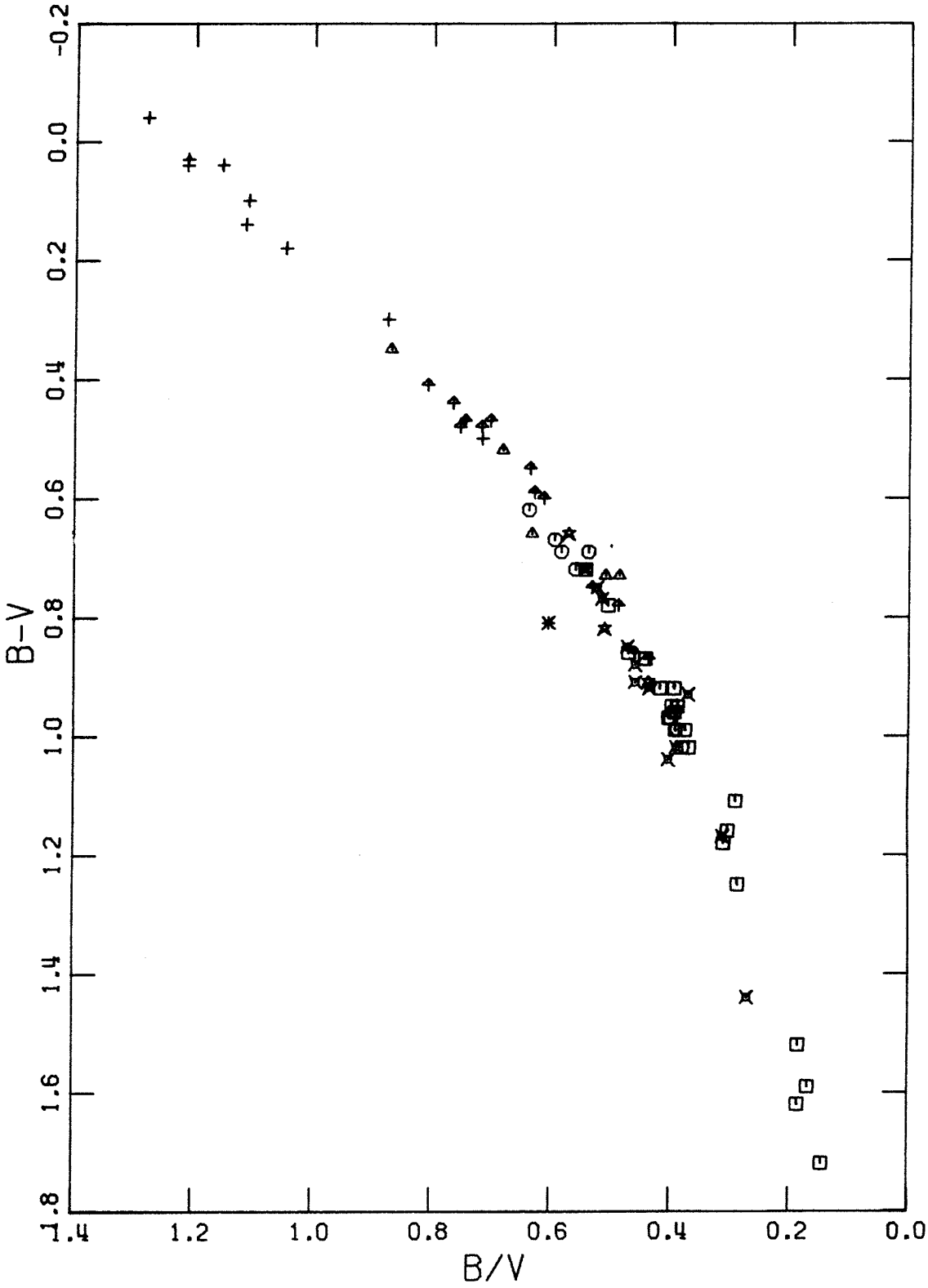

available are plotted. Later than $B/V \simeq 0.60$ ($B - V \simeq 0.80$), B/V varies more rapidly with respect to B - V for the mild sequence than for the extreme sequence. This indicates that B/V is more sensitive to differential blanketing effects than B - V. When two separate relationships, for the mild and extreme sequences, were drawn by eye in Figure 1, the mean scatter in B/V was only 0.02.

Figure B2 shows how B/V varies with V/R. A separation of about 0.1 in B/V is evident between the mild and extreme sequences. Thus B/V with its rather high sensitivity to differential blanketing effects is a good indicator of metal abundance.

B/V shows little evidence of luminosity sensitivity.

The dependences of the continuum indices are summarized as follows:

(1) V/R is strongly dependent on temperature.

(2) B/V is strongly dependent on temperature (except in very cool stars) and moderately dependent upon metal abundance.

(3) U/B is strongly dependent on surface gravity and moderately dependent on metal abundance.

Because of their highly convenient dependences these three parameters were extremely useful in fitting stellar population models to the clusters.

H 3798, H 3835, and H 4101 (Figures B3, B4, and B8)

These three indices which primarily measure H_{10} at λ3799, H9 at λ3837, and H delta at λ4103 show roughly the behaviors described by Aller (1960) and Keenan (1963). The feature strengths reach maxima between V/R = 1.2 and 1.4, in the vicinity of spectral type A0 as expected.

H 3835 exhibits considerable scatter. This scatter prompted a comparison with the index's behavior in O'Connell's (1970) population I sequence. Between V/R values of 1.0 and 0.4 the index is stronger in O'Connell's stars, especially near V/R = 0.7 where it is roughly 0.1 stronger in population I than population II. The evident conclusion is that the λ3835 bandpass is heavily blanketed, much more so than its sidebands. Absorption features of iron, magnesium, and cyanogen are all strong in this bandpass in the solar spectrum.

H 3798 and H 4101 show weaker evidence of abundance sensitivity. They are more nearly the same strength in population I and II. H 3798 is somewhat stronger in early mild population II giants than in extreme giants, indicating blanketing of the feature bandpass. Cyanogen bands are the probable cause. H 4101, on the other hand, is a bit stronger in the extreme population II giants, indicating sideband blanketing. Fairly strong iron lines in the λ4270 sideband are the strongest sideband features in the solar spectrum.

Some evidence of luminosity separation is evident for H 3798 and H 4101. The dispersion in blanketing in H 3835 completely overwhelms any evidence of luminosity effects.

Figure B8 clearly illustrates that H delta in clusters arises largely from the horizontal branch. The clusters are completely isolated in this figure, lying far below stars of the same V/R.

In blue horizontal-branch stars H delta may be even stronger than indicated by the H 4101 index because its width exceeds 20Å, the feature bandpass.

CN 3860 (Figure B5)

This index is primarily an indicator of the strength of the cyanogen band with bandhead at λ3883. However it suffers moderate blanketing from iron lines. It is extremely sensitive to abundances in giants, being much stronger ($\approx$0.3) in mildly deficient early giants than in extremely deficient early giants. The index is also sensitive to abundances in late subdwarfs. It exhibits a sensitivity to gravity, being stronger in giants than dwarfs. The behavior of the CN 3883 band is described in some detail by Keenan (1963).

CN 3880 (Figure B6)

This feature bandpass contains both the cyanogen bandhead at λ3883 and the blue wing of H_8 which is centered at λ3890. It is mildly blanketed by iron lines. For stars later than V/R $\simeq$ 0.8 this index behaves

similarly to the CN 3860 index. From $V/R \simeq 0.8$ to 1.2 it increases in strength with increasing temperature because of its dependence on H_8. It also exhibits a luminosity dependence in this region.

CaII 3933 (Figure B7)

This index is sensitive to the behavior of the K resonance line of CaII centered at λ3933. It exhibits a strong sensitivity to temperature from V/R = 1.0 to 0.6. A known luminosity sensitivity for spectral types later than K2 is not evident in Figure B7 because of the absence of late subdwarfs in the stellar sample. A strong abundance sensitivity for both giants and dwarfs is evident. More detailed descriptions of the behavior of the K-line are available by Barbier et al. (1941) and Aller (1960).

CN 4200 (Figure B9)

This index measures the blue cyanogen band with bandhead at λ4216. The feature is strongest in K giants. Its absence in extreme population II giants and in subdwarfs indicates a sensitivity to chemical composition. The behavior of this feature has been described in the literature by Griffin and Redman (1960), Aller (1963), Keenan (1963), and McClure and van den Bergh (1968).

CaI 4226 (Figure B10)

The neutral calcium line centered at λ4227 is detectable in the

present stellar sample only in late mild population II giants. Its sensitivity to abundance is readily apparent. The feature is stronger in late dwarfs than in giants due to pressure broadening, a fact not evident in Figure B10 because of the absence of late subdwarfs. Descriptions of this feature's behavior are provided by Aller (1960) and Fernie (1966).

CH 4305 (Figure B11)

This index is sensitive to the strength of the G-band, a blend of atomic lines and the CH band with bandhead at λ4314.

The feature shows a complex mixture of dependencies. It varies strongly with temperature between V/R = 1.1 and 0.3, reaching a maximum strength at V/R $\simeq$ 0.7 (K0). A weak luminosity separation, with the feature slightly stronger in giants than dwarfs, is evident. The feature shows only a moderate abundance sensitivity in giants but a substantial sensitivity in the subdwarfs.

Reference to Figure B11 makes it clear that the weakness of the G-band in clusters is largely a result of the fact that early spectral types contribute most of the blue flux.

Griffin and Redman (1960), Strömgren (1963), and Spinrad and Taylor (1969) provide additional information on the behavior of the G-band.

Is 4430 (Figure B12)

This index measures the strength of the diffuse interstellar line at

λ4430 of unknown origin. A correlation exists between this feature and interstellar reddening according to Stoeckly and Dressler (1964) and Wampler (1966). The index has a scatter of about 0.02 around unity (except in very red mildly deficient giants in which it is somewhat enhanced, probably by blanketing). The inferred upper limit on reddening, based on Wampler's line profile and the strength-color excess relation for stars in the galactic plane, is about $E_{B-V} \simeq 0.30$.

The highly reddened population II giant HDE 232078 has a feature index of 0.91. The indicated color excess is $E_{B-V} \simeq 1.4$. This value is too uncertain to justify use of HDE 232078 in the stellar population sequences.

MgH 4780 (Figure B13)

This index was chosen to detect MgH with bandhead at λ4845. According to Ohman (1934, 1936) and Merrill (1956) this feature becomes prominent in dwarfs later than K5, reaching a maximum strength near M0. In giants and late M dwarfs it is weaker and is overwhelmed by the TiO λ4762 bands. MgH is apparently undetected in the present sample because of the absence of late subdwarfs. Strengthening of the index in late mildly deficient giants is a result of TiO absorption.

The two M31 clusters well above unity in Figure B13 probably indicate observational errors.

TiO 4970 (Figure B14)

The behavior of the index, which measures the strength of the TiO bands with head at λ4954, is almost identical with the TiO dominated index, MgH 4780, except that the scatter about unity is smaller. The behavior of TiO bands has been described by Aller (1960).

MgI 5175 (Figure B15)

Except in late giants this index measures the strength of the "b" triplet of neutral magnesium. This feature appears initially at V/R $\simeq$ 1.0. Redward of this point the index strengthens much more rapidly in dwarfs than giants. Thus in the range V/R = 1.0 to 0.6 the feature is a sensitive indicator of luminosity. Redward of V/R $\simeq$ 0.6 MgH λ5211 and TiO λ5167 blanketing increases rapidly in the giants until at spectral type M0 (V/R $\simeq$ 0.4) the feature becomes stronger in giants than in dwarfs (according to O'Connell [1970]).

This feature is also a useful abundance discriminant. Mildly deficient giants have much stronger indices than extremely deficient giants. The mild and extreme subdwarfs also separate in this index, although not so much. Because of the relatively wide separation of the three lines of the "b" triplet ($\lambda\lambda$5183, 5173, 5167) it should be well-centered when observed with a narrow bandpass. Besides O'Connell, Fitch and Morgan (1951), Deeming (1960), Price (1966), Aller (1963), Spinrad and Taylor (1969), and Wood (1969) have described this feature.

NaI 5892 (Figure B16)

This index measures the D resonance lines of neutral sodium at $\lambda\lambda$5890 and 5896. The feature appears redward of V/R = 0.8, increasing in strength with decreasing temperature. A luminosity separation described elsewhere does not appear for the present sample because of the absence of late subdwarfs. They would, if present, show stronger NaD than giants.

The feature is moderately sensitive to abundance in giants.

In extremely hot stars (V/R $\simeq$ 1.35) the index is strengthened by He Iλ5876. This effect is barely apparent in Figure B16. In M Giants the NaIλ5892 bandpass is blanketed by TiOλ5861 and theλ5820 sideband is blanketed by TiOλ5814. The TiO blanketing does not dominate the D-lines as it does the "b" triplet however.

References for D-line behavior are O'Connell, Thackery (1949), Griffin (1961), and Spinrad (1962).

TiO 6180 and TiO 7100 (Figures B17 and B19)

These two TiO features behave similarly. TiO 6180 measures features with bandheads at$\lambda\lambda$6148 and 6158. TiO 7100 measures bands with heads at$\lambda\lambda$7054 and 7088. Those features appear only in objects redder than V/R = 0.6 (K2-3). Both features show only weak evidence of abundance sensitivity.

According to O'Connell (1970) TiO 7100 shows a luminosity separation, giants having a stronger feature than dwarfs at a given color. Again the absence of late subdwarfs prevents detection of such a separation in Figures B17 and B19.

Ohman (1936) and Spinrad and Taylor (1969) also have discussed the behavior of these features.

It should be noted that the λ7050 sideband contains the λ7054 bandhead. This does not destroy its usefulness as a sideband.

H 6564 (Figure B18)

H alpha (line center, λ6565) is the feature measured. The index is primarily an indicator of temperature. Peat (1964) detected a slight enhancement of H alpha strength in population II giants. The enhancement was much smaller than the dispersion in H alpha strengths and is not evident in Figure B18 because of the relatively small number of stars observed.

The feature shows slight evidence of being stronger in subdwarfs than in red-giants of the same temperature.

D) Observations of Globular Clusters of the Galaxy

The integrated light of globular clusters in the Galaxy was observed on 32 nights between November 3, 1969, and October 27, 1970, with a 4-inch Newtonian telescope with an f/3.3 focal ratio, matching

the f/3.3 collimator of the prime-focus scanner of the Palomar 200-inch telescope to which it was attached. The telescope and scanner were mounted on the side of the Palomar 18-inch Schmidt telescope. This equipment and the supporting pulse-counting data system were put together by Oke and Schild (1970) for their absolute calibration of Alpha Lyr and are described in some detail in their paper.

The small telescope aperture, the fast focal ratio of the telescope, and the fast exit focal ratio of the scanner (f/4.5) combined to reduce the spectral degradation of the system so that extended objects could be observed without great loss of spectral resolution. The scale at the scanner exit plane was 2.66Å per arc minute in the second order. An 8!1 scanner entrance aperture (0.79mm) was chosen. This aperture was large enough to admit most of the light from the clusters (the average $D_{0.9}$ diameter measured by Kron and Mayall [1960], that diameter which contains ninety per cent of the light, is 10!9 for the five clusters observed), while having been small enough to keep noise from background stars and sky to less than thirty per cent of the signal at most wavelengths and to keep spectral degradation effects small. Two other factors combined to minimize the effects of degradation:

(1) The strong central concentration of globular clusters reduces light contributed from aperture edges.

(2) The weakness of the globular cluster features insures the weakness of line wings with respect to cores.

Grating tilts were sufficiently accurate to yield bandpass positions with 1Å accuracy. This accuracy was preserved by applying appropriate corrections to bandpass wavelengths to compensate for the Doppler shift of each spectrum.

The procedural data for the 4-inch observations, as well as all other observations, are given in Table 5. The only comment necessary on the data there presented is that the red-leak corrections to the λ3448 count rates were typically about three per cent for the globular clusters and less than one per cent for the standards.

As mentioned before, a chopper was used to subtract sky and dark count rates from cluster and standard star count rates. Observations of each object were equally divided between the north and south apertures to compensate for a slight asymmetry in the system.

Because of the low surface brightnesses of the clusters, observations were confined to moonless nights. On a typical night the sky plus dark count rates ranged from about fifty per cent of the signal in the ultraviolet to twenty per cent in the yellow, except in the D-lines where fifty per cent was more typical, when the S-17 tube was used; and were about twenty to thirty per cent (mostly dark count) when the S-20 tube was used. On a few nights the sky background in the northwest became rather large (increases as large as a factor of two were noted in the red) because of contamination by scattered light from Los Angeles.

TABLE 5

OBSERVATIONAL PROCEDURAL DATA

Instrument	Chopper	Entrance Aperture ["]	λ [Å]	Δλ [Å]	Grating Order	Photo-cathode	Filter
Palomar 4-inch with 200-inch prime focus scanner	yes	486	3448	20	2	S-17	none, yellow*
			3570-4780	"	"	"	none
			4780-5892	30	1	"	"
			4780-7400	"	"	S-20	yellow
			8050	"	"	"	red
			8050-10800	"	"	S-1	"
Palomar 200-inch multi-channel spectrometer	yes	9.9	3400-5800	20	2	S-20	dichroic
			5800-8400	40	1	"	"
Mt. Wilson 60-inch Cassegrain scanner	no	23.0, 16.7, 11.7	3448-4270	20	2	S-20	liquid $CuSO_4$
			4270-4780	"	"	"	none
			4780-7400	30	1	"	yellow
			8050	"	"	"	amber
			8050-10800	"	"	S-1	"
Mt. Wilson 100-inch Cassegrain scanner	yes	20.0, 14.1, 10.0	3448-4270	20	2	S-20	liquid $CuSO_4$
			4270-4780	"	"	"	none
			4780-7400	30	1	"	yellow
			8050	"	"	"	amber
			8050-10800	"	"	S-1	"

* Count rate (adopted) = Count rate (no filter) - 1.08 × Count rate (yellow filter)

Because of this fact observational opportunities in the east were given preference over those in the west.

Because observed count rates seldom exceeded twenty per second and were as low a two per second in the ultraviolet, twenty to thirty hours of observing time was necessary with each object to obtain good accuracy. Perceptible systematic fluctuations in atmospheric extinction on most nights made it more practical to amass large numbers of scans of low accuracy than to attempt to obtain relatively few scans of high accuracy. The former approach minimized systematic errors in the individual scans. The large random errors in individual scans were reduced by averaging. (After gray corrections differences in individual scans were typically less than ten per cent. Thus it was possible to average magnitudes rather than fluxes.) The latter approach, on the other hand, would have minimized random errors in individual scans, but would have permitted the accumulation of large systematic errors which probably would not have been fully diluted in the averaging process. A further attempt to reduce errors from extinction variations was made by reversing the order of successive scans of an individual object on a single night.

The bright secondary standards of Oke (1964) were observed three or four times on most nights. Standard energy distributions were based on the recent calibration of Alpha Lyr by Oke and Schild (1970). Because of the small primary mirror, even observations of Alpha Lyr,

the brightest standard employed, required negligible coincidence corrections.

Except for a few occasions observations were restricted to times when the secant of the zenith angle was less than 1.5. Roughly speaking, this permitted about six hours of continuous observations on the low declination clusters M5 and M15 and about 8 hours on the high declination clusters M13 and M92.

The greatest problem in observing the globular clusters of the Galaxy was centering them in the 8!1 entrance aperture of the scanner. Because of their low surface brightnesses it was not possible to see their images on the thin quartz plate which covered the aperture when they approached its center. For this reason a 10-inch finding telescope, also mounted on the 18-inch Schmidt telescope, was used for guiding. Alignment of the two telescopes was achieved by centering on a star of fifth magnitude or brighter near the globular cluster being observed. Typically there was a star of sufficient brightness within a 2^{o} to 3^{o} radius of the cluster. Because of differential flexure between the two telescopes realignment was necessary about every two hours.

Using the techniques and procedures outlined above, two to four scans, each of one to two hours duration, could be obtained of a single cluster on a single night. Typically about 10^{3} counts at each wavelength were obtained in an individual scan. Intercomparison of scans shows that centering problems and variable extinction expanded the three per

cent errors expected statistically to about five per cent with occasional errors as large as ten per cent in individual scans. Averaging several scans together has reduced errors to about two per cent (three per cent in the ultraviolet) in the final energy distributions.

Data reduction procedures are described in Appendix A. The final energy distributions are given in magnitude form in Table B1. Energy distributions in flux form and spectral indices are given in section IV in comparison with model fluxes and indices.

E) Observations of M31 Globular Clusters

The M31 globular clusters and the nucleus of NGC 205 were observed with the 200-inch multi-channel spectrometer on three nights in August and November of 1970. This instrument has been described in detail by Oke (1969a). Data were collected in eighteen channels simultaneously, but since the spacing of these channels is fixed it was necessary to use nine separate grating tilts to observe fifteen of the seventeen features blueward of λ8050 (the features at λ3798 and λ3815 were omitted because of the low accuracies intrinsic to these bandpasses). Except for a few fortuitous cases program continuum bandpass wavelengths did not coincide with the wavelengths measured. Most continuum fluxes were therefore interpolated from fluxes at the non-program wavelengths observed.

The scale at the scanner exit plane, 2.5Å/" arc in the second order, was such that a cluster with an 8" diameter suffered about the same spectral degradation as an 8' cluster observed with the 4-inch telescope, a rather remarkable fact when it is realized that a cluster with an 8' diameter at 10 kpc, about the distance of the program clusters in the Galaxy, has about an 8" diameter at the distance of M31. Thus feature dilution in the second order by spectral degradation was about the same for clusters in the Galaxy and in M31, assuming of course that brightness profiles were similar. First order degradation was less for the M31 clusters because of the 40Å bandpasses employed. The price paid was loss of sensitivity to weak features.

Again grating tilts were sufficiently accurate to give accuracies of 1Å for the bandpass wavelengths. Doppler shift errors could not be completely compensated because the same correction had to be applied to all channels simultaneously (except that first order corrections were twice second order corrections). Residual errors of about 1Å were common after correction for Doppler shifts were applied.

The secant of the zenith angle was kept to less than 1.5 for all observations except those of MIV for which it exceeded 1.7.

Procedural data are given in Table 5. Integration times ranged from 45 to 150 seconds per grating setting. Each object was scanned twice. Apertures and the order in which the wavelengths were scanned were reversed for the second scan. The relatively short time required

to complete a scan (about 30 minutes) and the reversal of scanning order should have minimized the effect of systematic atmospheric extinction variations. When the pairs of scans were combined, photon statistical accuracies ranged from better than two per cent in the red to about ten per cent in the ultraviolet. Slight difficulty in centering the images in the 9".9 aperture, atmospheric extinction variations, and spectral degradation due to the extended images combined to reduce these accuracies somewhat. Final accuracies, estimated from the continuum smoothnesses are about two per cent in the red continuum, four or five per cent in most features, and eight per cent in the ultraviolet continuum. Continuum accuracies exceed photon statistical accuracies because continuum fluxes at program wavelengths were interpolated from several individual points.

The faint subdwarfs HD 19445 and BD+17^{c} 4708 were observed as secondary standards. Continuous energy distributions for these objects, based on Oke and Schild's (1970) calibration of Alpha Lyr, were provided by Oke (1970). These energy distributions were in satisfactory agreement with measurements made on the same objects with the 60-inch telescope as part of this program.

Final energy distributions for the M31 clusters and the nucleus of NGC 205 are given in Table B1 in magnitude form and in Tables 22 - 31 of section IV in flux form. Spectral indices are also given in section IV.

F) Observations of Stars

Stellar scans were accumulated during 29 fully or partially photometric nights with the Mt. Wilson Cassegrain scanner mounted on the 60-inch telescope and during four such nights with the same scanner mounted on the 100-inch telescope. All observations were made between February 4, 1970 and June 30, 1971. Because the same scanner was used and because of the similarity between the two telescopes and their data systems, observing techniques employed on the two instruments were similar. Thus the techniques are described together. (For a detailed description of the equipment used as well as standard observing and calibrating features, the reader is referred to Oke [1965], C. Anderson [1968] and K. Anderson [1968].)

Besides the difference in primary mirror size the chief difference between the two telescopes, affecting observing procedures, was in the data systems. The 100-inch data system accommodated the use of a chopper whereas the 60-inch system did not. The 100-inch system was operated in its chopping mode; asymmetries were cancelled in the same manner as has been described for the 4-inch and 200-inch observations. Sky and dark count corrections were made for 60-inch observations by interspersing sky with object plus sky measurements. The frequency with which sky measurements were made depended upon the brightness

of the star being observed. For the brightest program stars observed, sky plus dark count noise was less than one per cent of the signal. Noise was therefore unimportant and no attempt was made to moniter the sky. For the faintest program stars, sky plus dark count rates were comparable to the signal, especially in the ultraviolet. For these objects every stellar measurement was preceded or followed by a sky measurement. For most objects however, the noise was about 10 per cent of the signal. For these objects an entire scan of the object was followed by an entire scan of the sky. The greater convenience of the 100-inch system is obvious. However the 100-inch system yielded only the difference between signal plus noise and noise as output (a shortcoming not shared by the 4-inch and 200-inch data systems). Thus statistical accuracies were not so easily determinable as with the 60-inch system.

A second significant difference between the data systems was in the form of the output. A card punch at the 100-inch output recorded total signal counts, wavelength, integration time, sidereal time, and bandpass. The 60-inch output was more primitive. A paper tape printer indicated total counts. Sidereal times and integration times were recorded manually. Wavelengths and bandpasses were later added to the data from memory.

The scales at the scanner exit plane, e.g., 1.2Å/" arc in the second order with the scanner on the 60-inch telescope, generally caused

negligible spectral degradation problems as long as stellar images were kept relatively close to the aperture centers. Careful guiding was employed to insure that images were always within about 2" arc of the centers. On a few nights very bad seeing made guiding difficult and spread images to such an extent that feature dilution by spectral degradation was no longer negligible. On these nights a sufficient number of integrations were taken at each wavelength to permit the identification of bad data which were then rejected. Constant guiding was employed so that integrations could be terminated whenever images "blew up."

Procedural data for the stellar observations are again given in Table 5. The only comment necessary concerns the liquid copper sulfate filter used to remove first order red light from second order bandpasses between $\lambda\lambda$3448 and 4270. This filter was constructed by filling the region between two thin quartz plates with a nearly saturated solution of copper sulfate in distilled water. The filter edges were sealed with a silicone gel. Three problems affected the stability of the filter. (1) The filter was never successfully sealed. Despite numerous attempts to stop leaks it was necessary to add solution to the filter about every two months. (2) A detectable white film of unknown origin formed on the inside of the quartz plates after about a year. The filter was taken apart and the film removed but after several months it again appeared to be returning. (3) A nearly saturated solution was required to successfully remove first order red light. During one extremely

cold observing run a crystal began to grow in the filter. Fortunately it attached itself to the filter edge where it did no harm.

The transmission properties of the filter in the ultraviolet and blue were not noticeably affected by the aforementioned problems. However the red leak of the filter fluctuated significantly between successive observing runs, the range of fluctuations being almost an order of magnitude. Unfortunately the subtlety of the red-leak variation prevented its detection until about half the data were accumulated. Thereafter it was determined at the beginning of each run and appropriate corrections were made.

A few of the reddest objects which had been observed prior to the detection of the red-leak variation were reobserved in an attempt to determine the red leaks for early observations. However red leak determinations for given early runs made from separate stars varied by factors as large as two.

It is fortunate that despite its large fluctuations the red leak was so small that its effect on most of the energy distributions was minor. For example, on the last observing run, the copper sulfate filter transmitted only 0.02 per cent of λ6896 photons.

It is concluded that the effect of red-leak variations on final energy distributions was negligible for horizontal-branch stars, early subdwarfs, and early giants. For the reddest extreme population II giant observed, HD 165195, the uncertanties in ultraviolet flux are about 5

per cent at λ3448 and 2 per cent at $\lambda\lambda$3570 and 3620. For the reddest mildly deficient giants observed the uncertanties in flux could be as large as ten per cent at λ3448. For all stars the effects of red leak are negligible for all wavelengths except $\lambda\lambda$3448, 3570, and 3620.

Fortunately most of the ultraviolet flux in cluster models comes from horizontal-branch stars, subgiants, and early subdwarfs. Thus the uncertanties in the ultraviolet fluxes of the reddest stars had little effect on the cluster models.

Comments made in conjunction with the 4-inch observations concerning the accuracy of the bandpass centering, Doppler shift corrections to the program wavelengths, and selection and treatment of standards also apply here, with the qualification that preference was given to the faintest of Oke's (1964) secondary standards to avoid the necessity of large coincidence corrections.

Because various electronic components of the data systems varied from run to run coincidence corrections were determined separately for each run. Corrections were generally negligible for program stars and rarely exceeded 3 per cent for standards.

Observations were again restricted to zenith angles such that secant z was less than 1.5 except for a few of the objects of lowest declination. For these secant z ranged up to 2.0.

At least two scans were obtained for all program stars except HD 60778. Photon statistical accuracies of at least two per cent (except in

the ultraviolet regions of the reddest giants) were obtained for all stars and statistical accuracies of one per cent were obtained for most stars. Generally, because of the brightness criterion described in section II B, such accuracies could be reached in less than three hours of observing time. Stars observed on nights with suspected significant extinction variations were reobserved whenever possible. Apparently extinction variations were mostly gray and took place on a time scale of several hours. Scans of given stars taken on different nights varied in magnitude by as much as 0.2; however after the addition of gray corrections variations were typically about 2 per cent for all spectral regions except the ultraviolet where 5 per cent variations were more typical. Since such comparisons represented the nights of poorer photometric quality it is estimated that accuracies of the final energy distributions are about three per cent in the ultraviolet and better than two per cent elsewhere.

Energy distributions for the program stars are given in Appendix B. Spectral indices are not given for individual stars, but can be computed from the given energy distributions.

The stars HD 3546, HD 10700, and HD 37160 were observed both with the 60-inch telescope and the 4-inch telescope for purposes of comparison. Resultant energy distributions, after gray corrections, agreed within two per cent for HD 3546 and HD 37160 and within four

per cent for HD 10700, a subdwarf with a declination of -16° which was observed near secant $z = 1.6$ with both instruments.

III. SYNTHESES

A) Preparation of Stellar Sequences

The difficulties encountered in classifying population II stellar spectra are well known. Many of the program stars had no available spectral types. Others had been given spectral types by several authors, but these were in wide disagreement. Few of the program stars had abundance analyses. For these reasons it was realized early in the program that the stellar spectra could not be easily grouped in pre-labeled blocks for the purpose of averaging, as has been done in the syntheses of population I composite spectra.

The observed energy distributions provided a much simpler and more accurate means of classifying the spectra than data available in the literature.

After all the energy distributions had been plotted, the first step in classifying the spectra was to separate them into mildly and extremely metal-deficient sets. This was accomplished by reference to published abundance analyses, ultraviolet excesses, and the appearance of their energy distributions. Stars with logarithmic metal deficiencies greater than about $[-1.2]$ were considered to be extremely metal deficient. Those with lesser deficiencies were considered to be mildly deficient.

This point of separation corresponds to about 0.20 in ultraviolet excess for a G subdwarf according to the calibrations of $\delta(U-B)$ versus $[Fe/H]$ by Wallerstein and Carlson (1960) and Wallerstein (1962).

Horizontal-branch stars were not separated into two groups because of the relative insensitivity of their spectra to metal abundance. The use of a single horizontal-branch sequence probably caused no significant errors in final population models. In a recent study Newell (1970) found blue horizontal-branch stars of the metal-rich globular cluster M4 to be indistinguishable from the blue horizontal-branch stars of extremely metal-poor clusters to within the accuracy of his narrow-band filter photometry.

After the spectra were separated into two sets, each set was subdivided into giants and subdwarfs and these subsets were ordered according to the slopes of energy distributions, i.e., according to temperature. Thus mild and extreme population II sequences of giants and subdwarfs and a single sequence of horizontal-branch stars were formed.

A few stars fit into neither sequence. These were removed from the program. They are listed with appropriate comments in Table 6.

After the sequences had been formed, adjacent stars in each sequence were grouped into blocks for the purpose of averaging their energy distributions. This averaging was carried out in the same manner

TABLE 6

PROGRAM STARS NOT USED IN STELLAR SEQUENCES

Name	Comment
HD 6755*	Intermediate population II giant. Features too strong for E sequence, too weak for M sequence.
HD 73394*	Same as HD 6755.
HD 74462*	Intermediate population II subgiant? Did not fit well into either E or M sequence.
HD 126778*	May be mild population II subgiant. However was much redder than 47 Tuc subgiants.
HD 175305*	Same as HD 6755.
HDE 232078	Extreme population II giant. Very large but unknown reddening.
HD 196610	Variable? Energy distribution in spectral region $\lambda\lambda$4780-5300 very jagged, varied by more than $0^{m}.1$ from scan to scan.
HD 201626	CH star. Falls to right of cluster giant branches.
HD 205539*	Very blue subdwarf. Blue straggler?
HD 222107*	Same as 126778.

* These objects were tried in some models with negative results.

as the averaging of the separate scans of individual stars described in part C of Appendix A.

After preliminary attempts to synthesize the extremely metal-poor clusters M15 and M92, it was realized that the extremely metal-deficient sequence formed as described above was not sufficiently metal-poor to represent these two objects. For this reason a third sequence of subdwarfs and subgiants was formed using only the most metal-deficient members of the previously described extremely metal-deficient sequence. For obvious reasons introduction of a simple means of designating these three sequences becomes convenient at this point. Hereafter in this thesis the mildly deficient sequence will be designated the M sequence; the extremely metal deficient sequence introduced first, the E sequence; and the lastly introduced extremely deficient sequence composed of the most metal deficient subdwarfs and subgiants of the E sequence, the EE sequence or "extra-extreme" sequence.

The average stellar types, or blocks, formed by the averaging of individual stellar spectra could not meaningfully be given the labels of conventional spectral types for the reasons noted at the beginning of this section. Thus they are simply assigned a three parameter label. The first parameter, HB, SD, GI,or SG, designates whether the block represents a horizontal-branch star, a subdwarf, a giant, or a subgiant. The second parameter, M, E, or EE, designates a sequence as defined in the last paragraph. The third parameter is an integer which orders

blocks according to redness. Thus G M 1 designates that average stellar type corresponding to the bluest mildly deficient giants; SD EE 4 is the fourth bluest EE subdwarf block. The second parameter is omitted from the label of horizontal-branch blocks since only one horizontal-branch sequence is used.

The energy distributions and spectral indices for the mean stellar types are given in Tables B4 and B5 in Appendix B. Spectral indices are also plotted in Figures B1 - B19 of Appendix B.

In Figures 2, 3, and 4 the approximate positions of the average stellar types in conventional color-magnitude diagrams are indicated. B - V colors are the average of published B - V colors for the members of each block when available. Otherwise they are obtained from Figure 1 by entering B/V as taken from Table B5. V magnitudes have been obtained by entering the B - V colors in published color-magnitude diagrams for clusters of appropriate metal abundances. (Mean stellar type HB 5 has been placed 0.90 magnitudes above the cluster horizontal branches for reasons made clear later in this section.) The EE sequence V's were obtained from Sandage's (1968) diagram for M92. E sequence V's are from Arp's (1962) normal color-magnitude array for M5. The M sequence has been calibrated by reference to Tifft's (1963) mean diagram for 47 Tuc. Table 7 gives the reddening and distance modulus assumed for each of these three clusters in making the B - V

Figures 2, 3, and 4: The positions of mean stellar types in color-magnitude diagrams calibrated to M92, M5, and 47 Tuc normal relations. The positions of a few of the mean stellar types have been slightly misrepresented to prevent overlapping.

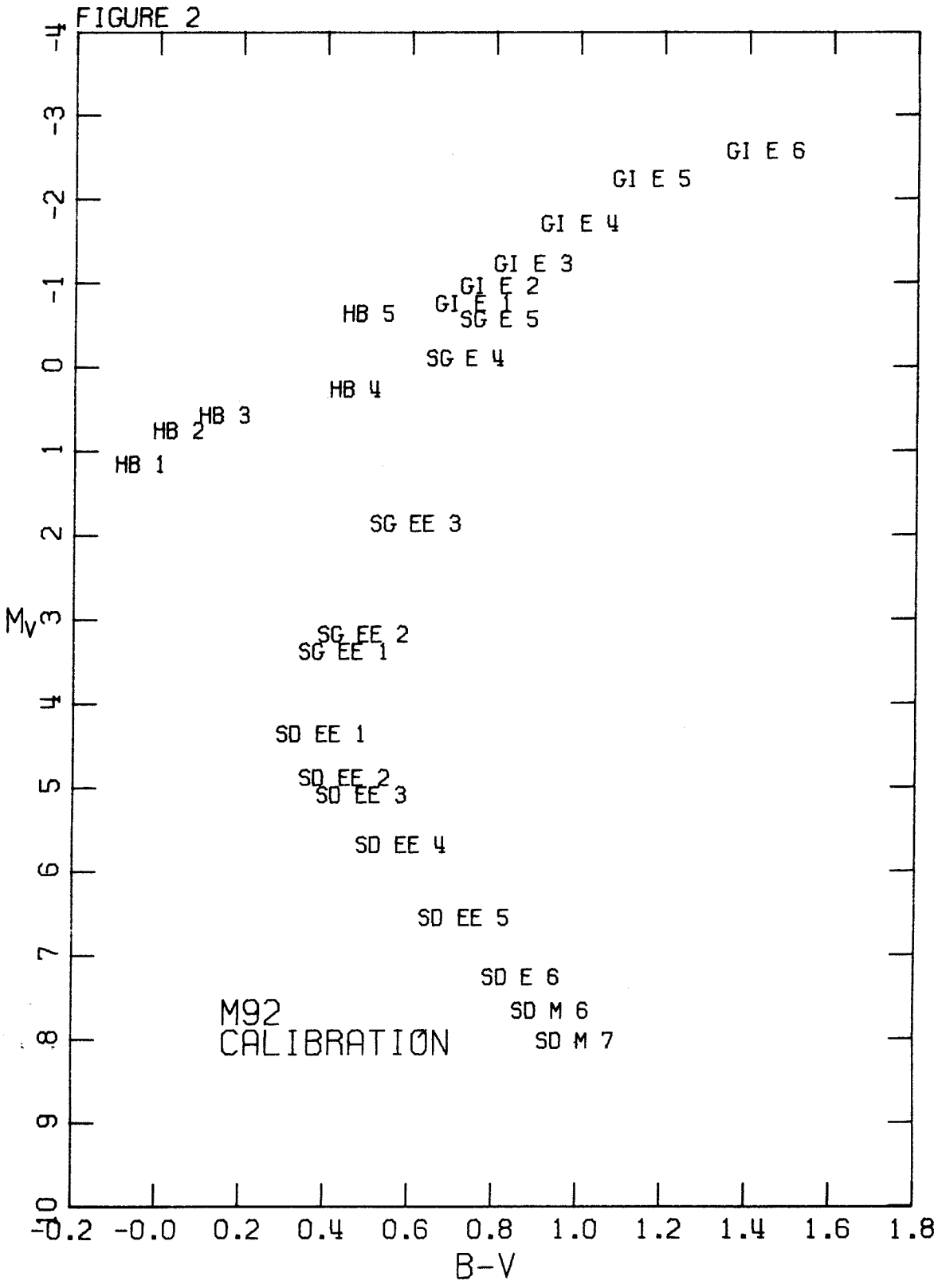
FIGURE 2
GI E 6
GI E 5
GI E 4
GI E 3
GI E 2
GI E 1
HB 5
SG E 5
SG E 4
HB 4
HB 3
HB 2
HB 1
SG EE 3
SG EE 2
SG EE 1
SD EE 1
SD EE 2
SD EE 3
SD EE 4
SD EE 5
SD E 6
SD M 6
SD M 7
M92
CALIBRATION
M_V
B-V
-4
-3
-2
-1
0
1
2
3
4
5
6
7
8
9
10
-0.2
-0.0
0.2
0.4
0.6
0.8
1.0
1.2
1.4
1.6
1.8

FIGURE 3

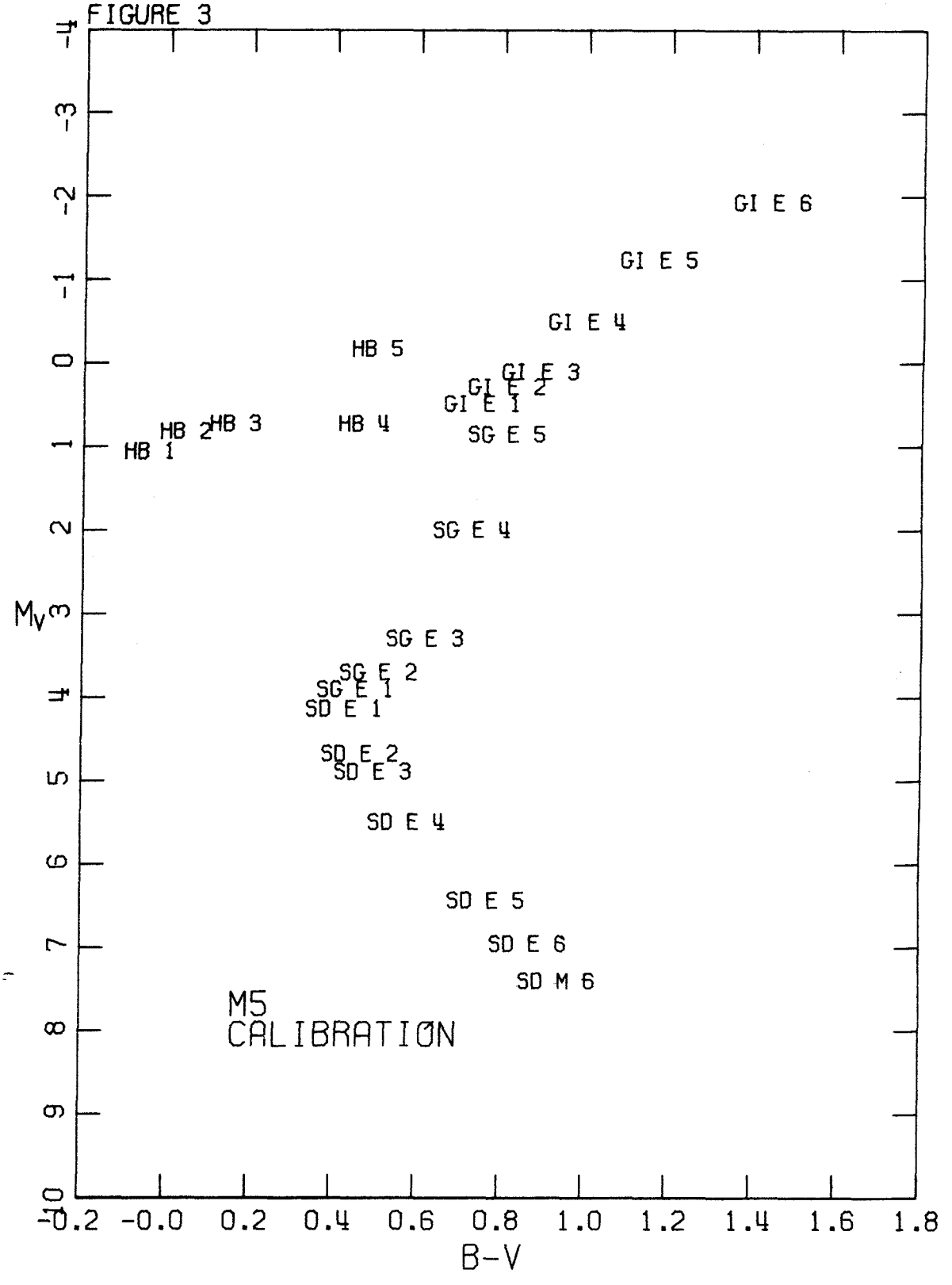
GI E 6
GI E 5
GI E 4
HB 5
GI E 3
GI E 2
GI E 1
HB 2
HB 3
HB 4
SG E 5
HB 1
SG E 4
SG E 3
SG E 2
SG E 1
SD E 1
SD E 2
SD E 3
SD E 4
SD E 5
SD E 6
SD M 6
M5
CALIBRATION
M_V
B-V
-4
-3
-2
-1
0
1
2
3
4
5
6
7
8
9
10
-0.2
-0.0
0.2
0.4
0.6
0.8
1.0
1.2
1.4
1.6
1.8

FIGURE 4

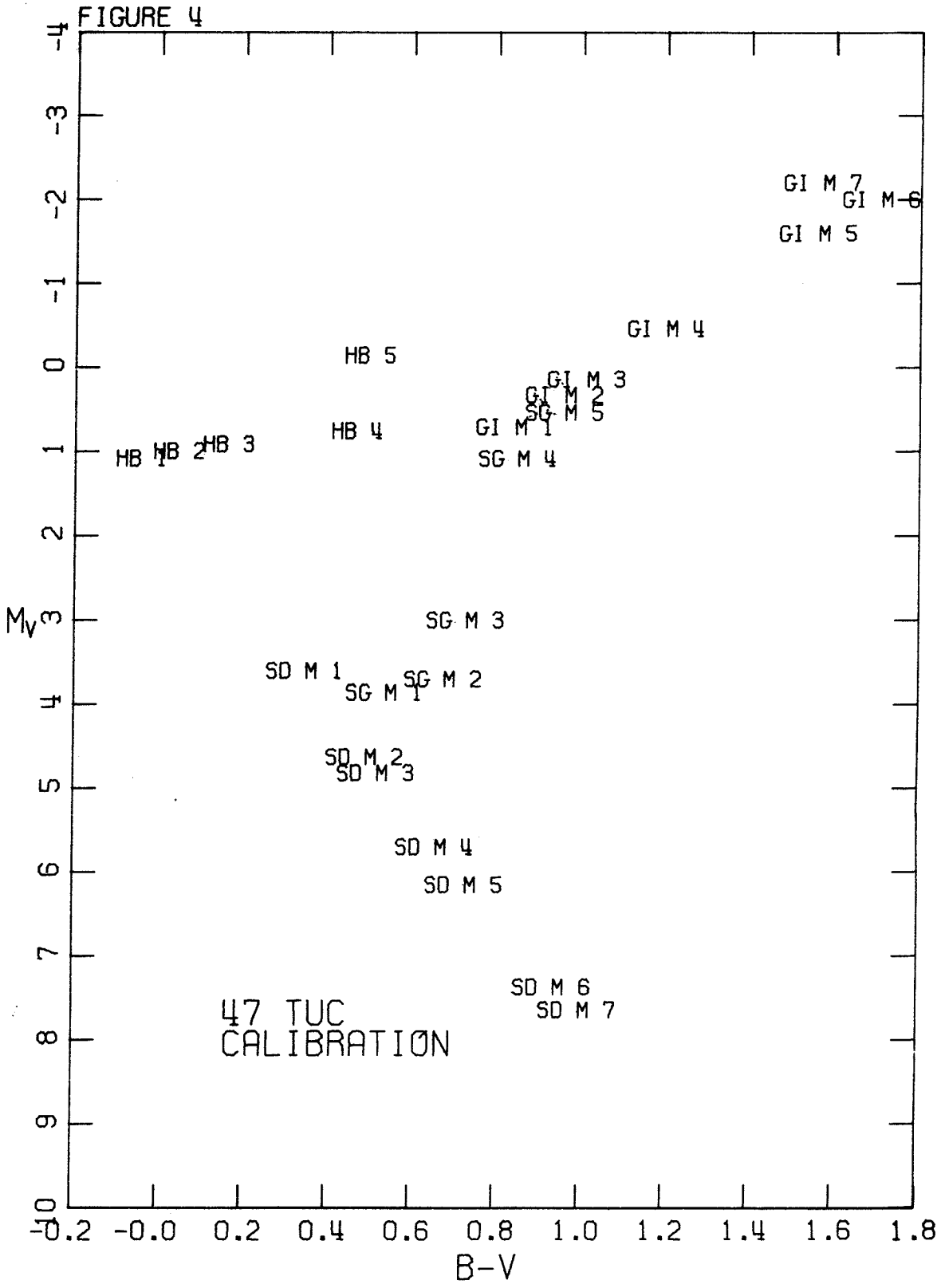
GI M 7
GI M 6
GI M 5
GI M 4
HB 5
GI M 3
GI M 2
SG M 5
HB 4
GI M 1
HB 1
HB 2
HB 3
SG M 4
SG M 3
SD M 1
SG M 1
SG M 2
SD M 2
SD M 3
SD M 4
SD M 5
SD M 6
SD M 7
47 TUC
CALIBRATION
M_V
B-V
-4
-3
-2
-1
0
1
2
3
4
5
6
7
8
9
10
-0.2
-0.0
0.2
0.4
0.6
0.8
1.0
1.2
1.4
1.6
1.8

versus V calibrations. Sources of information are also indicated. The numerical data for Figures 2 - 4 are included in Table 9.

Because of the scarcity of population II objects in the vicinity of the sun, the population II stellar sequences formed as described above lacked several kinds of stars essential to satisfactory population models. In particular subgiants and late subdwarfs of all abundances and extremely metal-deficient late red-giants were missing from the sequences.

To augment my data, Oke (1971) kindly provided energy distributions for red-giants near the M92 giant branch tip, obtained with the 200-inch multi-channel spectrometer. Unfortunately these scans had been obtained with 80Å and 160Å bandpasses, and therefore were insensitive to the weak spectral features present. It was, however, possible to approximate spectral feature strengths or otherwise compensate for their absence. The bluest of Oke's stars were averaged with the reddest of my observed population II giants, except that my observed feature strengths were adopted. For Oke's reddest stars spectral feature strengths were approximated by assuming that the ratios of the feature blocking fractions in these stars to the known blocking fractions in the cooler red-giants vary with V/R in the same way as these ratios vary with V/R in population I or in mildly deficient sequences. The population I and mild population II relationships were then taken from O'Connell (1970) and from the mild population II relationships

TABLE 7

PARAMETERS ASSUMED IN SEQUENCE CALIBRATIONS

Sequence	Normal Color-Magnitude Relation	E_{B-V}	m - M
M	47 Tuc (1)	0.02 (1)	13.35 (1)
E	M5 (2)	0.02 (2,3)	14.39 (2)
EE	M92 (4)	0.02 (3,5)	14.62 (6)

References: 1. Tifft (1963), 2. Arp (1962), 3. McNamara and Langford (1969), 4. Sandage (1968), 5. Sandage (1969), 6. Sandage and Walker (1966).

TABLE 8

DATA SUMMARY FOR ARTIFICAL SUBGIANT DERIVATIONS

Name	Derived From	$T_{eff}[^oK]$	V/R	$\triangle$m	$\triangle$(log g)
SG M 1	SD M 3	5700	0.86	-0.50	-0.20
SG M 2	SD M 4	5400	0.84	-0.90	-0.36
SG M 3	SD M 5	5100	0.78	-2.20	-0.88
SG M 4	GI M 1	4900	0.72	1.48	0.59
SG M 5	GI M 3	4500	0.69	0.92	0.37
SG E 1	SD E 2	5700	0.85	-0.55	-0.22
SG E 2	SD E 3	5400	0.83	-0.91	-0.36
SG E 3	SD E 4	5100	0.81	-2.01	-0.80
SG E 4	GI E 1	4900	0.72	1.48	0.59
SG E 5	GI E 2	4500	0.69	0.92	0.37
SG EE 1	SD EE 2	5700	0.84	-0.55	-0.22
SG EE 2	SD EE 3	5400	0.80	-0.86	-0.34
SG EE 3	SD EE 4	5100	0.79	-2.18	-0.87

TABLE 9

MEAN STELLAR PARAMETERS ASSUMED FOR SYNTHESES

Name	Members		V/R	B/V	B - V adopted	M_V calibrated by M92, M5, 47 Tuc	$M/M_\odot$ calibrated by M92, M5, 47 Tuc
	Name	B - V					
HB 1	HD 85504	-0.04	1.396	1.280	-0.04	1.15, 1.05, 1.04	0.70, 0.70, 0.70
HB 2	HD 60778	0.10	1.233	1.171	0.05	0.75, 0.81, 1.01	0.70, 0.70, 0.70
	HD 74721	0.03					
	HD 109995	0.04					
	HD 117880	0.04					
HB 3	HD 86986	0.14	1.098	1.079	0.16	0.57, 0.72, 0.91	0.70, 0.70, 0.70
	HD 161817	0.18					
HB 4	HD 106223	0.30	0.851	0.740	0.47	0.26, 0.72, 0.75	0.70, 0.70, 0.70
	-15° 4515	0.61[a]					
HB 5	HD 46703	0.50	0.876	0.715	0.50	-0.64, -0.18, -0.15	0.70[b], 0.70[b], 0.70[b]
GI E 1	HD 2665	0.93[c, d]	0.720	0.542	0.75	-0.74, 0.28	0.70, 0.70
	M92 II-12	0.75[c]					
GI E 2	HD 44007	0.85	0.691	0.492	0.81	-0.97, 0.28	0.70, 0.70
	M92 VI-18	0.77[c]					
GI E 3	HD 88609	0.90[a]	0.635	0.456	0.89	-1.23, 0.19	0.70, 0.70

TABLE 9 (continued)

Name	Members		V/R	B/V	B - V adopted	M_V calibrated by M92, M5, 47 Tuc	$M/M_\odot$ calibrated by M92, M5, 47 Tuc
	Name	B - V					
GI E 3 (cont.)	HD 122563	0.91					
	M92 VI-2	0.88[c]					
GI E 4	HD 165195	0.93[c,e]	0.604	0.387	1.00	-1.71, -0.50	0.70, 0.70
	HD 221170	1.02[c]					
	M92 XII-8	1.04[c]					
GI E 5	M92 X-49	1.17[c]	0.557	0.311	1.17	-2.24, -1.24	0.70, 0.70
GI E 6	M92 III-13	1.44[c]	0.516	0.270	1.44	-2.57, -1.93	0.70, 0.70
GI M 1	HD 3546	0.87	0.717	0.442	0.88	0.63	0.70
	HD 79452	0.86					
	HD 219615	0.92					
GI M 2	HD 9774	0.96	0.718	0.397	0.96	0.35	0.70
	HD 135722	0.95					
	HD 215373	0.97					
GI M 3	HD 37160	0.95	0.692	0.380	0.99	0.28	0.70
	HD 43039	1.02					
	HD 130952	0.99					
	HD 182762	0.99					
GI M 4	HD 6833	1.18	0.594	0.299	1.20	-0.47	0.70

TABLE 9 (continued)

Name	Members		V/R	B/V	B - V adopted	M_V calibrated by M92, M5, 47 Tuc	$M/M_\odot$ calibrated by M92, M5, 47 Tuc
	Name	B - V					
GI M 4 (cont.)	HD 107328 HD 151937	1.16 1.25					
GI M 5	HD 90362 HD 142574	1.52 1.59	0.438	0.175	1.56	-1.6	0.70
GI M 6	HD 148349	1.72	0.323	0.145	1.72	-2.0	0.70
GI M 7	HD 123598 HD 186776	1.62 1.58[a]	0.267	0.186	1.60	-2.2	0.70
SG EE 1	SD EE 2[f]		0.841	0.747	0.47[g]	3.34, 3.85	0.70, 0.70
SG EE 2	SD EE 3[f]		0.807	0.719	0.50[g]	3.21, 3.75	0.70, 0.70
SG EE 3	SD EE 4[f]		0.794	0.615	0.63[g]	1.86, 3.23	0.70, 0.70
SG E 1	SD E 2[f]		0.853	0.751	0.46[g]	3.88	0.70
SG E 2	SD E 3[f]		0.830	0.711	0.50[g]	3.75	0.70
SG E 3	SD E 4[f]		0.816	0.620	0.62[g]	3.29	0.70
SG E 4	GI E 1[f]		0.722	0.551	0.73[g]	-0.11, 1.99	0.70, 0.70

TABLE 9 (continued)

Name	Members		V/R	B/V	B - V adopted	M_V calibrated by M92, M5, 47 Tuc	$M/M_\odot$ calibrated by M92, M5, 47 Tuc
	Name	B - V					
SG E 5	GI E 2[f]		0.694	0.500	0.81[g]	-0.69, 0.85	0.70, 0.70
SG M 1	SG M 3[f]		0.863	0.684	0.54[g]	3.86	0.70
SG M 2	SD M 4[f]		0.846	0.634	0.66[h]	3.81	0.70
SG M 3	SD M 5[f]		0.781	0.493	0.73[h]	3.00	0.70
SG M 4	GI M 1[f]		0.718	0.449	0.85[g]	1.08	0.70
SG M 5	GI M 3[f]		0.695	0.386	0.96[g]	0.53	0.70
SD EE 1	HD 84937	0.41	0.873	0.807	0.41	4.36, 4.13	0.70, 0.70
SD EE 2	HD 19445	0.47	0.838	0.744	0.47	4.92, 4.69	0.63, 0.63
SD EE 3	HD 140283	0.48	0.804	0.717	0.50[g]	5.05, 4.83	0.62, 0.62
SD EE 4	HD 64090 HD 188510	0.60 0.59	0.789	0.619	0.60	5.68, 5.60	0.55, 0.54
SD EE 5	HD 103095	0.75	0.712	0.530	0.75	6.55, 6.38	0.48, 0.48
SD E 1	HD 84937 +17° 4708	0.41 0.44	0.862	0.786	0.43	4.13	0.70

TABLE 9 (continued)

Name	Members		V/R	B/V	B - V adopted	M_V calibrated by M92, M5, 47 Tuc	$M/M_\odot$ calibrated by M92, M5, 47 Tuc
	Name	B - V					
SD E 2	HD 19445 HD 94028	0.47 0.48	0.849	0.748	0.47	4.69	0.63
SD E 3	HD 140283 HD 219617	0.48 0.47	0.827	0.709	0.49[g]	4.83	0.62
SD E 4	HD 64090 HD 188510 HD 193901	0.60 0.59 0.55	0.811	0.624	0.58	5.49	0.55
SD E 5	HD 103095 HD 134439	0.75 0.78	0.735	0.508	0.77	6.43	0.47
SD E 6	HD 25329 HD 134440	0.87 0.86	0.707	0.447	0.87	7.26, 6.95	0.42, 0.43
SD M 1	HD 128167	0.35	0.973	0.869	0.35	3.60	0.70
SD M 2	HD 60552	0.50[a]	0.936	0.716	0.50	4.68	0.70
SD M 3	HD 165908	0.52	0.860	0.681	0.52	4.82	0.68
SD M 4	HD 157089	0.66	0.843	0.632	0.66	5.70	0.58
SD M 5	HD 10700	0.73	0.776	0.496	0.73	6.15	0.54

TABLE 9 (continued)

Name	Members		V/R	B/V	B - V adopted	M_V calibrated by M92, M5, 47 Tuc	$M/M_\odot$ calibrated by M92, M5, 47 Tuc
	Name	B - V					
SD M 5 (cont.)	HD 144579	0.73					
SD M 6	HD 81192	0.94[a]	0.705	0.398	0.94	7.66, 7.40, 7.37	0.40, 0.40, 0.44
SD M 7	HD 185657	1.00[a]	0.695	0.373	1.00	8.02, 7.64	0.38, 0.38

a No published B-V color was found. The value given is based on the observed energy distribution.
b The mass of HD 46703 is probably less than 0.70 $M_\odot$
c The value given is unreddened according to the color excess given in Table A1.
d HD 2665 probably has a true color nearer 0.73 than 0.93.
e HD 165195 appears to have a true color nearer 1.01 than 0.93.
f The mean stellar type from which the artificial subgiant spectrum was derived is given.
g The adopted value of B-V has been determined by entering B/V in Figure 1.
h The adopted value of B-V is based upon the mean stellar type from which the subgiant spectrum was derived.

determined in this thesis. Additionally the color dependence of H alpha for extreme population II giants was taken from Peat (1964). Although the feature strengths derived in this manner cannot be considered highly reliable, they should be sufficiently reliable to have had little effect on the cluster population models for at least two reasons: (1) Most spectral features are very weak in these giants. Only CaII K and the G-band have spectral indices less than 0.90. (2) CaII K, the G-band, and most of the other strongest spectral features of these stars occur in the ultraviolet or blue where their light contributions are only a few per cent of total cluster light.

It should be noted that Oke's magnitudes for the M92 giants in the spectral range $\lambda\lambda$5720-5880 were apparently almost $0^{m}.10$ too faint because of an obvious malfunction of channel 18 of the multichannel spectrometer. These magnitudes were corrected by interpolating between channels 17 and 19.

Artificial subgiant energy distributions for all three abundance sequences have been formed by adding differential corrections to observed giant and subdwarf energy distributions. Corrections have been interpolated from the grid of model atmospheres of Carbon and Gingerlich (1969). Temperatures have been approximated by comparing model and observed energy distribution slopes. Δlog g's have been derived using the assumption that vertical increments in the normal color-magnitude relationships for M5, M92, and 47 Tuc referred to earlier in

this section are due only to differences in gravity. Absolute values of log g chosen have little effect on the differential corrections derived. Log g = 4.5 and 2.0 have been assumed for the subdwarf and giant branches. Table 8 describes the derived subgiant blocks, the observed blocks from which they were derived, and the parameters assumed in the interpolation of differential corrections.

No attempt has been made to correct the subgiant feature strengths for luminosity effects. Since subgiant spectra were derived from both giants and subdwarfs, the net effect on model spectra should be slight.

Mean subgiant energy distributions and spectral indices are given in Tables B3 and B4 of Appendix B. Their spectral features are not plotted in Figures B1 - B19 however, as they tend to overlap the giant and subdwarf points from which they were derived, thereby obscuring the depicted relationships.

No suitable method was found for constructing energy distributions for late subdwarfs. Extrapolation of the synthesized luminosity functions indicates that although late subdwarfs contribute heavily to the mass of clusters they make nearly insignificant contributions to cluster luminosities in the visual region. It is concluded that even had late subdwarf energy distributions been available, their light, mass, and number contributions to the clusters would have been indeterminable.

It should be noted that SD M 7, SD M 6, and SD E 5 mean stellar types have been included with the SD E and SD EE sequences for

syntheses of some clusters. These mean stellar types are redder than any of the mean stellar types in the sequences to which they have been attached. The justification for mixing sequences lies in the insensitivity of strong features to abundances in late subdwarfs (Wilson 1962, Greenstein 1969). The largest errors resulting from the mixtures are probably from the blanketing effects of weak features on the continua.

Other than the aforementioned voids in the sequences which have been filled as explained, the biggest problem with the mean stellar sequences is probably the rather wide range of abundances in the mean stellar types. The GI E 1 and GI E 2 mean types which are used in both E and EE sequences have feature strengths based on those in HD 2665 and HD 44007 respectively. HD 2665 has a logarithmic iron deficiency of [-1.68] (Koelbloed 1967); HD 44007, for which no published abundance analysis is available, has slightly stronger features than HD 2665. Both of these objects have relatively strong G-bands. These giants certainly have features too strong for models of such metal-poor clusters as M15 and M92.

Similar problems are the uses of HD 103095 in SD EE 5, HD 103095 and HD 134439 in SD E 5, and HD 134440 in SD E 6. HD 103095 (= Groombridge 1830) has a logarithmic iron deficienty of [-1.50] (Cayrel and Cayrel de Strobel 1966). Line strengths indicate similar abundances in HD 134439 and HD 134440.

Mean stellar type HB 5 is the star HD 46703. HD 46703 is a rather peculiar star with a huge Balmer jump, indicating it probably lies considerably above cluster horizontal branches (Bond 1970a). It may be that HD 46703 is a star of the same type as those that lie well above the horizontal branches in most clusters. Recent observations by Strom et al. (1970) indicate that such stars are cluster members.

This star was included in the models only after it was found that model Balmer jumps were too small otherwise. The necessity of including a significant amount of light from HB 5 stars in the models may indicate that the sample field horizontal-branch stars have generally larger surface gravities than horizontal-branch stars in clusters. It may also result from an absence of asymptotic branch giants among sample field stars. If HD 46703 is one of the type of stars studied by Strom et al. it would lie close to the asymptotic branch, and therefore inclusion of such stars in the models could compensate for the luminosity difference between the asymptotic and red-giant branches.

In attempting to synthesize the spectra of the strong-lined M31 clusters, it was found that the three sequences described were all inadequate. O'Connell's (1970) population I sequences have been used in the syntheses for these clusters.

After preparation of the stellar sequences the spectral indices described in section II C and tabulated in Table B4 of Appendix B were calculated. The formation of these indices was described briefly in

section II C and in greater detail by O'Connell (1970). A feature index should approximate the quantity

$$I \simeq 1 - W/\Delta\lambda \qquad (1)$$

where W is the equivalent width of absorption in the feature bandpass $\Delta\lambda$. (W is not necessarily the total feature equivalent width since some features, particularly the molecular bands, are wider than the bandpasses used to observe them.) The above equality does not hold exactly because of differential blanketing in the feature bandpasses and sidebands. Thus the complete absence of a feature does not necessarily imply an index value of unity.

The spectral indices facilitated an easy comparison between cluster and model spectra, thereby simplifying preparation of model revisions.

In order to obtain the relative contributions of cluster components to cluster masses and the numbers of stars in the clusters it was necessary to determine absolute magnitudes and masses for the average stellar types. Absolute magnitudes, as already mentioned, were obtained for the three population II sequences from the normal color-magnitude relationships for M92, M5, and 47 Tuc. Absolute magnitudes for the population I sequence of O'Connell (1970) were taken from O'Connell.

The choice of appropriate masses for the mean stellar types was more difficult. Population II masses are not well known. Particularly controversial are horizontal-branch stars masses. It remains an open question whether or not red-giants suffer significant mass losses before migrating to the horizontal-branch region. Current estimates for the masses of stars at the main sequence turnoff point of globular clusters are about 0.70 $M_\odot$. (See Faulkner, et al. [1966] ; Hartwick [1970] .) This value has been assumed for the three population II sequences. Horizontal branch mass estimates have been based on both observational and theoretical considerations. The range of inferred values is at least from 0.3 $M_\odot$ (Graham and Doremus 1968) to 0.7 $M_\odot$ (Sargent's [1968] value for blue horizontal-branch stars in M67; also the value inferred by Stobie [1971] for metal-weak Osterhoff II cluster variables). Estimates within this range are also required by Christy (1966 a,b) for satisfactory RR Lyrae models. Kodaina, Greenstein, and Oke (1969) obtained masses of 0.34 $M_\odot$, 0.35 $M_\odot$, and 0.59 $M_\odot$ for the field horizontal-branch stars HD 86986, HD 109995, and HD 161817. Adoption of the value $M_{HB} = 0.70\ M_\odot$ in this thesis is prompted by convenience. Total cluster masses are almost independent of the masses of horizontal-branch stars because of domination by subdwarfs so the adopted value is not important.

Main sequence masses have been based on the homology relation

$$M \propto L^{1/5} \tag{2}$$

which has been shown by Dennis (1965) and Faulkner (1967) to apply to population II stars with masses near 0.7 $M_{\odot}$. Bolometric luminosities entered in equation (2) were obtained by adding to the absolute magnitudes of Table 9 bolometric corrections obtained by entering V/R's into a V/R - bolometric correction relation calibrated with data in O'Connell (1970) and Harris (1963). Since V/R is little affected by blanketing and since masses derived from relation (2) are insensitive to luminosity, any errors resulting from use of a population I calibrated, bolometric correction-color relation should be slight. Adopted masses are included in Table 9.

B) Construction of Models

It has been assumed that with the proper choice of mean stellar types the light of a cluster is described by a set of equations

$$l_j = R_j (E_{B-V}) \sum_{i=1}^{n} P_i I_{ij} \tag{3}$$

where l_j is the normalized flux of a cluster at the jth wavelength; I_{ij} is the unreddened normalized flux of the ith stellar type at the jth wavelength; P_i is the fractional contribution of the ith stellar type to the

cluster light at $\lambda 5050$, the wavelength arbitrarily chosen for normalization of fluxes; n is the number of stellar types; and $R_j(E_{B-V})$ is the non-logarithmic Whitford (1958) reddening at the jth wavelength, normalized to $\lambda 5050$, for the assumed color excess, E_{B-V}, of the cluster under consideration. (A detailed derivation of equation (3), except for the reddening factor, is provided by Spinrad and Taylor [1971].) Thus the problem of synthesis boils down to properly selecting the P_i's.

Despite Wood's (1963) claim that a straightforward least-squares solution of equations (3) for the P_i's would not work because of color and feature interdependences, such an approach was tried. Resultant models were unphysical.

After rejection of a direct least-squares solution for the P_i's, a semi-trial-and-error approach was adopted. The first step in applying the adopted method was to "guess" a population model vector $\vec{P}$. $\vec{P}$ was then used to calculate a model energy distribution $\vec{L}$. $\vec{L}$ and $\vec{l}$ were then compared by calculating the quantity

$$\Phi = \sum_j (l_j - L_j)^2 \qquad (4)$$

An algorithm by Marquardt (1963) was then used to minimize Φ by varying $\vec{P}$. This approach differed from a straightforward least-squares solution for $\vec{P}$ in three respects:

(1) There were apparently many minima in the Φ surface.

Marquardt's algorithm resulted in convergence to only the

nearest minimum. For most initial models $\vec{P}$ the corresponding final model did not represent a drastic revision. Changes in individual P_i's were typically from a few per cent to factors of about two.

(2) To prevent the possibility of unphysical negative P_i's, equation (3) was redefined

$$l_j = R_j(E_{B-V}) \sum_{i=1}^{n} |P_i| I_{ij} \qquad (3')$$

before Marquardt's algorithm was applied. Thus the dependence of $\vec{l}$ on $\vec{P}$ was linear only in a restricted sense.

(3) In some models E_{B-V} was treated as a free parameter.

Even with the aid of Marquardt's algorithm it was usually necessary to try several models before good agreement with observations could be obtained. (Good agreement could have been obtained much more easily if published cluster color-magnitude arrays and luminosity functions had been consulted. However, to preserve the fairness of the program as a test of the validity of synthesis techniques, such consultations were deferred until models giving satisfactory energy distributions were obtained.) After each initial model had been modified by application of Marquardt's algorithm a new initial model was concocted by applying changes which would correct for model deficiencies. References to feature behaviors described in section II C and plotted in Appendix B were helpful in varying models.

Guessed initial models and acceptable final models were subjected to two constraints. (1) The color-magnitude distributions were required to be smooth except along the horizontal branch where observed irregularities are common. (2) Mixtures of the stellar sequences of different metal content were restricted to adjacent sequences.

Application of the above approach led to models for the galactic globular clusters which agree with published color-magnitude arrays and luminosity functions. Comparison of the models with published data has led to the conclusion that fitting of continuum indices is somewhat more important than the fitting of line indices in deriving correct models. The preceding statement is made with the implicit assumption that continuum indices accurately represent average continua in their respective spectral regions. It is the general fitting of the continuum, not the fitting of individual continuum points, that is of greater importance than the fitting of individual feature strengths.

It should be emphasized that the indicated importance of fitting continuum indices is almost certainly a result of the high degree of accuracy with which the interstellar reddenings of the galactic globular clusters were known. It was found that variations in model color excesses of a few hundredths of a magnitude could be cancelled by small variations in model stellar contents with little effect on resultant model spectra. It is concluded that the relative importance of fitting continuum indices decreases with increasing uncertainty in color excesses.

It is further concluded that it is more accurate to use independently derived color excesses than to treat E_{B-V} as a free model parameter.

In summary, experience gained on clusters of the Galaxy led to the following fitting criteria for synthesizing M31 clusters. They are listed in order of importance.

(1) Models were required to satisfy astrophysical constraints (1) and (2) above. Independently derived E_{B-V}'s were used.

(2) Continua were fitted as accurately as possible.

(3) Line indices were fitted as accurately as possible.

IV. RESULTS

A) Comparisons of Cluster Spectra

Before discussing and comparing adopted cluster models it is enlightening to compare the observed cluster energy distributions. Figures 5-14, in which cluster and model spectra are plotted for comparison, serve to illustrate the discussion of this section.

Visual inspection of Figures 5-14 and perusal of object line indices enables one to subdivide the ten program systems into five groups with similar spectra. M15, M92, and MIV belong to the weakest-lined group. The K-line index, the most composition-sensitive program feature, is 0.82 for M15, 0.84 for M92, and 0.74 for MIV. (All spectral indices are easily compared by referring to Table B2 in Appendix B). Except for the K-line index these spectra are very similar. MIV is 0.03 bluer than M15 or M92 in its V/R index. H alpha and H delta indices are about 0.03 stronger in MIV than in the other two clusters. Van den Bergh (1969) has determined line indices of L = -1, 0, and 0 for M15, M92, and MIV.

The second group consists of M5 and M13. Although their K-line indices (0.74 for M5, 0.78 for M13) are comparable to that of MIV, other features are stronger.

Except for the troublesome indices, H 3798 and H 3835 (see section IV C), feature indices are about the same in these two objects. Van den Bergh line indices are L = 3 for M13 and L = 6 for M5.

The similar clusters H12 and H140 of M31 form the third group. K-line indices are 0.61 for H12 and 0.67 for H140. G-band indices are 0.84 and 0.92. (The relatively weak G-band in H140 is probably a bad datum since it is comparable to those in M15 and M92 while other spectral features are much stronger.) Van den Bergh line indices are L = 8 for both these objects. H140 is somewhat bluer than H12.

H55 (L = 11) and B282 (L = 15) form the fourth group. The K-line index of H55 (0.46) is slightly stronger than that of B282 (0.49). Most other spectral features are also slightly stronger in H55. Colors of the two clusters are similar.

The nucleus of NGC 205 is the sole member of its group. It has line strengths similar to those of H12 and H140. (The line index L = 3p may not be too meaningful. Van den Bergh (1969) states that he encountered difficulty in determining the line index because features were Doppler-broadened much more than in the clusters.) The color of the NGC 205 nucleus is comparable to that of M92, being much bluer than H12 or H140.

The position of the NGC 205 nucleus in Figure 1 indicates that the nucleus is considerably bluer than the integrated light of the galaxy. Entering the spectral index B/V = 0.603 in the curve of Figure 1 gives

B - V = 0.64 for the nucleus. The integrated color, according to de Vaucouleurs and de Vaucouleurs (1964), is 0.81. This value is plotted as the y-coordinate in the figure.

B) Cluster Models

Individual cluster models will be described and compared with observations and with published color-magnitude diagrams and luminosity functions in this section. For convenience similar clusters are discussed in sequence. Some general comments on the models and model fits, including comparisons of models, are deferred until section IV C.

Tables 10-31 and Figures 5-14 describe the adopted models and compare their spectra with observations. Fluxes in the tables are computed from the magnitudes in Appendix B with the simple relation

$$F_{\nu} = 10^{-0.4 \times m_{\nu}}. \qquad (5)$$

V-light contributions are based on V-fluxes interpolated from fluxes at $\lambda\lambda$5050, 5300, 5820, and 6100. The models lack late subdwarfs which contribute significantly to cluster masses and numbers of stars despite nearly negligible luminosity contributions. Thus the tabulated numbers of stars per model, model masses, and model mass-to-light ratios represent lower limits to these parameters in the clusters themselves.

M5

Tables 10-12 and Figure 5 describe the adopted model for M5. Table 12 is a normalized light contribution table. Such tables will not be included for the other clusters but can be computed from the energy distributions of Appendix B and the data of Tables 13-31.

The M5 model represents the best energy distribution fit achieved for any of the ten aggregate objects. For the thirty-two measured fluxes longward of the Balmer jump the mean difference between observations and the model is only 1.6 per cent. For the three wavelengths shortward of the Balmer jump the mean flux difference is 4.4 per cent.

The model energy distribution deviates from the observations in a systematic manner only in the vicinity of the Balmer jump. The faintness of the model redward of the discontinuity is a probable result of line blanketing. The fitting problem reflects slightly greater metal abundances in the model sequence than in M5 itself. According to Wildey et al. (1962) the average fractional blocking coefficient, excluding Balmer features, between $\lambda\lambda$3650 and 4000 is 0.08 in the subdwarf HD 19445 and 0.26 in the F8 V star 50 And. Thus the few per cent discrepancy in the fitting of the model in this region is not surprising.

The small excess of flux shortward of the Balmer jump may be a result of observational errors. It can be corrected by the addition of

TABLE 10

NGC 5904 M5

COMPARISON OF OBSERVED AND SYNTHESIZED SPECTRA

FLUXES

LAMBDA	OBSERVED	SYNTHESIZED	PCT. DIFF.
3448.	2.176E-01	2.313E-01	6.102
3570.	2.370E-01	2.496E-01	5.156
3620.	2.625E-01	2.681E-01	2.081
3784.	3.977E-01	3.780E-01	-5.088
3796.	3.678E-01	3.501E-01	-4.931
3815.	4.033E-01	3.940E-01	-2.329
3835.	3.342E-01	3.277E-01	-1.965
3860.	4.414E-01	4.376E-01	-0.868
3880.	3.934E-01	3.869E-01	-1.648
3910.	4.677E-01	4.523E-01	-3.352
3933.	3.571E-01	3.674E-01	2.849
4015.	5.516E-01	5.593E-01	1.386
4101.	5.026E-01	4.987E-01	-0.776
4200.	6.081E-01	6.183E-01	1.662
4226.	6.093E-01	6.206E-01	1.846
4270.	6.350E-01	6.397E-01	0.734
4305.	5.834E-01	5.772E-01	-1.084
4400.	7.060E-01	7.035E-01	-0.350
4430.	7.291E-01	7.236E-01	-0.754
4500.	7.929E-01	7.677E-01	-3.222
4780.	8.726E-01	8.852E-01	1.438
4970.	9.489E-01	9.673E-01	1.926
5050.	1.000E 00	9.941E-01	-0.597
5175.	9.845E-01	1.005E 00	2.081
5300.	1.093E 00	1.103E 00	0.883
5820.	1.307E 00	1.310E 00	0.222
5892.	1.294E 00	1.283E 00	-0.868
6100.	1.359E 00	1.394E 00	2.521
6180.	1.416E 00	1.410E 00	-0.424
6370.	1.482E 00	1.485E 00	0.189
6564.	1.443E 00	1.409E 00	-2.386
7050.	1.739E 00	1.713E 00	-1.536
7100.	1.727E 00	1.734E 00	0.432
7400.	1.795E 00	1.798E 00	0.187
8050.	1.932E 00	1.945E 00	0.663

LINE INDICES

NAME	OBSERVED	SYNTHESIZED	DIFFERENCE
H 3798	0.919	0.909	-0.010
H 3835	0.796	0.793	-0.002
CN 3860	1.019	1.039	0.020
CN 3880	0.880	0.893	0.012
CAII3933	0.736	0.774	0.038
H 4101	0.868	0.851	-0.017
CN 4200	0.995	1.002	0.007
CAI 4226	0.982	0.992	0.010
CH 4305	0.893	0.879	-0.013
IS 4430	0.997	1.002	0.005
MGH 4780	0.975	1.007	0.033
TIO 4970	0.980	1.009	0.029
MGI 5175	0.941	0.959	0.018
NAII5892	0.979	0.963	-0.016
TIO 6180	1.016	0.993	-0.023
H 6564	0.928	0.909	-0.019
TIO 7100	0.988	1.005	0.017

CONTINUUM INDICES

U/B	0.373	0.385	0.013
B/V	0.559	0.557	-0.002
V/R	0.679	0.687	0.008

TABLE 11

MISCELLANEOUS CONTRIBUTION TABLES

NGC 5904 M5 V= 5.97 DISTANCE MODULUS= 14.39

COMPONENT	INTRINSIC PARAMETERS			% CONTRIBUTION TO		
	V	MASS	M/L_V	V LIGHT	MASS	NUMBER
HB 1	1.05	0.70	2.23E-02	3.992	0.282	0.205
HB 2	0.81	0.70	1.79E-02	2.379	0.135	0.098
HB 3	0.72	0.70	1.65E-02	1.343	0.070	0.051
HB 4	0.72	0.70	1.65E-02	1.750	0.091	0.066
HB 5	-0.18	0.70	7.20E-03	2.533	0.058	0.042
GI E 1	0.28	0.70	1.10E-02	2.217	0.077	0.056
GI E 2	0.28	0.70	1.10E-02	3.533	0.123	0.089
GI E 3	0.19	0.70	1.01E-02	4.056	0.130	0.095
GI E 4	-0.50	0.70	5.36E-03	8.100	0.137	0.100
GI E 5	-1.24	0.70	2.71E-03	11.740	0.101	0.073
GI E 6	-1.93	0.70	1.44E-03	12.344	0.056	0.041
SG EE 1	3.85	0.70	2.55E-01	3.822	3.556	2.592
SG E 1	3.88	0.70	3.03E-01	2.714	2.598	1.893
SG EE 2	3.75	0.70	2.69E-01	5.426	4.607	3.357
SG E 2	3.75	0.70	2.69E-01	0.014	0.012	0.008
SG EE 3	3.23	0.70	1.66E-01	3.593	1.890	1.377
SG E 3	3.29	0.70	1.76E-01	0.198	0.110	0.080
SG E 4	1.99	0.70	5.31E-02	2.868	0.481	0.351
SG E 5	0.85	0.70	1.86E-02	6.346	0.373	0.272
SD EE 1	4.13	0.70	3.81E-01	2.053	2.474	1.802
SD E 1	4.13	0.70	3.81E-01	3.281	3.954	2.881
SD EE 2	4.69	0.63	5.75E-01	1.910	3.469	2.808
SD E 2	4.69	0.63	5.75E-01	1.160	2.107	1.706
SD EE 3	4.83	0.62	6.43E-01	1.555	3.161	2.600
SD E 3	4.83	0.62	6.43E-01	1.381	2.808	2.310
SD EE 4	5.60	0.54	1.14E 00	3.143	11.313	10.684
SD E 4	5.49	0.55	1.05E 00	0.002	0.005	0.005
SD EE 5	6.38	0.48	2.08E 00	2.801	18.384	19.533
SD E 5	6.43	0.47	2.13E 00	1.167	7.851	8.519
SD E 6	6.95	0.43	3.14E 00	1.606	15.965	18.936
SD M 6	7.40	0.40	4.43E 00	0.973	13.622	17.368

MODEL PARAMETERS: E(B-V)= 0.02 NUMBER OF STARS> 1.19E 05 MASS> 6.08E 04 M/L_V> 3.16E-01

FIGURE 5

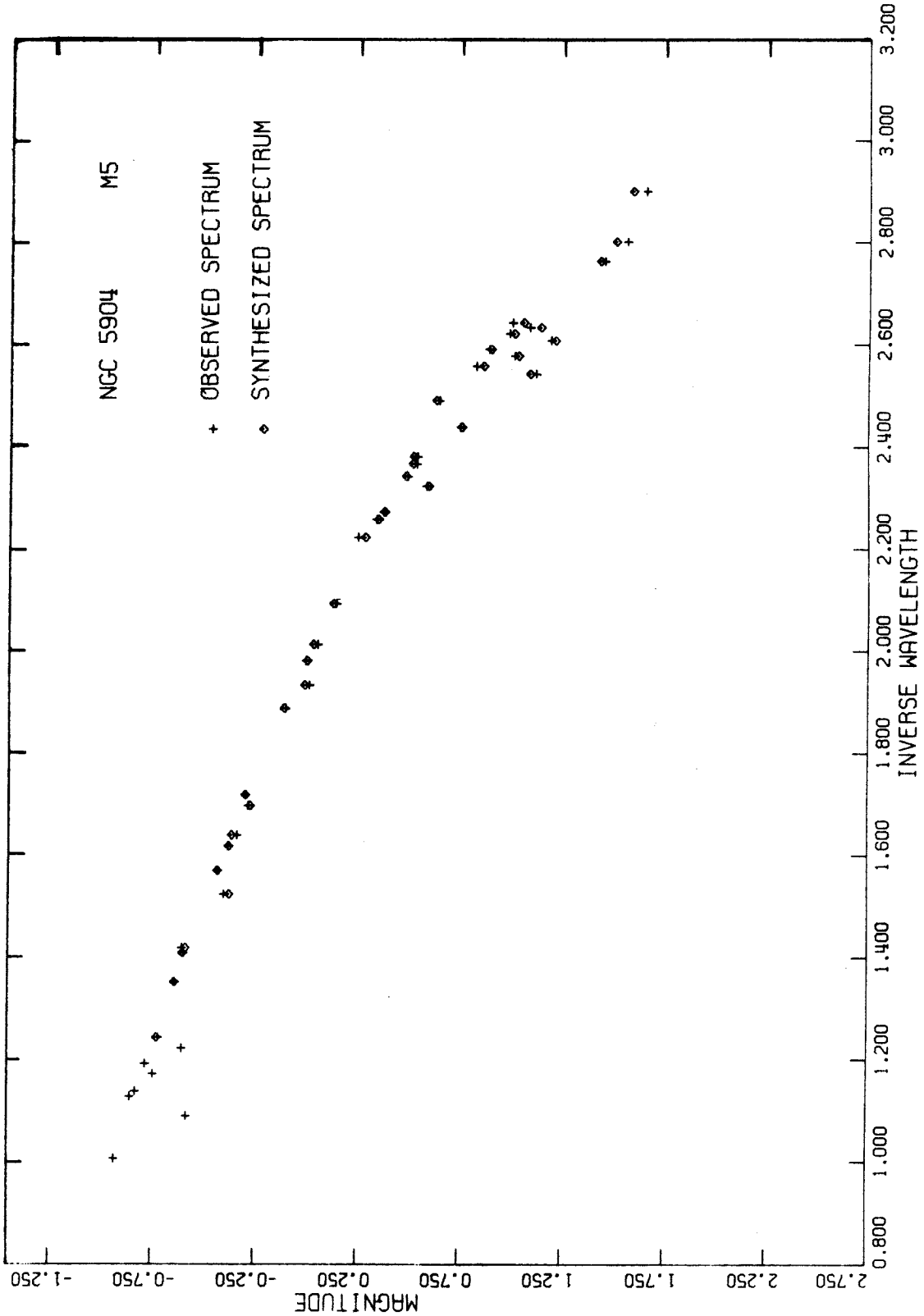
NGC 5904 M5
OBSERVED SPECTRUM
SYNTHESIZED SPECTRUM
MAGNITUDE
-1.250
-0.750
-0.250
0.250
0.750
1.250
1.750
2.250
2.750
INVERSE WAVELENGTH
0.800
1.000
1.200
1.400
1.600
1.800
2.000
2.200
2.400
2.600
2.800
3.000
3.200

TABLE 12

NGC 5904 M5

NORMALIZED LIGHT CONTRIBUTION

COMPONENT	WAVELENGTH 3448.	3570.	3620.	3784.	3798.	3815.	3835.	3860.	3860.
HB 1	0.911E-01	0.818E-01	0.774E-01	0.105E 00	0.885E-01	0.122E 00	0.949E-01	0.127E 00	0.115E 00
HB 2	0.392E-01	0.355E-01	0.332E-01	0.504E-01	0.444E-01	0.605E-01	0.480E-01	0.650E-01	0.520E-01
HB 3	0.183E-01	0.177E-01	0.170E-01	0.258E-01	0.233E-01	0.296E-01	0.246E-01	0.314E-01	0.280E-01
HB 4	0.242E-01	0.226E-01	0.210E-01	0.247E-01	0.224E-01	0.254E-01	0.239E-01	0.257E-01	0.235E-01
HB 5	0.202E-01	0.197E-01	0.206E-01	0.339E-01	0.366E-01	0.341E-01	0.364E-01	0.339E-01	0.320E-01
GI E 1	0.196E-01	0.219E-01	0.221E-01	0.206E-01	0.220E-01	0.201E-01	0.229E-01	0.195E-01	0.198E-01
GI E 2	0.287E-01	0.317E-01	0.318E-01	0.290E-01	0.317E-01	0.280E-01	0.311E-01	0.282E-01	0.293E-01
GI E 3	0.253E-01	0.273E-01	0.284E-01	0.276E-01	0.294E-01	0.273E-01	0.316E-01	0.268E-01	0.284E-01
GI E 4	0.366E-01	0.399E-01	0.403E-01	0.397E-01	0.432E-01	0.391E-01	0.431E-01	0.365E-01	0.414E-01
GI E 5	0.234E-01	0.327E-01	0.348E-01	0.349E-01	0.368E-01	0.356E-01	0.402E-01	0.348E-01	0.390E-01
GI E 6	0.171E-01	0.260E-01	0.279E-01	0.277E-01	0.307E-01	0.283E-01	0.327E-01	0.280E-01	0.317E-01
SG EE 1	0.670E-01	0.663E-01	0.659E-01	0.593E-01	0.567E-01	0.573E-01	0.591E-01	0.555E-01	0.566E-01
SG E 1	0.479E-01	0.472E-01	0.466E-01	0.421E-01	0.416E-01	0.409E-01	0.416E-01	0.400E-01	0.407E-01
SG EE 2	0.981E-01	0.893E-01	0.876E-01	0.813E-01	0.821E-01	0.815E-01	0.864E-01	0.787E-01	0.797E-01
SG E 2	0.234E-03	0.219E-03	0.214E-03	0.200E-03	0.198E-03	0.195E-03	0.200E-03	0.190E-03	0.193E-03
SG EE 3	0.477E-01	0.469E-01	0.483E-01	0.441E-01	0.453E-01	0.389E-01	0.396E-01	0.391E-01	0.415E-01
SG E 3	0.270E-02	0.262E-02	0.268E-02	0.245E-02	0.249E-02	0.218E-02	0.221E-02	0.219E-02	0.231E-02
SG E 4	0.283E-01	0.312E-01	0.313E-01	0.281E-01	0.300E-01	0.273E-01	0.310E-01	0.263E-01	0.267E-01
SG E 5	0.549E-01	0.603E-01	0.604E-01	0.547E-01	0.598E-01	0.528E-01	0.585E-01	0.527E-01	0.548E-01
SD EE 1	0.384E-01	0.376E-01	0.365E-01	0.333E-01	0.331E-01	0.341E-01	0.342E-01	0.340E-01	0.346E-01
SD E 1	0.570E-01	0.580E-01	0.558E-01	0.511E-01	0.508E-01	0.516E-01	0.521E-01	0.515E-01	0.532E-01
SD EE 2	0.348E-01	0.344E-01	0.341E-01	0.295E-01	0.292E-01	0.285E-01	0.294E-01	0.276E-01	0.282E-01
SD E 2	0.213E-01	0.209E-01	0.206E-01	0.180E-01	0.177E-01	0.174E-01	0.177E-01	0.170E-01	0.173E-01
SD EE 3	0.295E-01	0.268E-01	0.262E-01	0.232E-01	0.234E-01	0.233E-01	0.247E-01	0.225E-01	0.228E-01
SD E 3	0.250E-01	0.233E-01	0.227E-01	0.203E-01	0.201E-01	0.198E-01	0.202E-01	0.192E-01	0.196E-01
SD EE 4	0.466E-01	0.455E-01	0.465E-01	0.398E-01	0.408E-01	0.349E-01	0.355E-01	0.350E-01	0.371E-01
SD E 4	0.250E-04	0.241E-04	0.245E-04	0.209E-04	0.212E-04	0.180E-04	0.188E-04	0.186E-04	0.196E-04
SD EE 5	0.274E-01	0.248E-01	0.291E-01	0.256E-01	0.263E-01	0.187E-01	0.193E-01	0.208E-01	0.226E-01
SD E 5	0.115E-01	0.103E-01	0.117E-01	0.104E-01	0.105E-01	0.795E-02	0.718E-02	0.821E-02	0.910E-02
SD E 6	0.123E-01	0.121E-01	0.134E-01	0.114E-01	0.117E-01	0.824E-02	0.805E-02	0.764E-02	0.949E-02
SD M 6	0.585E-02	0.530E-02	0.573E-02	0.554E-02	0.524E-02	0.446E-02	0.364E-02	0.350E-02	0.386E-02

TABLE 12 (continued)

NGC 5904 M5

NORMALIZED LIGHT CONTRIBUTION

COMPONENT	WAVELENGTH 3910.	3933.	4015.	4101.	4200.	4226.	4270.	4305.	4400.
HB 1	0.124E 00	0.159E 00	0.113E 00	0.683E-01	0.986E-01	0.972E-01	0.933E-01	0.100E 00	0.833E-01
HB 2	0.652E-01	0.847E-01	0.604E-01	0.349E-01	0.540E-01	0.527E-01	0.512E-01	0.541E-01	0.453E-01
HB 3	0.308E-01	0.407E-01	0.300E-01	0.193E-01	0.275E-01	0.271E-01	0.264E-01	0.277E-01	0.238E-01
HB 4	0.257E-01	0.316E-01	0.250E-01	0.205E-01	0.236E-01	0.232E-01	0.232E-01	0.243E-01	0.220E-01
HB 5	0.381E-01	0.390E-01	0.361E-01	0.339E-01	0.324E-01	0.330E-01	0.323E-01	0.341E-01	0.314E-01
GI E 1	0.192E-01	0.162E-01	0.199E-01	0.229E-01	0.209E-01	0.205E-01	0.208E-01	0.184E-01	0.213E-01
GI E 2	0.274E-01	0.195E-01	0.284E-01	0.349E-01	0.302E-01	0.307E-01	0.306E-01	0.283E-01	0.308E-01
GI E 3	0.269E-01	0.252E-01	0.277E-01	0.334E-01	0.301E-01	0.309E-01	0.319E-01	0.324E-01	0.336E-01
GI E 4	0.386E-01	0.290E-01	0.432E-01	0.547E-01	0.501E-01	0.516E-01	0.534E-01	0.510E-01	0.573E-01
GI E 5	0.349E-01	0.246E-01	0.424E-01	0.581E-01	0.546E-01	0.590E-01	0.602E-01	0.614E-01	0.693E-01
GI E 6	0.287E-01	0.200E-01	0.354E-01	0.504E-01	0.486E-01	0.525E-01	0.540E-01	0.563E-01	0.645E-01
SG EE 1	0.554E-01	0.570E-01	0.525E-01	0.530E-01	0.515E-01	0.506E-01	0.507E-01	0.529E-01	0.490E-01
SG E 1	0.393E-01	0.380E-01	0.376E-01	0.377E-01	0.367E-01	0.361E-01	0.361E-01	0.373E-01	0.352E-01
SG EE 2	0.784E-01	0.869E-01	0.739E-01	0.731E-01	0.701E-01	0.696E-01	0.702E-01	0.721E-01	0.664E-01
SG E 2	0.188E-03	0.190E-03	0.180E-03	0.179E-03	0.173E-03	0.172E-03	0.173E-03	0.175E-03	0.164E-03
SG EE 3	0.384E-01	0.306E-01	0.402E-01	0.451E-01	0.393E-01	0.388E-01	0.384E-01	0.352E-01	0.391E-01
SG E 3	0.217E-02	0.170E-02	0.225E-02	0.248E-02	0.220E-02	0.217E-02	0.214E-02	0.200E-02	0.216E-02
SG E 4	0.258E-01	0.217E-01	0.266E-01	0.304E-01	0.277E-01	0.271E-01	0.275E-01	0.243E-01	0.280E-01
SG E 5	0.510E-01	0.362E-01	0.525E-01	0.642E-01	0.555E-01	0.563E-01	0.561E-01	0.480E-01	0.560E-01
SD EE 1	0.340E-01	0.387E-01	0.318E-01	0.294E-01	0.303E-01	0.303E-01	0.298E-01	0.322E-01	0.284E-01
SD E 1	0.520E-01	0.550E-01	0.483E-01	0.462E-01	0.470E-01	0.463E-01	0.459E-01	0.495E-01	0.443E-01
SD EE 2	0.276E-01	0.284E-01	0.261E-01	0.264E-01	0.256E-01	0.252E-01	0.252E-01	0.263E-01	0.244E-01
SD E 2	0.167E-01	0.161E-01	0.160E-01	0.160E-01	0.156E-01	0.154E-01	0.154E-01	0.159E-01	0.150E-01
SD EE 3	0.224E-01	0.248E-01	0.211E-01	0.208E-01	0.200E-01	0.199E-01	0.200E-01	0.206E-01	0.190E-01
SD E 3	0.191E-01	0.192E-01	0.182E-01	0.182E-01	0.175E-01	0.174E-01	0.176E-01	0.178E-01	0.167E-01
SD EE 4	0.342E-01	0.272E-01	0.355E-01	0.398E-01	0.347E-01	0.342E-01	0.339E-01	0.310E-01	0.344E-01
SD E 4	0.163E-04	0.143E-04	0.189E-04	0.207E-04	0.184E-04	0.182E-04	0.179E-04	0.167E-04	0.180E-04
SD EE 5	0.208E-01	0.139E-01	0.262E-01	0.308E-01	0.262E-01	0.242E-01	0.252E-01	0.230E-01	0.271E-01
SD E 5	0.848E-02	0.565E-02	0.105E-01	0.122E-01	0.104E-01	0.961E-02	0.990E-02	0.897E-02	0.108E-01
SD E 6	0.958E-02	0.636E-02	0.125E-01	0.147E-01	0.124E-01	0.115E-01	0.118E-01	0.111E-01	0.135E-01
SD M 6	0.476E-02	0.301E-02	0.618E-02	0.797E-02	0.665E-02	0.659E-02	0.651E-02	0.553E-02	0.717E-02

TABLE 12 (continued)

NGC 5904 M5

NORMALIZED LIGHT CONTRIBUTION

COMPONENT	WAVELENGTH 4430.	4500.	4780.	4970.	5050.	5175.	5360.	5820.	5892.
HB 1	0.806E-01	0.747E-01	0.610E-01	0.547E-01	0.524E-01	0.500E-01	0.446E-01	0.343E-01	0.338E-01
HB 2	0.445E-01	0.417E-01	0.346E-01	0.315E-01	0.304E-01	0.293E-01	0.264E-01	0.207E-01	0.206E-01
HB 3	0.232E-01	0.218E-01	0.187E-01	0.172E-01	0.166E-01	0.160E-01	0.147E-01	0.119E-01	0.119E-01
HB 4	0.214E-01	0.212E-01	0.196E-01	0.189E-01	0.190E-01	0.188E-01	0.181E-01	0.167E-01	0.165E-01
HB 5	0.314E-01	0.305E-01	0.290E-01	0.291E-01	0.283E-01	0.279E-01	0.261E-01	0.246E-01	0.237E-01
GI E 1	0.215E-01	0.214E-01	0.216E-01	0.223E-01	0.220E-01	0.218E-01	0.223E-01	0.219E-01	0.222E-01
GI E 2	0.321E-01	0.334E-01	0.336E-01	0.347E-01	0.348E-01	0.349E-01	0.351E-01	0.357E-01	0.365E-01
GI E 3	0.340E-01	0.344E-01	0.362E-01	0.388E-01	0.388E-01	0.399E-01	0.398E-01	0.417E-01	0.430E-01
GI E 4	0.582E-01	0.611E-01	0.687E-01	0.714E-01	0.735E-01	0.762E-01	0.781E-01	0.848E-01	0.852E-01
GI E 5	0.705E-01	0.744E-01	0.886E-01	0.978E-01	0.998E-01	0.105E 00	0.111E 00	0.125E 00	0.123E 00
GI E 6	0.658E-01	0.705E-01	0.876E-01	0.991E-01	0.102E 00	0.108E 00	0.115E 00	0.134E 00	0.130E 00
SG EE 1	0.470E-01	0.465E-01	0.452E-01	0.411E-01	0.417E-01	0.415E-01	0.397E-01	0.363E-01	0.367E-01
SG E 1	0.340E-01	0.337E-01	0.322E-01	0.297E-01	0.297E-01	0.295E-01	0.282E-01	0.259E-01	0.261E-01
SG EE 2	0.655E-01	0.627E-01	0.601E-01	0.593E-01	0.580E-01	0.582E-01	0.557E-01	0.523E-01	0.535E-01
SG E 2	0.162E-03	0.158E-03	0.152E-03	0.147E-03	0.145E-03	0.145E-03	0.140E-03	0.130E-03	0.132E-03
SG EE 3	0.399E-01	0.399E-01	0.395E-01	0.376E-01	0.377E-01	0.376E-01	0.365E-01	0.351E-01	0.356E-01
SG E 3	0.218E-02	0.220E-02	0.216E-02	0.207E-02	0.207E-02	0.207E-02	0.202E-02	0.193E-02	0.195E-02
SG E 4	0.282E-01	0.280E-01	0.282E-01	0.290E-01	0.285E-01	0.283E-01	0.269E-01	0.283E-01	0.287E-01
SG E 5	0.585E-01	0.607E-01	0.609E-01	0.627E-01	0.628E-01	0.628E-01	0.631E-01	0.640E-01	0.655E-01
SD EE 1	0.278E-01	0.269E-01	0.246E-01	0.237E-01	0.235E-01	0.231E-01	0.217E-01	0.194E-01	0.197E-01
SD E 1	0.433E-01	0.417E-01	0.391E-01	0.366E-01	0.365E-01	0.362E-01	0.343E-01	0.311E-01	0.317E-01
SD EE 2	0.234E-01	0.232E-01	0.226E-01	0.205E-01	0.208E-01	0.207E-01	0.198E-01	0.182E-01	0.184E-01
SD E 2	0.145E-01	0.144E-01	0.137E-01	0.127E-01	0.127E-01	0.126E-01	0.120E-01	0.111E-01	0.112E-01
SD EE 3	0.187E-01	0.179E-01	0.172E-01	0.170E-01	0.166E-01	0.167E-01	0.160E-01	0.150E-01	0.153E-01
SD E 3	0.164E-01	0.160E-01	0.155E-01	0.150E-01	0.146E-01	0.148E-01	0.142E-01	0.133E-01	0.134E-01
SD EE 4	0.351E-01	0.351E-01	0.346E-01	0.329E-01	0.330E-01	0.315E-01	0.320E-01	0.308E-01	0.307E-01
SD E 4	0.182E-04	0.183E-04	0.179E-04	0.172E-04	0.172E-04	0.165E-04	0.167E-04	0.160E-04	0.159E-04
SD EE 5	0.281E-01	0.298E-01	0.289E-01	0.281E-01	0.279E-01	0.243E-01	0.286E-01	0.280E-01	0.277E-01
SD E 5	0.115E-01	0.119E-01	0.116E-01	0.115E-01	0.114E-01	0.101E-01	0.116E-01	0.116E-01	0.115E-01
SD E 6	0.147E-01	0.155E-01	0.155E-01	0.158E-01	0.156E-01	0.134E-01	0.158E-01	0.164E-01	0.161E-01
SD M 6	0.779E-02	0.865E-02	0.917E-02	0.926E-02	0.932E-02	0.840E-02	0.953E-02	0.998E-02	0.992E-02

TABLE 12 (continued)

NGC 5904 M5

NORMALIZED LIGHT CONTRIBUTION

COMPONENT	WAVELENGTH 6100.	6180.	6370.	6564.	7050.	7100.	7400.	8050.
HB 1	0.305E-01	0.296E-01	0.271E-01	0.198E-01	0.209E-01	0.205E-01	0.182E-01	0.158E-01
HB 2	0.189E-01	0.183E-01	0.170E-01	0.128E-01	0.138E-01	0.134E-01	0.127E-01	0.111E-01
HB 3	0.110E-01	0.108E-01	0.102E-01	0.829E-02	0.871E-02	0.855E-02	0.807E-02	0.709E-02
HB 4	0.161E-01	0.161E-01	0.154E-01	0.135E-01	0.145E-01	0.141E-01	0.140E-01	0.134E-01
HB 5	0.234E-01	0.229E-01	0.225E-01	0.220E-01	0.206E-01	0.202E-01	0.197E-01	0.175E-01
GI E 1	0.220E-01	0.218E-01	0.218E-01	0.218E-01	0.214E-01	0.216E-01	0.214E-01	0.213E-01
GI E 2	0.359E-01	0.352E-01	0.339E-01	0.305E-01	0.356E-01	0.360E-01	0.357E-01	0.359E-01
GI E 3	0.430E-01	0.431E-01	0.437E-01	0.448E-01	0.448E-01	0.451E-01	0.450E-01	0.460E-01
GI E 4	0.880E-01	0.884E-01	0.898E-01	0.942E-01	0.937E-01	0.942E-01	0.951E-01	0.979E-01
GI E 5	0.129E 00	0.131E 00	0.135E 00	0.144E 00	0.146E 00	0.146E 00	0.151E 00	0.155E 00
GI E 6	0.141E 00	0.144E 00	0.150E 00	0.166E 00	0.166E 00	0.168E 00	0.173E 00	0.186E 00
SG EE 1	0.352E-01	0.350E-01	0.336E-01	0.310E-01	0.318E-01	0.314E-01	0.311E-01	0.292E-01
SG E 1	0.251E-01	0.250E-01	0.241E-01	0.223E-01	0.224E-01	0.221E-01	0.218E-01	0.206E-01
SG EE 2	0.505E-01	0.509E-01	0.498E-01	0.469E-01	0.468E-01	0.472E-01	0.464E-01	0.437E-01
SG E 2	0.126E-03	0.126E-03	0.122E-03	0.115E-03	0.114E-03	0.114E-03	0.113E-03	0.106E-03
SG EE 3	0.343E-01	0.344E-01	0.336E-01	0.326E-01	0.320E-01	0.319E-01	0.310E-01	0.303E-01
SG E 3	0.186E-02	0.186E-02	0.181E-02	0.173E-02	0.171E-02	0.172E-02	0.166E-02	0.163E-02
SG E 4	0.284E-01	0.282E-01	0.282E-01	0.282E-01	0.277E-01	0.279E-01	0.276E-01	0.275E-01
SG E 5	0.644E-01	0.632E-01	0.643E-01	0.654E-01	0.641E-01	0.644E-01	0.639E-01	0.643E-01
SD EE 1	0.191E-01	0.186E-01	0.182E-01	0.168E-01	0.167E-01	0.165E-01	0.160E-01	0.151E-01
SD E 1	0.301E-01	0.300E-01	0.290E-01	0.269E-01	0.269E-01	0.263E-01	0.258E-01	0.243E-01
SD EE 2	0.176E-01	0.175E-01	0.168E-01	0.155E-01	0.159E-01	0.157E-01	0.156E-01	0.147E-01
SD E 2	0.108E-01	0.107E-01	0.103E-01	0.955E-02	0.959E-02	0.946E-02	0.935E-02	0.886E-02
SD EE 3	0.145E-01	0.146E-01	0.143E-01	0.135E-01	0.135E-01	0.136E-01	0.134E-01	0.126E-01
SD E 3	0.128E-01	0.128E-01	0.125E-01	0.117E-01	0.116E-01	0.116E-01	0.115E-01	0.108E-01
SD EE 4	0.301E-01	0.302E-01	0.295E-01	0.286E-01	0.282E-01	0.280E-01	0.273E-01	0.267E-01
SD E 4	0.155E-04	0.154E-04	0.151E-04	0.144E-04	0.143E-04	0.143E-04	0.139E-04	0.136E-04
SD EE 5	0.280E-01	0.279E-01	0.281E-01	0.283E-01	0.278E-01	0.277E-01	0.271E-01	0.271E-01
SD E 5	0.114E-01	0.113E-01	0.114E-01	0.114E-01	0.112E-01	0.110E-01	0.109E-01	0.105E-01
SD E 6	0.164E-01	0.163E-01	0.163E-01	0.164E-01	0.158E-01	0.161E-01	0.161E-01	0.152E-01
SD M 6	0.100E-01	0.991E-02	0.100E-01	0.102E-01	0.996E-02	0.985E-02	0.942E-02	0.852E-02

horizontal-branch stars and/or red-giants only at the expense of the good fit in other spectral regions.

All continuum and line indices fit within observational accuracies. Discrepancies in line indices CaII 3933, MgH 4780, and TiO 4970 are relatively large because of the combined effects of smaller but compounding discrepancies in feature and sideband fluxes.

E and EE sequences have been combined in the M5 model. The population distribution of spectral types has been constrained to be smooth only when corresponding E and EE types are paired as units. For spectral types represented by both sequences the ratio of total E to total EE V-light is 0.41.

The cluster luminosity function along the giant, horizontal and upper subgiant branches agrees with the distribution of stars in Arp's (1962) color-magnitude diagram to within the statistical accuracies of Arp's counts, except at the blue end of the horizontal branch where model stars are too numerous by a factor of about two. This disagreement is believed to be a result of (1) the absence of RR Lyrae variables in Arp's diagram and (2) a possible incompleteness in his star counts at the faint blue tip of the branch.

M13

The M13 model is described in Tables 13 and 14. In Figure 6 model and observed energy distributions are plotted for comparison.

TABLE 13

NGC 6205 M13

COMPARISON OF OBSERVED AND SYNTHESIZED SPECTRA

FLUXES

LAMBDA	OBSERVED	SYNTHESIZED	PCT. DIFF.
3448.	2.554E-01	2.646E-01	3.556
3570.	2.709E-01	2.840E-01	4.715
3620.	3.059E-01	3.031E-01	-0.921
3784.	4.309E-01	4.161E-01	-3.502
3796.	4.223E-01	3.837E-01	-9.574
3815.	4.289E-01	4.347E-01	1.332
3835.	3.905E-01	3.612E-01	-7.777
3860.	4.734E-01	4.821E-01	1.819
3880.	4.270E-01	4.260E-01	-0.218
3910.	5.003E-01	4.946E-01	-1.142
3933.	4.059E-01	4.061E-01	0.057
4015.	6.121E-01	6.038E-01	-1.357
4101.	5.390E-01	5.315E-01	-1.396
4200.	6.613E-01	6.630E-01	0.263
4226.	6.457E-01	6.637E-01	2.753
4270.	6.912E-01	6.833E-01	-1.141
4305.	6.327E-01	6.184E-01	-2.279
4400.	7.311E-01	7.434E-01	1.662
4430.	7.741E-01	7.603E-01	-1.797
4500.	8.069E-01	8.013E-01	-0.693
4780.	9.078E-01	9.137E-01	0.646
4970.	9.781E-01	9.870E-01	0.898
5050.	1.000E 00	1.013E 00	1.304
5175.	1.007E 00	1.025E 00	1.775
5300.	1.096E 00	1.114E 00	1.659
5820.	1.300E 00	1.300E 00	0.025
5892.	1.276E 00	1.278E 00	0.121
6100.	1.407E 00	1.377E 00	-2.201
6180.	1.398E 00	1.392E 00	-0.442
6370.	1.435E 00	1.458E 00	1.602
6564.	1.418E 00	1.367E 00	-3.646
7050.	1.640E 00	1.664E 00	1.465
7100.	1.640E 00	1.684E 00	2.652
7400.	1.660E 00	1.741E 00	4.811
8050.	1.957E 00	1.875E 00	-4.261

LINE INDICES

NAME	OBSERVED	SYNTHESIZED	DIFFERENCE
H 3798	0.982	0.904	-0.078
H 3835	0.871	0.793	-0.078
CN 3860	1.024	1.042	0.018
CN 3880	0.895	0.897	0.002
CAII3933	0.775	0.784	0.010
H 4101	0.845	0.844	-0.001
CN 4200	0.988	1.003	0.015
CAI 4226	0.953	0.992	0.038
CH 4305	0.901	0.885	-0.017
IS 4430	1.028	1.000	-0.028
MGH 4780	1.005	1.009	0.003
TIO 4970	1.006	1.006	-0.001
MGI 5175	0.961	0.965	0.003
NAI5892	0.962	0.968	0.006
TIO 6180	0.987	0.994	0.007
H 6564	0.949	0.901	-0.048
TIO 7100	0.998	1.005	0.007

CONTINUUM INDICES

U/B	0.406	0.411	0.006
B/V	0.593	0.591	-0.002
V/R	0.726	0.709	-0.017

TABLE 14

MISCELLANEOUS CONTRIBUTION TABLES

NGC 6205 M13 V= 5.76 DISTANCE MODULUS= 14.30

COMPONENT	INTRINSIC PARAMETERS			% CONTRIBUTION TO		
	V	MASS	M/L_v	V LIGHT	MASS	NUMBER
HB 1	1.05	0.70	2.23E-02	3.424	0.291	0.249
HB 2	0.81	0.70	1.79E-02	3.081	0.210	0.175
HB 3	0.72	0.70	1.65E-02	2.066	0.130	0.108
HB 4	0.72	0.70	1.65E-02	0.0	0.0	0.0
HB 5	-0.18	0.70	7.20E-03	0.0	0.0	0.0
GI E 1	0.28	0.70	1.10E-02	2.051	0.086	0.072
GI E 2	0.28	0.70	1.10E-02	2.648	0.111	0.092
GI E 3	0.19	0.70	1.01E-02	3.888	0.150	0.125
GI E 4	-0.50	0.70	5.36E-03	7.430	0.152	0.126
GI E 5	-1.24	0.70	2.71E-03	8.310	0.086	0.071
GI E 6	-1.93	0.70	1.44E-03	11.141	0.061	0.051
SG EE 1	3.85	0.70	2.95E-01	4.846	5.436	4.529
SG E 1	3.88	0.70	3.03E-01	3.503	4.040	3.366
SG EE 2	3.75	0.70	2.69E-01	3.169	3.242	2.701
SG E 2	3.75	0.70	2.69E-01	2.565	2.645	2.204
SG EE 3	3.23	0.70	1.66E-01	2.886	1.829	1.524
SG E 3	3.29	0.70	1.76E-01	2.730	1.829	1.524
SG E 4	1.99	0.70	5.31E-02	5.509	1.114	0.928
SG E 5	0.85	0.70	1.86E-02	4.935	0.349	0.291
SD EE 1	4.13	0.70	3.81E-01	4.409	6.401	5.334
SD E 1	4.13	0.70	3.81E-01	3.405	4.943	4.119
SD EE 2	4.69	0.63	5.75E-01	2.654	6.247	5.783
SD E 2	4.69	0.63	5.75E-01	2.542	5.563	5.150
SD EE 3	4.83	0.62	6.43E-01	3.645	8.930	8.401
SD E 3	4.83	0.62	6.43E-01	1.841	4.512	4.244
SD EE 4	5.60	0.54	1.14E 00	2.693	11.678	12.613
SD E 4	5.49	0.55	1.05E 00	1.672	6.674	7.077
SD EE 5	6.38	0.48	2.08E 00	1.370	10.836	13.166
SD E 5	6.43	0.47	2.13E 00	1.110	9.003	11.172
SD E 6	6.95	0.43	3.14E 00	0.182	2.185	2.964
SD M 6	7.40	0.40	4.43E 00	0.075	1.266	1.847

MODEL PARAMETERS: E(B-V)= 0.02 NUMBER OF STARS> 9.67E 04 MASS> 5.64E 04 M/L_v > 2.63E-01

FIGURE 6

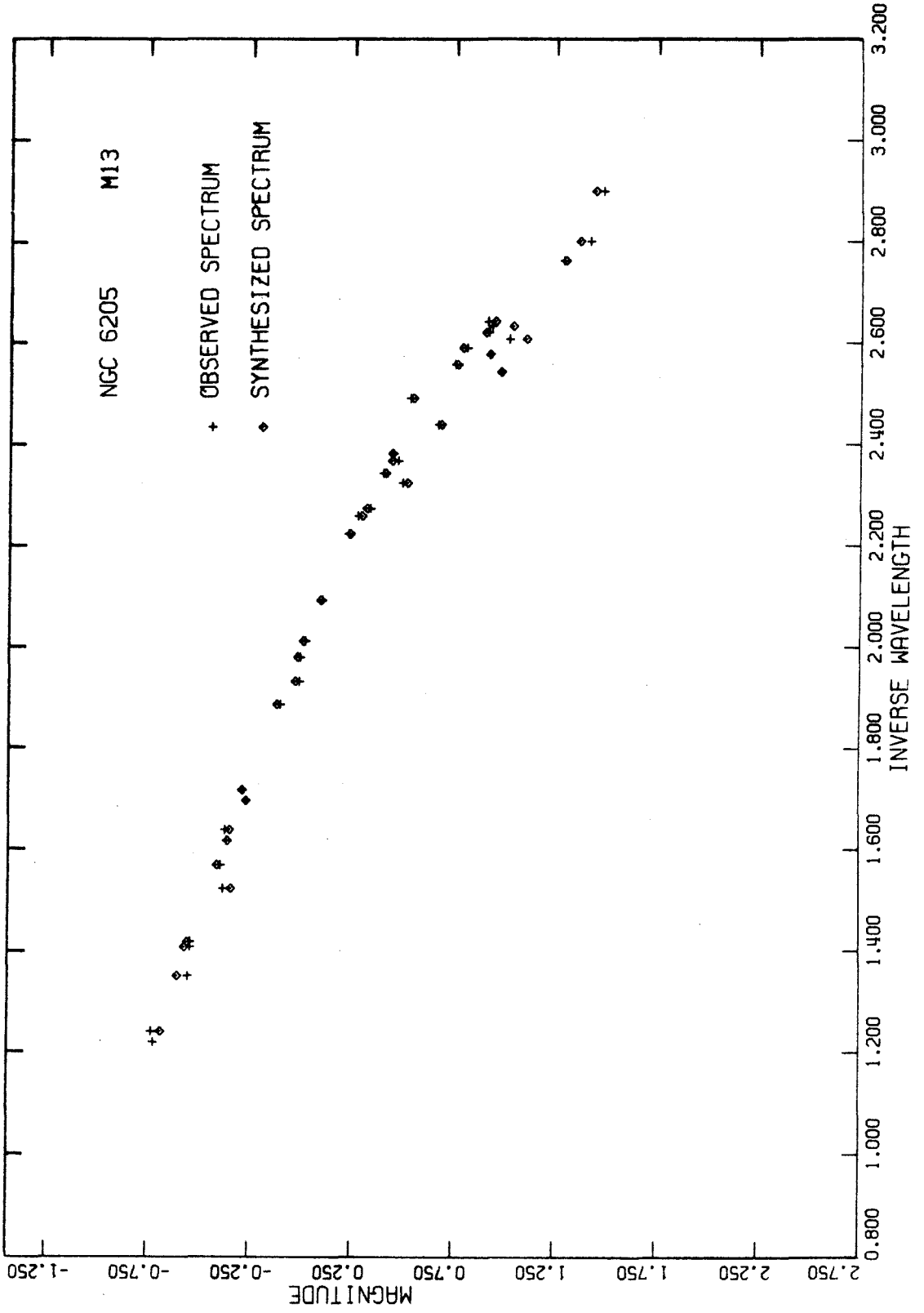
NGC 6205 M13
OBSERVED SPECTRUM
SYNTHESIZED SPECTRUM
MAGNITUDE
-1.250
-0.750
-0.250
0.250
0.750
1.250
1.750
2.250
2.750
INVERSE WAVELENGTH
0.800
1.000
1.200
1.400
1.600
1.800
2.000
2.200
2.400
2.600
2.800
3.000
3.200

Except for the Balmer features at $\lambda\lambda$3798 and 3835 the agreement between model and observed energy distributions is as good as for M5. Excluding these wavelengths, the mean differences in model and observed fluxes are 1.6 and 3.1 per cent longward and shortward of the Balmer jump.

The difficulty in fitting these two wavelengths is partly a result of the line blanketing discussed in section II C. The jaggedness of the energy distribution near these features also made them subject to larger observational errors than other bandpasses.

The adopted M13 model has an H alpha index 0.05 stronger than the observed index. The excessive strength of H alpha is common to all models and is believed to be a result of spectral degradation from observing extended sources and/or H alpha emission in the red-giants. The problem is discussed in detail in the next section.

As with M5, E and EE mean stellar types have been combined in the model. The ratio of E to EE V-light for spectral types represented by both sequences is 0.75.

M13 is one of only two of the galactic globular clusters (the other is M92) which has a published luminosity function (Simoda and Kimura 1968) with which its model can be compared. (Color-magnitude diagrams are often based on incomplete star counts except along giant and horizontal branches and therefore do not provide sufficient data for

extensive comparisons.) However before a comparison can be made certain difficulties need to be considered.

A meaningful comparison of a model and a conventional luminosity function is difficult over all regions of the color-magnitude plane for two reasons: (1) Model luminosity functions depend strongly upon assumed magnitudes for the mean stellar types. The assumed magnitudes for subgiants are quite uncertain, especially on the steep portion of the subgiant branch where they are extremely sensitive to the colors by which they were calibrated. On the red end of the horizontal branch the assumed magnitude for stellar type HB 5 is uncertain. (2) Mean stellar types along the steep portions of the subgiant branch and the blue tip of the horizontal branch represent wide spreads in luminosity. The magnitude of an "average stellar type" within a block may be quite different from the magnitude derived from the "average stellar luminosity" within the block. Adopted magnitudes were averages of the first kind since the second kind requires presupposition of a luminosity function and knowledge of exactly where boundaries between blocks fall in the color-magnitude diagrams. Model mass contributions suffer from the same difficulties; light contributions are not affected by the two problems discussed above.

Comparisons of giant branch and cluster main sequence luminosity functions can be made without concern for the above problems. In these regions the agreement between the model and published data are

satisfactory. For M13 the ratio of the number of red-giants brighter than $M_V = 0.30$ to the number of dwarfs in the magnitude range $M_V = 4.00$ to 4.41 is 0.057 for the model and 0.048 for the luminosity function of Simoda and Kimura (1968). (The data of Simoda and Kimura have been adjusted to a distance modulus of m - M = 14.3 rather than 14.6 as they assumed.)

A comparison of model and published horizontal-branch luminosity functions served to illustrate the difficulty that can be encountered in comparing numbers of stars rather than light contributions in troublesome regions such as the horizontal or subgiant branches. The ratio of the number of horizontal-branch stars to the number of main sequence stars within the magnitude range $M_V = 4.00$ to 4.41 is 0.056 for the model and 0.077 for the published luminosity function. The discrepancy is the result of a large number of stars blueward of and fainter than the bluest mean stellar type HB 1 with $M_V = 1.05$. Each of these stars is counted with a weight of

$$W = 10^{-0.4(M_V - 1.05)} \qquad (5)$$

in the model, where M_V is the star's absolute magnitude and W is the ratio of its luminosity to the luminosity of mean stellar type HB 1. This is because all HB 1 light in a model is assumed to come from stars with the same luminosity as the mean stellar type, i.e., with $M_V = 1.05$. If such weights are attached to faint horizontal-branch

stars in the published luminosity function then the discrepant ratio 0.077 becomes 0.054, in excellent agreement with the model.

The relative numbers of stars in M13 in the three regions considered are compared in Table 15 for the model and for the Simoda and Kimura luminosity function. The apparent small discrepancy in giant

TABLE 15

RELATIVE NUMBERS OF STARS IN M13

Source	Cluster Main Sequence $4.00 \leq M_V \leq 4.41$	Red-Giant Branch $M_V \leq 0.30$	Horizontal Branch
Model	899	51	50
Simoda and Kimura (1968) Luminosity Function**	907	43	49*

* Weighted. See text.
**Adjusted to m - M = 14.3.

branch populations is probably not as great as indicated. This is because the M13 model is based upon the M5 color-absolute magnitude calibration. The M13 giant branch is actually somewhat taller than the M5 giant branch (about $0^m.24$ at B - V = 1.20 if the red tips of the blue horizontal branches are aligned). Thus replacing the M5 giant

magnitudes with the somewhat brighter M13 magnitudes would reduce the number of giants required by the model to produce a given amount of light.

In addition to the preceding comparison, the M13 model can be compared to the color-magnitude array of Arp and Johnson (1955). Agreement is within the statistical accuracies of the star counts except near the blue tip of the horizontal branch where the counts of Arp and Johnson are incomplete.

M15

Tables 16 and 17 and Figure 7 describe the adopted M15 model. Excluding wavelengths $\lambda\lambda$3798 and 3815 the mean model flux residuals are 2.9 and 3.0 per cent longward and shortward of the Balmer jump. Disagreement between model and observed spectra occurs primarily in the spectral region between $\lambda\lambda$3700 and 4000 for reasons given in the discussion of the M5 model. Except for the G-band and the problem indices H 3798, H 3835, and H 6564 all model line and continuum indices fit the observations satisfactorily.

The excessive strength (0.03) of the model G-band index is not unique to M15. All models except that of NGC 205 have stronger G-bands than are observed. The average discrepancy is 0.03. Since the G-bandhead occurs at λ4314, at the edge of the feature bandpass, it is

TABLE 16

NGC 7078 M15

COMPARISON OF OBSERVED AND SYNTHESIZED SPECTRA

FLUXES

LAMBDA	OBSERVED	SYNTHESIZED	PCT. DIFF.
3448.	2.297E-01	2.476E-01	7.477
3570.	2.638E-01	2.666E-01	1.068
3620.	2.837E-01	2.848E-01	0.411
3764.	4.093E-01	3.968E-01	-3.095
3798.	4.003E-01	3.680E-01	-8.398
3815.	4.393E-01	4.170E-01	-5.222
3835.	4.011E-01	3.508E-01	-13.361
3860.	4.898E-01	4.625E-01	-5.726
3880.	4.329E-01	4.081E-01	-5.690
3910.	5.162E-01	4.771E-01	-7.660
3933.	4.341E-01	4.019E-01	-7.704
4015.	5.733E-01	5.812E-01	1.369
4101.	4.952E-01	5.114E-01	3.214
4200.	6.183E-01	6.405E-01	3.534
4226.	6.217E-01	6.413E-01	3.100
4270.	6.397E-01	6.614E-01	3.326
4305.	6.126E-01	5.986E-01	-2.311
4400.	7.413E-01	7.166E-01	-3.392
4430.	7.251E-01	7.337E-01	1.175
4500.	7.338E-01	7.723E-01	5.194
4780.	8.686E-01	8.872E-01	2.126
4970.	9.665E-01	9.662E-01	-0.027
5050.	1.000E 00	9.957E-01	-0.429
5175.	1.022E 00	1.016E 00	-0.640
5300.	1.090E 00	1.099E 00	0.784
5820.	1.282E 00	1.295E 00	0.965
5892.	1.278E 00	1.267E 00	0.710
6100.	1.377E 00	1.379E 00	0.140
6180.	1.389E 00	1.394E 00	0.341
6370.	1.423E 00	1.464E 00	2.831
* 6564.	1.449E 00	1.361E 00	-6.314
7050.	1.706E 00	1.693E 00	-0.867
7100.	1.684E 00	1.715E 00	1.834
7400.	1.746E 00	1.782E 00	2.054
8050.	1.999E 00	1.927E 00	-3.663

LINE INDICES

NAME		OBSERVED	SYNTHESIZED	DIFFERENCE
H	3798	0.947	0.907	-0.040
H	3835	0.869	0.803	-0.066
CN	3860	1.031	1.039	0.008
CN	3880	0.881	0.892	0.011
CAII	3933	0.822	0.805	-0.016
H	4101	0.832	0.842	0.010
CN	4200	0.995	1.003	0.007
CA I	4226	0.990	0.991	0.001
CH	4305	0.920	0.886	-0.034
IS	4430	0.981	1.001	0.020
MGH	4780	1.007	1.006	-0.001
TIO	4970	1.009	1.005	-0.004
MGI	5175	0.978	0.971	-0.008
NAI	5892	0.978	0.977	-0.000
TIO	6180	0.999	0.993	-0.006
H	6564	0.965	0.890	-0.075
TIO	7100	0.983	1.005	0.023

CONTINUUM INDICES

	OBSERVED	SYNTHESIZED	DIFFERENCE
U/B	0.396	0.400	0.004
B/V	0.582	0.576	-0.006
V/R	0.687	0.689	0.002

*NO ATTEMPT WAS MADE TO FIT THE MODEL TO THE OBSERVATIONS AT THESE WAVELENGTHS.

TABLE 17

MISCELLANEOUS CONTRIBUTION TABLES

NGC 7078 M15 V= 6.27 DISTANCE MODULUS= 15.50

COMPONENT	INTRINSIC PARAMETERS			% CONTRIBUTION TO		
	V	MASS	M/L_v	V LIGHT	MASS	NUMBER
HB 1	1.15	0.70	2.45E-02	2.650	0.330	0.296
HB 2	0.75	0.70	1.69E-02	2.600	0.224	0.201
HB 3	0.57	0.70	1.44E-02	3.829	0.279	0.251
HB 4	0.26	0.70	1.08E-02	0.641	0.035	0.032
HB 5	-0.64	0.70	4.71E-03	1.229	0.029	0.026
GI E 1	-0.74	0.70	4.30E-03	3.076	0.067	0.060
GI E 2	-0.97	0.70	3.48E-03	7.138	0.126	0.113
GI E 3	-1.23	0.70	2.74E-03	6.517	0.090	0.081
GI E 4	-1.71	0.70	1.76E-03	5.650	0.050	0.045
GI E 5	-2.24	0.70	1.08E-03	5.411	0.030	0.027
GI E 6	-2.57	0.70	7.96E-04	2.015	0.008	0.007
SG EE 1	3.34	0.70	1.84E-01	10.050	9.391	8.449
SG EE 2	3.21	0.70	1.63E-01	7.923	6.568	5.909
SG EE 3	1.86	0.70	4.71E-02	7.305	1.747	1.571
SG E 4	-0.11	0.70	7.68E-03	6.575	0.256	0.230
SG E 5	-0.69	0.70	4.50E-03	5.350	0.122	0.110
SD EE 1	4.36	0.70	4.71E-01	8.348	19.958	17.957
SD EE 2	4.92	0.63	7.10E-01	5.793	20.878	20.871
SD EE 3	5.05	0.62	7.88E-01	5.372	21.476	21.815
SD EE 4	5.68	0.55	1.25E 00	2.226	14.102	16.147
SD EE 5	6.55	0.48	2.43E 00	0.238	2.930	3.844
SD E 6	7.26	0.42	4.09E 00	0.063	1.304	1.956
SD M 6	7.66	0.40	5.62E 00	0.0	0.0	0.0
SD M 7	8.02	0.38	7.44E 00	0.0	0.0	0.0

MODEL PARAMETERS: E(B-V)= 0.12 NUMBER OF STARS> 1.27E 05 MASS> 7.99E 04 M/L_v> 1.97E-01

FIGURE 7

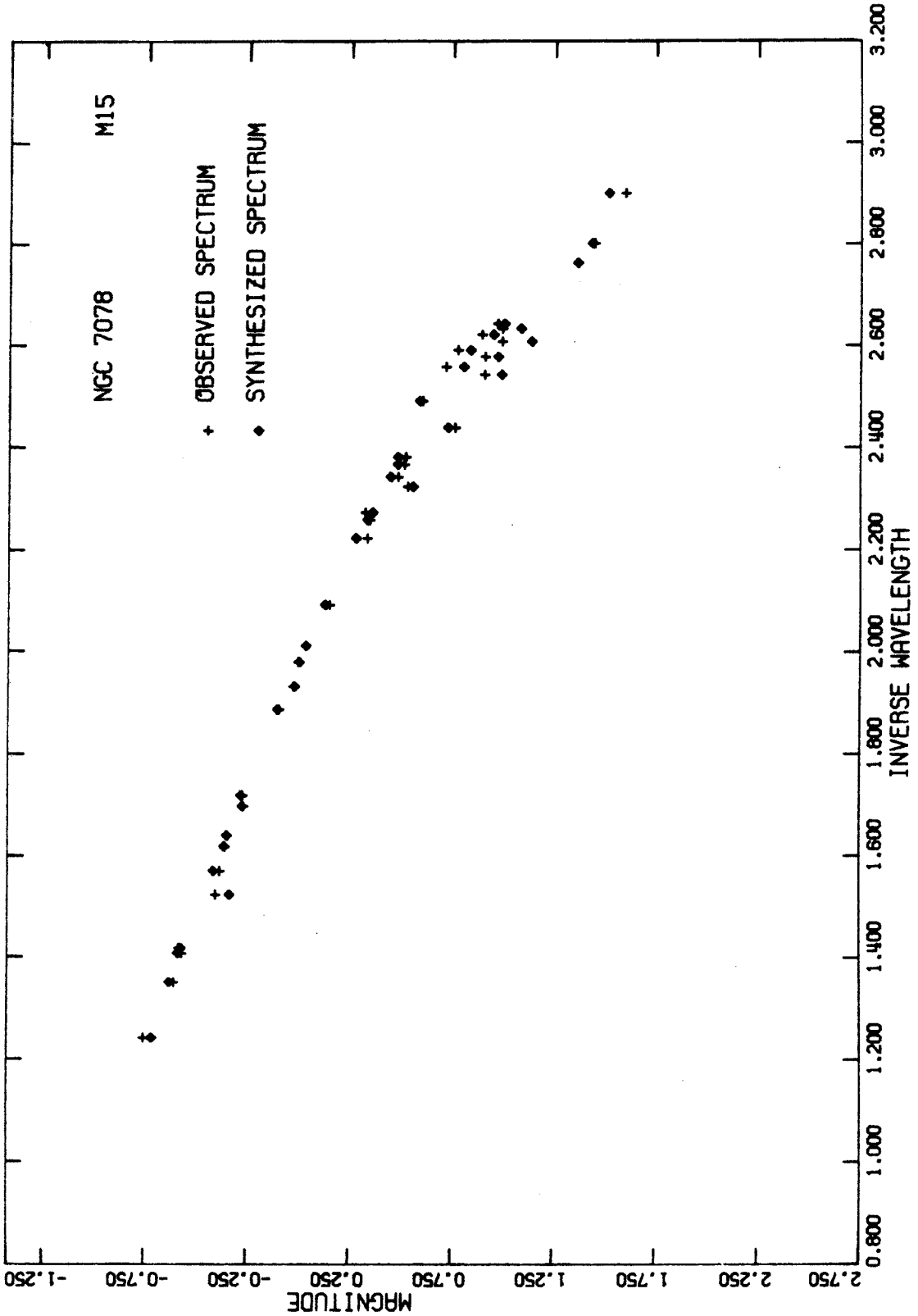
NGC 7078
M15
OBSERVED SPECTRUM
SYNTHESIZED SPECTRUM
MAGNITUDE
INVERSE WAVELENGTH
-1.250
-0.750
-0.250
0.250
0.750
1.250
1.750
2.250
2.750
0.800
1.000
1.200
1.400
1.600
1.800
2.000
2.200
2.400
2.600
2.800
3.000
3.200

believed that spectral degradation from the extended sources is responsible for this problem.

The model luminosity function agrees with the color-magnitude diagram of Sandage, Katem, and Kristian (1968) except along the blue horizontal branch. Subtraction of RR Lyrae variables from the model (they are excluded from the diagram) produces agreement at the red end of the blue branch. The disagreement at the blue tip of the branch may indicate a substantial number of blue stars in the cluster fainter than V = 17.0, the limiting magnitude of the diagram of Sandage et. al. Such a "plunging" blue extension of the horizontal branch is present in M13.

Late subdwarfs could not be successfully included in the model. This is not believed to be a result of an actual absence of subdwarfs in the cluster, but rather is interpreted as an indication that the metal deficiencies in the available mean stellar types are not so great as in M15. M15 has a metal content similar to M92 which has a logarithmic metal deficiency of [-2.2] (Helfer et al. 1959). This is a more extreme under-abundance than is observed in the stars from which the late subdwarf mean stellar types were derived.

M92

The adopted M92 model is described in Tables 18 and 19 and in Figure 8. Model fluxes differ from observed fluxes by mean values of 2.5

TABLE 18

NGC 6341 M92

COMPARISON OF OBSERVED AND SYNTHESIZED SPECTRA

FLUXES

LAMBDA	OBSERVED	SYNTHESIZED	PCT. DIFF.
3448.	2.640E-01	2.775E-01	4.991
3570.	2.816E-01	2.947E-01	4.560
3620.	3.107E-01	3.130E-01	0.731
3784.	4.426E-01	4.354E-01	-1.635
3798.	4.487E-01	4.006E-01	-11.345
3815.	4.764E-01	4.620E-01	-3.082
3835.	4.317E-01	3.855E-01	-11.323
3860.	5.365E-01	5.094E-01	-5.193
3880.	4.393E-01	4.471E-01	1.757
3910.	5.425E-01	5.254E-01	-3.197
3933.	4.682E-01	4.528E-01	-3.341
4015.	6.098E-01	6.290E-01	3.090
4101.	5.205E-01	5.397E-01	3.625
4200.	6.528E-01	6.822E-01	4.393
4226.	6.552E-01	6.837E-01	4.247
4270.	6.918E-01	7.030E-01	1.598
4305.	6.717E-01	6.469E-01	-3.766
4400.	7.413E-01	7.551E-01	1.836
4430.	7.663E-01	7.675E-01	0.161
4500.	7.914E-01	8.018E-01	1.299
4780.	8.694E-01	9.048E-01	3.995
4970.	9.663E-01	9.726E-01	0.440
5050.	1.000E 00	9.964E-01	-0.361
5175.	1.010E 00	1.011E 00	0.092
5300.	1.056E 00	1.084E 00	2.607
5820.	1.193E 00	1.248E 00	4.433
5892.	1.211E 00	1.229E 00	1.486
6100.	1.328E 00	1.314E 00	-1.040
6180.	1.323E 00	1.328E 00	0.349
6370.	1.413E 00	1.385E 00	-1.997
* 6564.	1.401E 00	1.284E 00	-8.711
7050.	1.555E 00	1.567E 00	0.796
7100.	1.608E 00	1.585E 00	-1.462
7400.	1.683E 00	1.636E 00	-2.792
8050.	1.690E 00	1.741E 00	2.966

LINE INDICES

NAME	OBSERVED	SYNTHESIZED	DIFFERENCE
H 3798	0.980	0.895	-0.085
H 3835	0.859	0.798	-0.060
CN 3860	1.058	1.036	-0.022
CN 3880	0.843	0.886	0.043
CAII3933	0.841	0.827	-0.014
H 4101	0.817	0.826	0.009
CN 4200	0.976	1.000	0.024
CAI 4226	0.967	0.991	0.023
CH 4300	0.953	0.903	-0.050
IS 4430	1.013	0.998	-0.015
MGH 4780	0.972	1.007	0.035
TIO 4970	1.000	1.006	0.006
MGI 5175	0.982	0.972	-0.010
NAII5892	0.987	0.972	-0.015
TIO 6180	0.978	0.994	0.016
H 6564	0.962	0.893	-0.069
TIO 7100	1.023	1.005	-0.018

CONTINUUM INDICES

U/B	0.413	0.417	0.004
B/V	0.637	0.625	-0.012
V/R	0.695	0.728	0.033

*NO ATTEMPT WAS MADE TO FIT THE MODEL TO THE OBSERVATIONS AT THESE WAVELENGTHS.

TABLE 19

MISCELLANEOUS CONTRIBUTION TABLES

NGC 6341 M92 V= 6.32 DISTANCE MODULUS= 14.62

COMPONENT	INTRINSIC PARAMETERS			% CONTRIBUTION TO		
	V	MASS	M/L_V	V LIGHT	MASS	NUMBER
HB 1	1.15	0.70	2.45E-02	4.592	0.546	0.507
HB 2	0.75	0.70	1.69E-02	2.681	0.221	0.205
HB 3	0.57	0.70	1.44E-02	1.881	0.131	0.122
HB 4	0.26	0.70	1.08E-02	0.0	0.0	0.0
HB 5	-0.64	0.70	4.71E-03	2.642	0.060	0.056
GI E 1	-0.74	0.70	4.30E-03	3.618	0.075	0.070
GI E 2	-0.97	0.70	3.48E-03	3.563	0.060	0.056
GI E 3	-1.23	0.70	2.74E-03	4.874	0.065	0.060
GI E 4	-1.71	0.70	1.76E-03	5.734	0.049	0.045
GI E 5	-2.24	0.70	1.08E-03	9.819	0.051	0.048
GI E 6	-2.57	0.70	7.96E-04	7.339	0.028	0.026
SG EE 1	3.34	0.70	1.84E-01	10.242	9.158	8.496
SG EE 2	3.21	0.70	1.63E-01	6.915	5.485	5.089
SG EE 3	1.86	0.70	4.71E-02	3.436	0.786	0.729
SG E 4	-0.11	0.70	7.68E-03	3.922	0.146	0.136
SG E 5	-0.69	0.70	4.50E-03	2.820	0.062	0.057
SD EE 1	4.36	0.70	4.71E-01	8.689	19.880	18.441
SD EE 2	4.92	0.63	7.10E-01	8.350	28.799	29.684
SD EE 3	5.05	0.62	7.88E-01	8.700	33.283	34.859
SD EE 4	5.68	0.55	1.25E 00	0.184	1.114	1.315
SD EE 5	6.55	0.48	2.43E 00	0.0	0.0	0.0
SD E 6	7.26	0.42	4.09E 00	0.0	0.0	0.0
SD M 6	7.66	0.40	5.62E 00	0.0	0.0	0.0
SD M 7	8.02	0.38	7.44E 00	0.0	0.0	0.0

MODEL PARAMETERS: E(B-V)= 0.02 NUMBER OF STARS> 5.46E 04 MASS> 3.55E 04 M/L_V> 2.06E-01

FIGURE 8

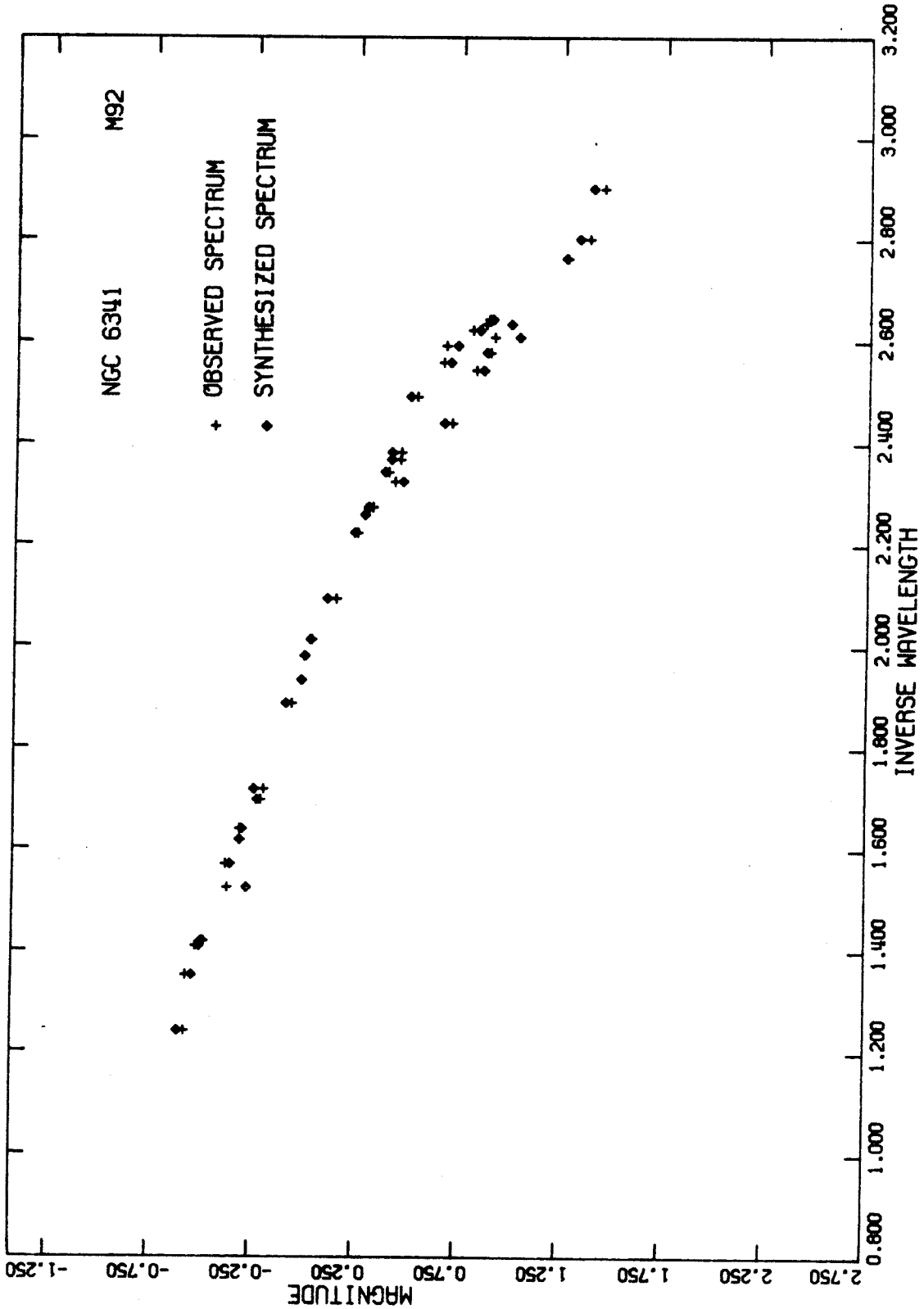
NGC 6341
M92
OBSERVED SPECTRUM
SYNTHESIZED SPECTRUM
MAGNITUDE
INVERSE WAVELENGTH
-1.250
-0.750
-0.250
0.250
0.750
1.250
1.750
2.250
2.750
0.800
1.000
1.200
1.400
1.600
1.800
2.000
2.200
2.400
2.600
2.800
3.000
3.200

per cent to the red of the Balmer jump and 3.4 per cent to the blue if fluxes at $\lambda\lambda$3798 and 3835 are ignored. Regions and features of disagreement are the same as for M15 for the same reasons.

The model luminosity function can be compared with the published function of Hartwick (1970). In both cases the ratio of the number of red-giants with absolute magnitude brighter than M = - 0.70 to the number of subdwarfs with absolute magnitudes in the range M_V = 3.85 to 4.98 is 0.0064. (The agreement in the second significant figure can be regarded as fortuitous.)

The model color-magnitude distribution can also be compared with the diagram of Sandage and Walker (1966). Agreement is within expected statistical accuracies except along the blue horizontal branch. The reasons for disagreement in this region are the same as those given for M15.

As with M15 late subdwarfs have been excluded from the model in order to promote the best possible agreement between observed and model spectra.

Schwarzchild and Bernstein (1955) give a mass $M = 1.4 \pm 0.7 \times 10^5 M_\odot$ and a mass-to-light ratio $M/L = 0.8 \pm 0.4\ M_\odot/L_\odot$ for M92. These values are compatible with the lower limits established from the adopted model. The model mass and mass-to-light ratio could be raised to these values with only small effects on the model spectrum if large numbers of late subdwarfs were added to the model. This fact is taken

as evidence that the shortage of late subdwarfs in the model reflects the inadequacy of the available mean stellar types rather than the luminosity function of the cluster.

M31: MIV

The weak-lined cluster MIV is described in Tables 20 and 21 and Figure 9. Mean residuals, when the model is compared with observations, are 2.4 per cent in the extreme ultraviolet and 3.2 elsewhere (excluding λ3784).

Substantial disagreements between the model and the observations at several wavelengths are believed to be the result of observational errors. MIV was observed through thin cirrus clouds at a large zenith angle (secant z $\simeq$ 1.7) and therefore probably has the largest errors in its energy distribution of any of the ten aggregate objects. (Correction of the MIV energy distribution for the effects of the clouds is given in Appendix A.)

The large discrepancy between the model and the observed CaII 3933 indices (ΔI = 0.08) is the result of moderate, but compounding, discrepancies in the λ3910 and λ3933 bandpasses. Over most of the visual region of the spectrum, model spectral features are somewhat stronger than observed features. This is probably the result of the smoothing process used to remove effects of gray cloud absorption.

Despite the observational difficulties associated with the MIV

TABLE 20

M31 MIV

COMPARISON OF OBSERVED AND SYNTHESIZED SPECTRA

FLUXES

LAMBDA	OBSERVED	SYNTHESIZED	PCT. DIFF.
3448.	2.601E-01	2.514E-01	-3.397
3570.	2.800E-01	2.700E-01	-3.658
3620.	2.879E-01	2.879E-01	0.000
* 3784.	3.532E-01	4.163E-01	16.400
* 3798.	0.0	3.811E-01	0.0
3815.	4.123E-01	4.441E-01	7.718
* 3835.	0.0	3.637E-01	0.0
3860.	4.853E-01	4.971E-01	2.398
3880.	4.450E-01	4.302E-01	-3.400
3910.	5.485E-01	5.118E-01	-6.937
3933.	4.180E-01	4.397E-01	5.045
4015.	6.240E-01	6.231E-01	-0.143
4101.	5.086E-01	5.254E-01	3.244
4200.	6.668E-01	6.806E-01	2.046
4226.	6.842E-01	6.798E-01	-0.650
4270.	6.893E-01	6.989E-01	1.383
4305.	6.564E-01	6.308E-01	-3.991
4400.	7.165E-01	7.527E-01	4.935
4430.	7.870E-01	7.715E-01	-1.997
4500.	8.341E-01	8.098E-01	-2.948
4780.	9.754E-01	9.195E-01	-5.908
4970.	1.025E 00	9.985E-01	-2.633
5050.	1.000E 00	1.026E 00	2.553
5175.	1.073E 00	1.042E 00	-3.021
5300.	1.146E 00	1.127E 00	-1.663
5820.	1.321E 00	1.318E 00	-0.201
5892.	1.340E 00	1.306E 00	-2.599
6100.	1.391E 00	1.399E 00	0.571
6180.	1.400E 00	1.413E 00	0.948
6370.	1.430E 00	1.482E 00	3.606
6564.	1.396E 00	1.372E 00	-1.722
7050.	1.641E 00	1.705E 00	3.825
7100.	1.565E 00	1.727E 00	9.895
7400.	1.783E 00	1.790E 00	0.379
8050.	2.061E 00	1.936E 00	-6.211

LINE INDICES

NAME	OBSERVED	SYNTHESIZED	DIFFERENCE
CN 3860	1.021	1.045	0.024
CN 3880	0.883	0.878	-0.004
CAII3933	0.740	0.821	0.081
H 4101	0.787	0.810	0.023
CN 4200	0.993	1.004	0.011
CAI 4226	1.009	0.992	-0.016
CH 4305	0.942	0.884	-0.058
FS 4430	1.048	1.003	-0.046
MGH 4780	1.062	1.003	-0.059
TIO 4970	1.051	1.006	-0.045
MGI 5175	1.002	0.968	-0.034
NAII5892	1.001	0.975	-0.026
TIO 6180	0.998	0.993	-0.005
H 6564	0.936	0.887	-0.049
TIO 7100	0.942	1.006	0.064

CONTINUUM INDICES

U/B	0.404	0.384	-0.020
B/V	0.570	0.594	0.024
V/R	0.720	0.700	-0.021

*NO ATTEMPT WAS MADE TO FIT THE MODEL TO THE OBSERVATIONS AT THESE WAVELENGTHS.

TABLE 21

MISCELLANEOUS CONTRIBUTION TABLES

M31 MIV V=15.06 DISTANCE MODULUS= 24.65

COMPONENT	INTRINSIC PARAMETERS			% CONTRIBUTION TO		
	V	MASS	M/L_V	V-LIGHT	MASS	NUMBER
HB 1	1.15	0.70	2.45E-02	4.763	0.566	0.468
HB 2	0.75	0.70	1.69E-02	5.164	0.424	0.351
HB 3	0.57	0.70	1.44E-02	4.464	0.311	0.257
HB 4	0.26	0.70	1.08E-02	1.615	0.084	0.070
HB 5	-0.64	0.70	4.71E-03	0.677	0.015	0.013
GI E 1	-0.74	0.70	4.30E-03	5.008	0.104	0.086
GI E 2	-0.97	0.70	3.48E-03	6.341	0.107	0.088
GI E 3	-1.23	0.70	2.74E-03	4.887	0.065	0.054
GI E 4	-1.71	0.70	1.76E-03	4.596	0.039	0.032
GI E 5	-2.24	0.70	1.08E-03	4.462	0.023	0.019
GI E 6	-2.57	0.70	7.96E-04	4.489	0.017	0.014
SG EE 1	3.34	0.70	1.84E-01	7.467	6.667	5.519
SG EE 2	3.21	0.70	1.63E-01	6.685	5.295	4.383
SG EE 3	1.86	0.70	4.71E-02	6.744	1.541	1.275
SG E 4	-0.11	0.70	7.68E-03	6.951	0.259	0.214
SG E 5	-0.69	0.70	4.50E-03	6.544	0.151	0.125
SD EE 1	4.36	0.70	4.71E-01	5.322	12.157	10.063
SD EE 2	4.92	0.63	7.10E-01	4.514	15.547	14.299
SD EE 3	5.05	0.62	7.88E-01	4.340	16.603	15.516
SD EE 4	5.68	0.55	1.25E 00	3.097	18.750	19.753
SD EE 5	6.55	0.48	2.43E 00	1.110	13.067	15.773
SD E 6	7.26	0.42	4.09E 00	0.221	4.360	6.042
SD M 6	7.66	0.40	5.62E 00	0.120	3.274	4.743
SD M 7	8.02	0.38	7.44E 00	0.015	0.552	0.842

MODEL PARAMETERS: E(B-V)= 0.11 NUMBER OF STARS> 2.01E 05 MASS> 1.16E 05 M/L_V> 2.06E-01

FIGURE 9

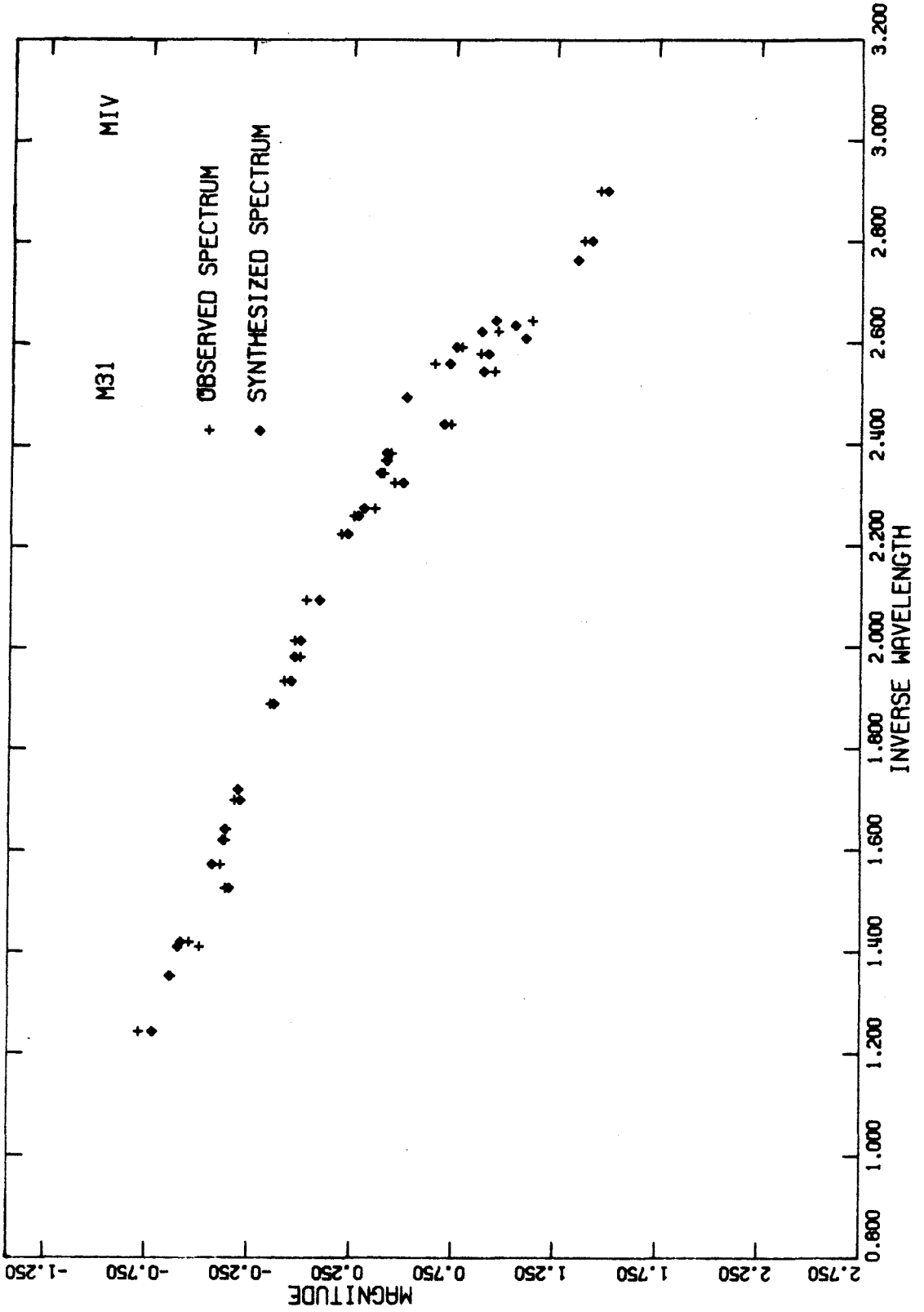
M31
MIV
OBSERVED SPECTRUM
SYNTHESIZED SPECTRUM
MAGNITUDE
INVERSE WAVELENGTH
-1.250
-0.750
-0.250
0.250
0.750
1.250
1.750
2.250
2.750
0.800
1.000
1.200
1.400
1.600
1.800
2.000
2.200
2.400
2.600
2.800
3.000
3.200

energy distribution, it is believed that its model is sufficiently accurate to support the conclusion that it has a metal content similar to M15 and M92. Its horizontal branch is probably even bluer than the branches in these two clusters. An apparent shortage of subdwarfs in the cluster may or may not be real. More accurate observations are needed to resolve the question.

M31: H12

The spectrum of H12 is well reproduced by a model consisting of mild population II objects found near the sun. In addition to these stars a few population I O and B main sequence stars have been tried in some models as was done by Spinrad and Schweizer (1972) in their models for B282 and MII. The best fitting model contains a 1.4 per cent light contribution from O stars. Such a small contribution from hot stars is not regarded as firm evidence that they exist in the cluster.

The adopted H12 model fits the observed spectrum with a mean accuracy of 2.4 per cent on both sides of the Balmer jump (excluding the heavily blanketed point λ3784). The excessive model flux in the region $\lambda\lambda$3700 through 4000 and the weakness of the K-line in the model indicate that the cluster has a slightly higher metal content than the mean stellar types of the model.

Tables 22 and 23 and Figure 10 describe the adopted H12 model.

TABLE 22

M31 H12

COMPARISON OF OBSERVED AND SYNTHESIZED SPECTRA

FLUXES

	LAMBDA	OBSERVED	SYNTHESIZED	PCT. DIFF.
	3448.	2.239E-01	2.146E-01	-4.234
	3570.	2.218E-01	2.180E-01	-1.742
	3620.	2.432E-01	2.406E-01	-1.090
*	3784.	2.979E-01	3.315E-01	10.691
*	3796.	0.0	3.045E-01	0.0
	3815.	3.076E-01	3.176E-01	3.206
*	3835.	0.0	2.521E-01	0.0
	3860.	3.203E-01	3.330E-01	3.879
	3880.	3.079E-01	3.053E-01	-0.860
	3910.	3.715E-01	3.811E-01	2.544
	3933.	2.443E-01	2.637E-01	7.608
	4015.	5.171E-01	5.115E-01	-1.100
	4101.	4.617E-01	4.808E-01	4.042
	4200.	5.435E-01	5.541E-01	1.936
	4226.	5.878E-01	5.623E-01	-4.427
	4270.	5.829E-01	5.756E-01	-1.270
	4305.	5.096E-01	4.900E-01	-3.905
	4400.	6.761E-01	6.530E-01	-3.471
	4430.	7.073E-01	6.964E-01	-1.548
	4500.	7.386E-01	7.708E-01	4.270
	4780.	8.726E-01	8.962E-01	2.668
*	4970.	0.0	9.665E-01	0.0
	5050.	1.000E 00	9.971E-01	-0.292
	5175.	1.025E 00	9.665E-01	-5.890
	5300.	1.132E 00	1.129E 00	-0.267
	5820.	1.339E 00	1.371E 00	2.383
	5892.	1.307E 00	1.305E 00	-0.176
	6100.	1.426E 00	1.451E 00	1.777
	6180.	1.420E 00	1.430E 00	0.682
	6370.	1.509E 00	1.538E 00	1.867
	6564.	1.518E 00	1.460E 00	-3.894
	7050.	1.811E 00	1.816E 00	0.251
	7100.	1.765E 00	1.773E 00	-0.687
	7400.	1.930E 00	1.933E 00	0.147
*	8050.	0.0	2.142E 00	0.0

LINE INDICES

NAME	OBSERVED	SYNTHESIZED	DIFFERENCE
CN 3860	0.950	0.959	0.010
CN 3880	0.878	0.847	-0.031
CAII3933	0.607	0.645	0.038
H 4101	0.857	0.903	0.046
CN 4200	0.963	0.994	0.031
CAI 4226	1.029	0.997	-0.032
CH 4305	0.839	0.822	-0.017
FS 4430	1.018	1.013	-0.005
MGH 4780	1.009	1.016	0.008
MGI 5175	0.963	0.910	-0.053
NAII5892	0.960	0.937	-0.023
TIO 6180	0.979	0.968	-0.011
H 6564	0.952	0.903	-0.049
TIO 7100	0.976	0.967	-0.009

CONTINUUM INDICES

U/B	0.369	0.373	0.004
B/V	0.509	0.491	-0.018
V/R	0.661	0.667	0.007

*NO ATTEMPT WAS MADE TO FIT THE MODEL TO THE OBSERVATIONS AT THESE WAVELENGTHS.

TABLE 23

MISCELLANEOUS CONTRIBUTION TABLES

M31 H12 V=14.24 DISTANCE MODULUS= 24.65

COMPONENT	INTRINSIC PARAMETERS			% CONTRIBUTION TO		
	V	MASS	M/L_V	V-LIGHT	MASS	NUMBER
0 V	-5.00	30.00	3.64E-03	1.364	0.016	0.000
80-4 V	-2.50	9.00	1.09E-02	0.001	0.000	0.000
HB 2	1.01	0.70	2.15E-02	0.0	0.0	0.0
HB 3	0.91	0.70	1.96E-02	0.379	0.024	0.020
HB 4	0.75	0.70	1.69E-02	1.650	0.090	0.074
HB 5	-0.15	0.70	7.40E-03	6.724	0.160	0.132
GI M 1	0.63	0.70	1.52E-02	7.994	0.390	0.321
GI M 2	0.35	0.70	1.17E-02	8.522	0.321	0.265
GI M 3	0.28	0.70	1.10E-02	4.287	0.151	0.125
GI M 4	-0.47	0.70	5.51E-03	3.668	0.065	0.054
GI M 5	-1.60	0.70	1.95E-03	2.597	0.016	0.013
GI M 6	-2.00	0.70	1.35E-03	2.222	0.010	0.008
GI M 7	-2.20	0.70	1.12E-03	1.542	0.006	0.005
SG M 1	3.86	0.70	2.97E-01	7.666	7.317	6.032
SG M 2	3.81	0.70	2.84E-01	6.780	6.180	5.096
SG M 3	3.00	0.70	1.35E-01	5.576	2.410	1.987
SG M 4	1.08	0.70	2.30E-02	8.375	0.618	0.509
SG M 5	0.53	0.70	1.38E-02	5.291	0.235	0.194
SD M 1	3.60	0.70	2.34E-01	6.573	4.938	4.071
SD M 2	4.68	0.70	6.33E-01	5.286	10.738	8.853
SD M 3	4.82	0.66	6.99E-01	5.982	13.426	11.397
SD M 4	5.70	0.58	1.34E 00	3.580	15.417	15.341
SD M 5	6.15	0.54	1.89E 00	2.651	16.090	17.196
SD M 6	7.37	0.44	4.74E 00	0.856	12.713	16.675
SD M 7	7.64	0.43	5.94E 00	0.455	8.668	11.633

MODEL PARAMETERS: E(B-V)= 0.11 NUMBER OF STARS> 6.49E 05 MASS> 3.74E 05 M/L_V> 3.11E-01

FIGURE 10

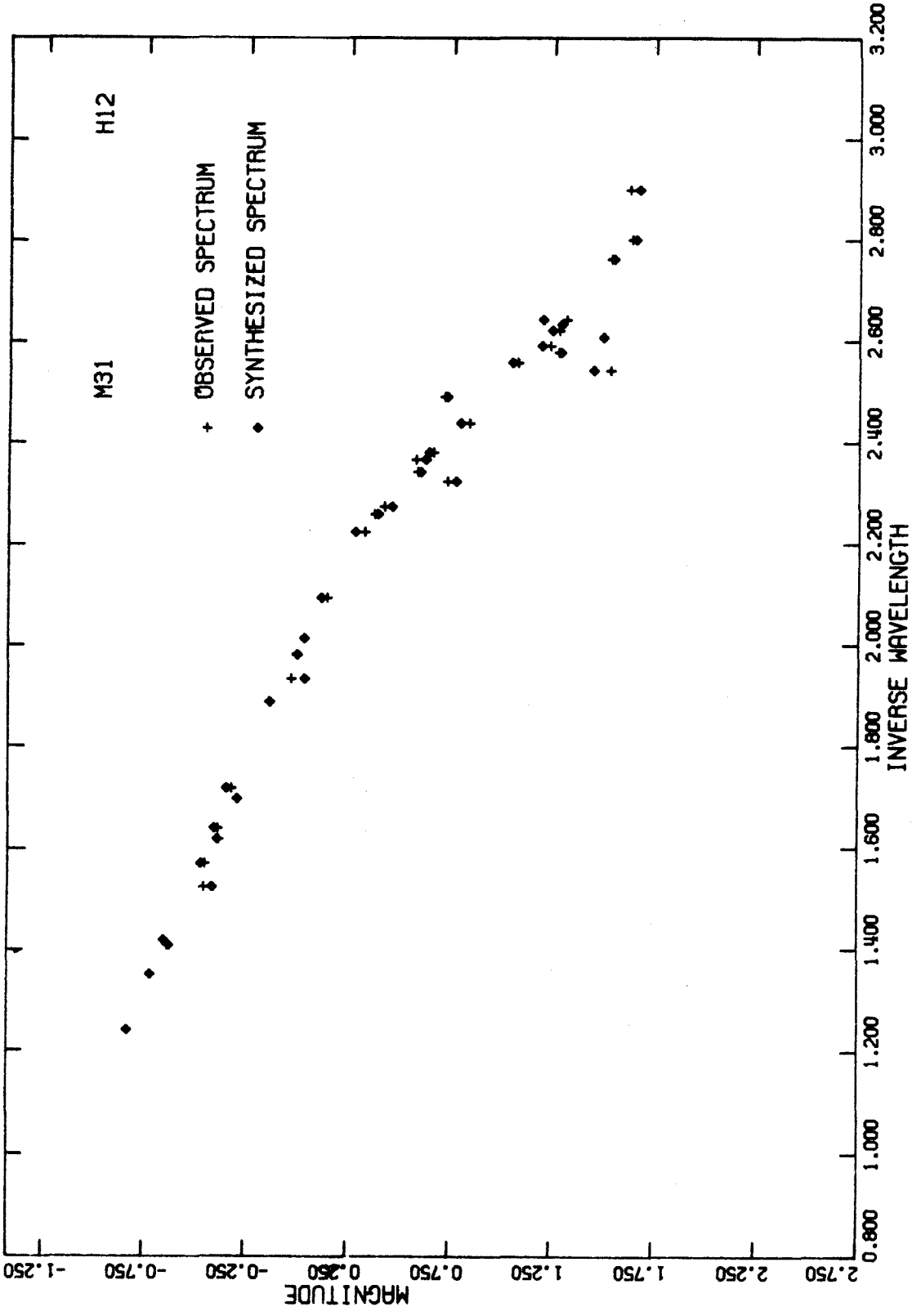
M31
H12
OBSERVED SPECTRUM
SYNTHESIZED SPECTRUM
MAGNITUDE
INVERSE WAVELENGTH
-1.250
-0.750
-0.250
0.250
0.750
1.250
1.750
2.250
2.750
0.800
1.000
1.200
1.400
1.600
1.800
2.000
2.200
2.400
2.600
2.800
3.000
3.200

M31: H140

Tables 24 and 25 and Figure 11 provide descriptions of the best H140 model. As with H12 a small amount of light from O V stars improves the model fit slightly. If $\lambda\lambda$3620 and 3784 are ignored the mean residuals between the model and observed fluxes are 3.8 per cent shortward of the Balmer jump and 2.8 per cent longward. The large discrepancy at λ3620 is believed to be a result of a bad datum. Excessive λ3784 flux in the model is probably a result of blanketing in the cluster. The relative weakness of the observed G-band (0.92) is attributed to an observational error since other features are relatively strong.

Redward of λ5000 H140 has an energy distribution almost identical to that of H12. However H140 is about one-tenth of a magnitude brighter than H12 in the blue and ultraviolet spectral regions. The best fitting model for H140 is similar to that for H12 except that it has a rather blue horizontal branch similar to that of M5.

M31: H55

Despite its apparent remoteness from the disk of M31, H55 has very strong spectral features (van den Bergh assigns L = +11). Its spectrum could not be satisfactorily reproduced with the mild population II sequence. Even the best model composed of O'Connell's population I sequence, which includes "super-metal-rich" K giants and

TABLE 24

M31 H140

COMPARISON OF OBSERVED AND SYNTHESIZED SPECTRA

FLUXES

	LAMBDA	OBSERVED	SYNTHESIZED	PCT. DIFF.
	3448.	2.524E-01	2.404E-01	-4.860
	3570.	2.500E-01	2.434E-01	-2.682
*	3620.	3.062E-01	2.653E-01	-14.296
*	3784.	3.248E-01	3.742E-01	14.139
*	3798.	0.0	3.382E-01	0.0
	3815.	3.516E-01	3.720E-01	5.658
*	3835.	0.0	2.884E-01	0.0
	3860.	3.887E-01	3.999E-01	2.855
	3880.	3.364E-01	3.552E-01	5.437
	3910.	4.278E-01	4.434E-01	3.580
	3933.	3.116E-01	3.363E-01	7.611
	4015.	6.009E-01	5.805E-01	-3.453
	4101.	5.058E-01	5.084E-01	0.501
	4200.	6.223E-01	6.223E-01	-0.008
	4226.	6.368E-01	6.276E-01	-1.446
	4270.	6.257E-01	6.421E-01	2.585
	4305.	6.015E-01	5.569E-01	-7.695
	4400.	7.211E-01	7.133E-01	-1.087
	4430.	7.551E-01	7.549E-01	-0.024
	4500.	8.806E-01	8.250E-01	-6.522
	4780.	9.550E-01	9.388E-01	-1.707
*	4970.	0.0	1.003E 00	0.0
	5050.	1.000E 00	1.030E 00	2.999
	5175.	1.039E 00	9.985E-01	-4.019
	5300.	1.112E 00	1.156E 00	3.862
	5820.	1.374E 00	1.380E 00	0.396
	5892.	1.298E 00	1.313E 00	1.163
	6100.	1.426E 00	1.454E 00	1.983
	6180.	1.369E 00	1.430E 00	4.373
	6370.	1.532E 00	1.535E 00	0.179
	6564.	1.485E 00	1.438E 00	-3.159
	7050.	1.811E 00	1.799E 00	-0.671
	7100.	1.795E 00	1.752E 00	-2.438
	7400.	1.934E 00	1.913E 00	-1.065
	8050.	2.084E 00	2.111E 00	1.302

LINE INDICES

NAME	OBSERVED	SYNTHESIZED	DIFFERENCE
CN 3860	1.005	0.987	-0.017
CN 3880	0.835	0.845	0.011
CAII3933	0.671	0.712	0.041
H 4101	0.829	0.846	0.017
CN 4200	1.004	0.995	-0.009
CAI 4226	1.024	0.994	-0.030
CH 4305	0.924	0.843	-0.082
FE 4430	0.984	1.012	0.028
MGH 4780	1.012	1.013	0.001
MGI 5175	0.985	0.914	-0.071
NAI5892	0.935	0.938	0.003
TIO 6180	0.940	0.967	0.028
H 6564	0.922	0.894	-0.028
TIO 7100	0.981	0.965	-0.017

CONTINUUM INDICES

U/B	0.413	0.375	-0.038
B/V	0.542	0.535	-0.007
V/R	0.664	0.683	0.019

*NO ATTEMPT WAS MADE TO FIT THE MODEL TO THE OBSERVATIONS AT THESE WAVELENGTHS.

TABLE 25

MISCELLANEOUS CONTRIBUTION TABLES

M31 H140 V=15.16 DISTANCE MODULUS= 24.65

COMPONENT	INTRINSIC PARAMETERS			% CONTRIBUTION TO		
	V	MASS	M/L_V	V-LIGHT	MASS	NUMBER
D V	-5.00	30.00	3.64E-03	1.892	0.024	0.000
BO-4 V	-2.50	9.00	1.09E-02	0.002	0.000	0.000
HB 2	1.01	0.70	2.15E-02	1.852	0.140	0.118
HB 3	0.91	0.70	1.96E-02	5.896	0.407	0.341
HB 4	0.75	0.70	1.69E-02	0.055	0.003	0.003
HB 5	-0.15	0.70	7.40E-03	3.627	0.094	0.079
GI M 1	3.63	0.70	1.52E-02	6.101	0.326	0.273
GI M 2	0.35	0.70	1.17E-02	6.017	0.248	0.208
GI M 3	0.26	0.70	1.10E-02	4.755	0.184	0.154
GI M 4	-0.47	0.70	5.51E-03	2.967	0.056	0.046
GI M 5	-1.60	0.70	1.95E-03	3.196	0.022	0.018
GI M 6	-2.00	0.70	1.35E-03	1.929	0.009	0.008
GI M 7	-2.20	0.70	1.12E-03	1.725	0.007	0.006
SG M 1	3.86	0.70	2.97E-01	6.651	6.961	5.832
SG M 2	3.81	0.70	2.84E-01	5.180	5.178	4.338
SG M 3	3.00	0.70	1.35E-01	7.088	3.360	2.815
SG M 4	1.08	0.70	2.30E-02	7.064	0.571	0.479
SG M 5	0.53	0.70	1.38E-02	6.668	0.325	0.272
SD M 1	3.60	0.70	2.34E-01	10.490	8.641	7.239
SD M 2	4.68	0.70	6.33E-01	4.487	9.993	8.372
SD M 3	4.82	0.68	6.99E-01	5.984	14.729	12.703
SD M 4	5.70	0.58	1.34E 00	2.835	13.366	13.535
SD M 5	6.15	0.54	1.89E 00	2.432	16.185	17.577
SD M 6	7.37	0.44	4.74E 00	1.026	17.110	22.805
SD M 7	7.64	0.43	5.94E 00	0.097	2.037	2.778

MODEL PARAMETERS: E(B-V)= 0.11 NUMBER OF STARS> 2.50E 05 MASS> 1.46E 05 M/L_V> 2.84E-01

FIGURE 11

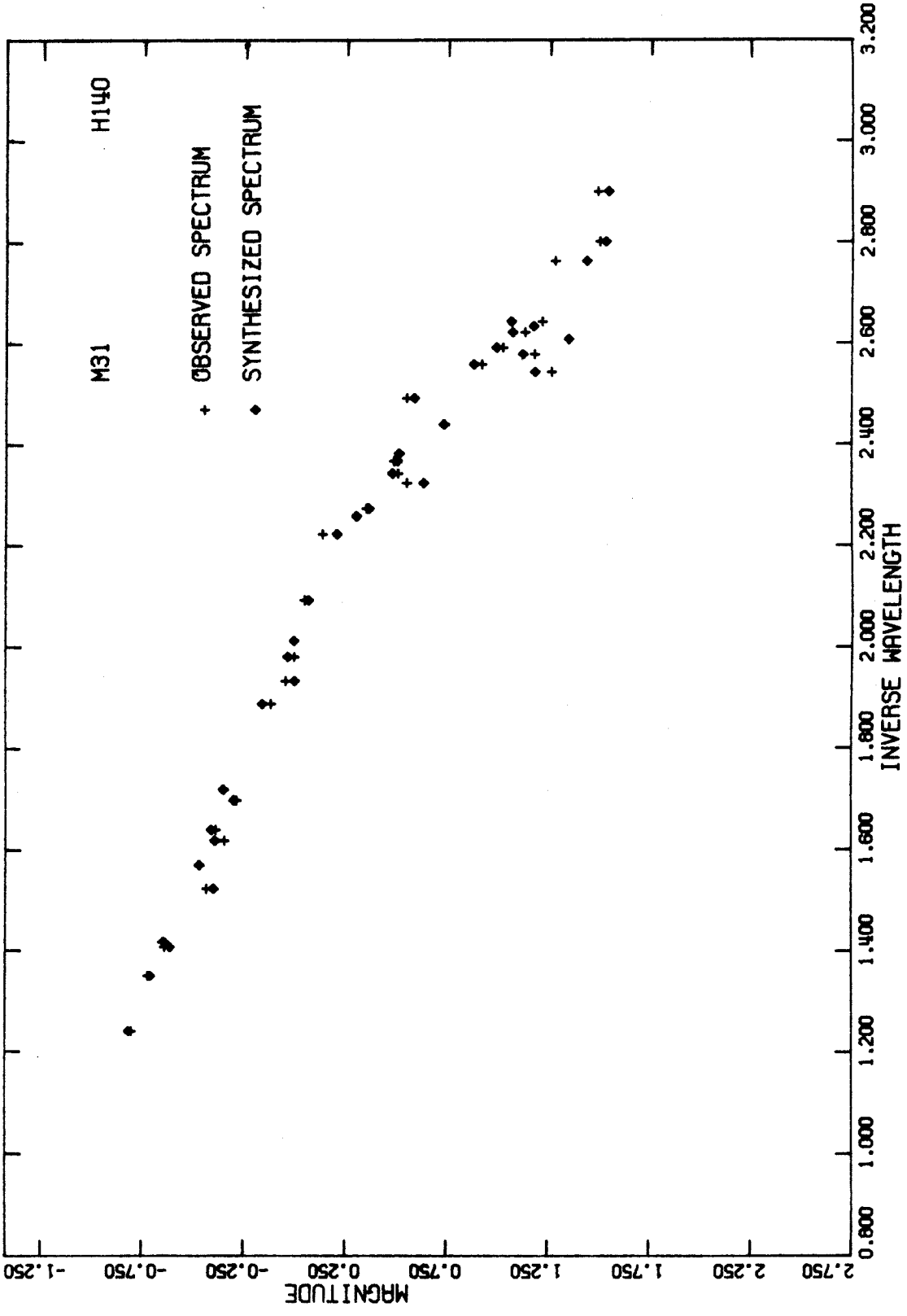
H140
M31
OBSERVED SPECTRUM
SYNTHESIZED SPECTRUM
MAGNITUDE
INVERSE WAVELENGTH
-1.250
-0.750
-0.250
0.250
0.750
1.250
1.750
2.250
2.750
0.800
1.000
1.200
1.400
1.600
1.800
2.000
2.200
2.400
2.600
2.800
3.000
3.200

subgiants, did not duplicate the observed strengths of the K- and D-lines. The strength of the cluster K-line is so great that the λ3910 sideband is depressed about twenty per cent by its blue wing. (λ3910 also serves as a sideband for the CN 3860 index; thus the observed index is about ten per cent too weak.)

Tables 26 and 27 and Figure 12 summarize the adopted H55 model. The agreement between model and observed fluxes is 4.2 per cent in the extreme ultraviolet (excluding λ3448, a probable observational error) and 3.0 per cent elsewhere (excluding $\lambda\lambda$3784, 3910, and 3933). O'Connell's data do not generally include the points $\lambda\lambda$3880, 4226, 4780, 4970, and 6564. Thus synthetic fluxes given for these wavelengths in Table 27 are not meaningful.

The H55 color-magnitude diagram has a heavily populated dwarf sequence and a lightly populated horizontal branch. The best model contains only a small contribution from population II horizontal-branch components HB 4 and HB 5; however late A and early F population I giants contribute about 5 per cent of the model V-light. These spectral types probably represent a horizontal branch too metal-rich to be duplicated by population II spectra. The color of the inferred horizontal branch is not clear since late A and early F giants have colors characteristic of the RR Lyrae gap.

The H55 model shows clearly that stars earlier than F0 have evolved away from the main sequence. Only a very small amount of

TABLE 26

M31 M55

COMPARISON OF OBSERVED AND SYNTHESIZED SPECTRA

FLUXES

LAMBDA	OBSERVED	SYNTHESIZED	PCT. DIFF.
* 3448.	1.893E-01	1.427E-01	-28.097
3570.	1.449E-01	1.502E-01	3.566
3620.	1.722E-01	1.806E-01	4.765
* 3784.	2.222E-01	2.764E-01	21.718
* 3798.	0.0	2.389E-01	0.0
3815.	2.519E-01	2.493E-01	-1.020
* 3835.	0.0	1.817E-01	0.0
3860.	2.662E-01	2.494E-01	-6.515
* 3880.	1.900E-01	5.955E-03	0.0
3910.	2.704E-01	3.250E-01	18.348
3933.	1.401E-01	2.013E-01	35.654
4015.	4.459E-01	4.624E-01	3.645
4101.	4.063E-01	4.252E-01	4.546
4200.	4.742E-01	4.879E-01	2.835
* 4226.	4.567E-01	9.316E-02	0.0
4270.	4.971E-01	5.165E-01	3.833
4305.	4.406E-01	4.231E-01	-4.055
4400.	6.565E-01	5.963E-01	-9.610
4430.	6.534E-01	6.451E-01	-1.281
4500.	7.132E-01	7.242E-01	1.530
* 4780.	9.489E-01	1.268E-02	0.0
* 4970.	1.001E 00	1.387E-02	0.0
5050.	1.000E 00	9.761E-01	-2.415
5175.	9.333E-01	8.973E-01	-3.927
5300.	1.162E 00	1.150E 00	-1.069
5820.	1.483E 00	1.442E 00	-2.646
5892.	1.297E 00	1.347E 00	3.820
6100.	1.560E 00	1.551E 00	-0.592
6180.	1.600E 00	1.529E 00	-4.524
6370.	1.641E 00	1.644E 00	0.135
* 6564.	1.631E 00	1.151E-01	0.0
7050.	1.920E 00	2.003E 00	4.269
7100.	1.916E 00	1.936E 00	1.012
7400.	2.202E 00	2.215E 00	0.587
8050.	2.585E 00	2.552E 00	-1.273

LINE INDICES

NAME	OBSERVED	SYNTHESIZED	DIFFERENCE
CN 3860	1.022	0.877	-0.145
CAII3933	0.456	0.569	0.113
H 4101	0.878	0.885	0.007
CN 4200	0.982	0.973	-0.009
CH 4305	0.818	0.787	-0.031
FE 4430	0.971	1.018	0.047
MGI 5175	0.865	0.846	-0.019
NAI5892	0.862	0.917	0.054
TIO 6180	1.009	0.968	-0.041
TIO 7100	0.978	0.952	-0.026

CONTINUUM INDICES

U/B	0.275	0.297	0.022
B/V	0.436	0.429	-0.007
V/R	0.642	0.614	-0.028

*NO ATTEMPT WAS MADE TO FIT THE MODEL TO THE OBSERVATIONS AT THESE WAVELENGTHS.

TABLE 27

MISCELLANEOUS CONTRIBUTION TABLES

M31 H55 V=15.56 DISTANCE MODULUS= 24.65

COMPONENT	INTRINSIC PARAMETERS			% CONTRIBUTION TO		
	V	MASS	M/L	V LIGHT	MASS	NUMBER
O V	-5.00	30.00	3.64E-03	0.0	0.0	0.0
B0-4 V	-2.50	9.00	1.09E-02	0.0	0.0	0.0
A5-9 V	2.30	1.70	1.72E-01	0.419	0.100	0.054
F0-5 V	3.10	1.40	2.95E-01	4.716	1.975	1.300
F6-9 V	4.20	1.20	6.97E-01	8.801	8.700	6.682
G0-5 V	4.90	1.00	1.11E 00	9.285	14.575	13.432
G6-9 V	5.60	0.85	1.79E 00	9.226	23.454	25.428
K0-2 V	6.10	0.80	2.67E 00	7.227	27.408	31.572
K3 V	6.80	0.75	3.97E 00	1.334	7.516	9.235
K5-7 V	7.90	0.56	1.02E 01	0.118	1.705	2.709
M0 4	0.72	1.40	3.30E-02	0.584	0.027	0.018
M0 5	-0.18	1.40	1.44E-02	0.658	0.013	0.009
G0-5 IV	3.00	1.40	2.69E-01	13.193	5.038	3.316
G6-9 IV	3.10	1.40	2.95E-01	8.860	3.710	2.442
K0-3 IV	3.20	1.40	3.24E-01	4.696	2.156	1.419
K0-3 IV SMR	3.20	1.40	3.24E-01	3.797	1.744	1.148
A5-9 III	1.20	1.40	5.13E-02	2.547	0.185	0.122
F0-5 III	1.60	1.40	7.42E-02	2.658	0.280	0.184
G5-9 III	1.50	1.40	6.76E-02	8.419	0.808	0.532
K0-3 III	0.90	1.40	3.89E-02	5.945	0.328	0.216
K0-3 III SMR	0.90	1.40	3.89E-02	3.549	0.196	0.129
K4-5 III	0.10	1.40	1.86E-02	1.051	0.028	0.018
K4-5 III SMR	0.10	1.40	1.86E-02	1.409	0.037	0.025
M4-5 III	-0.80	1.40	8.13E-03	0.639	0.007	0.005
M6-8 III	-1.00	1.40	6.76E-03	0.876	0.008	0.006

MODEL PARAMETERS: E(B-V)= 0.11 NUMBER OF STARS> 2.73E 05 MASS> 2.51E 05 M/L > 7.05E-01

FIGURE 12

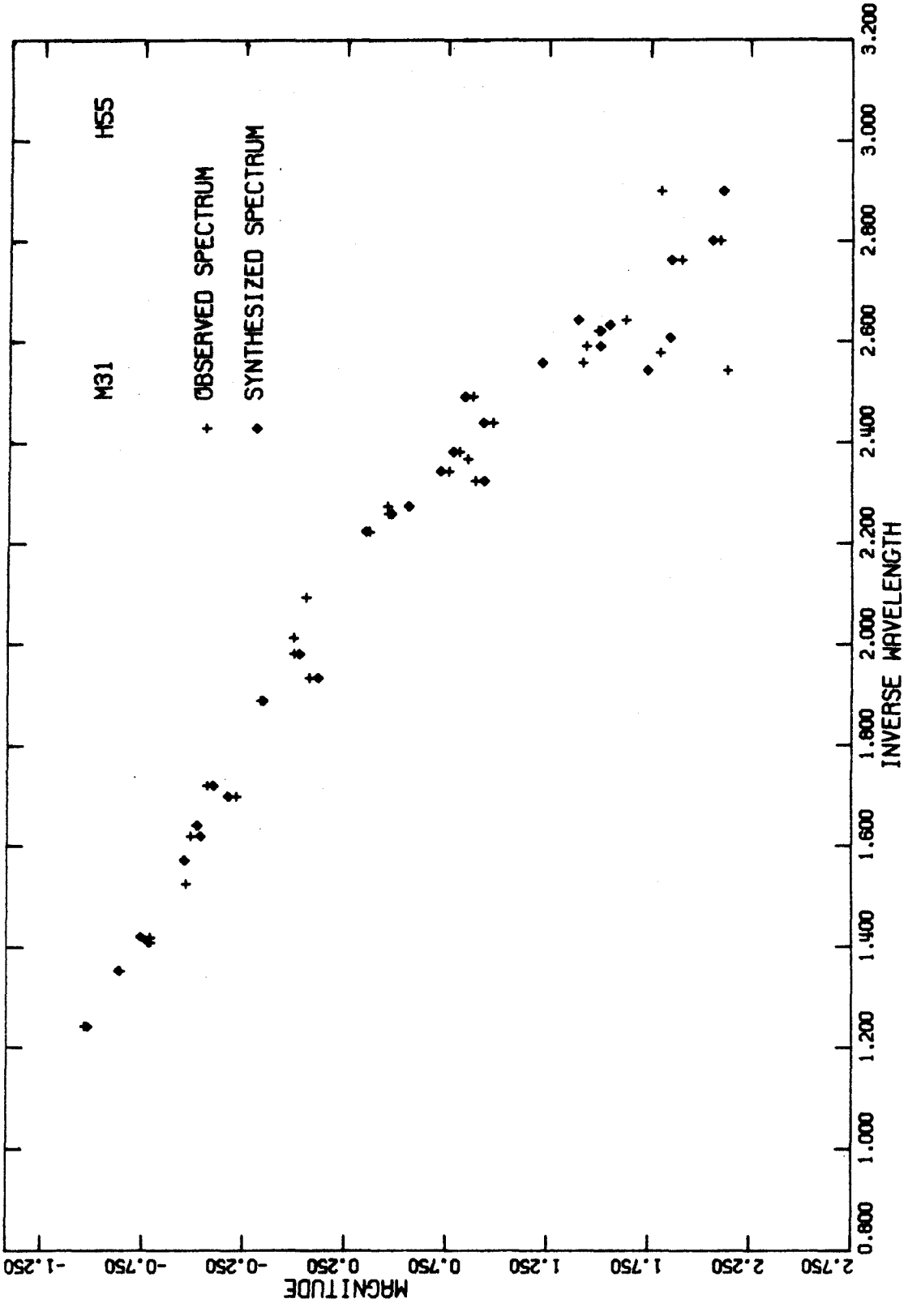
M31
M55
OBSERVED SPECTRUM
SYNTHESIZED SPECTRUM
MAGNITUDE
-1.250
-0.750
-0.250
0.250
0.750
1.250
1.750
2.250
2.750
INVERSE WAVELENGTH
0.800
1.000
1.200
1.400
1.600
1.800
2.000
2.200
2.400
2.600
2.800
3.000
3.200

light from late A stars could be successfully included in the model. Early A and late B main sequence stars (not shown in Table 28) were tried unsuccessfully. It is concluded that H55 is an old metal-rich cluster.

No evidence is found for O or B stars in H55.

M31: B282

The strong-lined cluster B282 (L = 15) is best represented by the model in Tables 28 and 29 and Figure 13. It is similar to the adopted H55 model. The only significant disimilarity is a somewhat redder horizontal branch in B282 (based on mean spectral types A 5-9 III and F 0-5 III).

A comparison of the model and observed spectra produces mean residuals of 4.5 per cent shortward of the Balmer jump (excluding λ3620) and 2.9 per cent longward (excluding $\lambda\lambda$3784, 3910, and 3933). As with H55 an extremely strong K-line (though not quite so strong as in H55) depresses its λ3910 sideband and cannot be synthetically reproduced. Depression of the λ3910 flux again destroys the meaningfulness of the CN 3660 index. Unlike H55, the D-line is reproduced in the model as is the G-band. Apparently a bad datum at λ3620 ruins the fit at that point.

B282 is one of the three clusters for which Spinrad and Schweizer (1972) inferred the presence of hot blue stars to explain the blue and

TABLE 28

M31 B282

COMPARISON OF OBSERVED AND SYNTHESIZED SPECTRA

FLUXES

LAMBDA	OBSERVED	SYNTHESIZED	PCT. DIFF.
3448.	1.535E-01	1.420E-01	-7.749
3570.	1.479E-01	1.497E-01	1.204
3620.	2.068E-01	1.793E-01	-14.232
* 3784.	2.134E-01	2.727E-01	24.386
* 3798.	0.0	2.357E-01	0.0
3815.	2.280E-01	2.462E-01	7.666
* 3835.	0.0	1.794E-01	0.0
3860.	2.432E-01	2.462E-01	1.237
* 3880.	1.815E-01	2.757E-04	0.0
3910.	2.692E-01	3.183E-01	16.733
3933.	1.462E-01	1.946E-01	28.439
4015.	4.127E-01	4.515E-01	8.994
4101.	4.003E-01	4.172E-01	4.125
4200.	4.682E-01	4.779E-01	2.058
* 4226.	4.782E-01	6.773E-02	0.0
4270.	5.058E-01	5.048E-01	-0.212
4305.	4.438E-01	4.137E-01	-7.031
4400.	6.053E-01	5.825E-01	-3.850
4430.	6.143E-01	6.308E-01	2.645
4500.	7.015E-01	7.143E-01	1.808
* 4760.	9.307E-01	5.658E-04	0.0
* 4970.	9.621E-01	6.071E-04	0.0
5050.	1.000E 00	9.503E-01	-5.092
5175.	8.954E-01	8.738E-01	-2.437
5300.	1.132E 00	1.120E 00	-1.136
5820.	1.430E 00	1.402E 00	-1.918
5892.	1.316E 00	1.311E 00	-0.387
6100.	1.493E 00	1.513E 00	1.330
6180.	1.493E 00	1.485E 00	-0.509
6370.	1.632E 00	1.605E 00	-1.706
* 6564.	1.670E 00	8.059E-02	0.0
7050.	1.897E 00	1.975E 00	4.040
7100.	1.905E 00	1.890E 00	-0.815
7400.	2.184E 00	2.233E 00	2.248
8050.	2.667E 00	2.610E 00	-2.162

LINE INDICES

NAME	OBSERVED	SYNTHESIZED	DIFFERENCE
CN 3860	0.984	0.881	-0.104
CAII3933	0.488	0.562	0.074
H 4101	0.904	0.889	-0.015
CN 4200	0.977	0.975	-0.002
CH 4305	0.835	0.768	-0.067
FE 4430	0.970	1.016	0.046
MGI 5175	0.841	0.846	0.005
NAI5892	0.910	0.916	0.007
TIO 6160	0.973	0.964	-0.009
TIO 7100	0.984	0.940	-0.044

CONTINUUM INDICES

U/B	0.319	0.303	-0.017
B/V	0.434	0.431	-0.003
V/R	0.628	0.599	-0.029

*NO ATTEMPT WAS MADE TO FIT THE MODEL TO THE OBSERVATIONS AT THESE WAVELENGTHS.

TABLE 29

MISCELLANEOUS CONTRIBUTION TABLES

M31 8282 V=14.18 DISTANCE MODULUS= 24.65

COMPONENT	INTRINSIC PARAMETERS			% CONTRIBUTION TO		
	V	MASS	M/L_V	V-LIGHT	MASS	NUMBER
O V	-5.00	30.00	3.64E-03	0.0	0.0	0.0
B0-4 V	-2.50	9.00	1.09E-02	0.142	0.002	0.000
A5-9 V	2.30	1.70	1.72E-01	0.329	0.074	0.039
F0-5 V	3.10	1.40	2.95E-01	4.170	1.622	1.031
F6-9 V	4.20	1.20	6.97E-01	8.694	7.981	5.920
G0-5 V	4.90	1.00	1.11E 00	9.126	13.303	11.843
G6-9 V	5.60	0.85	1.79E 00	8.771	20.707	21.687
K0-2 V	6.10	0.80	2.67E 00	6.603	23.255	25.877
K3 V	6.60	0.75	3.97E 00	2.529	13.235	15.709
K5-7 V	7.90	0.58	1.02E 01	0.439	5.883	9.029
M0 4	0.72	1.40	3.30E-02	0.054	0.002	0.002
M0 5	-0.18	1.40	1.44E-02	0.003	0.000	0.000
G0-5 IV	3.00	1.40	2.69E-01	13.472	4.778	3.038
G6-9 IV	3.10	1.40	2.95E-01	9.503	3.695	2.350
K0-3 IV	3.20	1.40	3.24E-01	5.182	2.209	1.405
K0-3 IV SMR	3.20	1.40	3.24E-01	3.112	1.327	0.844
A5-9 III	1.20	1.40	5.13E-02	1.884	0.127	0.081
F0-5 III	1.60	1.40	7.42E-02	5.804	0.567	0.361
G5-9 III	1.50	1.40	6.76E-02	8.544	0.761	0.484
K0-3 III	0.90	1.40	3.89E-02	4.940	0.253	0.161
K0-3 III SMR	0.90	1.40	3.89E-02	3.167	0.162	0.103
K4-5 III	0.10	1.40	1.86E-02	0.916	0.022	0.014
K4-5 III SMR	0.10	1.40	1.86E-02	0.630	0.015	0.010
M4-5 III	-0.80	1.40	8.13E-03	0.743	0.008	0.005
M0-8 III	-1.00	1.40	6.76E-03	1.241	0.011	0.007

MODEL PARAMETERS: E(B-V)= 0.11 NUMBER OF STARS> 1.08E 06 MASS> 9.65E 05 M/L_V> 7.59E-01

FIGURE 13

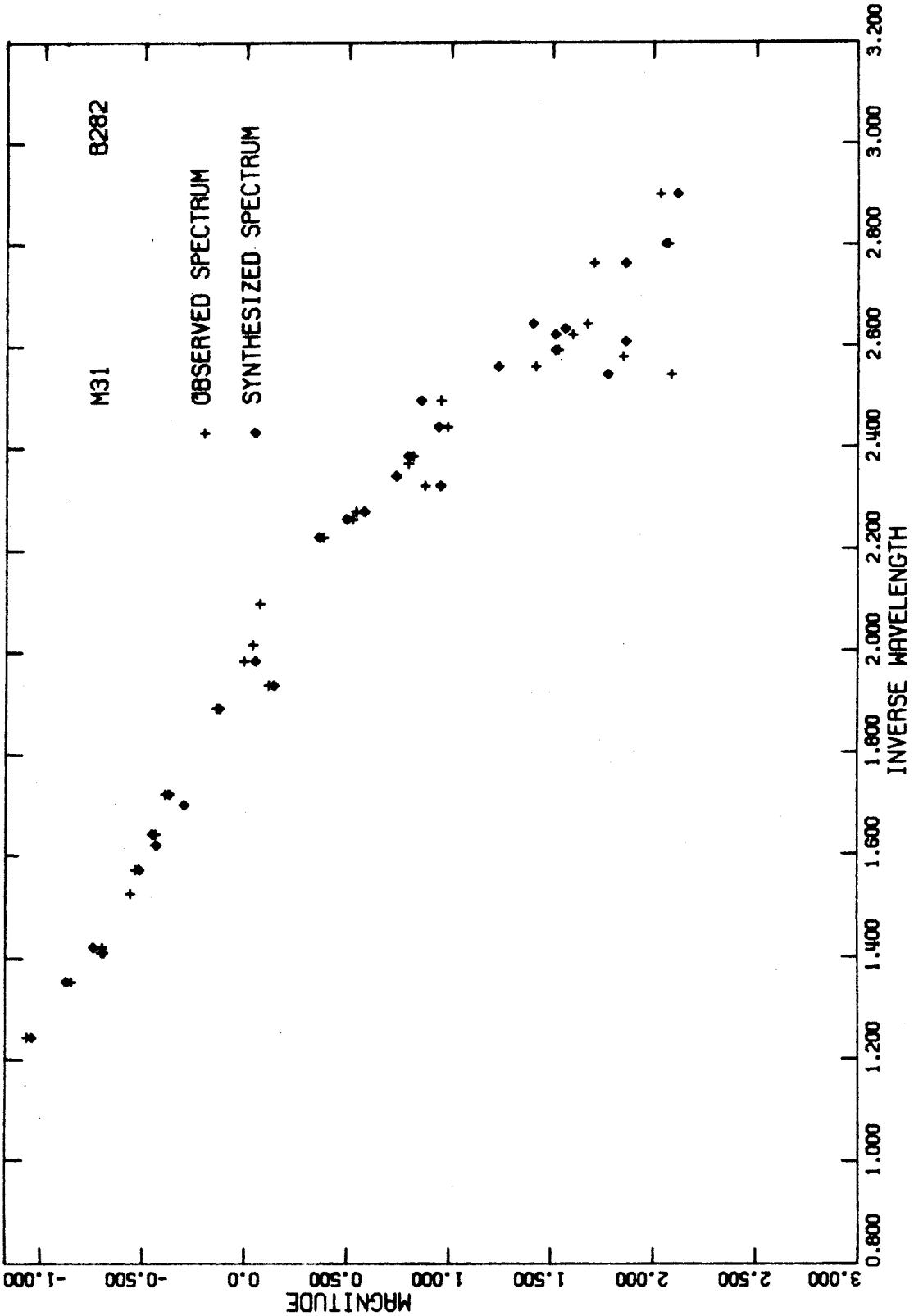
B282
M31
OBSERVED SPECTRUM
SYNTHESIZED SPECTRUM
MAGNITUDE
-1.000
-0.500
0.0
0.500
1.000
1.500
2.000
2.500
3.000
INVERSE WAVELENGTH
0.800
1.000
1.200
1.400
1.600
1.800
2.000
2.200
2.400
2.600
2.800
3.000
3.200

ultraviolet fluxes. The present model does not support their conclusion. Spinrad and Schweizer had 25 per cent of the V-light contributed by the cluster main sequence in their model. In the present model 41 per cent comes from the main sequence. Increasing the main sequence contribution has apparently increased the blue and ultraviolet fluxes sufficiently to remove the need for very hot stars.

Using the giant-to-dwarf ratio of Spinrad and Schweizer in the model does improve the K-line fit at the expense of the continuum fit. This does not open the way for the addition of hot blue stars however since such stars worsen the K-line fit.

NGC 205 Nucleus

Tables 30 and 31 and Figure 14 describe the best NGC 205 model. Mean residuals are 4.9 per cent shortward of the Balmer jump and 3.7 per cent redward (excluding λ3784). The extreme observed weakness of H delta is believed to be a bad datum. A shortage of flux in the λ3910 sideband weakens the observed cyanogen indices at $\lambda\lambda$3860 and 3880.

The adopted model has a three per cent V-light contribution from O and early B main sequence stars. This result suggests that a hot blue star such as those discovered by Baade (1951) in NGC 205 was included in the observing aperture. The blueness of the nucleus with respect to the cluster as a whole (see part A of this section) also leads to this

TABLE 30

NGC 205 NUCLEUS

COMPARISON OF OBSERVED AND SYNTHESIZED SPECTRA

FLUXES

	LAMBDA	OBSERVED	SYNTHESIZED	PCT. DIFF.
	3448.	2.793E-01	2.670E-01	-4.486
	3570.	2.998E-01	2.777E-01	-7.634
	3620.	3.028E-01	2.951E-01	-2.580
*	3704.	3.436E-01	3.945E-01	13.805
*	3798.	0.0	3.597E-01	0.0
	3815.	3.715E-01	3.906E-01	5.016
*	3835.	0.0	3.048E-01	0.0
	3860.	4.188E-01	4.249E-01	1.440
	3880.	3.869E-01	3.782E-01	-2.264
	3910.	4.111E-01	4.485E-01	8.701
	3933.	2.860E-01	3.148E-01	9.591
	4015.	5.670E-01	5.739E-01	1.196
	4101.	5.824E-01	5.151E-01	-12.257
	4200.	6.546E-01	6.234E-01	-4.695
	4226.	6.504E-01	6.227E-01	-5.277
	4270.	6.292E-01	6.332E-01	0.628
	4305.	5.205E-01	5.439E-01	4.407
	4400.	7.278E-01	6.973E-01	-4.271
	4430.	7.475E-01	7.345E-01	-1.745
	4500.	8.128E-01	7.882E-01	-3.073
	4780.	9.621E-01	8.872E-01	-8.099
	4970.	9.827E-01	9.330E-01	-5.185
	5050.	1.000E 00	9.544E-01	-4.670
	5175.	9.078E-01	9.290E-01	2.309
	5300.	1.052E 00	1.041E 00	-1.052
	5820.	1.197E 00	1.195E 00	-0.130
	5892.	1.141E 00	1.158E 00	1.478
	6100.	1.219E 00	1.237E 00	1.475
	6180.	1.208E 00	1.242E 00	2.813
	6370.	1.276E 00	1.289E 00	0.978
	6564.	1.222E 00	1.159E 00	-5.349
	7050.	1.400E 00	1.416E 00	1.167
	7100.	1.344E 00	1.427E 00	5.972
	7400.	1.423E 00	1.444E 00	1.461
	8050.	1.521E 00	1.536E 00	1.015

LINE INDICES

NAME	OBSERVED	SYNTHESIZED	DIFFERENCE
CN 3860	1.074	1.018	-0.056
CN 3880	0.971	0.880	-0.091
CAII3933	0.644	0.663	0.019
H 4101	0.991	0.868	-0.123
CN 4200	1.070	1.011	-0.059
CAI 4226	1.062	1.000	-0.062
CH 4305	0.795	0.837	0.042
IS 4430	0.993	1.015	0.022
MGH 4780	1.061	1.018	-0.044
TIO 4970	1.011	1.003	-0.008
MGI 5175	0.884	0.932	0.047
NAII5892	0.948	0.959	0.012
TIO 6180	0.977	0.991	0.015
H 6564	0.930	0.872	-0.057
TIO 7100	0.957	1.004	0.047

CONTINUUM INDICES

U/B	0.444	0.431	-0.014
B/V	0.603	0.595	-0.008
V/R	0.797	0.782	-0.015

*NO ATTEMPT WAS MADE TO FIT THE MODEL TO THE OBSERVATIONS AT THESE WAVELENGTHS.

TABLE 31

MISCELLANEOUS CONTRIBUTION TABLES

NGC 205 NUCLEUS V= 8.25 DISTANCE MODULUS= 24.65

COMPONENT	INTRINSIC PARAMETERS			% CONTRIBUTION TO		
	V	MASS	M/L_v	V-LIGHT	MASS	NUMBER
O V	-5.00	30.00	3.64E-03	0.173	0.001	0.000
BO-4 V	-2.50	9.00	1.09E-02	2.939	0.041	0.002
HB 2	1.01	0.70	2.15E-02	0.0	0.0	0.0
HB 3	0.91	0.70	1.96E-02	0.0	0.0	0.0
HB 4	0.75	0.70	1.69E-02	0.0	0.0	0.0
HB 5	-0.15	0.70	7.40E-03	0.0	0.0	0.0
GI M 1	0.63	0.70	1.52E-02	1.980	0.038	0.030
GI M 2	0.35	0.70	1.17E-02	0.755	0.011	0.009
GI M 3	0.28	0.70	1.10E-02	0.114	0.002	0.001
GI M 4	-0.47	0.70	5.51E-03	0.014	0.000	0.000
GI M 5	-1.60	0.70	1.95E-03	0.022	0.000	0.000
GI M 6	-2.00	0.70	1.35E-03	0.017	0.000	0.000
GI M 7	-2.20	0.70	1.12E-03	0.012	0.000	0.000
SG M 1	3.86	0.70	2.97E-01	11.455	4.305	3.367
SG M 2	3.81	0.70	2.84E-01	8.101	2.907	2.274
SG M 3	3.00	0.70	1.35E-01	5.632	0.959	0.750
SG M 4	1.08	0.70	2.30E-02	3.965	0.115	0.090
SG M 5	0.53	0.70	1.38E-02	2.327	0.041	0.032
SD M 1	3.60	0.70	2.34E-01	14.702	4.349	3.401
SD M 2	4.68	0.70	6.33E-01	13.523	10.816	8.458
SD M 3	4.82	0.68	6.99E-01	12.021	10.625	8.553
SD M 4	5.70	0.56	1.34E 00	10.360	17.566	16.578
SD M 5	6.15	0.54	1.89E 00	7.150	17.084	17.318
SD M 6	7.37	0.44	4.74E 00	2.911	17.432	21.607
SD M 7	7.64	0.43	5.94E 00	1.827	13.708	17.450

MODEL PARAMETERS: E(B-V)= 0.11 NUMBER OF STARS> 4.32E 08 MASS> 2.37E 08 M/L_v > 7.91E-01

FIGURE 14

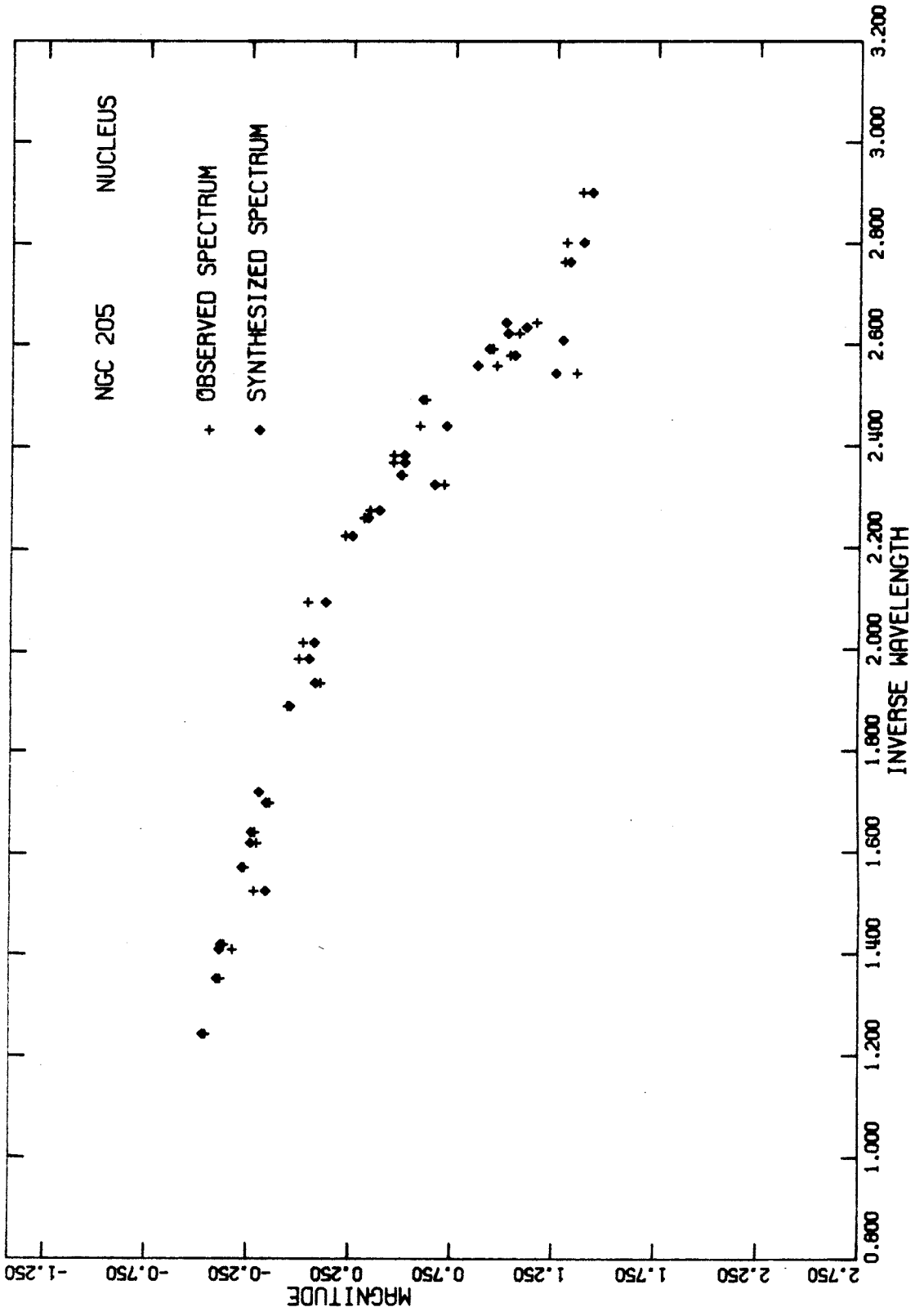
NGC 205 NUCLEUS
OBSERVED SPECTRUM
SYNTHESIZED SPECTRUM
MAGNITUDE
INVERSE WAVELENGTH
-1.250
-0.750
-0.250
0.250
0.750
1.250
1.750
2.250
2.750
0.800
1.000
1.200
1.400
1.600
1.800
2.000
2.200
2.400
2.600
2.800
3.000
3.200

conclusion. Whether such stars occur in the vicinity of the nucleus is not clear from Baade's plate because the nuclear region is "burned out."

It should be emphasized that the V magnitude of the 9!'9 nuclear region observed for NGC 205 was about 14.6 as compared with 8.25 for the total V-light of the system. Thus only 0.3 per cent of the integrated light was observed. The integrated spectrum of the galaxy could therefore be quite different from the observed nuclear spectrum.

C) General Comments and Model Comparisons

Most of the general difficulties encountered in fitting the models are well understood. Spectral region $\lambda\lambda$3650-4000 is heavily blanketed by metallic lines and cyanogen bands as well as Balmer lines. It is not accurately reproduced in the models because of dispersion in metal content within the mean stellar sequences and because cluster and model metal contents are not identical. The continuum in this region is too faint in M5, M13, and M92 models and too bright in H12, H55, H140, B282, and the NGC 205 models. It is concluded that the models are correspondingly too metal-rich and too metal-poor.

The CaII K-line index is somewhat too weak in all the M31 cluster models and in the NGC 205 model. The weakness in the MIV model appears to be at least partly a result of an erroneus measurement of

excessive flux in the λ3910 sideband. The weakness in the other models is probably a result of excessive calcium deficiencies in the model stellar types with respect to the clusters. This conclusion corroborates that made from the $\lambda\lambda$3650-4000 continuum. CaII K is by far the strongest spectral feature measured in the clusters, (e.g., its index is 0.40 smaller than any other index in H55), and is highly sensitive to chemical composition. Relatively small composition differentials could noticeably affect this index while being lost in the noise of other features.

The Balmer features at $\lambda\lambda$3798 and 3835 are subject to both heavy blanketing and observational errors because of the extreme sensitivity of observations to bandpass position and width in this spectral region. Galactic globular cluster models did not fit observations at these wavelengths. Average discrepancies in the indices were about 0.05. No observations were made of these features in the M31 clusters and NGC 205.

The tendency for model G-bands to be slightly too strong has been attributed to spectral degradation (see the M15 model description).

A general problem that applies to all models, and that is not well understood, is the excessive strength of H alpha in the models. The problem appears to be correlated with metal abundance. The most metal-deficient clusters, M92 and M15, have the weakest H alpha features and show the largest discrepancies between observations and

models. The source of this problem is not clear, especially when one considers the results of Peat (1964) who found that high-velocity field giants have stronger H alpha at a given color than low-velocity field giants.

One possible explanation is spectral degradation due to the extended sources. Accurate calculations of the effects of spectral degradation are not possible without accurate brightness profiles for the clusters. However the absence of evidence of spectral degradation effects upon the wide MgI "b" triplet indicates that degradation should have had minor effects on H alpha.

Another possible explanation is that chromospheric emission in the globular cluster red-giants fills the H alpha line. (It is unfortunate that the reddest population II giants used in the syntheses, those of M92, were not observed at H alpha.) The strength of the H alpha feature in the clusters arises primarily from the horizontal branch, but about half of the flux in H alpha comes from red-giants. Thus relatively weak emission in the giants could overwhelm the strong absorption from the horizontal-branch stars. However it should be noted that no H alpha emission is seen in late giants of the field (Weymann 1963), nor are circumstellar absorption lines seen to occur in giants earlier than M0 (Deutsch 1968). However both Deutsch (1960) and Weymann (1963) have expressed belief that giants earlier than M0 support mass flows which are too highly ionized for detection through absorption features.

The evidence that mass loss does take place in globular cluster giants is quite convincing. The theoretical work of Paczynski and Ziolkowsky (1968) on red-giant models suggests mass loss as do Christy's (1966a, b) RR Lyrae models which require masses near $0.5M_{\odot}$.

Three facts are interpreted as evidence for the emission line hypothesis. First, both H delta and H alpha arise primarily from horizontal-branch stars. Incorrect numbers of these stars in the models is therefore not likely an explanation for the H alpha problem since H delta is about the right strength in all the models. However Balmer line emission could easily cause the discrepancy in H alpha but not affect H delta, both because such emission would not be so strong in H delta as in H alpha, and also because most of the flux in H alpha is from red-giants, which is not true of H delta. (Problems in fitting H9 and H10 are probably due to other sources, as explained earlier, and are not interpreted as evidence that horizontal-branch contributions in the models are incorrect). The second indication is the fact that H alpha is so weak in most of the globular clusters (see Figure B18) as to be unreproducible by any mixture of stellar types. Third, it should be noted that those clusters with the largest discrepancies in H alpha, namely the most metal deficient clusters, are known to have (in the case of the clusters in the Galaxy) the most luminous red-giant branches at a given color and therefore the smallest giant surface gravities. Because supergiants exhibit evidences of mass loss more commonly than giants

(Deutsch 1968) it might be expected that those clusters with the most luminous red-giants would show the greatest evidence of mass loss through emission features. (For a description of Rho Cas, a F8 supergiant showing evidence of chromospheric emission in the Balmer lines see Sargent [1961].)

Agreement between models and observations were generally good in all other continuum regions and spectral features. No other features with systematic disagreements were noted. Occasional large discrepancies at other wavelengths between models and observations of individual objects were probably caused by observational errors.

In a few cases, when observations at individual wavelengths were felt to severely misrepresent true fluxes, no attempt was made to reproduce observed fluxes in the models. All such exceptions were noted in the tabulated model descriptions.

The described comparisons of models with published luminosity functions and color-magnitude arrays, plus the experience gained in fitting models to observed data has led to the conclusion that light contribution models for the clusters have accuracies of better than ten per cent when large regions of the color-magnitude diagram are considered, e.g., the V-light contribution of the red-giants or the blue horizontal branch. However distribution of light contributions from individual mean stellar types within a branch depends somewhat upon how initial models were smoothed, especially for stellar types which make

relatively small light contributions. Uncertainties in the light contributions of individual blocks are estimated to range from near ten per cent for the red-giant branch and the top of the main sequence to more than a factor of two at the faint end of the main sequence.

Model mass and luminosity functions are not so accurate for the reasons previously stated. These distributions probably have errors of ten to twenty per cent for comparison between the giant branches and tops of the cluster main sequences. Accuracies are somewhat less for the horizontal and subgiant branches and especially the faint end of the main sequence.

In Table 32 the V-light contributions from the various branches of the color-magnitude diagram are given for the ten stellar systems of the program. The table serves as a convenient reference for object comparisons.

One interesting feature of Table 32 is the evidence for an abnormally large light contribution from the red-giant branch of M5. There also exists other published evidence that this is the case. Comparison of Arp's (1962) M5 color-magnitude array with that of the similar cluster M3 (Johnson and Sandage 1956) implies that the ratio of the number of giants brighter than the horizontal branch and redder than $B - V = 0.80$ to the number of subgiants less than one magnitude fainter than the horizontal branch is about 1.4 in M5 and near unity in M3. (The population distributions of these arrays are proportional to

TABLE 32

COMPARATIVE V-LIGHT CONTRIBUTIONS

Cluster	BHB	RHB	HB	RG	SG	SD
M5	7.7	4.3	12.0	42.0	25.0	21.0
M13	8.6	0.0	8.6	35.5	30.2	25.8
M15	9.1	1.9	10.9	29.8	37.2	22.0
M92	9.2	2.6	11.8	34.9	27.3	25.9
H12	1.7*	8.4	10.1*	30.8	33.7	25.4
H55	2.5@	3.8#	6.4	21.9	30.5	41.1
H140	9.6*	3.7	13.3*	26.7	32.7	27.4
B282	2.0*,@	5.9#	7.9*	20.2	31.3	40.7
MIV	14.4	2.3	16.7	29.8	34.8	18.7
NGC 205 (nucl.)	3.1*	0.0	3.1*	2.9	31.5	62.5

*BHB and HB contain some contributions from O- and B-type stars.
@BHB consists of population I A 5-9 III stars.
#RHB consists of population I F 0-5 III stars.

cluster luminosity functions over their upper regions only.) A comparison of the M3 luminosity function with that of M13 and M92 in Figure 1 of Simoda and Kimura (1968) implies that in M3 red-giants contribute relatively more light than in M13 and M92. The comparison can be illustrated by the fact that the ratio of the M3 luminosity function at absolute magnitude -1.0 to that at $+2.0$ is more than a factor 1.5 greater than the corresponding ratios in M13 and M92.

The two metal-rich clusters H55 and B282 have relatively small giant-branch light contributions. These two clusters also have dwarf light contributions which are a factor 1.5 to 2.0 larger than corresponding contributions in the other clusters. These wide variations in light distributions in the clusters may be evidence of luminosity function variations at birth. (The rather unusual light distribution in MIV has been overlooked because the observational difficulties encountered in obtaining its spectrum would cast doubt upon any conclusions based thereon.)

The most interesting comparison to be made from the data of Table 32 is that of the two moderately metal-rich clusters H12 and H140. Similar line indices were obtained for these two clusters. Van den Bergh has assigned L = 8 to both clusters. Their luminosity functions are very much alike except along the horizontal branch. The H12 horizontal branch is heavily populated on the red side of the variable gap and sparsely populated or absent on the blue side as in the metal-similar

galactic globular clusters 47 Tuc (Tifft 1963), NGC 6171 (Sandage and Katem 1964), and NGC 6712 (Sandage and Smith 1966). Van den Bergh (1969) line indices are L = 7 for NGC 6171 and L = 8 for NGC 6712 so the similarities in color-magnitude arrays are not unexpected. In contrast, H140 has a very blue horizontal branch and thus violates the usual correlation between metal content and blueness of the horizontal branch as do the globular clusters M13 and NGC 7006 (Sandage and Wildey). The evident conclusion is that M31 clusters belong to at least a two-parameter family as do their galactic counterparts.

H55 and B282 provide much weaker but significant evidence for the same conclusion. Stellar types A5-9 III and F0-5 III which populate inferred horizontal branches in these similar clusters contribute 2.5 and 2.7 per cent of the V-light in H55 and 1.9 and 5.8 per cent in B282.

Although composed of mildly metal-deficient population II stars the adopted NGC 205 nuclear model has a luminosity function extremely different from those of the clusters. Dwarfs contribute over sixty per cent of the V-light. This compares with forty per cent in the metal-rich clusters H55 and B282 and about 25 per cent in the other clusters. Giants contribute only three per cent of the V-light. This is an order of magnitude less than cluster giant branch contributions.

The color-magnitude array for NGC 205 is somewhat similar to that of the old galactic cluster M67 (Johnson and Sandage 1955). The shortage of giants with respect to brighter dwarfs and the steep

luminosity function gradient along the subgiant branch are common to both arrays. However faint dwarfs are relatively much more numerous than in M67.

The V-light contributions of dwarfs in the nuclei of M31, M32, and M81 are about twenty to thirty per cent according to Spinrad and Taylor (1971). Thus the sixty per cent contribution in NGC 205 is quite surprising.

V. CONCLUSIONS

A) Validity and Applicability of Spectral Synthesis

Comparisons of best models with color-magnitude arrays and luminosity functions for globular clusters in the Galaxy provide evidence of the validity of the Spinrad and Taylor (1971) synthesis technique. However in a rigorous sense the approach is not completely satisfactory since best-fitting models do not generally satisfy the physical constraints of a smooth luminosity function and a relatively narrow range in chemical composition. The application of these constraints to galaxies and parts of galaxies other than our own is an extrapolation of locally observed phenomena to other regions of the universe.

In a practical sense the validity of the approach, since it is one of trial and error, depends upon the thoroughness with which reasonable models are considered.

The technique of spectral synthesis shows particular promise of applicability to the study of globular clusters of other galaxies. The method yields the metal content of a cluster and the color of its horizontal branch. Thus the two independent parameters which seem adequate for describing clusters in the Galaxy are revealed.

Comparison of various models for M5, M13, M15, and M92 with their known color-magnitude distributions has led to a ranking by importance for fitting criteria. In relative order of significance they are:

(1) That the physical constraints of a smooth luminosity function and narrow range in chemical composition be satisfied.

(2) That the model continuum fit the observed continuum.

(3) That the model and observed feature strengths agree.

Criterion (2) is, of course, dependent upon the accuracy with which the continuum of the composite spectrum is known. Its relative importance decreases with increasing uncertainty in reddening.

Because small color changes arising from interstellar extinction variations in the models can be easily compensated by varying stellar population mixtures, spectral synthesis is not a good method for determining reddening. Independently determined color excesses should be used in models.

B) Astrophysical Conclusions

Applications of spectral synthesis to the five M31 globular clusters and to the nucleus of NGC 205 have led to several interesting conclusions. Perhaps most interesting is the result that M31 clusters belong to at least a two-parameter family as do galactic globular clusters. The very different horizontal-branch luminosity functions of the

otherwise similar clusters H12 and H140 serve as evidence that this is the case. H12 has a fairly prominent red horizontal branch much like the metal-similar cluster 47 Tuc. H140, a cluster of similar line strength, has a rather blue horizontal branch similar to that of moderately metal-poor M5.

The clusters H55 and B282 have extremely strong spectral features. Even population I mixtures enriched with some "super-metal-rich" components do not adequately reproduce the strong features of these clusters. This result is in agreement with that of Spinrad and Schweizer (1972).

The strong-lined cluster H55 is especially interesting because of its location in the M31 halo. It confirms van den Bergh's (1969) claim that some remote M31 clusters have strong lines.

The presence of metal-poor MIV, moderately metal-rich H140, and metal-rich H55 in the halo of M31 corroborates van den Bergh's discovery of the absence of a strong position-metallicity correlation in M31. It is difficult to reconcile the metal contents and spatial distribution of the M31 clusters with a model of galactic collapse highly similar to that of Eggen, Lynden-Bell, and Sandage (1962). At least three possible explanations can be considered.

(1) Rapid metal enrichment of the M31 interstellar medium was well in progress before the system collapsed to a disk. Early enrichment was highly non-uniform, leading to the present wide

dispersion in cluster line strengths.

(2) The metal-rich clusters were ejected from the collapsing young disk.

(3) Star formation persisted beyond one generation in the clusters.

Of the three explanations, (2) seems least feasible for want of an ejection mechanism. Although possibility (3) seems rather speculative because of the lack of observed interstellar matter in galactic globular clusters, it is interesting to consider in combination with van den Bergh's (1969) observation that M31 globular clusters may be systematically brighter than globular clusters in the Galaxy. The present work suggests that clusters in both systems have similar luminosity functions. Thus differences in brightness would reflect differences in numbers of stars or masses of the systems. Two alternatives can be considered. (a) M31 clusters were born more massive than galactic globular clusters. Because of their greater masses, residual gas and dust after the initial burst of star formation was not swept quickly out of the systems, but persisted long enough for some metal-enriched younger stars to form. This possibility would seem to require a correlation between metal content and absolute luminosity which does not exist. (b) M31 and galactic globular clusters may have been born with similar masses but with different orbital distributions such that M31 globular clusters have avoided the central region of M31. Interstellar matter within the M31 clusters after the initial star formation thus

persisted and has condensed into younger stars of higher metal content. No abundance-luminosity correlation is required by alternative (b) which would explain both the lack of a strong spatial-metal content correlation and the inferred greater masses of the M31 clusters. However the absence of an early main sequence (earlier than F0) in both H55 and B282 weakens the status of explanation (3).

There is fairly strong evidence for significant dispersion in the luminosity functions of clusters. The best models for the two metal-rich clusters H55 and B282 have about forty per cent V-light contributions from their main sequences as opposed to about 25 per cent for the other clusters. The best M5 model has about one-third more V-light arising from its giant branch than do other cluster models. There exists independent published evidence for a more heavily populated giant branch in M5 than in most clusters. The absence of a significant luminosity function differential between H12 and H140 except along the horizontal branch seems to imply that luminosity function dispersion is not the second parameter implied by comparisons of color-magnitude arrays.

Only very weak evidence is found for hot blue stars in the metal-rich M31 clusters like those inferred by Spinrad and Schweizer for H87, B282, and MII. The best B282 model, the only cluster common to both studies, has less than a 0.2 per cent V-light contribution from hot blue stars. Spinrad and Schweizer's model has 4.6 per cent. The best

model for H55, another very strong-lined cluster, has no O- or B-type stars. The best models for H12 and H140, two clusters of moderate metal content, have between one and two per cent V-light contributions from hot blue stars. These contributions can be assimilated by the blue horizontal branches in these clusters with only small effects on integrated spectra. It is concluded that such small V-light contributions constitute only marginal evidence for the presence of very hot stars. (The presence of hot stars in the clusters would strengthen the status of hypothesis (3) concerning the evolution of the M31 clusters, i.e., that they are self-metal-enriched.) The relatively strong blue and ultraviolet fluxes which Spinrad and Schweizer felt necessitated the inclusion of O- and B-type stars in their models have been reproduced in the present models by increasing the numbers of dwarfs with respect to giants and subgiants.

Although the nucleus of NGC 205 is best represented by a model of moderate metal-deficiency as are M31 globular clusters H12 and H140, the model color-magnitude distribution is unlike that of any known globular cluster. It is somewhat similar to that of the old galactic cluster M67; however faint dwarfs are much more numerous than in M67. Dwarfs are more numerous by a factor of two and giants are less numerous by a factor of ten than in the Spinrad and Taylor (1971) models of the nuclei of M31, M32, and M81. The apparent implication of the result is the existence of wide variations in the luminosity functions of

galactic systems. This conclusion is perhaps not too surprising when one considers that the Spinrad and Taylor models represent large departures from the van Rhijn luminosity function of the solar neighborhood.

C) Future Modifications and Programs

Experience gained in performing the syntheses has led to several conclusions as to how similar future work might be more efficiently performed. Several of the observed wavelengths were of little value in fitting models and should probably be excluded from future observational programs. The troublesome bandpasses at $\lambda\lambda$3798 and 3835 could certainly be dropped as could the heavily blanketed sideband λ3784 which is also difficult to observe accurately. It would probably be well to replace these two Balmer features with H beta, and perhaps H gamma.

The interstellar feature at λ4430 is too weak to yield quantitative information on interstellar extinction and too close to the continuum bandpasses $\lambda\lambda$4400 and 4500 to yield independent information on continuum shapes. λ4430 should be dropped and continuum bandpass λ4500 should be moved closer to λ4780 for which it serves as a sideband.

The feature indices MgH 4780, TiO 4970, TiO 6180, and TiO 7100 exhibit nearly identical behaviors. They are all sensitive to TiO bands which are generally extremely weak in clusters because of the absence of late red-giants. MgH 4780 is also sensitive to the MgH λ4845 band which is very weak in clusters because of the relatively small light contributions from late dwarfs. At least two of these bandpasses, probably $\lambda\lambda$4970 and 6180 should be dropped from the program.

A significant fraction of the total observing time was spent on the three ultraviolet continuum bandpasses at $\lambda\lambda$3448, 3570, and 3620. Most program objects were relatively faint at these wavelengths. Observations were important however because of the great sensitivity of the Balmer discontinuity to luminosity class. It would probably be helpful to reduce the number of observed ultraviolet points to two and to increase bandpasses in this region to 50Å to improve accuracies and to reduce observing time.

It would be helpful in discriminating among models if the continuum could be extended over a larger spectral region. Infrared colors would be especially useful.

It also might be helpful to observe atomic lines of additional chemical elements. The iron line at λ4325 would probably be one good choice.

The disimilarities in the properties of the globular clusters of the Galaxy and those of M31 are justification for extensive future studies

of the globular clusters of other nearby galaxies. Certainly the clusters of other galaxies of the local group should be studied by spectral synthesis. Table 33, which is based on a paper by van den Bergh (1968), lists the members of the local group and indicates which have known globular clusters.

Studies of individual globular clusters in other nearby clusters of galaxies are also possible out to about the distance of the Virgo cluster. If a distance modulus of 30.7 is assumed for the Virgo cluster (Sandage 1961), and if the brightest globular clusters in the Virgo cluster have luminosities comparable to the brightest clusters in M31, then their magnitudes are near 20.0. At such a faint magnitude a three-hour scan with the 200-inch multi-channel spectrometer, using 160Å bandpasses in the second order, would yield accuracies near ten per cent in the visual region. Clearly the long observing times and loss of spectral resolution rule out studies of large numbers of globular clusters at this distance. However it would probably be worthwhile to study a few of the brightest clusters in M87. Investigation of the clusters of this giant elliptical galaxy, which is more massive than M31, might reveal how globular clusters vary with mass and morphological type of their parent galaxy.

TABLE 33

MEMBERS OF THE LOCAL GROUP OF GALAXIES*

Name	Type	M_V	Globular Clusters
M31 = NGC 224	Sb I-II	-21.1	yes
Galaxy	Sb or Sc	-20?	yes
M33 = NGC 598	Sc II-III	-18.9	yes
LMC	Ir or SBc III-IV	-18.5	yes
SMC	Ir IV or Ir IV-V	-16.8	yes
NGC 205	E6p	-16.4	yes
M32 = NGC 221	E2	-16.4	?
NGC 6822	Ir IV-V	-15.7	?
NGC 185	dE0	-15.2	yes
NGC 147	dE4	-14.9	yes
IC 1613	Ir V	-14.8	no
Fornax	Spheroidal	-13.6	yes
Sculptor	Spheroidal	-11.7	no
Leo I	Spheroidal	-11.0	no
Leo II	Spheroidal	-9.4	no
Ursa Minor	Spheroidal	-8.8	no
Draco	Spheroidal	-8.6	no

*Recently discovered Maffei I and Maffei II are not included in the table.

APPENDIX A

DATA REDUCTION

A) Basic Reduction Procedure

The reduction procedure for photometric scanner data has been described in detail by Oke (1965). OB_λ, the count rate or deflection per wavelength interval in magnitudes that would be observed outside the earth's atmosphere, is obtained at each program wavelength by adding an atmospheric extinction correction, $-a_\lambda \sec z$, to the observed count rate per wavelength expressed in magnitudes for each observation of each object. An instrumental response function $OB_\lambda - AB_\lambda$, where AB_λ is flux outside the earth's atmosphere measured in magnitudes, is determined from observations of standard stars. Fluxes, in magnitudes, are then determined for the unknown objects by adding $-(OB_\lambda - AB_\lambda)$ to each OB_λ. Ignoring for a moment the possibility of errors introduced through use of observing instruments, fluxes obtained in this manner are subject to three kinds of errors: (1) random photon statistical errors, (2) gray extinction terms, and (3) the calibrational accuracy of the standards. If the objects observed are to be compared with one another rather than with theoretical models, error (3) is of no

importance. Since scanner observations are generally employed to obtain colors rather than absolute magnitudes, error (2) is also inconsequential if extinction does not vary with time.

B) Modifications and Corrections

Before data can be reduced by this straightforward method it is necessary to correct observed count rates for coincidence errors. Because of high-speed electronic components in the data systems these corrections were fortunately small, usually less than one per cent, for the observations of this program. Even for the brightest standards observed with the 60-inch and 100-inch telescopes coincidence corrections did not exceed three per cent for the highest count rates observed (about 400 KHz).

Oke's (1964) secondary standards are all early spectral type stars. These and the two extreme subdwarf standards employed, HD 19445 and BD +17° 4708, have few prominent spectral features except for Balmer and Paschen lines and discontinuities. For this reason the OB's of the standards were generally insensitive to variations in bandpass and displacements of a few Angstroms. However in spectral regions of Balmer or Paschen features they were extremely sensitive to such variations. This was particularly a problem in regions of series convergences. For this reason the instrumental response function

OB - AB was interpolated in spectral regions $\lambda\lambda$3650 - 4000 and $\lambda\lambda$8400-9000 as well as at $\lambda\lambda$4101 and 6564, the positions of H delta and H alpha.

All the data reduction procedures, including corrections, which have been mentioned to this point were performed on the Caltech IBM 360/75 computer. A number of small corrections which could not be conveniently programmed because they depended on somewhat subjective judgements were also applied. A discussion of these corrections follows.

As previously stated OB - AB between $\lambda\lambda$3650 and 4000 was interpolated from OB - AB determined from the standards at $\lambda\lambda$3570, 3620, 4015, and 4200. Because of the nature of the interpolation formula (Lagrange's) and the rather narrow increments between the pairs of wavelengths on either side of the interpolated gap as compared with the size of the gap, a small error in OB - AB for one of these wavelengths, especially λ3570, can be magnified as a larger error at an interpolated wavelength. For this reason a smooth OB - AB curve was drawn by eye for each night and compared with the computed interpolated curve at λ3815, near the middle of the gap. If a disagreement larger than $0^m.02$ was found, the eye-smoothed curve was adopted and appropriate corrections were applied to the AB's. Data for nine nights were corrected in this manner. The largest correction needed was $-0^m.030$.

For the same reasons as mentioned above OB - AB at λ4101, which

was interpolated from OB - AB at $\lambda\lambda$3620, 4015, 4200, and 4226, was especially sensitive to errors at $\lambda\lambda$4200 and 4226. Again the eye-drawn interpolation curve was compared with the computed curve. Appropriate corections were made to the data of eighteen nights. Except for one night when missing data at λ4226 greatly distorted the computed interpolated curve, the largest correction was $+0\overset{m}{.}034$.

Although corrections comparable to those already mentioned were also probably needed at λ6564, the OB - AB curves were quite steep at this wavelength because of rapid loss of sensitivity in the S-20 photo-tubes. OB - AB curves, which could be drawn with accuracies better than $0\overset{m}{.}01$ at the previously mentioned wavelengths, could not be drawn with accuracies better than about $0\overset{m}{.}03$ or $0\overset{m}{.}04$ near H alpha. Thus it was not practical to attempt to improve upon the computed curves. The result is probable larger random errors at λ6564 than in adjacent spectral regions.

There is an apparent problem in the calibration of the standards near the Na D - lines which caused unnatural "dips" in the instrumental response curves OB - AB at $\lambda\lambda$5820 and 5892. Apparently the standards are not so bright in this region as indicated by their calibrations. This irregularity was independent of choice of standards which seems to indicate an error in the calibration of Alpha Lyr. (Reference to Figure 1 of Oke and Schild (1970) shows that except for the ultraviolet region of the spectrum their greatest scatter in the calibration of Alpha Lyr

occurred at λ5840. Reference to their Figure 2 shows that their flux of Alpha Lyr at λ5840 is somewhat greater than that of Hayes' 1970 calibration.) It was not possible to correct for this problem by a visual smoothing of the OB - AB curves since the points $\lambda\lambda$5820 and 5892 fell near the peak of the Mt. Wilson response curves where accurate interpolation was impossible. The Palomar curves were not peaked in this region because of a different grating blaze. However these curves suggest a correction of $0\overset{m}{.}05$ at λ5820, a correction which appears too large when applied because it creates unnatural "saddles" in the unknown energy distributions. A differential correction of $0\overset{m}{.}025$ was determined between $\lambda\lambda$5820 and 5890 by comparing the measured D-feature strength in HD 19445 with its equivalent width measured from a microphotometer tracing (tracings were also made of MgI "b" and H alpha which agreed with scanner measurements). Thus $0\overset{m}{.}025$ has been added to all λ5892 magnitudes. An additional correction between $0\overset{m}{.}00$ and $0\overset{m}{.}05$ should probably be added to all $\lambda\lambda$5820 and 5892 magnitudes. In any case there can be no resultant error in the synthesized models arising from this problem since the error appears to be the same for all observations.

The blue wing of H gamma depressed the flux in the G-band λ4305 bandpass by as much as $0\overset{m}{.}06$ in the A0 standards Alpha Lyr, Gamma Gem, 109 Vir, and 58 Aql and by lesser amounts in the other standards. A separate correction to the OB-AB curves was determined for each

standard and appropriate corrections were determined and applied to the λ4305 fluxes of program objects.

200-inch observations of M31 clusters were reduced in the same manner as the other observations. OB - AB curves were smoothed visually for each channel and compared with computed OB - AB curves. Appropriate corrections were then made.

During the observations of H55, B282, MIV, and NGC 205 channel 21 of the multi-channel spectrometer had an extremely insensitive response. Resultant data did not fit smoothly into the derived energy distributions. The flux at λ7050, which fell within this channel, has therefore been interpolated from continuum measurements made with adjacent channels.

Channel 24 inadvertently remained disconnected during the scans of H12. The flux at λ8050 was consequently not measured; nor could it be interpolated because no reliable data were accumulated at longer wavelengths.

The two scans of MIV were taken through thin cirrus clouds. Data reductions for MIV were accomplished by assuming that a separate gray correction applied to each integration. Since each gray correction applied to not one but eighteen channels, it was possible to determine the corrections by requiring a smooth continuum. This method seemed to produce satisfactory results, but the energy distribution of MIV should be regarded as somewhat less accurate than those of the

other M31 clusters.

C) Averaging of Scans

Except for HD 60778 the number of scans obtained for program objects ranged from two for many objects to seventeen for M15. Scans of each object were intercompared and gray corrections were added to bring them into as close agreement as possible. Scans which then appeared discrepant (fewer than 5 per cent of the total) were discarded. If only two disagreeing scans were available a third was obtained to permit discrimination of the discrepant scan. Scans were then averaged to yield the final energy distributions. Since scans of a given object differed from one another by only a few hundredths of a magnitude, averaging of magnitudes introduced no significant errors despite their logarithmic nature.

Errors in the final energy distributions have been estimated from the scatter of the individual scans about the final distributions. Their accuracies are discussed in section II, except for wavelengths longward of λ8050. Errors in this spectral region are probably about five per cent. Poor photon statistics and H_2O atmospheric absorption are responsible for the relatively large errors. Because of their unimportance in the present program no corrections such as those described in part B of this appendix have been applied to these data.

D) Reddening Corrections

Interstellar extinction data are not available for most of the program stars. Those stars with known color excesses have been unreddened according to the Whitford (1958) law. Stars thus corrected are listed in Table A1.

Most of the stars observed were high-velocity stars lying away from the galactic plane. If the reddening at the galactic poles is only $E_{B-V} = 0.02$ or 0.03 as the work of Sturch (1966) and Peterson (1968) suggests, reddenings of most objects are only a few hundredths of a magnitude. ($E_{\lambda 3448-\lambda 8050} = 2.95\ E_{B-V}$.)

The population II red-giant HDE 232078 has a very large but unknown color excess. For this reason it has been excluded from the stellar population sequences.

Interstellar extinction corrections have not been applied to the globular cluster spectra. Their color excesses have been taken into consideration in the synthesis process.

TABLE A1

STARS CORRECTED FOR REDDENING

Name	E_{B-V}	Reference
HD 2665	0.07	Koelbloed (1967)
HD 165195	0.25	Wallerstein et al. (1963)
HD 221170	0.05	Wallerstein et al. (1963)
M92 giants	0.02	McNamara and Langford (1969), Sandage (1969)

APPENDIX B

BASIC DATA

A) Observational Data

Table B1 gives the observed energy distributions in magnitude form for the ten program clusters and for the nucleus of NGC 205. The magnitudes are defined

$$m_\nu = -2.5 \log F_\nu + \text{constant} \quad , \qquad \text{(B-1)}$$

where F is the flux per unit frequency interval outside the earth's atmosphere. The data are reduced to the absolute calibration of Alpha Lyr of Oke and Schild (1970). Except at λ5050, the arbitrarily chosen zero point for the magnitude scale, a null entry in the table indicates an absence of data. Cluster line indices are given in Table B2.

Energy distributions for the program stars are given in Table B3. Unlike the clusters, a few of these objects have been corrected for interstellar reddening. HD 2665, HD 165195, HD 221170, and the M92 cluster members have had their spectra adjusted by the Whitford (1958) law for the color excesses in Table A1. Line indices of individual stars are not given.

B) Mean Stellar Types

The individual stellar data of Table B3 have been combined into mean stellar types as described in section III A. Table B4 gives mean stellar energy distributions in magnitude form and Table B5 gives the mean stellar indices.

The data of Table B5 are plotted in Figures B1 - B19. The index V/R, a temperature parameter, serves as abscissa in all plots. Figures B1 and B2 illustrate the behavior of the continuum indices U/B and B/V. Figures B3 - B19 depict feature index behaviors.

TABLE B1

GLOBULAR CLUSTER MAGNITUDES

LAMBDA	M3	M5	M13	M15	M92	M31 H12
3448.	1.376	1.656	1.482	1.597	1.446	1.625
3570.	1.392	1.563	1.418	1.447	1.376	1.635
3620.	1.386	1.452	1.286	1.368	1.269	1.535
3784.	0.940	1.001	0.914	0.970	0.885	1.315
3798.	1.075	1.086	0.936	0.994	0.870	0.0
3815.	0.848	0.986	0.919	0.893	0.805	1.280
3835.	1.011	1.190	1.021	0.992	0.912	0.0
3860.	0.930	0.888	0.812	0.775	0.676	1.236
3880.	0.933	1.013	0.924	0.909	0.893	1.279
3910.	0.762	0.825	0.752	0.718	0.664	1.075
3933.	0.975	1.118	0.979	0.906	0.824	1.530
4015.	0.603	0.646	0.533	0.604	0.537	0.716
4101.	0.609	0.747	0.671	0.763	0.709	0.839
4200.	0.477	0.540	0.449	0.522	0.463	0.662
4226.	0.491	0.538	0.475	0.516	0.459	0.577
4270.	0.489	0.493	0.401	0.485	0.400	0.586
4305.	0.0	0.585	0.497	0.532	0.432	0.732
4400.	0.395	0.378	0.340	0.325	0.325	0.425
4430.	0.394	0.343	0.278	0.349	0.289	0.376
4500.	0.236	0.252	0.233	0.336	0.254	0.329
4780.	0.085	0.148	0.105	0.153	0.152	0.148
4970.	0.005	0.057	0.024	0.037	0.035	0.0
5050.	0.0	0.0	0.0	0.0	0.0	0.0
5175.	-0.049	0.017	-0.008	-0.024	-0.011	-0.027
5300.	-0.169	-0.097	-0.100	-0.094	-0.059	-0.135
5820.	-0.384	-0.291	-0.285	-0.270	-0.192	-0.317
5892.	-0.245	-0.280	-0.265	-0.266	-0.208	-0.291
6100.	0.0	-0.333	-0.371	-0.347	-0.308	-0.385
6180.	0.0	-0.378	-0.364	-0.357	-0.304	-0.381
6370.	0.0	-0.427	-0.392	-0.383	-0.375	-0.447
6564.	0.0	-0.398	-0.379	-0.403	-0.366	-0.453
7050.	0.0	-0.601	-0.537	-0.581	-0.479	-0.645
7100.	0.0	-0.593	-0.537	-0.566	-0.516	-0.629
7400.	0.0	-0.635	-0.559	-0.615	-0.565	-0.714
8050.	0.0	-0.715	-0.729	-0.752	-0.570	0.0
8190.	0.0	-0.600	-0.717	0.0	0.0	0.0
8400.	0.0	-0.778	0.0	0.0	0.0	0.0
8543.	0.0	-0.739	0.0	0.0	0.0	0.0
8800.	0.0	-0.825	0.0	0.0	0.0	0.0
8880.	0.0	-0.851	0.0	0.0	0.0	0.0
9190.	0.0	-0.578	0.0	0.0	0.0	0.0
9950.	0.0	-0.927	0.0	0.0	0.0	0.0
10400.	0.0	0.0	0.0	0.0	0.0	0.0
10800.	0.0	0.0	0.0	0.0	0.0	0.0

TABLE B1 (CONTINUED)

GLOBULAR CLUSTER MAGNITUDES

LAMBDA	M31 H55	M31 H140	M31 B282	M31 MIV	NGC205 NUCL
3448.	1.807	1.495	2.035	1.462	1.385
3570.	2.097	1.505	2.075	1.382	1.308
3620.	1.910	1.285	1.711	1.352	1.297
3784.	1.633	1.221	1.677	1.130	1.160
3798.	0.0	0.0	0.0	0.0	0.0
3815.	1.497	1.135	1.605	0.962	1.075
3835.	0.0	0.0	0.0	0.0	0.0
3860.	1.437	1.026	1.535	0.785	0.945
3880.	1.803	1.183	1.853	0.879	1.031
3910.	1.420	0.922	1.425	0.652	0.965
3933.	2.134	1.266	2.088	0.947	1.359
4015.	0.877	0.553	0.961	0.512	0.616
4101.	0.978	0.740	0.994	0.734	0.587
4200.	0.810	0.515	0.824	0.449	0.461
4226.	0.851	0.490	0.801	0.412	0.457
4270.	0.759	0.509	0.740	0.404	0.503
4305.	0.899	0.552	0.882	0.457	0.709
4400.	0.457	0.355	0.545	0.362	0.345
4430.	0.462	0.305	0.529	0.260	0.316
4500.	0.367	0.138	0.385	0.197	0.225
4780.	0.057	0.050	0.078	0.027	0.042
4970.	-0.001	0.0	0.042	-0.027	0.019
5050.	0.0	0.0	0.0	0.0	0.0
5175.	0.075	-0.042	0.120	-0.077	0.105
5300.	-0.163	-0.115	-0.135	-0.148	-0.155
5820.	-0.428	-0.345	-0.388	-0.302	-0.195
5892.	-0.282	-0.283	-0.298	-0.318	-0.143
6100.	-0.483	-0.385	-0.435	-0.358	-0.215
6180.	-0.510	-0.341	-0.435	-0.365	-0.205
6370.	-0.538	-0.463	-0.532	-0.388	-0.265
6564.	-0.531	-0.429	-0.557	-0.362	-0.218
7050.	-0.708	-0.645	-0.695	-0.538	-0.365
7100.	-0.706	-0.635	-0.700	-0.486	-0.321
7400.	-0.857	-0.716	-0.848	-0.628	-0.383
8050.	-1.031	-0.797	-1.065	-0.785	-0.455
8190.	0.0	0.0	0.0	0.0	0.0
8400.	0.0	0.0	0.0	0.0	0.0
8543.	0.0	0.0	0.0	0.0	0.0
8800.	0.0	0.0	0.0	0.0	0.0
8880.	0.0	0.0	0.0	0.0	0.0
9190.	0.0	0.0	0.0	0.0	0.0
9950.	0.0	0.0	0.0	0.0	0.0
10400.	0.0	0.0	0.0	0.0	0.0
10800.	0.0	0.0	0.0	0.0	0.0

TABLE B2

GLOBULAR CLUSTER INDICES

INDEX	M3	M5	M13	M15	M92	M31 H12	M31 H55	M31 H140	M31 B282
H 3798	[illegible]	[illegible]	[illegible]	[illegible]	[illegible]	[illegible]	[illegible]	[illegible]	[illegible]
H 3835	0.889	0.796	0.871	0.869	0.859	0.0	0.0	0.0	0.0
CN 3860	0.893	1.019	1.024	1.031	1.058	0.950	1.022	1.005	0.984
CN 3880	[illegible]	[illegible]	[illegible]	[illegible]	[illegible]	[illegible]	0.719	0.835	0.709
CAII3933	0.795	0.736	0.775	0.822	0.841	0.607	0.456	0.671	0.488
H 4101	0.959	0.868	0.845	0.832	0.817	0.857	[illegible]	[illegible]	[illegible]
CN 42[illegible]	1.040	0.995	0.988	0.995	0.976	0.963	0.982	1.004	0.977
CAI 4226	1.016	0.982	0.953	0.990	0.967	1.029	0.936	1.024	0.978
CH 4305	0.0	[illegible]	[illegible]	[illegible]	[illegible]	[illegible]	[illegible]	[illegible]	[illegible]
IS 4430	0.904	0.997	1.028	0.981	1.013	1.018	0.971	0.984	0.970
MGH 4780	1.025	0.975	1.005	1.007	0.972	1.009	1.115	1.012	1.102
TIO 497[illegible]	[illegible]	[illegible]	[illegible]	[illegible]	[illegible]	[illegible]	[illegible]	[illegible]	1.010
MGI 5175	0.967	0.941	0.961	0.978	0.982	0.963	0.865	0.985	0.841
NAI 5892	0.858	0.979	0.962	0.978	0.987	0.960	0.862	[illegible]	[illegible]
TIO 618[illegible]	[illegible]	1.016	0.987	0.999	0.978	0.979	1.009	0.940	0.973
H 6564	0.0	0.928	0.949	0.965	0.962	0.952	0.948	0.922	0.978
TIO 7100	0.0	0.988	[illegible]	[illegible]	[illegible]	[illegible]	[illegible]	[illegible]	[illegible]
NAI 8190	0.0	0.878	0.955	0.0	0.0	0.0	0.0	0.0	0.0
CAII8543	0.0	0.949	0.0	0.0	0.0	0.0	0.0	0.0	0.0
TIO 888[illegible]	[illegible]	1.[illegible]65	[illegible]	[illegible]	[illegible]	[illegible]	[illegible]	[illegible]	[illegible]
CN 9190	0.0	0.767	0.0	0.0	0.0	0.0	0.0	0.0	0.0
U/B	[illegible]	[illegible]	[illegible]	[illegible]	.413	[illegible]	.275	[illegible]	[illegible]
B/V	0.537	0.559	0.593	0.582	0.637	0.509	0.436	0.542	0.434
V/R	0.0	0.679	0.726	0.687	0.695	0.661	0.642	0.664	0.628
V/I	[illegible]	[illegible]	[illegible]	0.0	0.0	0.0	0.0	0.0	0.0
V/J	0.0	0.0	0.0	0.0	0.0	0.0	0.0	0.0	0.0

TABLE B2 (CONTINUED)

GLOBULAR CLUSTER INDICES

INDEX	M31 MIV	NGC205 NUCL
H 3798	0.0	0.0
H 3835	[illegible]	[illegible]
CN 3860	1.021	1.074
CN 3880	0.883	0.971
CAII3933	[illegible]	[illegible]
H 4101	0.787	0.991
CN 4200	0.993	1.070
CAI 4226	1.009	1.062
CH 4305	0.942	0.795
IS 4430	1.048	0.993
MGH 4780	1.062	1.051
TIO 4970	1.051	1.011
MGI 5175	1.002	1.884
NAI 5892	1.001	0.948
TIO 6180	0.998	0.977
H 6564	[illegible]	[illegible]
TIO 7100	0.942	0.957
NAI 8190	0.0	0.0
CAII8543	[illegible]	[illegible]
TIO 8880	0.0	0.0
CN 9190	0.0	0.0
U/B	0.404	0.444
B/V	0.570	0.603
V/R	[illegible]	[illegible]
V/I	0.0	0.0
V/J	0.0	0.0

TABLE B3

STELLAR MAGNITUDES

LAMBDA	HD 2665	HD 3546	HD 6755	HD 6833	HD 9774	HD 10700
3448.	1.519	2.072	1.564	2.509	2.367	1.662
3570.	1.408	2.086	1.413	2.649	2.452	1.568
3620.	1.334	1.816	1.358	2.355	2.057	1.503
3784.	1.019	1.440	1.062	2.046	1.866	1.105
3798.	1.041	1.520	1.107	2.152	2.072	1.240
3815.	1.023	1.670	1.122	2.341	2.147	1.290
3835.	1.076	1.873	1.220	2.469	2.481	1.861
3860.	0.930	1.767	0.977	2.388	2.429	1.338
3880.	1.047	1.658	1.074	2.316	2.206	1.335
3910.	0.913	1.384	0.979	2.023	1.631	1.131
3933.	1.316	1.960	1.522	2.796	2.380	1.730
4015.	0.629	0.894	0.698	1.356	1.101	0.719
4101.	0.620	0.838	0.653	1.207	1.004	0.680
4200.	0.498	0.762	0.559	1.114	1.038	0.612
4226.	0.529	0.751	0.558	1.095	0.889	0.627
4270.	0.494	0.758	0.541	1.011	0.836	0.635
4305.	0.744	0.971	0.758	1.289	1.148	0.895
4400.	0.379	0.538	0.403	0.771	0.656	0.489
4430.	0.327	0.429	0.358	0.678	0.556	0.358
4500.	0.260	0.286	0.268	0.446	0.381	0.246
4780.	0.100	0.098	0.081	0.155	0.131	0.075
4970.	0.004	0.033	0.043	0.061	0.044	0.005
5050.	0.0	0.0	0.0	0.0	0.0	0.0
5175.	0.005	0.017	0.004	0.020	0.057	0.103
5300.	-0.106	-0.128	-0.119	-0.212	-0.160	-0.127
5820.	-0.263	-0.353	-0.267	-0.543	-0.377	-0.317
5892.	-0.261	-0.339	-0.254	-0.507	-0.333	-0.255
6100.	-0.345	-0.394	-0.337	-0.626	-0.415	-0.337
6180.	-0.353	-0.400	-0.347	-0.641	-0.414	-0.334
6370.	-0.410	-0.458	-0.379	-0.736	-0.482	-0.386
6564.	-0.363	-0.410	-0.311	-0.729	-0.460	-0.300
7050.	-0.562	-0.595	-0.536	-0.965	-0.659	-0.486
7100.	-0.573	-0.599	-0.531	-0.989	-0.651	-0.503
7400.	-0.590	-0.616	-0.558	-1.046	-0.644	-0.505
8050.	-0.650	-0.695	-0.602	-1.227	-0.712	-0.545
8190.	0.0	0.0	0.0	0.0	0.0	0.0
8400.	0.0	0.0	0.0	0.0	0.0	0.0
8543.	0.0	0.0	0.0	0.0	0.0	0.0
8800.	0.0	0.0	0.0	0.0	0.0	0.0
8880.	0.0	0.0	0.0	0.0	0.0	0.0
9190.	0.0	0.0	0.0	0.0	0.0	0.0
9950.	0.0	0.0	0.0	0.0	0.0	0.0
10400.	0.0	0.0	0.0	0.0	0.0	0.0
10800.	0.0	0.0	0.0	0.0	0.0	0.0

TABLE B3 (CONTINUED)

STELLAR MAGNITUDES

LAMBDA	HD 19445	HD 25329	HD 37160	HD 43039	HD 44007	HD 46703
3448.	0.997	1.966	2.431	2.301	1.589	1.923
3570.	0.930	1.775	2.335	2.457	1.567	1.869
3620.	0.861	1.548	2.056	2.117	1.499	1.745
3734.	0.647	1.436	1.620	1.850	1.226	0.831
3798.	0.742	1.459	1.757	2.099	1.216	0.831
3815.	0.640	1.783	1.880	2.206	1.262	0.779
3835.	0.807	1.937	2.247	2.555	1.338	0.911
3860.	0.563	1.806	2.054	2.461	1.122	0.673
3880.	0.675	1.661	1.952	2.282	1.221	0.870
3910.	0.530	1.419	1.534	1.693	1.135	0.511
3933.	0.725	2.080	2.252	2.443	1.701	0.712
4015.	0.360	0.837	1.022	1.112	0.808	0.341
4101.	0.475	0.829	0.922	0.999	0.757	0.536
4200.	0.275	0.780	0.865	1.047	0.695	0.355
4226.	0.290	0.855	0.867	0.894	0.687	0.330
4270.	0.255	0.795	0.824	0.891	0.672	0.320
4305.	0.321	0.982	1.147	1.224	0.946	0.375
4400.	0.190	0.532	0.634	0.677	0.555	0.250
4430.	0.206	0.407	0.499	0.533	0.427	0.219
4500.	0.152	0.281	0.304	0.341	0.314	0.189
4780.	0.032	0.134	0.104	0.099	0.157	0.096
4970.	0.044	0.009	-0.003	0.020	0.031	-0.001
5050.	0.0	0.0	0.0	0.0	0.0	0.0
5175.	-0.005	0.172	0.057	0.072	-0.001	0.004
5300.	-0.056	-0.132	-0.178	-0.172	-0.096	-0.021
5820.	-0.140	-0.350	-0.420	-0.426	-0.304	-0.135
5892.	-0.130	-0.292	-0.377	-0.363	-0.303	-0.074
6100.	-0.170	-0.410	-0.483	-0.473	-0.372	-0.144
6180.	-0.178	-0.427	-0.488	-0.482	-0.361	-0.134
6370.	-0.188	-0.478	-0.544	-0.541	-0.430	-0.168
6564.	-0.042	-0.436	-0.516	-0.516	-0.387	-0.087
7050.	-0.277	-0.579	-0.704	-0.704	-0.572	-0.224
7100.	-0.275	-0.614	-0.711	-0.704	-0.585	-0.215
7400.	-0.305	-0.648	-0.725	-0.731	-0.610	-0.222
8050.	-0.316	-0.618	-0.841	-0.849	-0.718	-0.177
8190.	0.0	0.0	0.0	-0.865	0.0	0.0
8400.	0.0	0.0	0.0	-0.898	0.0	0.0
8543.	0.0	0.0	0.0	-0.799	0.0	0.0
8800.	0.0	0.0	0.0	-0.926	0.0	0.0
8880.	0.0	0.0	0.0	-0.967	0.0	0.0
9190.	0.0	0.0	0.0	-0.879	0.0	0.0
9950.	0.0	0.0	0.0	-1.001	0.0	0.0
10400.	0.0	0.0	0.0	-1.015	0.0	0.0
10800.	0.0	0.0	0.0	-0.699	0.0	0.0

TABLE B3 (CONTINUED)

STELLAR MAGNITUDES

LAMBDA	HD 60552	HD 60778	HD 64090	HD 73394	HD 74462	HD 74721
3448.	1.148	1.373	1.159	2.078	1.860	1.272
3570.	1.110	1.406	1.139	2.178	2.015	1.274
3620.	1.091	1.358	1.020	2.064	1.821	1.267
3784.	0.778	0.562	0.843	1.761	1.589	0.465
3798.	0.888	0.792	0.874	1.770	1.587	0.688
3815.	0.741	0.300	0.961	1.923	1.829	0.195
3835.	0.986	0.779	1.079	1.917	1.694	0.664
3860.	0.663	0.134	0.821	1.855	1.627	0.023
3880.	0.810	0.582	0.904	1.856	1.603	0.455
3910.	0.640	0.095	0.822	1.711	1.581	-0.032
3933.	0.968	0.024	1.292	2.391	1.997	-0.080
4015.	0.399	-0.100	0.528	1.174	1.018	-0.148
4101.	0.593	0.649	0.537	1.070	0.937	0.579
4200.	0.341	-0.047	0.461	0.968	0.843	-0.135
4226.	0.349	-0.014	0.476	0.989	0.868	-0.135
4270.	0.307	-0.035	0.461	0.882	0.867	-0.125
4305.	0.505	0.063	0.662	1.070	0.917	-0.076
4400.	0.227	0.020	0.312	0.664	0.644	-0.100
4430.	0.194	-0.008	0.258	0.612	0.560	-0.113
4500.	0.141	0.009	0.194	0.424	0.406	-0.099
4780.	0.053	0.063	0.072	0.190	0.201	-0.028
4970.	0.009	0.006	0.028	0.038	0.048	-0.022
5050.	0.0	0.0	0.0	0.0	0.0	0.0
5175.	0.016	0.078	0.039	-0.012	-0.011	0.025
5300.	-0.055	0.072	-0.069	-0.165	-0.098	0.054
5820.	-0.135	0.138	-0.225	-0.439	-0.382	0.140
5892.	-0.099	0.147	-0.183	-0.412	-0.360	0.160
6100.	-0.139	0.163	-0.268	-0.538	-0.450	0.195
6130.	-0.136	0.202	-0.289	-0.551	-0.490	0.201
6370.	-0.156	0.226	-0.323	-0.627	-0.512	0.232
6564.	0.024	0.593	-0.231	-0.610	-0.538	0.616
7050.	-0.176	0.294	-0.427	-0.812	-0.732	0.348
7100.	-0.178	0.302	-0.433	-0.839	-0.734	0.345
7400.	-0.158	0.352	-0.429	-0.900	-0.761	0.384
8050.	-0.185	0.364	-0.498	-0.976	-0.884	0.473
8190.	0.0	0.0	-0.527	0.0	0.0	0.0
8400.	0.0	0.0	-0.551	0.0	0.0	0.0
8543.	0.0	0.0	-0.443	0.0	0.0	0.0
8800.	0.0	0.0	-0.567	0.0	0.0	0.0
8880.	0.0	0.0	-0.570	0.0	0.0	0.0
9190.	0.0	0.0	-0.534	0.0	0.0	0.0
9950.	0.0	0.0	-0.518	0.0	0.0	0.0
10400.	0.0	0.0	-0.548	0.0	0.0	0.0
10800.	0.0	0.0	-0.109	0.0	0.0	0.0

TABLE B3 (CONTINUED)

STELLAR MAGNITUDES

LAMBDA	HD 79452	HD 81192	HD 84937	HD 85504	HD 86986	HD 88609
3448.	1.875	2.099	1.022	0.954	1.416	1.924
3570.	1.814	2.087	0.964	0.990	1.402	1.884
3620.	1.737	1.927	0.921	0.973	1.364	1.758
3784.	1.332	1.592	0.647	0.272	0.549	1.417
3798.	1.470	1.736	0.740	0.541	0.754	1.431
3815.	1.483	1.784	0.577	0.067	0.338	1.395
3835.	1.812	2.204	0.776	0.537	0.763	1.378
3860.	1.638	1.932	0.469	-0.089	0.142	1.271
3880.	1.688	1.961	0.583	0.153	0.397	1.330
3910.	1.274	1.565	0.432	-0.102	0.162	1.198
3932.	1.920	2.287	0.519	-0.145	0.018	1.483
4015.	0.851	1.052	0.278	-0.225	-0.056	0.968
4101.	0.753	0.902	0.489	0.443	0.603	0.893
4200.	0.731	0.867	0.224	-0.187	-0.067	0.782
4226.	0.696	0.874	0.220	-0.175	-0.043	0.747
4270.	0.708	0.854	0.206	-0.163	-0.049	0.674
4305.	1.021	1.143	0.236	-0.128	-0.008	0.722
4400.	0.528	0.648	0.159	-0.141	-0.050	0.520
4430.	0.417	0.528	0.149	-0.136	-0.044	0.486
4500.	0.280	0.351	0.125	-0.116	-0.048	0.409
4780.	0.117	0.139	0.072	-0.045	0.0	0.192
4970.	0.015	0.036	0.019	-0.019	-0.014	0.020
5050.	0.0	0.0	0.0	0.0	0.0	0.0
5175.	0.023	0.104	0.011	0.040	0.038	-0.044
5300.	-0.100	-0.133	-0.021	0.065	0.042	-0.137
5820.	-0.304	-0.363	-0.079	0.169	0.094	-0.385
5892.	-0.283	-0.332	-0.074	0.211	0.124	-0.403
6100.	-0.360	-0.434	-0.125	0.235	0.121	-0.509
6180.	-0.372	-0.431	-0.113	0.255	0.123	-0.517
6370.	-0.425	-0.498	-0.141	0.296	0.134	-0.583
6564.	-0.388	-0.456	0.008	0.694	0.431	-0.553
7050.	-0.556	-0.639	-0.195	0.429	0.181	-0.763
7100.	-0.575	-0.637	-0.193	0.439	0.196	-0.788
7400.	-0.589	-0.628	-0.201	0.530	0.212	-0.807
8050.	-0.677	-0.599	-0.220	0.601	0.268	-0.918
8190.	-0.718	0.0	-0.222	0.0	0.0	0.0
8400.	-0.720	0.0	-0.269	0.0	0.0	0.0
8543.	-0.648	0.0	-0.244	0.0	0.0	0.0
8800.	-0.813	0.0	-0.368	0.0	0.0	0.0
8880.	-0.861	0.0	-0.291	0.0	0.0	0.0
9190.	-0.711	0.0	-0.162	0.0	0.0	0.0
9950.	-0.729	0.0	0.0	0.0	0.0	0.0
10400.	-0.689	0.0	0.0	0.0	0.0	0.0
10800.	-0.317	0.0	0.0	0.0	0.0	0.0

TABLE B3 (CONTINUED)

STELLAR MAGNITUDES

LAMBDA	HD 90362	HD 94028	HD 103095	HD 106223	HD 107328	HD 109995
3448.	2.917	0.989	1.576	1.156	2.616	1.287
3570.	3.315	0.930	1.603	1.105	2.836	1.304
3620.	3.079	0.878	1.351	1.082	2.440	1.272
3784.	2.912	0.651	1.121	0.574	2.237	0.418
3798.	3.077	0.752	1.173	0.708	2.430	0.652
3815.	3.196	0.634	1.416	0.462	2.612	0.190
3835.	3.343	0.836	1.584	0.713	2.901	0.674
3860.	3.172	0.537	1.189	0.376	2.738	-0.004
3880.	3.126	0.657	1.230	0.595	2.570	0.442
3910.	2.824	0.540	1.153	0.318	2.075	-0.089
3933.	3.446	0.872	1.821	0.308	2.834	-0.082
4015.	1.971	0.349	0.675	0.164	1.356	-0.198
4101.	1.770	0.477	0.626	0.499	1.264	0.559
4200.	1.688	0.273	0.569	0.150	1.260	-0.175
4226.	1.882	0.283	0.650	0.160	1.160	-0.154
4270.	1.469	0.253	0.576	0.136	1.075	-0.144
4305.	1.473	0.342	0.786	0.199	1.314	-0.079
4400.	0.994	0.173	0.396	0.089	0.775	-0.119
4430.	0.831	0.173	0.327	0.090	0.646	-0.114
4500.	0.526	0.119	0.200	0.068	0.394	-0.104
4780.	0.314	0.034	0.084	0.047	0.152	-0.060
4970.	0.051	0.006	0.022	0.015	0.022	-0.018
5050.	0.0	0.0	0.0	0.0	0.0	0.0
5175.	0.234	0.0	0.142	0.014	0.104	0.020
5300.	-0.398	-0.050	-0.112	-0.014	-0.216	0.043
5820.	-0.831	-0.141	-0.293	-0.052	-0.526	0.114
5892.	-0.587	-0.121	-0.258	-0.008	-0.464	0.145
6100.	-0.984	-0.179	-0.357	-0.052	-0.584	0.160
6180.	-0.816	-0.181	-0.363	-0.069	-0.607	0.179
6370.	-1.057	-0.206	-0.427	-0.072	-0.688	0.197
6564.	-1.137	-0.061	-0.373	0.148	-0.674	0.540
7050.	-1.439	-0.250	-0.564	-0.093	-0.875	0.277
7100.	-1.269	-0.248	-0.572	-0.068	-0.882	0.276
7400.	-1.612	-0.267	-0.586	-0.087	-0.920	0.330
8050.	-1.817	-0.300	-0.667	-0.044	-1.061	0.388
8190.	-1.831	-0.297	-0.697	0.0	0.0	0.394
8400.	-1.902	-0.305	-0.712	0.0	0.0	0.450
8543.	-1.789	-0.294	-0.640	0.0	0.0	0.416
8800.	-2.033	-0.428	-0.738	0.0	0.0	0.148
8880.	-2.054	-0.449	-0.761	0.0	0.0	0.266
9190.	-1.981	-0.262	-0.728	0.0	0.0	0.439
9950.	-2.192	0.0	-0.758	0.0	0.0	0.413
10400.	-2.248	0.0	-0.697	0.0	0.0	0.0
10800.	-1.893	0.0	0.0	0.0	0.0	0.0

TABLE B3 (CONTINUED)

STELLAR MAGNITUDES

LAMBDA	HD 117880	HD 122563	HD 123598	HD 126778	HD 128167	HD 130952
3448.	1.194	1.941	2.629	2.233	1.071	2.159
3570.	1.255	1.808	3.123	2.256	1.045	2.340
3620.	1.325	1.694	3.045	1.950	0.996	1.994
3784.	0.476	1.329	2.844	1.717	0.649	1.812
3798.	0.675	1.361	2.980	1.849	0.781	1.949
3815.	0.269	1.309	3.028	2.008	0.584	2.109
3835.	0.637	1.392	3.161	2.272	0.855	2.347
3860.	0.035	1.217	2.975	2.182	0.431	2.277
3880.	0.209	1.278	2.945	2.038	0.651	2.051
3910.	0.056	1.175	2.772	1.578	0.430	1.620
3933.	-0.059	1.506	3.335	2.305	0.717	2.267
4015.	-0.110	0.931	2.005	1.020	0.216	1.031
4101.	0.555	0.862	1.706	0.947	0.519	0.950
4200.	-0.126	0.741	1.567	0.922	0.175	0.963
4226.	-0.093	0.730	1.844	0.874	0.165	0.880
4270.	-0.091	0.678	1.407	0.831	0.128	0.853
4305.	-0.094	0.795	1.335	1.130	0.230	1.116
4400.	-0.076	0.530	0.958	0.671	0.094	0.616
4430.	-0.084	0.473	0.874	0.540	0.074	0.489
4500.	-0.087	0.403	0.586	0.343	0.049	0.296
4780.	-0.041	0.205	0.570	0.147	0.0	0.087
4970.	-0.002	0.041	0.303	0.019	0.008	0.025
5050.	0.0	0.0	0.0	0.0	0.0	0.0
5175.	0.004	-0.031	0.203	0.060	0.032	0.066
5300.	0.021	-0.124	-0.502	-0.158	-0.016	-0.164
5820.	0.124	-0.358	-0.822	-0.365	-0.066	-0.408
5892.	0.147	-0.374	-0.408	-0.341	-0.028	-0.358
6100.	0.157	-0.463	-1.127	-0.433	-0.063	-0.455
6180.	0.174	-0.493	-0.611	-0.449	-0.063	-0.471
6370.	0.196	-0.565	-1.204	-0.492	-0.074	-0.514
6564.	0.584	-0.537	-1.365	-0.465	0.141	-0.483
7050.	0.255	-0.739	-1.840	-0.650	-0.082	-0.661
7100.	0.332	-0.749	-1.376	-0.651	-0.080	-0.666
7400.	0.283	-0.795	-2.268	-0.677	-0.060	-0.688
8050.	0.664	-0.893	-2.478	-0.788	-0.072	-0.786
8190.	0.0	0.0	0.0	0.0	-0.076	0.0
8400.	0.0	0.0	0.0	0.0	-0.067	0.0
8543.	0.0	0.0	0.0	0.0	0.001	0.0
8800.	0.0	0.0	0.0	0.0	-0.078	0.0
8880.	0.0	0.0	0.0	0.0	-0.056	0.0
9190.	0.0	0.0	0.0	0.0	-0.018	0.0
9950.	0.0	0.0	0.0	0.0	-0.032	0.0
10400.	0.0	0.0	0.0	0.0	0.002	0.0
10800.	0.0	0.0	0.0	0.0	0.0	0.0

TABLE B3 (CONTINUED)

STELLAR MAGNITUDES

LAMBDA	HD 134439	HD 134440	HD 135722	HD 140283	HD 142574	HD 144579
3448.	1.512	1.666	2.153	0.932	3.072	1.617
3570.	1.568	1.725	2.250	0.955	3.499	1.622
3620.	1.382	1.576	2.007	0.902	3.297	1.424
3784.	1.132	1.289	1.700	0.663	3.067	1.152
3798.	1.233	1.379	1.900	0.737	3.270	1.237
3815.	1.335	1.568	1.983	0.617	3.372	1.426
3835.	1.789	1.867	2.393	0.754	3.510	1.743
3860.	1.265	1.482	2.255	0.541	3.328	1.334
3880.	1.268	1.425	2.172	0.662	3.315	1.382
3910.	1.160	1.309	1.606	0.510	3.026	1.165
3933.	1.827	1.988	2.322	0.625	3.622	1.809
4015.	0.725	0.855	1.044	0.348	2.114	0.687
4101.	0.690	0.756	0.929	0.487	1.879	0.655
4200.	0.641	0.717	0.951	0.299	1.785	0.572
4226.	0.716	0.794	0.875	0.303	1.880	0.654
4270.	0.661	0.733	0.846	0.261	1.540	0.626
4305.	0.890	0.916	1.154	0.344	1.567	0.857
4400.	0.444	0.507	0.646	0.219	1.067	0.425
4430.	0.325	0.390	0.522	0.203	0.893	0.323
4500.	0.243	0.269	0.337	0.188	0.552	0.192
4780.	0.116	0.127	0.120	0.084	0.291	0.079
4970.	0.017	0.022	0.034	0.005	0.087	0.012
5050.	0.0	0.0	0.0	0.0	0.0	0.0
5175.	0.096	0.137	0.062	-0.014	0.169	0.161
5300.	-0.143	-0.113	-0.144	-0.065	-0.408	-0.124
5820.	-0.321	-0.338	-0.370	-0.176	-0.866	-0.298
5892.	-0.281	-0.310	-0.330	-0.178	-0.673	-0.222
6100.	-0.348	-0.410	-0.433	-0.204	-1.021	-0.333
6180.	-0.348	-0.401	-0.438	-0.224	-0.880	-0.335
6370.	-0.410	-0.454	-0.486	-0.255	-1.117	-0.389
6564.	-0.346	-0.394	-0.442	-0.131	-1.167	-0.312
7050.	-0.523	-0.584	-0.624	-0.338	-1.481	-0.494
7100.	-0.499	-0.619	-0.627	-0.360	-1.333	-0.502
7400.	-0.546	-0.651	-0.633	-0.380	-1.632	-0.496
8050.	-0.637	-0.721	-0.728	-0.395	-1.683	-0.585
8190.	0.0	0.0	0.0	0.0	0.0	0.0
8400.	0.0	0.0	0.0	0.0	0.0	0.0
8543.	0.0	0.0	0.0	0.0	0.0	0.0
8800.	0.0	0.0	0.0	0.0	0.0	0.0
8880.	0.0	0.0	0.0	0.0	0.0	0.0
9190.	0.0	0.0	0.0	0.0	0.0	0.0
9950.	0.0	0.0	0.0	0.0	0.0	0.0
10400.	0.0	0.0	0.0	0.0	0.0	0.0
10800.	0.0	0.0	0.0	0.0	0.0	0.0

TABLE B3 (CONTINUED)

STELLAR MAGNITUDES

LAMBDA	HD 148349	HD 151937	-15° 4515	HD 157089	HD 161817	HD 165195
3448.	2.954	2.673	1.431	1.362	1.479	2.229
3570.	3.555	2.922	1.463	1.284	1.406	2.259
3620.	3.404	2.512	1.494	1.213	1.371	2.167
3784.	3.192	2.331	0.912	0.919	0.544	1.830
3798.	3.313	2.442	1.152	0.979	0.724	1.796
3815.	3.388	2.722	0.869	0.943	0.369	1.791
3835.	3.473	2.789	1.154	1.234	0.745	1.856
3860.	3.316	2.724	0.707	0.855	0.207	1.678
3880.	3.288	2.610	0.952	0.958	0.470	1.709
3910.	3.119	2.200	0.690	0.815	0.158	1.626
3933.	3.636	2.992	0.705	1.376	0.153	2.144
4015.	2.377	1.464	0.447	0.537	-0.019	1.241
4101.	2.068	1.360	0.793	0.586	0.531	1.105
4200.	1.883	1.277	0.376	0.418	-0.035	0.963
4226.	2.096	1.239	0.397	0.424	-0.031	0.927
4270.	1.707	1.114	0.355	0.437	-0.037	0.856
4305.	1.600	1.335	0.413	0.637	0.048	0.988
4400.	1.147	0.842	0.313	0.330	-0.010	0.664
4430.	1.042	0.767	0.312	0.276	-0.018	0.623
4500.	0.718	0.490	0.231	0.204	-0.011	0.490
4780.	0.502	0.208	0.122	0.064	-0.017	0.205
4970.	0.222	0.046	0.046	0.039	-0.010	0.054
5050.	0.0	0.0	0.0	0.0	0.0	0.0
5175.	0.184	0.089	-0.015	0.053	0.015	-0.051
5300.	-0.451	-0.215	-0.098	-0.063	0.003	-0.172
5820.	-0.916	-0.540	-0.249	-0.167	0.048	-0.461
5892.	-0.572	-0.485	-0.217	-0.139	0.070	-0.436
6100.	-1.129	-0.615	-0.292	-0.198	0.065	-0.567
6180.	-0.759	-0.631	-0.303	-0.203	0.070	-0.580
6370.	-1.224	-0.715	-0.309	-0.225	0.081	-0.646
6564.	-1.360	-0.693	-0.124	-0.109	0.354	-0.643
7050.	-1.761	-0.940	-0.450	-0.290	0.081	-0.838
7100.	-1.471	-0.933	-0.447	-0.306	0.082	-0.856
7400.	-2.087	-0.973	-0.489	-0.313	0.119	-0.908
8050.	-2.370	-1.128	-0.594	-0.363	0.180	-1.024
8190.	-2.421	-1.168	0.0	0.0	0.0	-1.057
8400.	-2.472	-1.214	0.0	0.0	0.0	-1.076
8543.	-2.411	-1.115	0.0	0.0	0.0	-1.068
8800.	-2.789	-1.285	0.0	0.0	0.0	-1.289
8880.	-2.829	-1.320	0.0	0.0	0.0	-1.314
9190.	-2.668	-1.285	0.0	0.0	0.0	-1.139
9950.	-2.907	-1.437	0.0	0.0	0.0	-1.263
10400.	0.0	-1.465	0.0	0.0	0.0	0.0
10800.	0.0	-1.156	0.0	0.0	0.0	0.0

TABLE B3 (CONTINUED)

STELLAR MAGNITUDES

LAMBDA	HD 165908	HD 175305	HD 182762	HDE 232078	HD 185657	HD 186776
3448.	1.197	1.619	2.321	3.004	2.395	3.286
3570.	1.150	1.585	2.473	3.535	2.470	3.441
3620.	1.089	1.478	2.117	3.590	2.108	3.216
3784.	0.830	1.215	1.890	3.508	1.898	2.967
3798.	0.895	1.192	2.038	3.444	2.109	3.003
3815.	0.817	1.265	2.218	3.531	2.244	3.084
3835.	1.080	1.281	2.597	3.569	2.569	3.210
3860.	0.710	1.136	2.485	3.529	2.440	2.997
3880.	0.840	1.214	2.292	3.463	2.282	2.992
3910.	0.692	1.120	1.737	3.246	1.702	2.793
3933.	1.141	1.690	2.439	3.889	2.423	3.432
4015.	0.425	0.767	1.110	2.615	1.109	1.996
4101.	0.536	0.707	1.021	2.355	1.031	1.665
4200.	0.350	0.635	1.045	2.066	1.049	1.487
4226.	0.358	0.635	0.939	2.046	0.917	1.715
4270.	0.346	0.625	0.892	1.820	0.883	1.302
4305.	0.511	0.829	1.189	1.788	1.153	1.300
4400.	0.243	0.472	0.675	1.373	0.677	0.902
4430.	0.189	0.405	0.542	1.311	0.556	0.857
4500.	0.126	0.303	0.350	0.986	0.358	0.563
4780.	0.051	0.129	0.124	0.500	0.109	0.571
4970.	0.013	0.036	0.050	0.189	0.018	0.335
5050.	0.0	0.0	0.0	0.0	0.0	0.0
5175.	0.029	-0.005	0.086	0.016	0.073	0.224
5300.	-0.072	-0.098	-0.159	-0.463	-0.176	-0.564
5820.	-0.173	-0.239	-0.403	-1.051	-0.401	-0.873
5892.	-0.134	-0.275	-0.349	-0.973	-0.355	-0.432
6100.	-0.196	-0.360	-0.449	-1.298	-0.457	-1.148
6180.	-0.198	-0.363	-0.459	-1.172	-0.469	-0.570
6370.	-0.227	-0.402	-0.520	-1.487	-0.521	-1.258
6564.	-0.086	-0.345	-0.486	-1.598	-0.501	-1.416
7050.	-0.232	-0.572	-0.676	-2.040	-0.680	-1.966
7100.	-0.235	-0.576	-0.668	-1.930	-0.672	-1.421
7400.	-0.292	-0.600	-0.689	-2.254	-0.700	-2.385
8050.	-0.332	-0.664	-0.750	-2.527	-0.787	-2.609
8190.	-0.339	-0.679	0.0	0.0	0.0	0.0
8400.	-0.333	-0.698	0.0	0.0	0.0	0.0
8543.	-0.303	-0.705	0.0	0.0	0.0	0.0
8800.	-0.446	-0.893	0.0	0.0	0.0	0.0
8880.	-0.481	-0.955	0.0	0.0	0.0	0.0
9190.	-0.301	-0.709	0.0	0.0	0.0	0.0
9950.	-0.307	-0.685	0.0	0.0	0.0	0.0
10400.	0.0	0.0	0.0	0.0	0.0	0.0
10800.	0.0	0.0	0.0	0.0	0.0	0.0

TABLE B3 (CONTINUED)

STELLAR MAGNITUDES

LAMBDA	HD 188510	HD 193901	HD 196610	HD 201626	HD 205539	+17° 4708
3448.	1.203	1.090	2.826	1.799	1.287	1.126
3570.	1.110	1.071	2.904	2.142	1.222	0.983
3620.	1.023	0.996	2.495	1.745	1.171	0.956
3784.	0.802	0.793	1.914	1.856	0.732	0.678
3798.	0.885	0.886	2.039	1.983	0.846	0.766
3815.	0.880	0.854	2.153	2.101	0.647	0.639
3835.	1.126	1.054	2.196	2.271	0.915	0.819
3860.	0.790	0.747	2.056	2.444	0.492	0.525
3880.	0.848	0.840	1.969	2.151	0.678	0.607
3910.	0.768	0.718	1.755	1.652	0.476	0.472
3933.	1.251	1.236	2.499	1.904	0.796	0.715
4015.	0.523	0.460	0.967	1.194	0.253	0.329
4101.	0.518	0.533	0.727	1.104	0.561	0.467
4200.	0.428	0.394	0.656	1.103	0.181	0.232
4226.	0.436	0.403	1.296	0.918	0.187	0.258
4270.	0.410	0.389	0.809	1.046	0.153	0.228
4305.	0.622	0.546	0.752	1.509	0.243	0.260
4400.	0.321	0.305	0.608	0.868	0.132	0.149
4430.	0.273	0.282	0.840	0.557	0.114	0.151
4500.	0.211	0.194	0.713	0.370	0.084	0.126
4780.	0.065	0.090	1.036	0.055	0.016	0.024
4970.	0.034	0.027	0.942	-0.034	0.009	0.032
5050.	0.0	0.0	0.0	0.0	0.0	0.0
5175.	0.041	0.022	0.321	-0.110	0.022	-0.010
5300.	-0.080	-0.087	-0.571	-0.269	-0.029	-0.060
5820.	-0.200	-0.204	-0.888	-0.505	-0.061	-0.146
5892.	-0.188	-0.168	-0.207	-0.454	-0.038	-0.145
6100.	-0.238	-0.206	-1.261	-0.564	-0.067	-0.162
6180.	-0.247	-0.209	-0.529	-0.568	-0.061	-0.189
6370.	-0.270	-0.235	-1.437	-0.634	-0.063	-0.192
6564.	-0.180	-0.097	-1.814	-0.589	0.164	-0.060
7050.	-0.364	-0.302	-2.605	-0.791	-0.084	-0.275
7100.	-0.375	-0.340	-1.728	-0.788	-0.080	-0.250
7400.	-0.393	-0.332	-3.564	-0.845	-0.062	-0.279
8050.	-0.437	-0.404	-3.979	-0.920	-0.073	-0.292
8190.	0.0	0.0	0.0	0.0	0.0	0.0
8400.	0.0	0.0	0.0	0.0	0.0	0.0
8543.	0.0	0.0	0.0	0.0	0.0	0.0
8800.	0.0	0.0	0.0	0.0	0.0	0.0
8880.	0.0	0.0	0.0	0.0	0.0	0.0
9190.	0.0	0.0	0.0	0.0	0.0	0.0
9950.	0.0	0.0	0.0	0.0	0.0	0.0
10400.	0.0	0.0	0.0	0.0	0.0	0.0
10800.	0.0	0.0	0.0	0.0	0.0	0.0

TABLE B3 (CONTINUED)

STELLAR MAGNITUDES

LAMBDA	HD 215373	HD 219615	HD 219617	HD 221170	HD 222107	M92 II-12
3448.	2.429	2.060	1.040	2.157	2.235	1.842
3570.	2.523	2.136	1.008	2.051	2.288	1.550
3620.	2.098	1.865	0.963	1.957	1.967	1.446
3784.	1.932	1.621	0.704	1.592	1.763	1.176
3798.	2.093	1.776	0.821	1.628	1.886	0.0
3815.	2.241	1.878	0.720	1.607	2.045	1.135
3835.	2.581	2.199	0.930	1.729	2.256	0.0
3860.	2.522	2.131	0.628	1.514	2.094	1.073
3880.	2.191	1.974	0.736	1.585	2.007	0.0
3910.	1.666	1.497	0.609	1.476	1.620	1.045
3933.	2.346	2.227	0.926	2.010	2.176	0.0
4015.	1.046	0.974	0.416	1.112	1.050	0.797
4101.	1.033	0.887	0.531	0.999	0.949	0.0
4200.	1.055	0.890	0.337	0.879	0.896	0.0
4226.	0.882	0.801	0.339	0.860	0.867	0.0
4270.	0.817	0.792	0.293	0.802	0.815	0.552
4305.	1.051	1.092	0.410	0.993	1.082	0.0
4400.	0.628	0.613	0.246	0.615	0.607	0.412
4430.	0.552	0.516	0.239	0.584	0.508	0.385
4500.	0.355	0.343	0.182	0.450	0.292	0.340
4780.	0.100	0.110	0.061	0.184	0.074	0.0
4970.	0.032	0.033	0.025	0.065	0.015	0.0
5050.	0.0	0.0	0.0	0.0	0.0	0.0
5175.	0.068	0.051	-0.006	-0.046	0.107	0.0
5300.	-0.152	-0.143	-0.065	-0.174	-0.209	-0.140
5820.	-0.378	-0.353	-0.165	-0.448	-0.468	-0.307
5892.	-0.296	-0.318	-0.145	-0.442	-0.402	0.0
6100.	-0.415	-0.405	-0.190	-0.559	-0.533	-0.363
6180.	-0.420	-0.409	-0.190	-0.580	-0.541	0.0
6370.	-0.462	-0.463	-0.212	-0.650	-0.605	-0.411
6564.	-0.425	-0.419	-0.075	-0.643	-0.587	0.0
7050.	-0.603	-0.606	-0.267	-0.854	-0.793	-0.519
7100.	-0.594	-0.610	-0.274	-0.869	-0.801	0.0
7400.	-0.606	-0.620	-0.316	-0.909	-0.835	-0.585
8050.	-0.697	-0.717	-0.325	-1.024	-0.959	-0.674
8190.	0.0	0.0	0.0	0.0	0.0	-0.699
8400.	0.0	0.0	0.0	0.0	0.0	-0.744
8543.	0.0	0.0	0.0	0.0	0.0	0.746
8800.	0.0	0.0	0.0	0.0	0.0	-0.740
8880.	0.0	0.0	0.0	0.0	0.0	-0.713
9190.	0.0	0.0	0.0	0.0	0.0	-0.753
9950.	0.0	0.0	0.0	0.0	0.0	-0.851
10400.	0.0	0.0	0.0	0.0	0.0	-0.992
10800.	0.0	0.0	0.0	0.0	0.0	-1.061

TABLE B3 (CONTINUED)

STELLAR MAGNITUDES

LAMBDA	M92 III-13	M92 IV-2	M92 VI-18	M92 X-49	M92 XII-8
3448.	3.489	2.201	1.937	3.132	2.554
3570.	2.954	1.874	1.579	2.687	2.106
3620.	2.803	1.760	1.488	2.542	2.023
3784.	2.441	1.426	1.224	2.168	1.664
3798.	0.0	0.0	0.0	0.0	0.0
3815.	2.373	1.388	1.171	2.101	1.604
3835.	0.0	0.0	0.0	0.0	0.0
3860.	2.270	1.329	1.074	2.014	1.519
3880.	0.0	0.0	0.0	0.0	0.0
3910.	2.207	1.324	1.051	1.976	1.497
3933.	0.0	0.0	0.0	0.0	0.0
4015.	1.723	1.016	0.844	1.320	0.0
4101.	0.0	0.0	0.0	0.0	0.0
4200.	0.0	0.0	0.0	0.0	0.0
4226.	0.0	0.0	0.0	0.0	0.0
4270.	1.151	0.678	0.531	1.014	0.776
4305.	0.0	0.0	0.0	0.0	0.0
4400.	0.857	0.505	0.437	0.759	0.592
4430.	0.806	0.468	0.410	0.711	0.555
4500.	0.668	0.394	0.312	0.589	0.474
4780.	0.0	0.0	0.0	0.0	0.0
4970.	0.0	0.0	0.0	0.0	0.0
5050.	0.0	0.0	0.0	0.0	0.0
5175.	0.0	0.0	0.0	0.0	0.0
5300.	-0.241	-0.150	-0.142	-0.221	-0.180
5820.	-0.588	-0.359	-0.330	-0.532	-0.423
5892.	0.0	0.0	0.0	0.0	0.0
6100.	-0.710	-0.419	-0.403	-0.633	-0.517
6180.	0.0	0.0	0.0	0.0	0.0
6370.	-0.840	-0.492	-0.475	-0.744	-0.612
6564.	0.0	0.0	0.0	0.0	0.0
7050.	-1.101	-0.667	-0.627	-0.996	-0.800
7100.	0.0	0.0	0.0	0.0	0.0
7400.	-1.191	-0.731	-0.681	-1.068	-0.874
8050.	-1.355	-0.837	-0.748	-1.176	-0.980
8190.	-1.397	-0.881	-0.787	-1.227	-1.014
8400.	-1.415	-0.889	-0.823	-1.254	-1.007
8543.	-1.446	-0.910	-0.838	-1.292	-1.070
8800.	-1.501	-0.943	-0.825	-1.338	-1.115
8880.	-1.499	-0.934	-0.849	-1.341	-1.122
9190.	-1.569	-1.000	-0.929	-1.412	-1.190
9950.	-1.698	-1.088	-0.980	-1.539	-1.278
10400.	-1.777	-1.132	-1.044	-1.602	-1.333
10800.	-1.872	-1.215	-1.106	-1.696	-1.405

TABLE B4

MEAN STELLAR MAGNITUDES

LAMBDA	HB 1	HB 2	HB 3	HB 4	HB 5	GI E 1
3446.	0.954	1.281	1.447	1.293	1.923	1.680
3570.	0.990	1.309	1.404	1.284	1.869	1.478
3620.	0.973	1.305	1.367	1.288	1.745	1.389
3784.	0.272	0.480	0.546	0.743	0.831	1.097
3798.	0.541	0.741	0.739	0.930	0.831	1.108
3815.	0.067	0.238	0.353	0.665	0.779	1.078
3835.	0.537	0.688	0.754	0.933	0.911	1.139
3860.	-0.089	0.047	0.174	0.541	0.673	1.001
3880.	0.153	0.422	0.435	0.773	0.870	1.115
3910.	-0.102	0.007	0.160	0.504	0.511	0.978
3933.	-0.145	-0.050	0.085	0.506	0.712	1.390
4015.	-0.225	-0.137	-0.038	0.305	0.341	0.712
4101.	0.443	0.585	0.567	0.646	0.536	0.689
4200.	-0.187	-0.121	-0.051	0.263	0.355	0.553
4226.	-0.175	-0.099	-0.037	0.278	0.330	0.576
4270.	-0.163	-0.099	-0.043	0.245	0.320	0.522
4305.	-0.128	-0.047	0.020	0.306	0.375	0.766
4400.	-0.141	-0.069	-0.030	0.201	0.250	0.395
4430.	-0.136	-0.080	-0.031	0.201	0.219	0.355
4500.	-0.116	-0.071	-0.030	0.149	0.189	0.299
4780.	-0.045	-0.019	-0.009	0.084	0.096	0.139
4970.	-0.019	-0.009	-0.012	0.030	-0.001	0.014
5050.	0.0	0.0	0.0	0.0	0.0	0.0
5175.	0.040	0.031	0.026	-0.001	0.004	-0.004
5300.	0.065	0.047	0.022	-0.056	-0.021	-0.124
5820.	0.169	0.129	0.071	-0.151	-0.135	-0.286
5892.	0.211	0.149	0.097	-0.113	-0.074	-0.278
6100.	0.235	0.168	0.093	-0.172	-0.144	-0.355
6180.	0.255	0.189	0.096	-0.186	-0.134	-0.359
6370.	0.296	0.212	0.107	-0.191	-0.168	-0.411
6564.	0.694	0.583	0.392	0.012	-0.087	-0.353
7050.	0.429	0.293	0.131	-0.272	-0.224	-0.541
7100.	0.439	0.313	0.139	-0.258	-0.215	-0.562
7400.	0.530	0.337	0.165	-0.288	-0.222	-0.588
8150.	0.691	0.400	0.224	-0.319	-0.177	-0.663
8190.	0.0	0.410	0.0	0.0	0.0	-0.696
8400.	0.0	0.466	0.0	0.0	0.0	-0.741
8543.	0.0	0.432	0.0	0.0	0.0	-0.743
8800.	0.0	0.164	0.0	0.0	0.0	-0.737
8880.	0.0	0.282	0.0	0.0	0.0	-0.710
9190.	0.0	0.455	0.0	0.0	0.0	-0.750
9950.	0.0	0.429	0.0	0.0	0.0	-0.848
12400.	0.0	0.0	0.0	0.0	0.0	-0.989
16800.	0.0	0.0	0.0	0.0	0.0	-1.058

TABLE B4 (CONTINUED)

MEAN STELLAR MAGNITUDES

LAMBDA	GI E 2	GI E 3	GI E 4	GI E 5	GI E 6	GI M 1
3448.	1.764	2.022	2.313	3.132	3.489	2.003
3570.	1.574	1.856	2.139	2.687	2.954	2.012
3620.	1.494	1.738	2.049	2.542	2.803	1.866
3784.	1.226	1.391	1.695	2.168	2.441	1.465
3798.	1.213	1.411	1.688	2.138	2.413	1.589
3815.	1.217	1.364	1.667	2.101	2.373	1.677
3835.	1.304	1.405	1.763	2.170	2.416	1.962
3860.	1.099	1.273	1.570	2.014	2.270	1.846
3880.	1.189	1.342	1.625	2.025	2.271	1.774
3910.	1.094	1.233	1.533	1.976	2.207	1.385
3933.	1.690	1.529	2.071	2.581	2.825	2.036
4015.	0.827	0.972	1.183	1.535	1.723	0.907
4101.	0.729	0.895	1.052	1.320	1.494	0.826
4200.	0.653	0.776	0.915	1.156	1.302	0.795
4226.	0.631	0.745	0.881	1.067	1.215	0.750
4270.	0.602	0.677	0.811	1.014	1.151	0.753
4305.	0.882	0.772	0.974	1.105	1.218	1.028
4400.	0.497	0.519	0.624	0.759	0.857	0.560
4430.	0.419	0.476	0.587	0.711	0.806	0.454
4500.	0.314	0.402	0.471	0.589	0.668	0.393
4780.	0.157	0.197	0.194	0.250	0.283	0.109
4970.	0.031	0.029	0.059	0.050	0.057	0.027
5450.	0.0	0.0	0.0	0.0	0.0	0.0
5175.	-0.012	-0.040	-0.049	-0.068	-0.074	0.031
5300.	-0.118	-0.137	-0.175	-0.221	-0.241	-0.123
5820.	-0.316	-0.367	-0.444	-0.532	-0.588	-0.336
5892.	-0.317	-0.376	-0.426	-0.492	-0.528	-0.313
6100.	-0.387	-0.463	-0.548	-0.633	-0.716	-0.386
6180.	-0.379	-0.479	-0.566	-0.662	-0.742	-0.393
6370.	-0.452	-0.546	-0.636	-0.744	-0.840	-0.448
6564.	-0.412	-0.516	-0.629	-0.754	-0.889	-0.405
7050.	-0.599	-0.723	-0.831	-0.976	-1.101	-0.585
7100.	-0.616	-0.742	-0.849	-0.996	-1.122	-0.594
7400.	-0.645	-0.777	-0.897	-1.068	-1.191	-0.608
8050.	-0.732	-0.882	-1.009	-1.176	-1.355	-0.696
8190.	-0.764	-0.930	-1.045	-1.227	-1.397	-0.741
8400.	-0.800	-0.938	-1.051	-1.254	-1.415	-0.743
8543.	-0.815	-0.959	-1.079	-1.292	-1.446	-0.671
8800.	-0.802	-0.992	-1.212	-1.338	-1.501	-0.836
8880.	-0.826	-0.983	-1.228	-1.341	-1.499	-0.884
9190.	-0.926	-1.149	-1.174	-1.412	-1.569	-0.934
9950.	-0.957	-1.137	-1.280	-1.539	-1.698	-0.752
10400.	-1.021	-1.181	-1.360	-1.602	-1.777	-0.712
12800.	-1.083	-1.264	-1.432	-1.696	-1.872	0.0

TABLE B4 (CONTINUED)

MEAN STELLAR MAGNITUDES

LAMBDA	GI M 2	GI M 3	GI M 4	GI M 5	GI M 6	GI M 7
3448.	2.316	2.303	2.599	2.995	2.954	2.957
3570.	2.408	2.401	2.802	3.407	3.555	3.282
3620.	2.054	2.071	2.435	3.166	3.404	3.130
3784.	1.833	1.793	2.204	2.990	3.192	2.855
3798.	2.022	1.973	2.341	3.174	3.313	2.991
3815.	2.124	2.103	2.558	3.284	3.388	3.056
3835.	2.485	2.436	2.719	3.427	3.473	3.185
3860.	2.402	2.319	2.616	3.250	3.316	2.986
3880.	2.190	2.144	2.498	3.221	3.288	2.966
3910.	1.634	1.646	2.099	2.925	3.119	2.782
3933.	2.349	2.350	2.874	3.534	3.636	3.383
4015.	1.064	1.068	1.392	2.043	2.377	2.000
4101.	0.989	0.973	1.277	1.825	2.068	1.685
4200.	1.015	0.980	1.217	1.737	1.883	1.527
4226.	0.882	0.895	1.164	1.881	2.096	1.779
4270.	0.833	0.865	1.066	1.535	1.747	1.354
4305.	1.118	1.169	1.312	1.520	1.600	1.317
4400.	0.643	0.650	0.796	1.031	1.147	0.938
4430.	0.543	0.515	0.697	0.862	1.042	0.865
4500.	0.358	0.322	0.443	0.539	0.718	0.574
4780.	0.117	0.103	0.171	0.303	0.502	0.570
4970.	0.037	0.023	0.043	0.069	0.222	0.319
5050.	0.0	0.0	0.0	0.0	0.0	0.0
5175.	0.062	0.070	0.071	0.202	0.184	0.213
5300.	-0.152	-0.169	-0.215	-0.403	-0.451	-0.533
5820.	-0.375	-0.415	-0.537	-0.848	-0.916	-0.848
5892.	-0.320	-0.362	-0.486	-0.630	-0.572	-0.420
6100.	-0.421	-0.465	-0.609	-1.002	-1.129	-1.138
6180.	-0.424	-0.475	-0.627	-0.848	-0.759	-0.591
6370.	-0.477	-0.530	-0.713	-1.087	-1.224	-1.231
6564.	-0.442	-0.501	-0.699	-1.152	-1.360	-1.391
7050.	-0.629	-0.687	-0.927	-1.469	-1.761	-1.993
7100.	-0.624	-0.688	-0.935	-1.301	-1.471	-1.399
7400.	-0.628	-0.709	-0.980	-1.622	-2.087	-2.327
8150.	-0.712	-0.807	-1.139	-1.750	-2.370	-2.544
8190.	0.0	-0.833	-1.167	-1.843	-2.421	0.0
8400.	0.0	-0.866	-1.213	-1.914	-2.472	0.0
8543.	0.0	-0.767	-1.114	-1.801	-2.411	0.0
8800.	0.0	-0.894	-1.284	-2.045	-2.789	0.0
8885.	0.0	-0.935	-1.319	-2.156	-2.829	0.0
9190.	0.0	-0.847	-1.284	-1.993	-2.668	0.0
9950.	0.0	-0.969	-1.436	-2.204	-2.907	0.0
10400.	0.0	-1.983	-1.464	-2.260	0.0	0.0
10800.	0.0	0.0	0.0	0.0	0.0	0.0

TABLE B4 (CONTINUED)

MEAN STELLAR MAGNITUDES

LAMBDA	SG EE 1	SG EE 2	SG EE 3	SG E 1	SG E 2	SG E 3
3448.	1.040	0.986	1.300	1.036	1.044	1.270
3570.	0.971	1.007	1.237	0.971	1.033	1.220
3620.	0.900	0.951	1.130	0.908	0.981	1.121
3784.	0.644	0.661	0.857	0.646	0.681	0.848
3798.	0.739	0.734	0.911	0.744	0.776	0.914
3815.	0.636	0.614	0.950	0.633	0.665	0.928
3835.	0.803	0.751	1.130	0.817	0.839	1.114
3860.	0.559	0.538	0.830	0.546	0.581	0.811
3880.	0.674	0.659	0.899	0.661	0.696	0.887
3910.	0.525	0.507	0.814	0.530	0.556	0.768
3933.	0.720	0.622	1.288	0.793	0.772	1.277
4015.	0.355	0.343	0.537	0.349	0.377	0.516
4101.	0.470	0.482	0.538	0.471	0.504	0.540
4200.	0.271	0.295	0.454	0.270	0.314	0.438
4226.	0.286	0.299	0.466	0.282	0.317	0.448
4270.	0.251	0.258	0.444	0.250	0.274	0.429
4305.	0.317	0.341	0.651	0.327	0.374	0.619
4400.	0.187	0.217	0.324	0.178	0.230	0.321
4430.	0.203	0.201	0.272	0.185	0.219	0.278
4500.	0.150	0.186	0.208	0.133	0.183	0.206
4780.	0.032	0.083	0.069	0.033	0.071	0.077
4970.	0.044	0.004	0.031	0.025	0.014	0.030
5050.	0.0	0.0	0.0	0.0	0.0	0.0
5175.	-0.005	-0.014	-0.006	-0.003	-0.010	-0.007
5300.	-0.056	-0.065	-0.075	-0.053	-0.065	-0.079
5820.	-0.139	-0.175	-0.212	-0.140	-0.170	-0.209
5892.	-0.128	-0.176	-0.202	-0.124	-0.160	-0.196
6100.	-0.168	-0.202	-0.251	-0.173	-0.195	-0.235
6180.	-0.176	-0.222	-0.265	-0.178	-0.205	-0.245
6370.	-0.185	-0.252	-0.293	-0.194	-0.231	-0.272
6564.	-0.089	-0.128	-0.201	-0.049	-0.100	-0.164
7050.	-0.273	-0.334	-0.389	-0.260	-0.299	-0.357
7100.	-0.271	-0.356	-0.397	-0.258	-0.313	-0.376
7400.	-0.300	-0.375	-0.403	-0.281	-0.343	-0.377
8050.	-0.311	-0.389	-0.459	-0.303	-0.354	-0.437
8190.	0.0	0.0	-0.491	-0.396	0.0	-0.471
8400.	0.0	0.0	-0.515	-0.314	0.0	-0.495
8543.	0.0	0.0	-0.406	-0.303	0.0	-0.386
8800.	0.0	0.0	-0.530	-0.437	0.0	-0.510
8880.	0.0	0.0	-0.532	-0.458	0.0	-0.512
9190.	0.0	0.0	-0.496	-1.271	0.0	-0.476
9950.	0.0	0.0	-0.478	0.0	0.0	-0.458
10400.	0.0	0.0	-0.507	0.0	0.0	-0.487
10800.	0.0	0.0	0.0	0.0	0.0	0.0

TABLE B4 (CONTINUED)

MEAN STELLAR MAGNITUDES

LAMBDA	SG E 4	SG E 5	SG M 1	SG M 2	SG M 3	SG M 4
3448.	1.566	1.701	1.240	1.416	1.759	1.889
3570.	1.376	1.518	1.191	1.336	1.708	1.910
3620.	1.296	1.440	1.128	1.262	1.570	1.713
3784.	1.043	1.176	0.827	0.917	1.164	1.411
3798.	1.056	1.184	0.892	0.976	1.271	1.537
3815.	1.029	1.170	0.813	0.940	1.388	1.628
3835.	1.092	1.260	1.076	1.231	1.830	1.915
3869.	0.957	1.059	0.726	0.852	1.361	1.802
3880.	1.074	1.152	0.835	0.955	1.382	1.733
3910.	0.942	1.061	0.667	0.812	1.167	1.349
3933.	1.356	1.659	1.136	1.373	1.787	2.002
4015.	0.683	0.861	0.420	0.532	0.715	0.878
4101.	0.665	0.757	0.531	0.581	0.679	0.802
4200.	0.534	0.635	0.346	0.414	0.602	0.776
4226.	0.552	0.614	0.354	0.420	0.651	0.732
4270.	0.506	0.587	0.342	0.434	0.640	0.737
4305.	0.752	0.868	0.507	0.634	0.885	1.014
4400.	0.384	0.487	0.240	0.328	0.465	0.549
4430.	0.346	0.410	0.186	0.274	0.348	0.445
4500.	0.292	0.307	0.124	0.202	0.225	0.296
4780.	0.134	0.154	0.051	0.063	0.078	0.134
4970.	0.012	0.030	0.013	0.038	0.009	0.025
5050.	0.0	0.0	0.0	0.0	0.0	0.0
5175.	-0.002	-0.010	0.029	0.053	0.024	0.033
5300.	-0.121	-0.114	-0.072	-0.063	-0.125	-0.120
5820.	-0.280	-0.310	-0.172	-0.166	-0.306	-0.330
5892.	-0.272	-0.311	-0.132	-0.137	-0.267	-0.307
6100.	-0.349	-0.380	-0.194	-0.196	-0.333	-0.380
6180.	-0.353	-0.372	-0.196	-0.201	-0.331	-0.387
6370.	-0.404	-0.445	-0.224	-0.222	-0.383	-0.441
6564.	-0.346	-0.404	-0.083	-0.106	-0.301	-0.398
7050.	-0.534	-0.590	-0.278	-0.286	-0.483	-0.578
7100.	-0.555	-0.607	-0.281	-0.302	-0.495	-0.587
7400.	-0.581	-0.636	-0.287	-0.308	-0.492	-0.601
8050.	-0.656	-0.723	-0.327	-0.357	-0.546	-0.689
8190.	-0.689	-0.755	-0.334	0.0	0.0	-0.734
8400.	-0.734	-0.791	-0.328	0.0	0.0	-0.736
8543.	-0.736	-0.807	-0.298	0.0	0.0	-0.664
8800.	-0.751	-0.794	-0.441	0.0	0.0	-0.830
8880.	-0.784	-0.818	-0.476	0.0	0.0	-0.878
9190.	-0.744	-0.898	-0.295	0.0	0.0	-0.926
9950.	-0.844	-0.949	-0.301	0.0	0.0	-0.748
10400.	-0.986	-1.014	0.0	0.0	0.0	-0.767
10800.	-1.054	-1.077	0.0	0.0	0.0	0.0

TABLE B4 (CONTINUED)

MEAN STELLAR MAGNITUDES

LAMBDA	SG M 5	SD EE 1	SD EE 2	SD EE 3	SD EE 4	SD EE 5
3448.	2.240	1.022	0.997	0.932	1.181	1.576
3570.	2.345	0.964	0.930	0.955	1.124	1.605
3620.	2.017	0.921	0.861	0.902	1.024	1.351
3784.	1.743	0.647	0.647	0.663	0.822	1.121
3798.	1.924	0.740	0.742	0.737	0.879	1.173
3815.	2.056	0.577	0.640	0.617	0.920	1.416
3835.	2.392	0.776	0.807	0.754	1.102	1.584
3860.	2.279	0.469	0.563	0.541	0.805	1.189
3880.	2.167	0.583	0.675	0.662	0.876	1.230
3910.	1.613	0.432	0.530	0.510	0.795	1.155
3933.	2.321	0.519	0.725	0.625	1.271	1.821
4015.	1.042	0.278	0.360	0.348	0.525	0.675
4101.	0.951	0.489	0.475	0.487	0.527	0.626
4200.	0.962	0.224	0.275	0.299	0.444	0.569
4226.	0.878	0.220	0.290	0.303	0.456	0.650
4270.	0.850	0.206	0.255	0.261	0.435	0.576
4305.	1.155	0.236	0.321	0.344	0.642	0.786
4400.	0.640	0.159	0.190	0.219	0.316	0.396
4430.	0.506	0.149	0.206	0.203	0.265	0.327
4500.	0.315	0.125	0.152	0.188	0.202	0.230
4780.	0.100	0.072	0.032	0.084	0.068	0.084
4970.	0.022	0.019	0.044	0.005	0.031	0.022
5050.	0.0	0.0	0.0	0.0	0.0	0.0
5175.	0.072	0.011	-0.005	-0.014	0.040	0.142
5300.	-0.165	-0.021	-0.056	-0.065	-0.075	-0.112
5820.	-0.409	-0.079	-0.140	-0.176	-0.213	-0.293
5892.	-0.356	-0.074	-0.130	-0.178	-0.186	-0.258
6100.	-0.458	-0.125	-0.179	-0.204	-0.253	-0.357
6180.	-0.468	-0.113	-0.178	-0.224	-0.268	-0.363
6370.	-0.523	-0.141	-0.188	-0.255	-0.297	-0.427
6564.	-0.493	0.008	-0.042	-0.131	-0.206	-0.373
7050.	-0.678	-0.195	-0.277	-0.338	-0.396	-0.564
7100.	-0.679	-0.193	-0.275	-0.368	-0.404	-0.572
7400.	-0.700	-0.201	-0.305	-0.380	-0.411	-0.586
8050.	-0.798	-0.220	-0.316	-0.395	-0.468	-0.667
8190.	-0.824	-0.222	0.0	0.0	-0.501	-0.697
8400.	-0.857	-0.269	0.0	0.0	-0.525	-0.712
8543.	-0.759	-0.244	0.0	0.0	-0.417	-0.640
8800.	-0.886	-0.368	0.0	0.0	-0.541	-0.738
8880.	-0.927	-0.291	0.0	0.0	-0.544	-0.761
9190.	-0.939	-0.162	0.0	0.0	-0.508	-0.728
9950.	-0.961	0.0	0.0	0.0	-0.492	-0.758
10400.	-0.976	0.0	0.0	0.0	-0.522	-0.697
12800.	0.0	0.0	0.0	0.0	0.0	0.0

TABLE B4 (CONTINUED)

MEAN STELLAR MAGNITUDES

LAMBDA	SD E 1	SD E 2	SD E 3	SD E 4	SD E 5	SD E 6
3448.	1.074	0.993	0.986	1.151	1.544	1.816
3570.	0.974	0.930	0.981	1.107	1.585	1.75.
3620.	0.939	0.869	0.932	1.015	1.366	1.562
3784.	0.663	0.649	0.683	0.813	1.126	1.3c3
3798.	0.753	0.747	0.779	0.882	1.203	1.419
3815.	0.608	0.637	0.668	0.898	1.375	1.676
3835.	0.798	0.821	0.842	1.086	1.686	1.902
3860.	0.497	0.550	0.584	0.786	1.227	1.644
3880.	0.595	0.666	0.699	0.864	1.249	1.543
3910.	0.452	0.535	0.559	0.769	1.156	1.364
3933.	0.617	0.798	0.775	1.260	1.824	2.034
4015.	0.304	0.354	0.382	0.504	0.700	0.846
4101.	0.478	0.476	0.509	0.529	0.658	0.793
4200.	0.228	0.274	0.318	0.428	0.605	0.749
4226.	0.239	0.286	0.321	0.438	0.683	0.825
4270.	0.217	0.254	0.277	0.420	0.618	0.764
4305.	0.248	0.331	0.377	0.610	0.838	0.949
4460.	0.154	0.181	0.232	0.313	0.420	0.520
4430.	0.150	0.189	0.221	0.271	0.326	0.399
4500.	0.126	0.135	0.185	0.200	0.221	0.275
4780.	0.048	0.033	0.072	0.076	0.109	0.131
4970.	0.026	0.025	0.015	0.030	0.019	0.016
5050.	0.0	0.0	0.0	0.0	0.0	0.0
5175.	0.001	-0.003	-0.010	0.034	0.119	0.155
5300.	-0.040	-0.053	-0.065	-0.079	-0.128	-0.122
5820.	-0.112	-0.141	-0.171	-0.210	-0.307	-0.344
5892.	-0.109	-0.126	-0.162	-0.180	-0.270	-0.301
6100.	-0.143	-0.175	-0.197	-0.237	-0.353	-0.410
6180.	-0.151	-0.180	-0.207	-0.248	-0.356	-0.414
6370.	-0.166	-0.197	-0.234	-0.276	-0.419	-0.466
6564.	-0.026	-0.052	-0.103	-0.169	-0.360	-0.415
7050.	-0.235	-0.264	-0.303	-0.364	-0.544	-0.581
7100.	-0.221	-0.262	-0.317	-0.383	-0.536	-0.616
7400.	-0.240	-0.286	-0.348	-0.385	-0.566	-0.649
8050.	-0.256	-0.308	-0.360	-0.446	-0.652	-0.669
8190.	-0.253	-0.311	0.0	-0.481	-0.684	0.0
8400.	-0.300	-0.319	0.0	-0.505	-0.699	0.0
8543.	-0.275	-0.308	0.0	-0.397	-0.627	0.0
8800.	-0.399	-0.442	0.0	-0.521	-0.725	0.0
8880.	-0.322	-0.463	0.0	-0.524	-0.748	0.0
9190.	-0.193	-0.276	0.0	-0.488	-0.715	0.0
9950.	0.0	0.0	0.0	-0.472	-0.745	0.0
10400.	0.0	0.0	0.0	-0.502	-0.684	0.0
10800.	0.0	0.0	0.0	0.0	0.0	0.0

TABLE B4 (CONTINUED)

MEAN STELLAR MAGNITUDES

LAMBDA	SD M 1	SD M 2	SD M 3	SD M 4	SD M 5	SD M 6
3448.	1.071	1.148	1.197	1.362	1.640	2.099
3570.	1.045	1.110	1.150	1.284	1.595	2.087
3620.	0.996	1.091	1.089	1.213	1.464	1.927
3784.	0.649	0.778	0.830	0.919	1.129	1.592
3798.	0.781	0.888	0.895	0.979	1.239	1.736
3815.	0.584	0.741	0.817	0.943	1.358	1.784
3835.	0.655	0.986	1.080	1.234	1.802	2.204
3860.	0.431	0.663	0.710	0.855	1.336	1.932
3889.	0.651	0.810	0.840	0.958	1.359	1.961
3910.	0.430	0.640	0.692	0.815	1.148	1.565
3933.	0.717	0.968	1.141	1.376	1.770	2.287
4015.	0.216	0.399	0.425	0.537	0.703	1.052
4101.	0.519	0.593	0.536	0.586	0.668	0.902
4200.	0.175	0.341	0.350	0.418	0.592	0.867
4226.	0.165	0.349	0.358	0.424	0.641	0.874
4270.	0.128	0.307	0.346	0.437	0.631	0.854
4335.	0.230	0.505	0.511	0.637	0.876	1.143
4400.	0.094	0.227	0.243	0.330	0.457	0.648
4430.	0.074	0.194	0.189	0.276	0.341	0.528
4500.	0.049	0.141	0.126	0.204	0.219	0.351
4780.	0.0	0.053	0.051	0.064	0.077	0.139
4970.	0.008	0.009	0.013	0.039	0.009	0.036
5050.	0.0	0.0	0.0	0.0	0.0	0.0
5175.	0.032	0.016	0.029	0.053	0.132	0.104
5300.	-0.016	-0.055	-0.072	-0.063	-0.125	-0.133
5620.	-0.066	-0.135	-0.173	-0.167	-0.307	-0.363
5892.	-0.028	-0.099	-0.134	-0.139	-0.238	-0.352
6100.	-0.063	-0.139	-0.196	-0.198	-0.335	-0.434
6180.	-0.063	-0.136	-0.198	-0.203	-0.334	-0.431
6370.	-0.074	-0.156	-0.227	-0.225	-0.387	-0.498
6564.	0.141	0.024	-0.086	-0.109	-0.306	-0.456
7050.	-0.082	-0.176	-0.282	-0.290	-0.490	-0.639
7100.	-0.080	-0.178	-0.285	-0.306	-0.502	-0.637
7400.	-0.060	-0.158	-0.292	-0.313	-0.500	-0.628
8050.	-0.072	-0.185	-0.332	-0.363	-0.565	-0.599
8190.	-0.176	0.0	-0.339	0.0	0.0	0.0
8400.	-0.067	0.0	-0.333	0.0	0.0	0.0
8543.	0.001	0.0	-0.303	0.0	0.0	0.0
8800.	-0.078	0.0	-0.446	0.0	0.0	0.0
8880.	-0.056	0.0	-0.481	0.0	0.0	0.0
9190.	-0.018	0.0	-0.361	0.0	0.0	0.0
9950.	-0.032	0.0	-0.307	0.0	0.0	0.0
10400.	0.002	0.0	0.0	0.0	0.0	0.0
10870.	0.0	0.0	0.0	0.0	0.0	0.0

TABLE B4 (CONTINUED)

MEAN STELLAR MAGNITUDES

LAMBDA	SD M 7
3448.	2.395
3570.	2.470
3620.	2.108
3784.	1.898
3798.	2.109
3815.	2.244
3835.	2.569
3860.	2.440
3880.	2.282
3910.	1.782
3933.	2.423
4015.	1.109
4101.	1.031
4200.	1.049
4226.	0.917
4270.	0.883
4335.	1.153
4400.	0.677
4430.	0.556
4500.	0.358
4780.	0.189
4970.	0.018
5050.	0.0
5175.	0.073
5300.	-0.176
5820.	-0.401
5892.	-0.355
6100.	-0.457
6180.	-0.469
6370.	-0.521
6564.	-0.501
7050.	-0.680
7150.	-0.672
7400.	-0.700
8050.	-0.787
8190.	0.0
8400.	0.0
8543.	0.0
8800.	0.0
8880.	0.0
9190.	0.0
9950.	0.0
10400.	0.0
10800.	0.0

TABLE B5

MEAN STELLAR INDICES

INDEX	HB 1	HB 2	HB 3	HB 4	HB 5	GI E 1	GI E 2	GI E 3	GI E 4
H 3798	0.714	0.734	0.770	0.815	0.878	0.982	1.008	0.971	0.995
H 3835	0.607	0.609	0.641	0.742	0.847	0.916	0.879	0.927	0.879
CN 3860	1.071	1.074	1.082	1.044	0.976	1.027	1.056	1.026	1.030
CN 3883	0.829	0.728	0.821	0.817	0.773	0.907	0.949	0.939	0.955
CAII3933	1.014	1.023	1.028	0.957	0.802	0.646	0.545	0.720	0.564
H 4101	0.549	0.519	0.571	0.716	0.828	0.962	1.019	0.976	0.999
CN 4216	1.002	1.007	1.006	0.997	0.972	1.019	1.009	0.981	0.993
CAI 4226	0.998	0.992	0.994	0.979	0.993	0.985	1.008	0.982	0.991
CH 4305	0.973	0.959	0.946	0.935	0.934	0.774	0.753	0.880	0.826
IS 4430	1.002	1.009	1.001	0.986	1.012	1.010	1.020	1.007	0.991
MGH 4780	0.972	0.972	0.983	0.986	0.993	1.004	0.994	0.995	1.026
TIO 4970	0.993	0.991	1.001	0.993	1.025	1.026	1.012	1.025	1.005
MGI 5175	0.990	0.990	0.984	0.975	0.985	0.947	0.957	0.973	0.964
NAI 5892	0.975	0.989	0.980	0.960	0.942	0.976	0.984	0.985	0.959
TIO 6180	0.996	0.991	1.000	1.007	0.984	0.988	0.975	0.992	0.992
H 6564	0.709	0.719	0.769	0.809	0.911	0.914	0.925	0.926	0.942
TIO 7100	1.002	0.986	0.996	0.984	0.991	1.013	1.009	1.010	1.008
NAI 8190	0.0	1.012	0.0	0.0	0.0	1.001	1.004	1.023	1.017
CAII8543	0.0	0.930	0.0	0.0	0.0	1.002	1.012	1.001	0.972
TIO 8880	0.0	0.938	0.0	0.0	0.0	0.972	1.002	0.981	1.021
CN 9190	0.0	0.807	0.0	0.0	0.0	0.972	1.044	1.002	0.939
U/B	0.352	0.278	0.270	0.376	0.246	0.407	0.404	0.331	0.281
B/V	1.280	1.171	1.079	0.740	0.715	0.542	0.492	0.456	0.387
V/R	1.396	1.233	1.098	0.851	0.876	0.726	0.691	0.635	0.604
V/I	0.0	1.222	0.0	0.0	0.0	0.613	0.586	0.521	0.471
V/J	0.0	0.0	0.0	0.0	0.0	0.472	0.465	0.411	0.370

TABLE B5 (CONTINUED)

MEAN STELLAR INDICES

INDEX	GI E 5	GI E 6	GI M 1	GI M 2	GI M 3	GI M 4	GI M 5	GI M 6	GI M 7
H 3798	0.999	0.997	0.969	0.939	0.953	1.007	0.944	0.966	0.954
H 3835	0.905	0.921	0.821	0.796	0.799	0.882	0.864	0.898	0.863
CN 3860	1.025	1.021	0.749	0.613	0.660	0.762	0.873	0.945	0.941
CN 3880	0.991	0.988	0.757	0.680	0.712	0.785	0.838	0.922	0.908
CAII3933	0.518	0.506	0.492	0.452	0.455	0.410	0.452	0.515	0.470
H 4101	1.021	1.014	1.026	0.996	1.023	1.000	1.017	1.048	1.065
CN 42[illegible]	0.988	0.994	0.999	0.895	0.946	0.941	0.913	0.984	0.983
CAI 4226	1.025	1.021	1.027	0.991	1.004	0.960	0.763	0.765	0.738
CH 4305	0.860	0.870	0.739	0.733	0.715	0.743	0.864	0.940	0.921
IS 4430	0.996	0.993	1.023	1.008	1.027	0.985	1.001	0.965	0.954
MGH 4780	1.021	1.020	1.034	1.051	1.048	1.036	0.954	0.849	0.756
TIO 4970	1.026	1.027	1.014	1.012	1.020	1.016	1.003	0.887	0.809
MGI 5175	0.960	0.956	0.918	0.880	0.866	0.847	0.683	0.677	0.630
NAI 5892	0.941	0.919	0.967	0.940	0.941	0.938	0.788	0.692	0.627
TIO 618[illegible]	0.996	0.994	0.989	0.987	0.991	0.988	0.848	0.693	0.589
H 6564	0.948	0.975	0.925	0.928	0.932	0.931	0.959	0.973	0.951
TIO 7100	1.006	1.007	1.005	0.995	0.997	1.000	0.845	0.731	0.591
NAI 8190	1.018	1.016	1.024	0.0	1.002	0.998	1.025	1.009	0.0
CAII8543	1.007	1.000	0.907	0.0	0.904	0.891	0.863	0.847	0.0
TIO 8860	0.989	0.985	1.026	0.0	1.046	1.032	1.028	1.058	0.0
CN 9190	1.002	0.997	1.107	0.0	0.929	0.949	0.903	0.857	0.0
U/B	0.203	0.177	0.316	0.255	0.258	0.213	0.151	0.146	0.147
B/V	0.311	0.270	0.442	0.397	0.380	0.299	0.175	0.145	0.186
V/R	0.557	0.516	0.717	0.718	0.692	0.594	0.438	0.323	0.267
V/I	0.433	0.387	0.599	0.0	0.586	0.452	0.293	0.168	0.0
V/J	0.313	0.276	0.644	0.0	0.533	0.371	0.227	0.0	0.0

TABLE B5 (CONTINUED)

MEAN STELLAR INDICES

INDEX	SG EE 1	SG EE 2	SG EE 3	SG E 1	SG E 2	SG E 3	SG E 4	SG E 5	SG M 1
H 3798	0.913	0.917	0.988	0.909	0.910	0.972	0.982	1.009	0.936
H 3835	0.831	0.854	0.806	0.814	0.823	0.802	0.916	0.879	0.751
CN 3883	1.022	1.023	1.052	1.035	1.030	1.047	1.028	1.056	1.044
CN 3880	0.903	0.896	0.961	0.913	0.907	0.950	0.908	0.949	0.905
CAII3933	0.807	0.869	0.609	0.756	0.790	0.601	0.646	0.545	0.624
H 4101	0.870	0.856	0.970	0.866	0.861	0.951	0.961	1.019	0.880
CN 4200	1.007	0.987	1.014	1.006	0.988	1.013	1.018	1.009	1.015
CAI 4226	0.984	0.975	0.994	0.986	0.976	0.996	0.985	1.008	1.001
CH 4305	0.926	0.917	0.802	0.915	0.902	0.817	0.773	0.753	0.837
IS 4430	0.975	1.006	1.015	0.981	0.997	1.007	1.009	1.020	1.017
MGH 4780	1.035	1.004	1.027	1.025	1.014	1.019	1.005	0.993	1.004
TIO 4970	0.978	1.020	0.998	0.992	1.010	0.998	1.027	1.012	1.002
MGI 5175	0.978	0.982	0.971	0.978	0.979	0.970	0.947	0.957	0.941
NAI 5892	0.982	0.994	0.981	0.977	0.984	0.981	0.976	0.984	0.958
TIO 6180	1.002	1.004	1.001	0.998	0.999	0.998	0.988	0.975	0.993
H 6564	0.851	0.870	0.893	0.856	0.867	0.882	0.914	0.925	0.862
TIO 7100	0.994	1.014	1.005	0.995	1.007	1.014	1.013	1.009	1.001
NAI 8190	0.0	0.0	1.008	0.998	0.0	1.009	1.001	1.004	1.005
CAII8543	0.0	0.0	0.899	0.950	0.0	0.899	1.001	1.012	0.937
TIO 8860	0.0	0.0	1.007	1.047	0.0	1.007	0.972	1.002	1.057
CN 9190	0.0	0.0	0.973	0.786	0.0	0.973	0.971	1.044	0.897
U/B	0.517	0.505	0.479	0.513	0.499	0.481	0.440	0.420	0.449
B/V	0.747	0.719	0.615	0.751	0.711	0.620	0.551	0.500	0.684
V/R	0.841	0.807	0.794	0.853	0.830	0.816	0.722	0.694	0.863
V/I	0.0	0.0	0.707	0.773	0.0	0.720	0.614	0.588	0.765
V/J	0.0	0.0	0.717	0.0	0.0	0.736	0.471	0.466	0.0

TABLE B5 (CONTINUED)

MEAN STELLAR INDICES

INDEX	SG M 2	SG M 3	SG M 4	SG M 5	SD EE 1	SD EE 2	SD EE 3	SD EE 4	SD EE 5
H 3798	0.956	0.989	0.969	0.953	0.891	0.914	0.916	0.987	1.067
H 3835	0.738	0.658	0.821	0.799	0.796	0.831	0.854	0.806	0.777
CN 3860	1.025	0.928	0.750	0.660	1.036	1.023	1.023	1.052	1.094
CN 3880	0.909	0.872	0.758	0.712	0.907	0.903	0.896	0.962	1.002
CAII3933	0.502	0.509	0.492	0.455	0.894	0.807	0.870	0.609	0.484
H 4101	0.926	1.009	1.026	1.023	0.804	0.870	0.855	0.970	1.014
CN 4200	1.043	1.054	0.999	0.946	1.001	1.007	0.986	1.014	1.031
CAI 4226	1.028	1.001	1.027	1.004	0.998	0.984	0.975	0.994	0.948
CH 4305	0.810	0.763	0.738	0.715	0.961	0.926	0.917	0.802	0.787
IS 4430	1.014	1.039	1.022	1.027	1.000	0.975	1.006	1.015	1.007
MGH 4780	1.030	1.027	1.035	1.048	0.985	1.036	1.004	1.025	1.010
TIO 4970	0.990	1.020	1.015	1.020	0.997	0.978	1.019	0.997	1.005
MGI 5175	0.924	0.923	0.917	0.867	0.979	0.978	0.982	0.930	0.833
NAI 5892	0.966	0.956	0.967	0.941	0.984	0.983	0.994	0.966	0.953
TIO 6180	0.997	0.984	0.989	0.991	0.984	1.002	1.004	1.001	0.986
H 6504	0.880	0.900	0.925	0.932	0.856	0.851	0.873	0.893	0.915
TIO 7100	1.011	1.009	1.005	0.997	0.997	0.994	1.014	1.005	1.004
NAI 8190	0.0	0.0	1.024	1.002	0.983	0.0	0.0	1.009	1.010
CAII8543	0.0	0.0	0.987	0.934	0.945	0.0	0.0	0.899	0.927
TIO 8880	0.0	0.0	1.026	1.046	0.963	0.0	0.0	1.008	1.022
CN 9190	0.0	0.0	1.107	0.929	0.758	0.0	0.0	0.973	0.976
U/B	0.429	0.367	0.341	0.268	0.497	0.538	0.530	0.525	0.403
B/V	0.634	0.493	0.449	0.386	0.807	0.744	0.717	0.619	0.530
V/R	0.846	0.781	0.718	0.695	0.873	0.838	0.804	0.789	0.712
V/I	0.0	0.0	0.000	0.587	0.780	0.0	0.0	0.700	0.620
V/J	0.0	0.0	0.645	0.534	0.0	0.0	0.0	0.727	0.636

TABLE B5 (CONTINUED)

MEAN STELLAR INDICES

INDEX	SD E 1	SD E 2	SD E 3	SD E 4	SD E 5	SD E 6	SD M 1	SD M 2	SD M 3
H 3738	0.899	0.909	0.910	0.971	1.026	1.070	0.862	0.890	0.937
H 3835	0.802	0.814	0.823	0.803	0.706	0.801	0.731	0.773	0.751
CN 3860	1.033	1.036	1.030	1.047	1.038	0.892	1.075	1.028	1.044
CN 3880	0.916	0.913	0.907	0.951	0.976	0.923	0.852	0.880	0.904
CAII3933	0.833	0.756	0.790	0.601	0.487	0.478	0.734	0.702	0.624
H 4101	0.828	0.866	0.860	0.951	1.012	1.022	0.735	0.812	0.880
CN 4200	1.011	1.006	0.988	1.013	1.032	1.034	0.978	0.991	1.015
CAI 4226	0.993	0.986	0.976	0.996	0.954	0.957	0.979	0.976	1.001
CH 4305	0.957	0.915	0.902	0.817	0.776	0.792	0.902	0.817	0.837
IS 4430	0.996	0.980	0.997	1.007	1.030	1.041	1.006	1.006	1.017
MGH 4780	1.008	1.026	1.014	1.017	1.004	1.000	1.015	1.010	1.005
TIO 4970	0.991	0.993	1.009	0.997	1.011	1.021	0.995	1.008	1.002
MGI 5175	0.980	0.978	0.979	0.934	0.844	0.819	0.962	0.960	0.941
NAI 5892	0.989	0.978	0.985	0.966	0.955	0.946	0.965	0.965	0.959
TIO 6180	1.000	0.998	0.998	0.999	0.984	0.988	0.996	0.992	0.993
H 6564	0.860	0.856	0.867	0.882	0.914	0.923	0.814	0.838	0.862
TIO 7100	0.986	0.995	1.007	1.014	0.989	1.023	1.000	1.003	1.001
NAI 8190	0.981	0.998	0.0	1.010	1.012	0.0	1.004	0.0	1.005
CAII8543	0.945	0.950	0.0	0.899	0.927	0.0	0.935	0.0	0.937
TIO 8880	0.963	1.047	0.0	1.008	1.022	0.0	0.989	0.0	1.057
CN 9190	0.758	0.787	0.0	0.973	0.976	0.0	0.948	0.0	0.897
U/B	0.491	0.533	0.524	0.527	0.415	0.392	0.433	0.464	0.467
B/V	0.786	0.748	0.709	0.624	0.508	0.447	0.869	0.716	0.681
V/R	0.862	0.849	0.827	0.811	0.735	0.707	0.973	0.936	0.866
V/I	0.777	0.770	0.0	0.713	0.636	0.0	0.972	0.0	0.782
V/J	0.0	0.0	0.0	0.721	0.653	0.0	1.041	0.0	0.0

TABLE B5 (CONTINUED)

MEAN STELLAR INDICES

INDEX	SD M 4	SD M 5	SD M 6	SD M 7
H 3798	0.956	0.988	0.944	0.938
H 3835	0.738	0.658	0.719	0.799
CN 3860	1.025	0.929	0.791	0.643
CN 3880	0.909	0.873	0.738	0.672
CAII3933	0.562	0.509	0.456	0.446
H 4101	0.926	1.009	1.078	1.000
CN 4200	1.043	1.054	1.038	0.907
CAI 4226	1.028	1.001	1.012	1.004
CH 4305	0.810	0.763	0.727	0.740
IS 4430	1.014	1.038	1.023	1.017
MGH 4780	1.030	1.025	1.027	1.059
TIO 4970	0.990	1.020	1.012	1.030
MGI 5175	0.924	0.835	0.854	0.861
NAI 5892	0.967	0.931	0.955	0.945
TIO 6180	0.996	0.984	0.980	0.993
H 6564	0.880	0.900	0.925	0.939
TIO 7100	1.011	1.009	0.999	0.989
NAI 8190	0.0	0.0	0.0	0.0
CAII8543	0.0	0.0	0.0	0.0
TIO 8880	0.0	0.0	0.0	0.0
CN 9190	0.0	0.0	0.0	0.0
U/B	0.451	0.403	0.314	0.251
B/V	0.632	0.496	0.398	0.373
V/R	0.843	0.776	0.705	0.695
V/I	0.0	0.0	0.0	0.0
V/J	0.0	0.0	0.0	0.0

Figures B1 - B19: Continuum and feature index behaviors in the mean stellar types and in the program clusters. The symbols represent object types as follows:

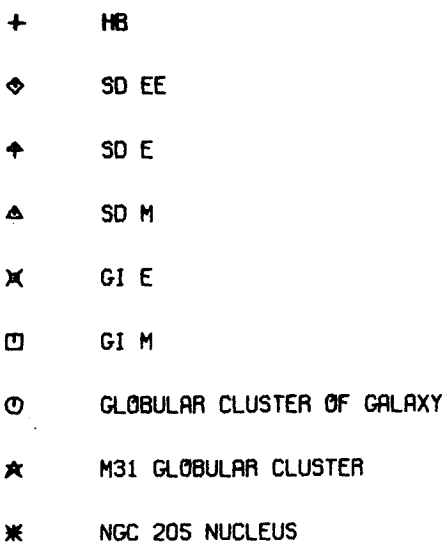

FIGURE B1

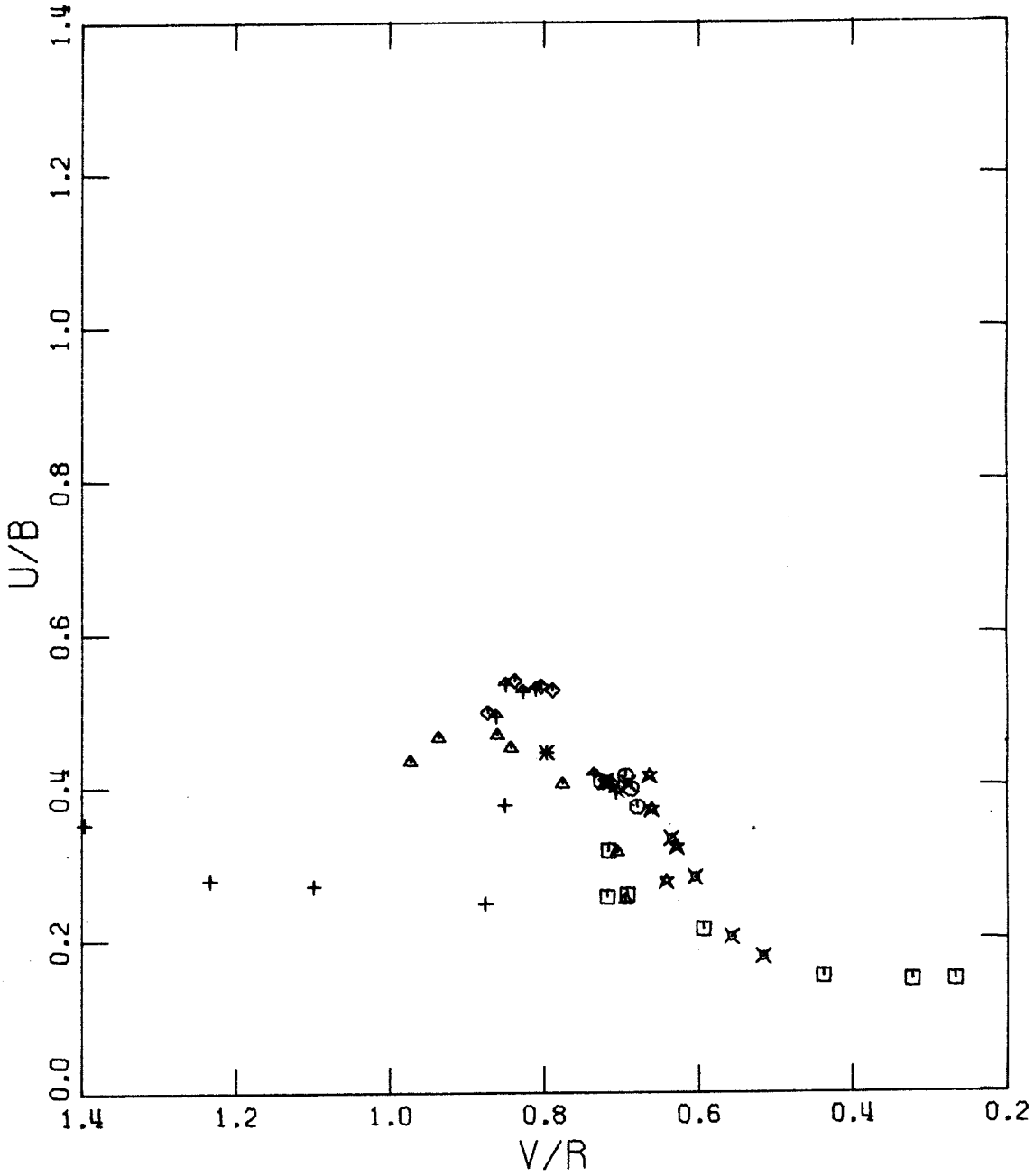

FIGURE B2

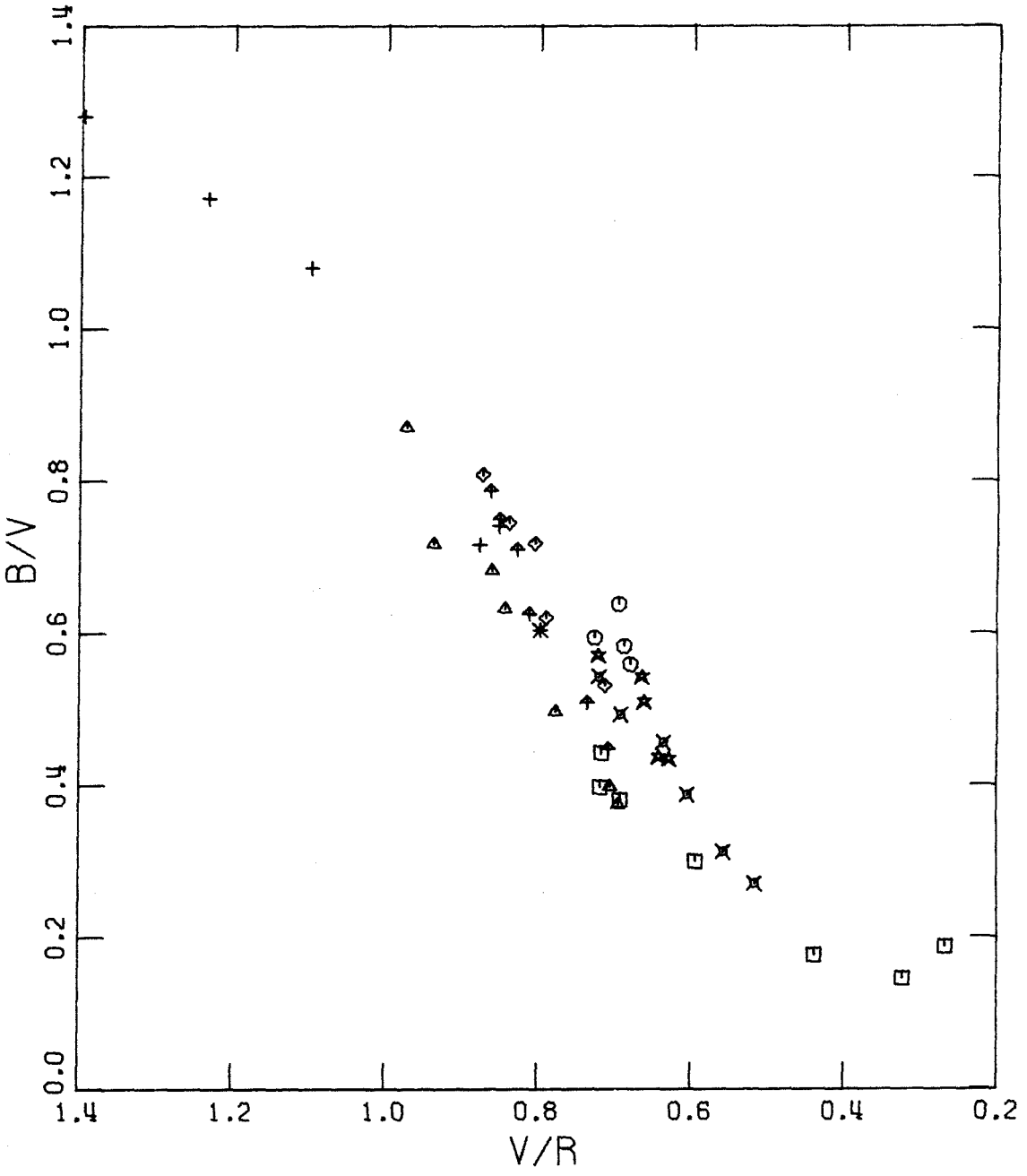

FIGURE B3

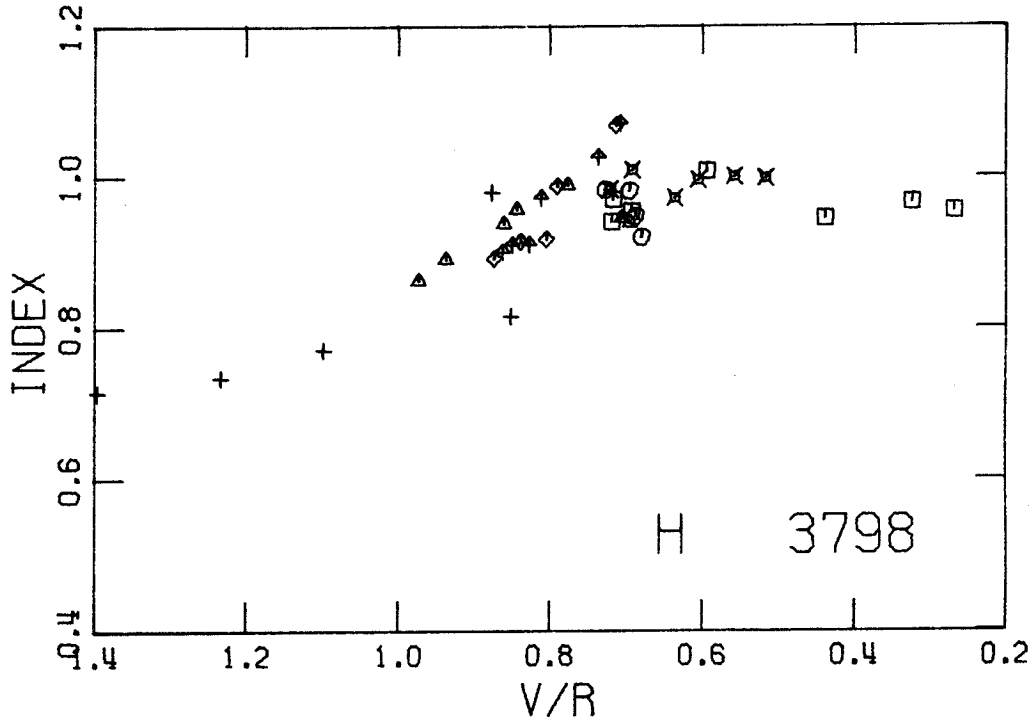

FIGURE B4

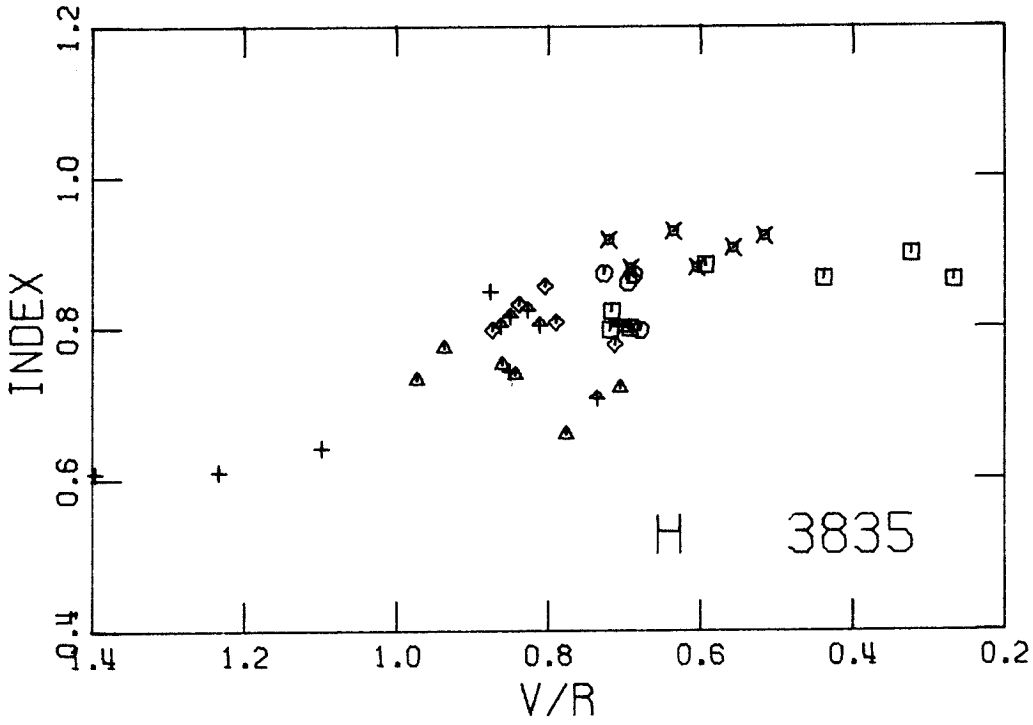

FIGURE B5

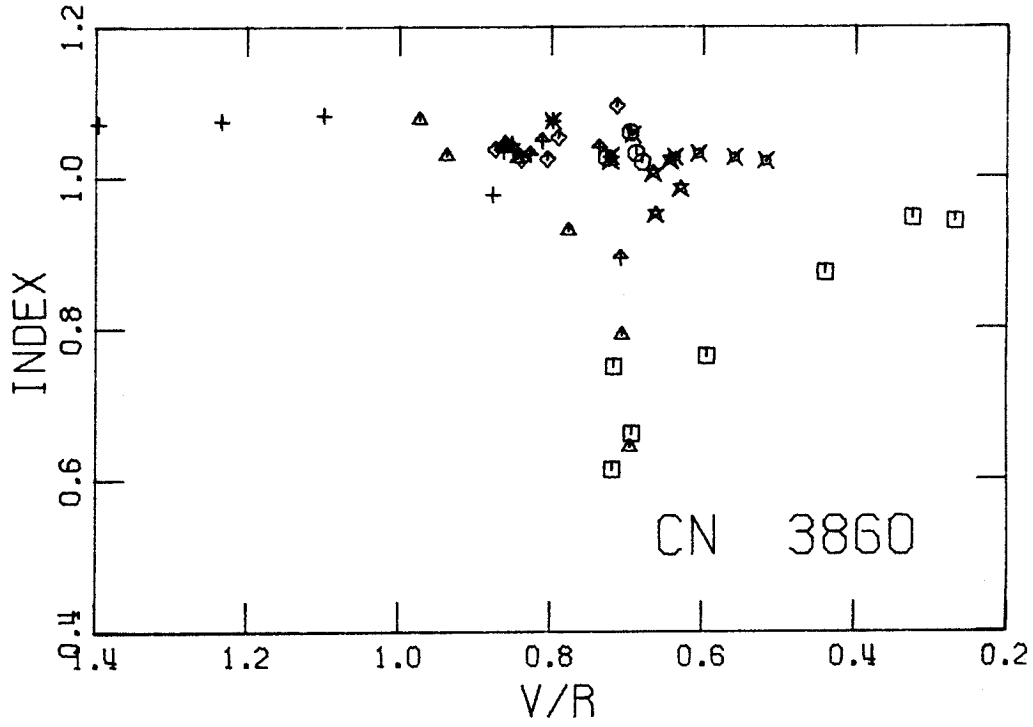

FIGURE B6

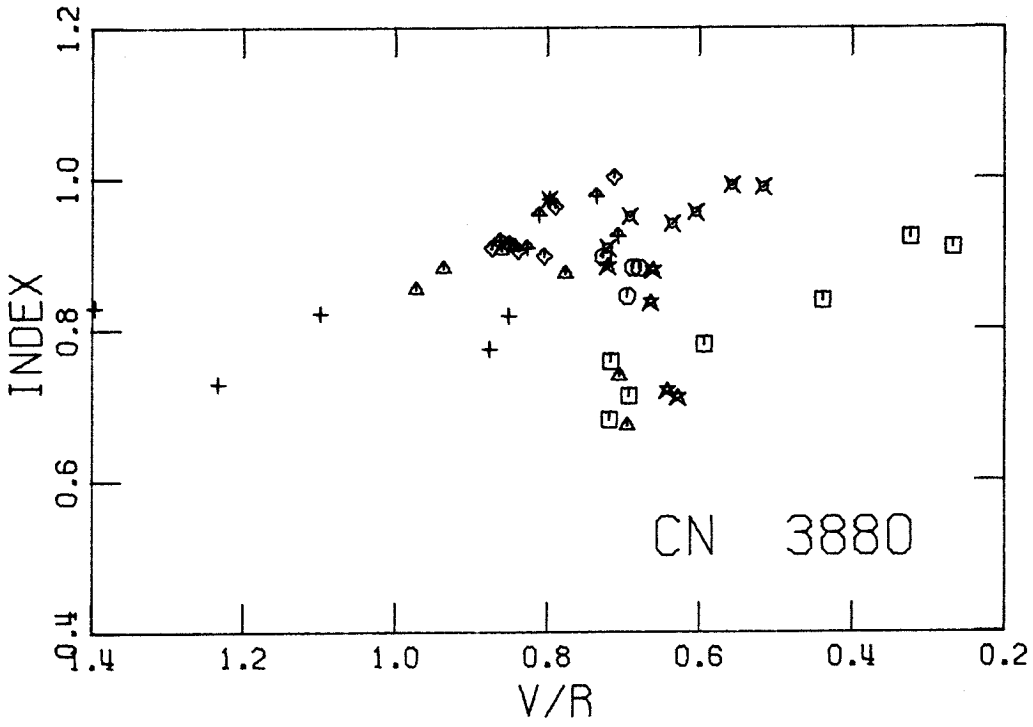

FIGURE B7

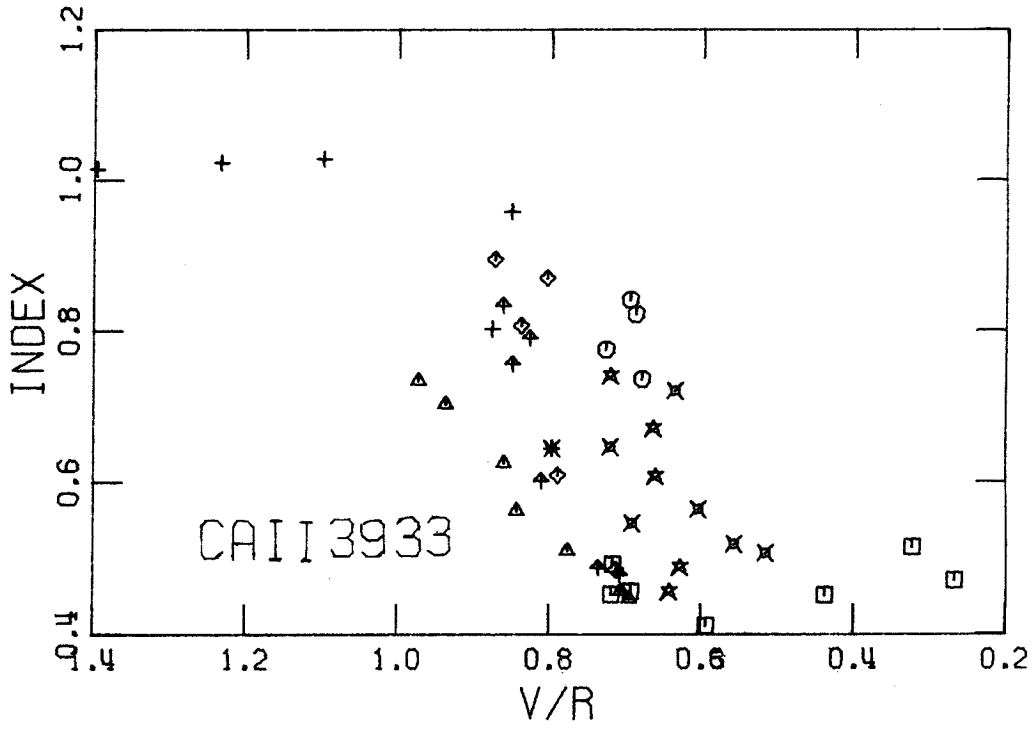

FIGURE B8

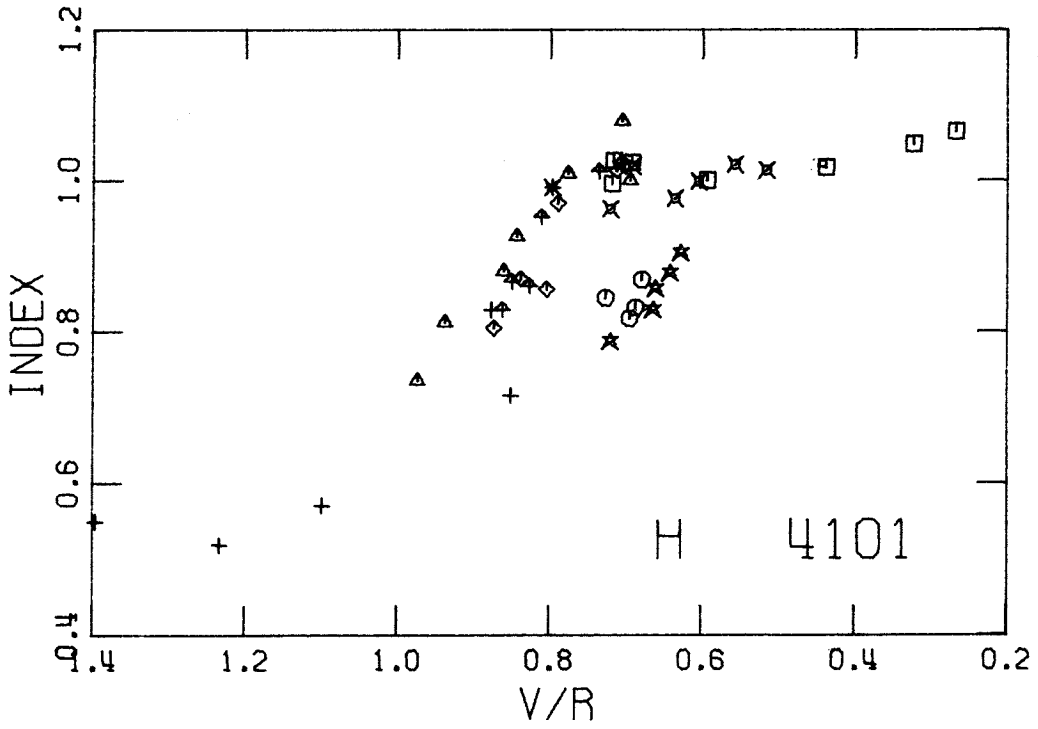

FIGURE B9

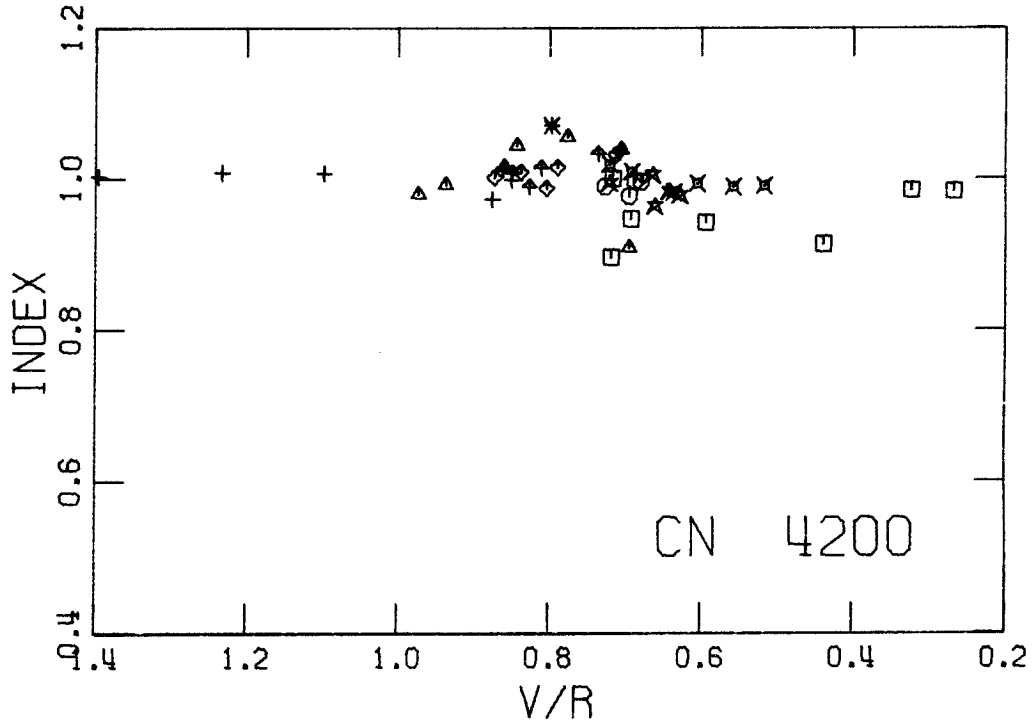

FIGURE B10

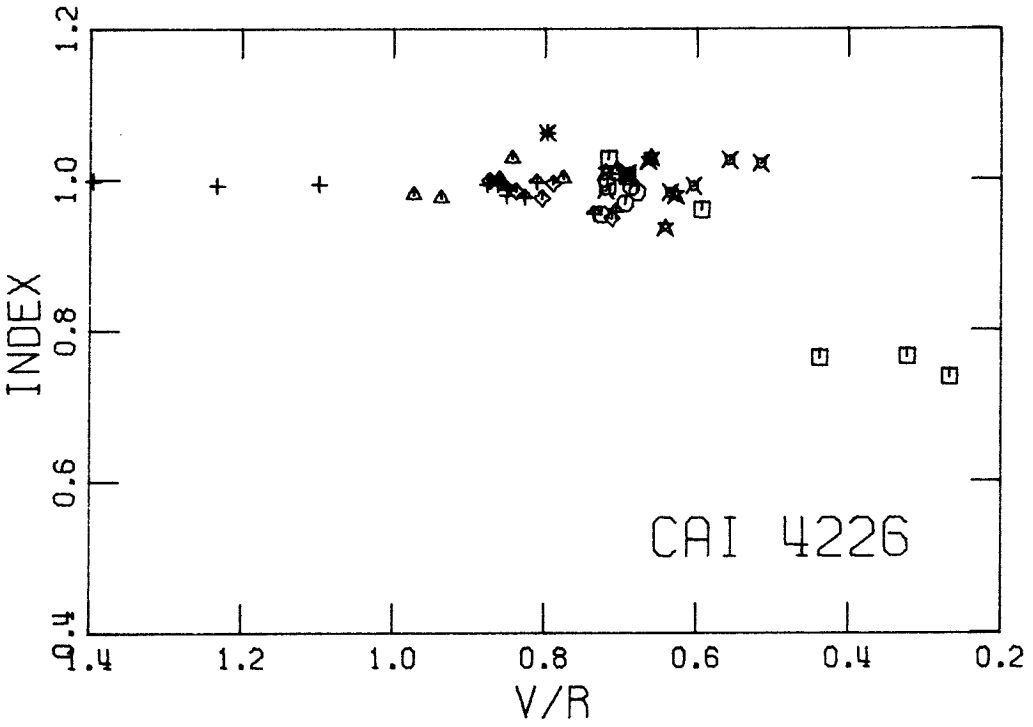

FIGURE B11

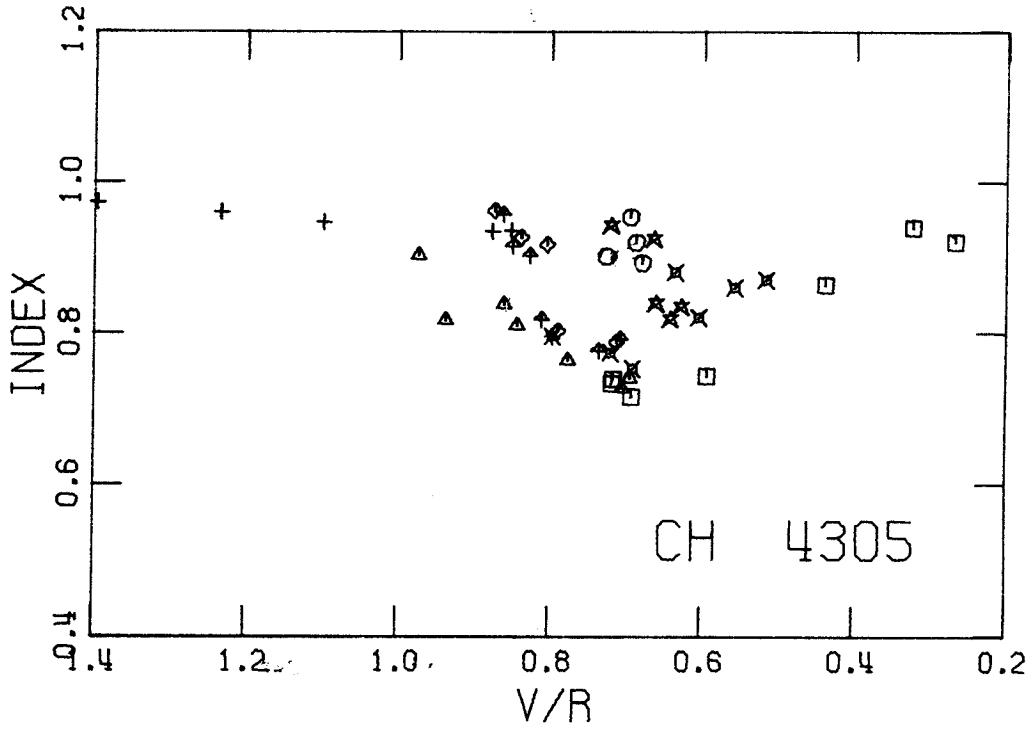

FIGURE B12

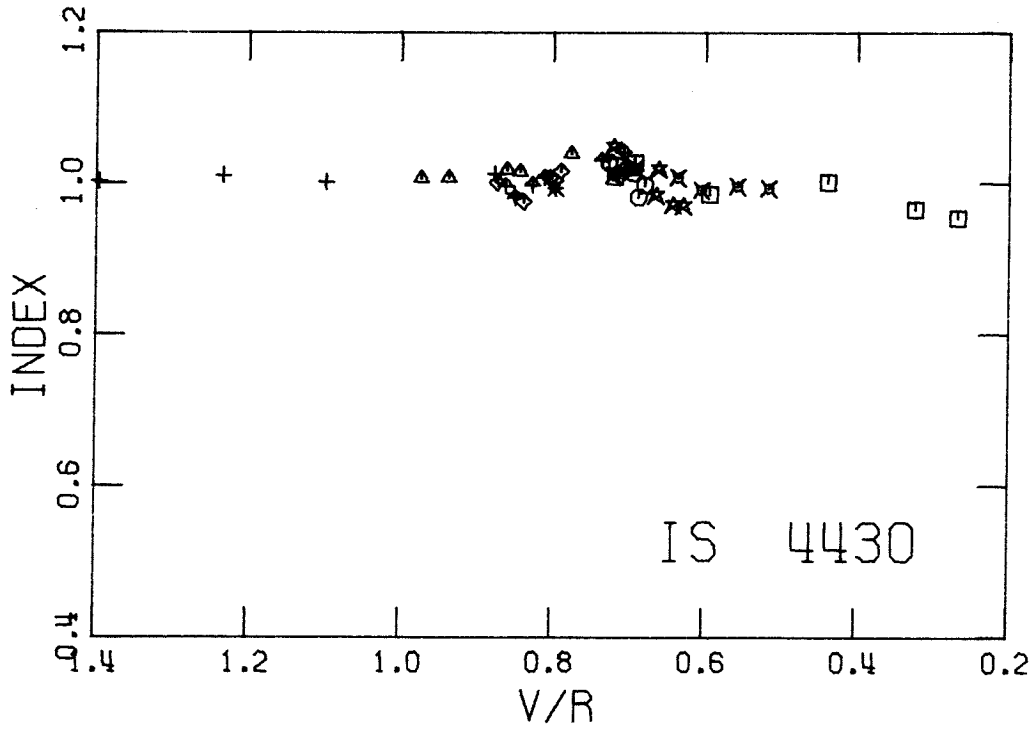

FIGURE B13

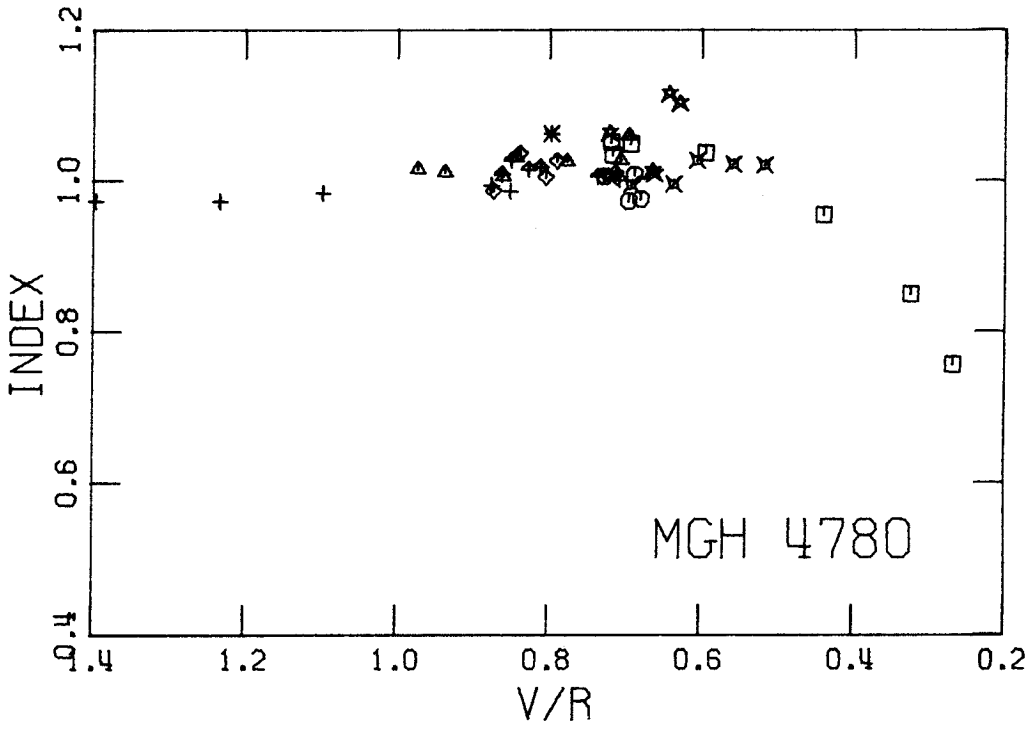

FIGURE B14

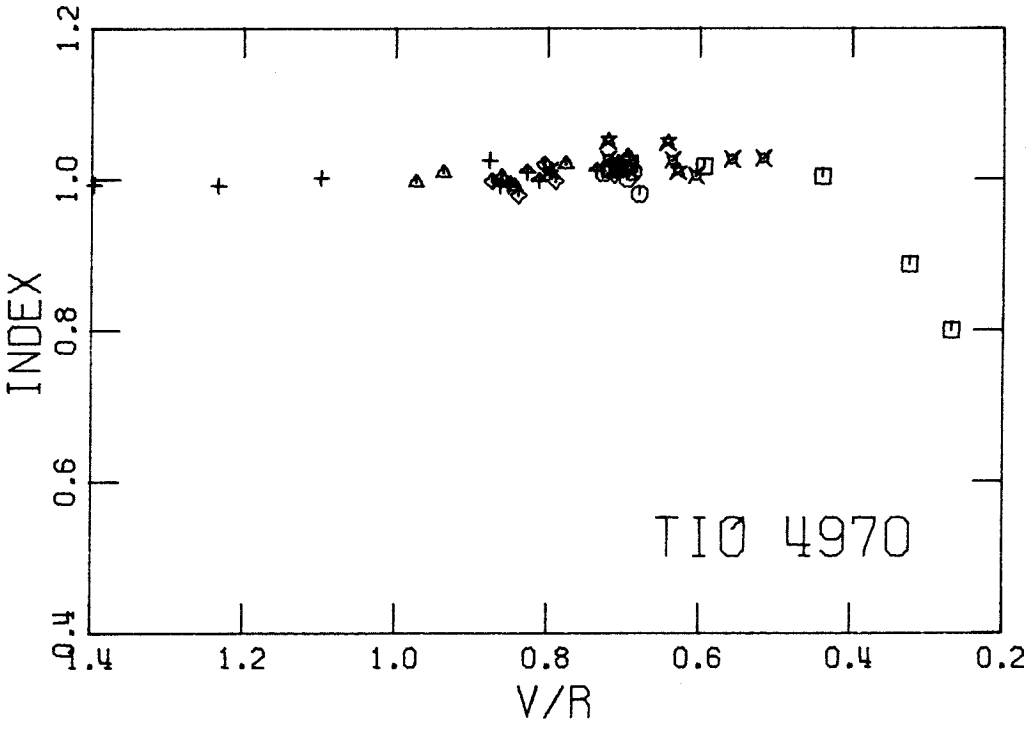

FIGURE B15

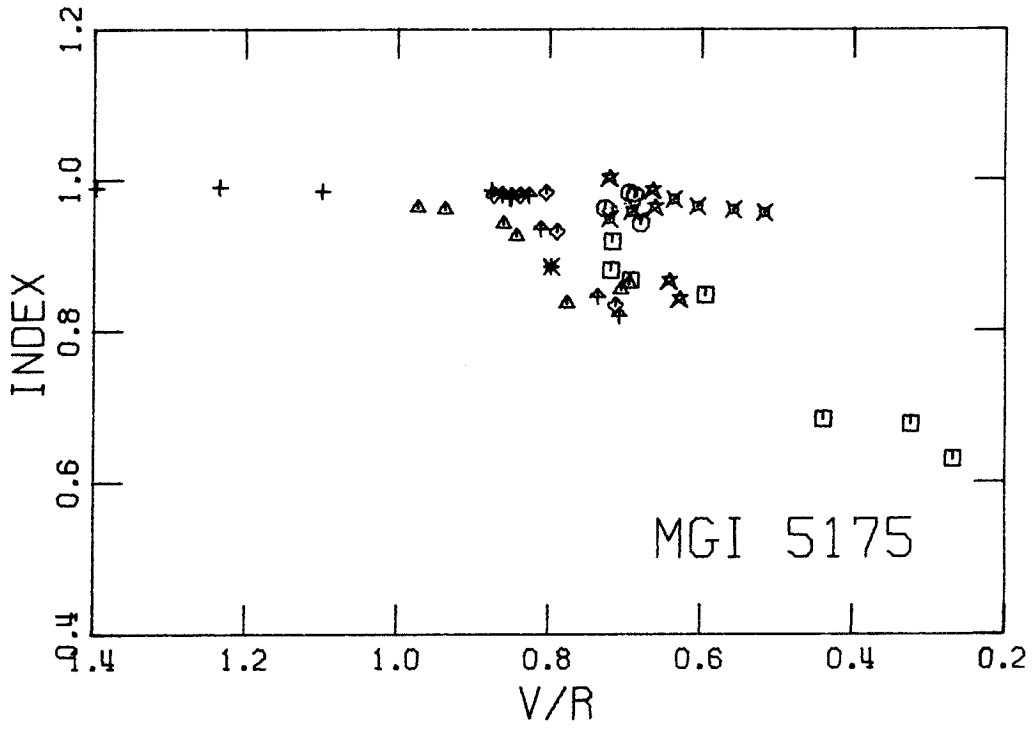

FIGURE B16

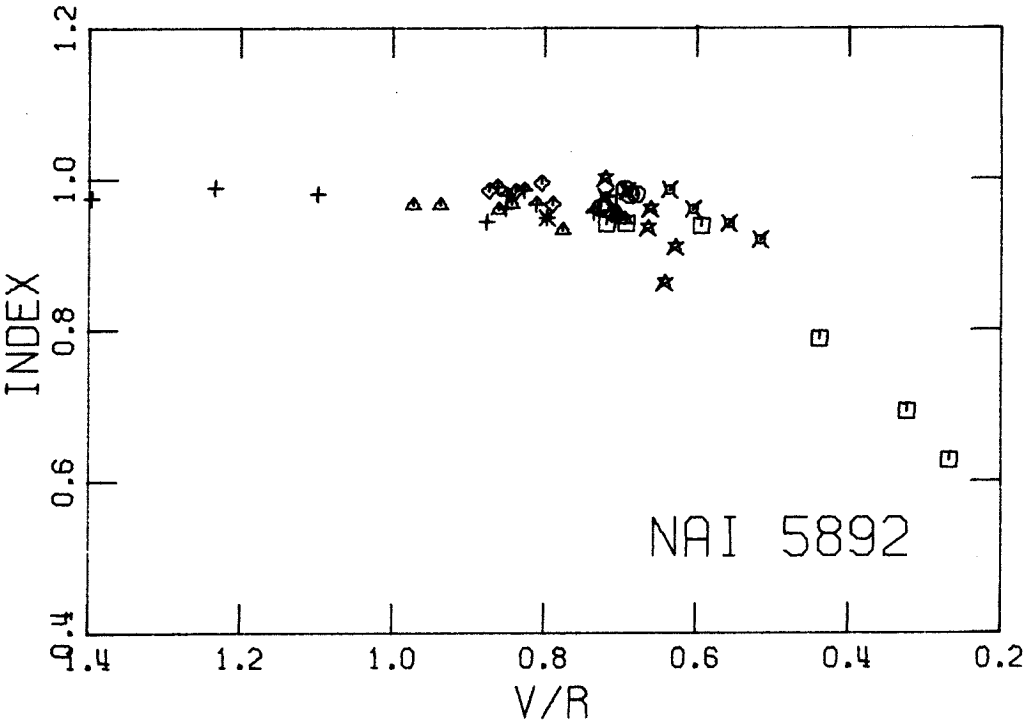

FIGURE B17

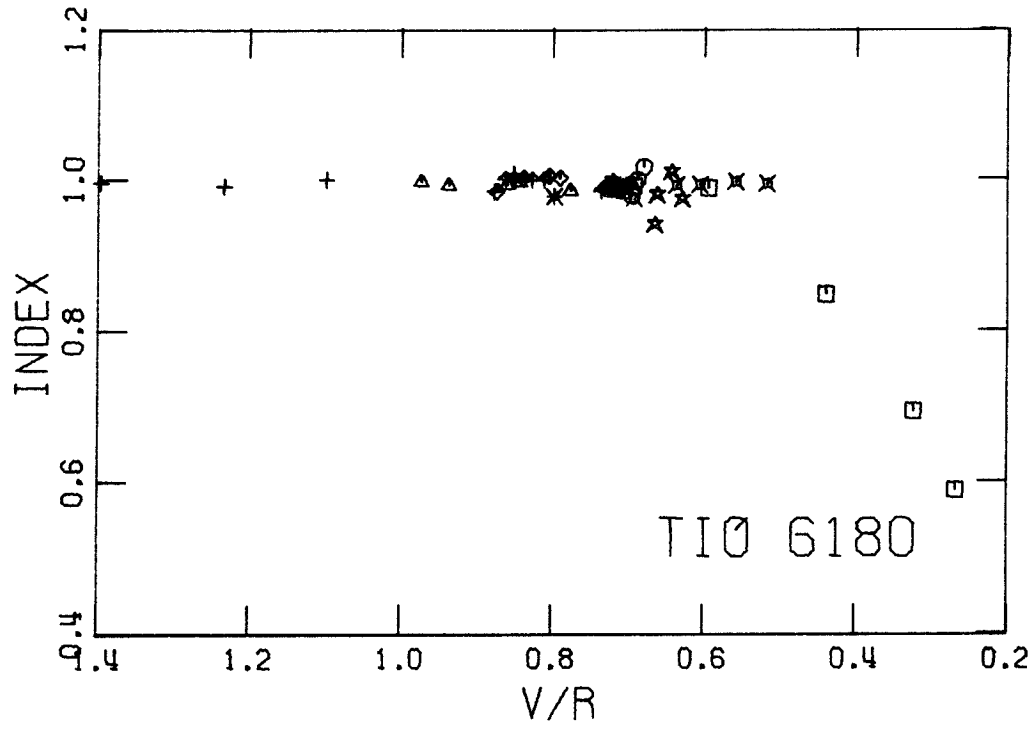

FIGURE B18

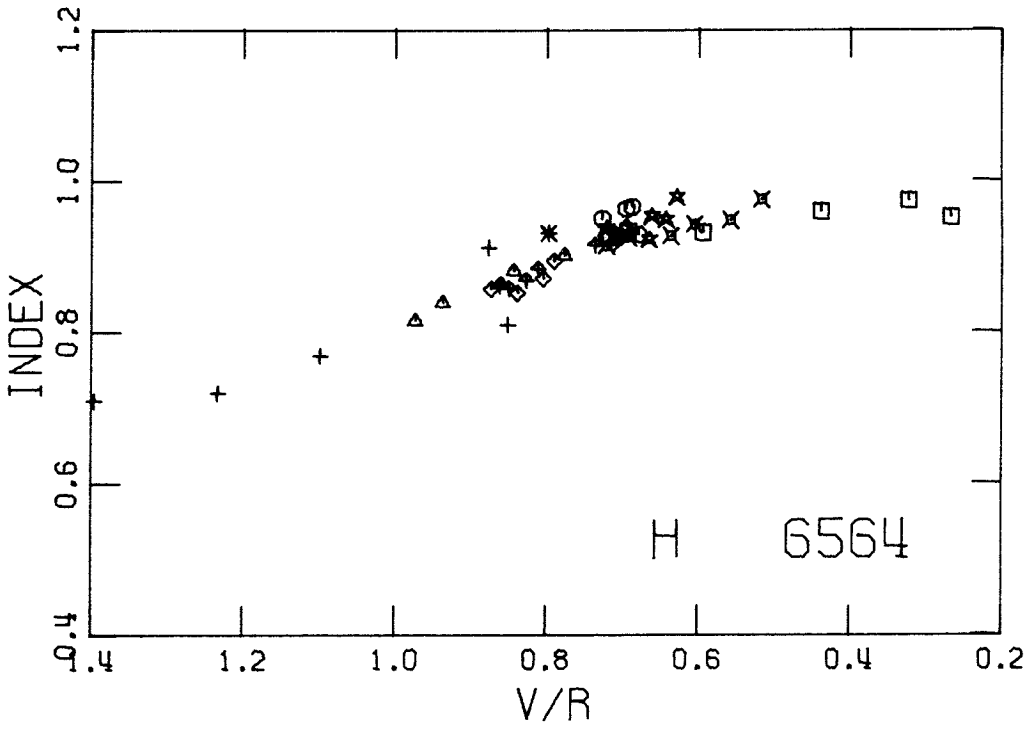

FIGURE B19

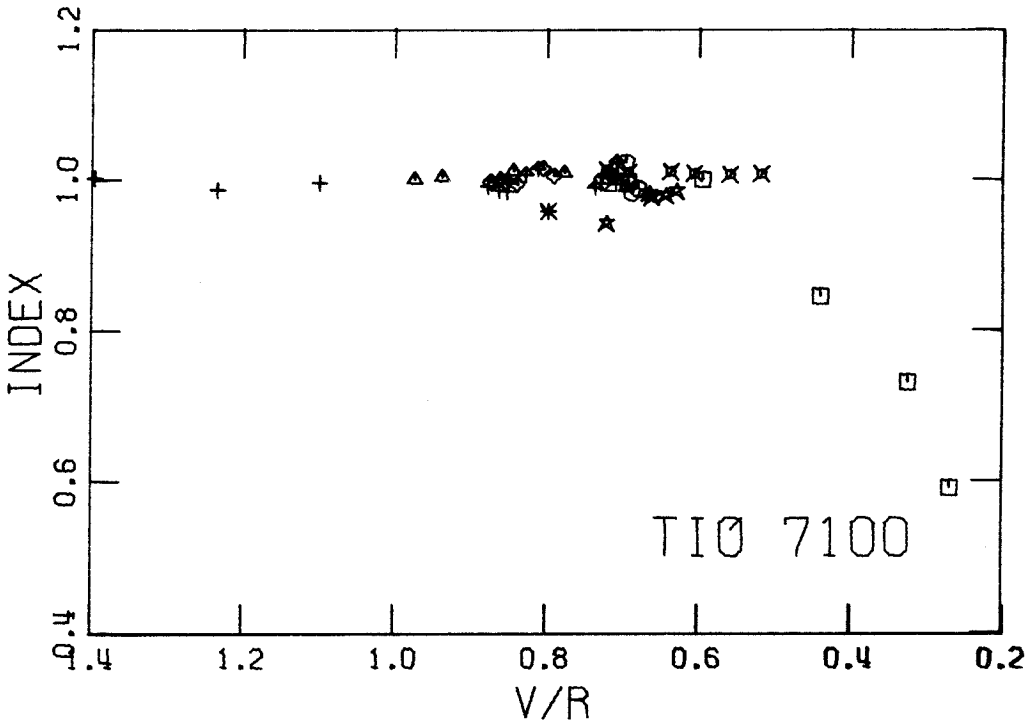

REFERENCES

Aller, L. H. 1960, in Stars and Stellar Systems, Vol. 6, Stellar Atmospheres, ed. J. L. Greenstein (Chicago: University of Chicago Press), pp. 156, 232.

-----. 1963, Astrophysics, the Atmospheres of the Sun and Stars, (New York: Ronald Press).

Aller, L. H., and Greenstein, J. L. 1960, Ap. J. Suppl., 5, 139.

Anderson, C. M. 1968, thesis, California Institute of Technology.

Anderson, K. S. 1968, thesis, California Institute of Technology.

Arp, H. 1962, Ap. J. 135, 311.

-----. 1965, in Stars and Stellar Systems, Vol. 5, Galactic Structure, ed. A. Blaauw and M. Schmidt (Chicago: University of Chicago Press), p. 401.

Arp, H. C., and Johnson, H. L. 1955, Ap. J., 122, 171.

Baade, W. 1944, Ap. J., 100, 137.

-----. 1951, Pub. Univ. Mich. Obs., 10, 7.

Barbier, D., Chalonge, D., and Morguleff, N. 1941, Ann. d'Ap., 4, 137.

Baum, W. A., Hiltner, W. A., Johnson, H. L., and Sandage, A. R. 1959, Ap. J., 130, 749.

Bergh, S. van den 1965, J. R. A. S. Canada, 59, 151.

-----. 1967, A. J., 72, 70.

-----. 1968, J. R. A. S. Canada, 62, 1.

-----. 1969, Ap. J. Suppl., 19, 145.

Bidelman, W. P. 1965, in Vistas in Astronomy, 8, ed. A. Beer (Oxford: Pergamon Press), 53.

Blanco, V. M., Demers, S., Douglass, G. G., and Fitzgerald, M. P. 1968, Pub. U. S. Naval Obs., Ser II, XXI.

Bond, H. E. 1970a (private communication).

------. 1970b, Ap. J. Suppl., 22, 117.

Burbidge, E. M., and Burbidge, G. R. 1956, Ap. J., 124, 116.

Burbidge, E. M., Burbidge, G. R., Fowler, W. A., and Hoyle, F. 1957, Rev. Mod. Phys., 29, 547.

Burbidge, G. 1969, Comments on Ap. and Space Phys., 1, 101.

Carbon, D. F., and Gingerlich, O. 1969, in Theory and Observation of Normal Stellar Atmospheres, ed. O. Gingerlich (Cambridge: The MIT Press).

Castellani, V., Giannone, P., and Renzini, A. 1970, Ap. and Space Sci., 9, 418.

Cayrel, R. 1968, Ap. J., 151, 997.

Cayrel, R., and Cayrel de Strobel, G. 1966, Ann. Rev. Astr. and Ap., 4, 1.

Cayrel de Strobel, G. 1966, Ann. d'Ap., 29, 413.

Chamberlain, J. W., and Aller, L. H. 1951, Ap. J., 114, 52.

Christy, R. F. 1966a, Ann. Rev. Astr. and Ap., 4, 353.

------. 1966b, Ap. J., 144, 108.

Crawford, D. L., and Barnes, J. V. 1969, A. J., 74, 1008.

Deeming, T. J. 1960, M. N. R. A. S., 121, 52.

Dennis, T. R. 1965, Pub. A. S. P., 77, 283.

Deutsch, A. J. 1960, in Stars and Stellar Systems, vol. 6, Stellar Atmospheres, ed. J. L. Greenstein (Chicago: University of Chicago Press), p. 543.

-----. 1968, in Mass Loss from Stars, ed. M. Hack (Dordrecht, Holland: D. Reidel Pub. Co.), p. 1.

Deutsch, A. J., Wilson, O. C., Keenan, P. C. 1969, Ap. J., 156, 107.

Eggen, O. J. 1962, R. O. B., No. 51.

-----. 1964, R. O. B., No. 84.

-----. 1966 (private communication to W. L. W. Sargent).

-----. 1969, Pub. A. S. P., 81, 346.

Eggen, O. J., Lynden-Bell, D., and Sandage, A. R. 1962, Ap. J., 136, 748.

Eggen, O. J., and Sandage, A. R. 1959, M. N. R. A. S., 119, 255.

Faulkner, J. 1967, Ap. J., 147, 617.

Faulkner, J., and Iben, I., Jr. 1966, Ap. J., 144, 995.

Fernie, J. D. 1966, M. N. R. A. S., 132, 485.

Fitch, W. S., and Morgan, W. W. 1951, Ap. J., 114, 548.

Graham, J. A., and Doremus, C. 1968, A. J., 73, 226.

Greenstein, J. L. 1965, in Stars and Stellar Systems, Vol. 5, Galactic Structure, ed. A. Blaauw and M. Schmidt (Chicago: University of Chicago Press) p. 361.

-----. 1969, in Low Luminosity Stars, ed. S. S. Kumar (New York: Gordan and Breach Science Publishers), p. 281.

Greenstein, J. L., and Keenan, P. C. 1958, Ap. J., 127, 172.

Griffin, R. F. 1961, M. N. R. A. S., 122, 181.

Griffin, R. F. 1968, A Photometric Atlas of the Spectrum of Arcturas, (Cambridge: Cambridge Philosophical Society).

Griffin, R., and Redman, R. O. 1960, M. N. R. A. S., 120, 287.

Harris, D. L. III 1963, in Stars and Stellar Systems, Vol. 3, Basic Astronomical Data, ed. K. Aa. Strand (Chicago: University of Chicago Press), p. 263.

Hartwick, F. D. A. 1968, Ap. J., 154, 475.

-----. 1970, Ap. J., 161, 845.

Hayes, D. S. 1970, Ap. J., 159, 165.

Helfer, H. L., and Wallerstein, G., Ap. J. Suppl., 16, 1.

Helfer, H. L., Wallerstein, G., and Greenstein, J. L. 1959, Ap. J., 129, 700.

Hoyle, F., and Schwarzchild, M. 1955, Ap. J. Suppl., 2, 1.

Iben, I., Jr. 1971, Pub. A. S. P., 83 (in press).

Johnson, H. L. 1963, in Stars and Stellar Systems, Vol. 3, Basic Astronomical Data, ed. K. Aa. Strand (Chicago: University of Chicago Press), p. 204.

-----. 1966, Ann. Rev. Astr. and Ap., 4, 193.

Johnson, H. L., and Sandage, A. R. 1955, Ap. J., 121, 616.

-----. 1956, Ap. J., 124, 379.

Keenan, P. C. 1963, in Stars and Stellar Systems, Vol. 3, Basic Astronomical Data, ed. K. Aa. Strand (Chicago: University of Chicago Press), p. 78.

Kodiara, K. 1964, Zs. f. Ap., 59, 139.

Kodiara, K., Greenstein, J. L., and Oke, J. B. 1969, Ap. J., 155, 525.

Koelbloed, D. 1967, Ap. J., 149, 299.

Kron, G. E., and Mayall, N. U. 1960, A. J., 65, 581.

Lindblad, B. 1922, Ap. J., 55, 85.

MacConnell, D. J. 1970 (private communication).

McClure, R. D., and Bergh, S. van den 1968, A. J., 73, 313.

McClure, R. D., and Racine, R. 1969, A.J., 74, 1000.

McNamara, D. H., and Langford, W. R. 1969, Pub. A. S. P., 81, 141.

Marquardt, D. W. 1963, S I A M J. Indust. and Appl. Math., 11, 431.

Melbourne, W. G. 1960, Ap. J., 132, 101.

Merrill, P. 1956, Lines of the Chemical Elements in Astronomical Spectra (Washington: Carnegie Institute of Washington), Pub. 610.

Minnaert, M. 1940, A Photometric Atlas of the Solar Spectrum (Amsterdam: Schnabel).

Morgan, W. W. 1959, A. J., 64, 432.

Newell, E. B. 1970, Ap. J., 161, 789.

O'Connell, R. 1970, thesis, California Institute of Technology.

Ohman, Y. 1934, Ap. J., 80, 171.

-----. 1936, Stockholm Obs. Ann., 12, No. 8.

Oke, J. B. 1964, Ap. J., 140, 689.

-----. 1965, Ann. Rev. Astr. and Ap., 3, 23.

-----. 1969a, Pub. A. S. P., 81, 11.

-----. 1969b (private communication).

-----. 1970 (private communication).

-----. 1971 (private communication).

Oke, J. B., and Conti, P. S. 1966, Ap. J., 143, 134.

Oke, J. B., Greenstein, J. L., and Gunn, J. 1966, in Stellar Evolution, ed. R. F. Stein and A. G. W. Cameron (New York: Plenum Press), p. 399.

Oke, J. B., and Schild, R. E. 1970, Ap. J., 161, 1015.

Oort, J. H. 1926, Groningen Pub., No. 40.

Paczynski, B., and Ziolkowsky, J. 1968, Acta Astron., 18, 255.

Pagel, B. E. J. 1964, R. O. B., No. 87.

Pagel, B. E. J., and Powell, A. L. T. 1966, R. O. B., No. 124.

Peat, D. W. 1964, M. N. R. A. S., 128, 435.

Penzias, A. A., and Wilson, R. W. 1965, Ap. J., 142, 419.

Peterson, B. 1968, thesis, California Institute of Technology.

Preston, G. W., and Bidelman, W. P. 1956, Pub. A. S. P., 68, 533.

Price, M. J. 1966, M. N. R. A. S., 134, 135.

Rood, R. and Iben, I. 1968, Ap. J., 154, 215.

Sandage, A. 1961, The Hubble Atlas of Galaxies (Washington: Carnegie Institution of Washington).

-----. 1964, Ap. J., 139, 442.

-----. 1968, in Galaxies and the Universe, ed. L. Woltjer (New York: Columbia University Press), p. 75.

-----. 1969, Ap. J., 157, 515.

Sandage, A. R., and Eggen, O. J. 1959, M. N. R. A. S., 119, 278.

Sandage, A., and Katem, B. 1964, Ap. J., 139, 1088.

Sandage, A., Katem, B., and Kristian, J. 1968, Ap. J., 153, L129.

Sandage, A., and Smith, L. L. 1966, Ap. J., 144, 886.

Sandage, A., and Walker, M. F. 1966, Ap. J., 143, 313.

Sandage, A., and Wildey, R. L. 1967, Ap. J. 150, 469.

Sargent, W. L. W. 1961, Ap. J., 134, 142.

-----. 1968, Ap. J., 152, 885.

Schwarzchild, M., and Bernstein, S. 1955, Ap. J., 122, 200.

Simoda, M., and Kimura, H. 1968, Ap. J., 151, 133.

Slettebak, A., Bahner, K., and Stock, J. 1961, Ap. J., 134, 195.

Spinrad, H. 1962, Ap. J., 135, 715.

-----. 1966, Pub. A. S. P., 78, 367.

Spinrad, H., and Schweizer, F. 1972 (in preparation).

Spinrad, H., and Taylor, B. 1969, Ap. J., 157, 1279.

-----. 1971, Ap. J. Suppl., 22, 445.

Stobie, R. S. 1971, Ap. J., 168, 381.

Stoeckly, R., and Dressler, K. 1964, Ap. J., 139, 240.

Strom, S. E., Cohen, J. G., and Strom, K. M., Ap. J., 147, 1038.

Strom, S. E., and Strom, K. M. 1967, Ap. J., 150, 501.

Strom, S. E., Strom, K. M., Rood, R. T., and Iben, I., Jr. 1970, Astr. and Ap. 8, 243.

Strömgren, B. 1963, in Stars and Stellar Systems, Vol. 3, Basic Astronomical Data, ed. K. Aa. Strand (Chicago: University of Chicago Press) p. 123.

Sturch, C. 1966, Ap. J., 143, 774.

Thackeray, A. D. 1949, M. N. R. A. S., 109, 436.

Tifft, W. G. 1963, M. N. R. A. S., 126, 209.

Tull, R. G. 1963, thesis, University of Michigan.

Vaucouleurs, G. de, and Vaucouleurs, A. de 1964, Reference Catalogue of Bright Galaxies (Austin: University of Texas Press).

Vetešnik, M. 1962, Bull. Astr. Inst. Czechoslovakia, 13, 180.

Wallerstein, G. 1962, Ap. J. Suppl., 6, 407.

Wallerstein, G., and Carlson, M. 1960, Ap. J., 132, 276.

Wallerstein, G., and Greenstein, J. L. 1964, Ap. J., 139, 1163.

Wallerstein, G., Greenstein, J. L., Parker, R., Helfer, H. L., and Allen, L. H. 1963, Ap. J., 137, 280.

Wallerstein, G., and Helfer, H. L. 1966, A. J., 71, 350.

Wallerstein, G., and Hunziker, W. 1964, Ap. J. 140, 214.

Wampler, E. J. 1966, Ap. J., 144, 921.

Weymann, R. 1963, Ann. Rev. Astr. and Ap., 1, 97.

Whitford, A. E. 1958, A. J., 63, 201.

Wildey, R. L., Burbidge, E. M., Sandage, A. R., and Burbidge, G. R. 1962, Ap. J., 135, 94.

Wilson, R. E. 1953, General Catalogue of Stellar Radial Velocities (Washington: Carnegie Institute of Washington), Pub. 601.

Wilson, O.C. 1962, Ap. J., 136, 793.

Wood, D. B. 1963, thesis, University of California, Berkley.

-----. 1966, Ap. J., 145, 36.

-----. 1969, A. J., 74, 177.